UNIVERSITY OF SOUTHAMPTON

Faculty of Social and Human Sciences

School of Mathematics

MOLECULAR FIELD THEORIES FOR BIAXIAL LIQUID CRYSTALS

by

Tung B. T. To

Supervisors: Geoffrey R. Luckhurst and Timothy J. Sluckin
A thesis submitted in partial fulfillment for the
degree of Doctor of Philosophy

March 2012

UNIVERSITY OF SOUTHAMPTON

ABSTRACT

FACULTY OF SOCIAL AND HUMAN SCIENCES
SCHOOL OF MATHEMATICS

Doctor of Philosophy

MOLECULAR FIELD THEORIES FOR BIAXIAL LIQUID CRYSTALS

by Tung B. T. To

This thesis consists of five studies on the applications of the molecular field theory to model systems of biaxial molecules which form biaxial and uniaxial nematic and smectic A phases. The first study extends the original theory for biaxial nematic phases of D_{2h} symmetry to allow the phase symmetry to be C_{2h}. In the second study, a dipolar interaction is introduced to the original model of biaxial nematic phases formed from V-shaped molecules to explain a disagreement between theory and experiment. This leads to the stabilisation of the novel polar biaxial nematic phase. In the third study, we introduce molecular flexibility at a simplified level into an existing model of V-shaped molecules to investigate its effects on the stability of the biaxial nematic phases. The fourth study aims to explain and predict various effects of magnetic field on the uniaxial nematic to isotropic phase transition for a system of rigid V-shaped molecules. In the fifth study, we develop a model for biaxial smectic A phases. The theory is simplified by using several approximations which facilitates the calculations.

Contents

List of Figures

List of Tables

DECLARATION OF AUTHORSHIP

I, Tung B. T. To,
declare that the thesis entitled
"Molecular Field Theories for Biaxial Liquid Crystals"
and the work presented in the thesis are both my own, and have been generated by me as the result of my own original research. I confirm that:

- this work was done wholly or mainly while in candidature for a research degree at this University;
- where any part of this thesis has previously been submitted for a degree or any other qualification at this University or any other institution, this has been clearly stated;
- where I have consulted the published work of others, this is always clearly attributed;
- where I have quoted from the work of others, the source is always given. With the exception of such quotations, this thesis is entirely my own work;
- I have acknowledged all main sources of help;
- where the thesis is based on work done by myself jointly with others, I have made clear exactly what was done by others and what I have contributed myself;
- parts of this work have been published as a modified version of chapter 3, entitled 'Molecular field theory for biaxial nematic liquid crystals composed of molecules with C_{2h} point group symmetry' by G. R. Luckhurst, S. Naemura, T. J. Sluckin, T. B. T. To and S. Turzi, in Physical Review E, volume 84, page 011704, 2011.

Signed: .....

Date: .....

To my dear parents

Acknowledgements

I would like to extend my deepest gratitude to Professor Luckhurst. His extensive knowledge and passion for science helped me to develop my understanding and my inspiration in carrying out this research.

I would like to express my gratitude to Professor Sluckin. He has not only kindly accepted to be my formal supervisor but also given me much valuable advice that has helped this research to progress.

I also would like to thank Doctor D'Alessandro for his fruitful advice and for his help with the administration and correction of this thesis.

I would like to thank Professor Naemura, Mr Nguan and Dr Turzi for their productive collaborations. I also would like to thank Dr Bisi, Dr Daly and Mr Le for their helpful discussions. Especially Dr Daly who helped me with the correction of this thesis.

I ackowledge my thanks to the School of Mathematics, University of Southampton for generous financial support and its members of staff for their help with administration.

I owe my special thanks to my parents for all their support during this study.

And finally, thanks to my relatives and friends. They have provided me very kind and valuable support throughout my time working on this project.

Chapter 1

Introduction

In this chapter we introduce the liquid crystal phases of matter. Then we concentrate on the discussion of biaxial low molar mass thermotropic nematic and smectic A liquid crystals. We also give a plan for subsequent chapters.

1.1 Liquid Crystals

Liquid crystal phases are intermediate between the liquid and the solid phases in that they possess orientational order, like a solid, but have little or no positional order, like a liquid. Therefore, a common behaviour of liquid crystals is a combination of liquid-like fluidity and crystal-like properties. Hence they are sometimes known as *mesomorphic* phases. Similarly the compounds out of which they are constructed are often called *mesogens* [1]. Liquid crystal phases can be broadly classified into *lyotropic* and *thermotropic* systems according to whether their phase structure is changed by adding solvent. The difference is at high enough concentration, the lyotropic mesogenic molecules begin to arrange themselves in *micellar* structures, which causes their phase behaviour with solvent different from thermotropic liquid crystals. In micellar structure, the molecules arrange themselves into spheres, with the mesogenic groups on the outside and the hydrocarbon end chains towards the centre. The rigid core is also called *mesogenic group*.

Thermotropic liquid crystals are often made of elongated molecules which can be classified into three types: *nematic*, *smectic* and *cholesteric* phases. Nematic liquid crystals are those that possess only orientational long-range order and no positional long-range order. In a nematic phase, the molecules have a preferred direction which is unique throughout a uniform domain and often called the director. In contrast, in a cholesteric phase, the director forms a twisted structure. While nematic and cholesteric liquid crystals do not have long-range positional orders, smectic phases are formed of two dimensional layers which confine molecular position. The type of liquid crystals that may be observed depends strongly on the structure of the constituent molecules or groups of molecules. For example, if the constituent molecules are disc-like instead of elongated then they can form *columnar* phases instead of smectic phases. In a columnar phase, the molecules stack face to face to form columns. Depending upon the nature of the building

blocks and upon the external parameters (temperature, pressure, concentration, solvents, fields, etc.), we can observe a wide variety of phenomena and transitions amongst liquid crystals [2]. The system may pass through one or more mesophases before it goes into the isotropic liquid. The crucial input for their building blocks is almost always a central core of some benzene or cyclohexane rings, connected to a flexible chain having a number of carbon atoms and other substituent groups [1]. While the rigid cores help the molecules to achieve ordering, their flexible chains allow them to move around in the fluid.

Thermotropic nematic liquid crystals are ubiquitous materials in *liquid crystal display devices*. The constituent molecules are often elongated (*calamitic* or rod-like). In a conventional nematic phase, the molecular long axis is parallel to the director on average while they can rotate freely around that averaged direction. Because of this orientational order of the molecules, nematic physical properties are anisotropic and cylindrically symmetric. An example is their optical behaviour. For example, a plane polarised light can propagate along the director without its state of polarisation being modified [3]. This director is also called the *optical axis* and since the material has one optical axis, it is called a *uniaxial* nematic, a nomenclature adopted from the field of *optics*. In addition, the anisotropic properties of nematic liquid crystals cause light polarized along the director to propagate at a different velocity than light polarised perpendicular to the director. In other words, an incoming light beam is split into two orthogonal components, called the *ordinary ray* and the *extraordinary ray*, which propagate with different wave vector, which leads to double images [4]. Nematic liquid crystals are, therefore, *birefringent* [5]. The degree of orientational order in nematic liquid crystals depends on the alignment of the constituent molecules with respect to one another. This order is characterised by a set of orientational order parameters.

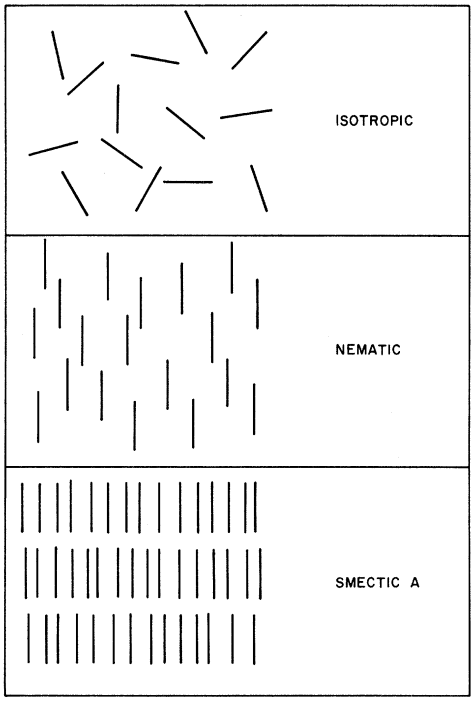

FIGURE 1.1: Schematic representations of the isotropic, nematic and smectic phases formed from elongated molecules. Reproduced from [6].

Another main subdivision of thermotropic liquid crystals which is formed from rod-like molecules is *smectic* mesophases [7]. In addition to orientational order, like nematic phases, smectic phases have a positional order in at least one dimension. There exists many types of smectic phases. They differ in: (i) the orientation of the preferred direction of the molecules with respect to the layer normal and (ii) the organisation of the centres of the molecules within the layers [7]. We are only concerned with the smectic A phase. In this phase, the molecular density oscillates in a direction parallel to the director which forms a density wave in that direction. At large density, the molecules are essentially confined into layers [1]. Hence, the centres of the molecules are, on average, arranged in equidistant planes and smectic phases are often approximated as having a layered structure. The molecules are arranged in layers with a thickness about equal to the

length of the molecules [7]. In addition, smectic A phases have long-range orientational order with the director of molecules in one layer is parallel to the layer normal. Inside each layer, the centres of gravity show no long-range positional order [2]. In figure 1.1, we show schematic representations of the isotropic, nematic and smectic A phases which are formed from elongated molecules. Because of the orientational order of the molecules, like nematics, many physical properties of smectic A liquid crystals are also anisotropic. In smectic A liquid crystals, an incoming light beam is also split into the *ordinary ray* and the *extraordinary ray*, which propagate with different wave vector. Therefore, smectic A liquid crystals are also birefringent. However, there is a difference between the nematic and the smectic A phases in their interaction with light. [5]. In nematic liquid crystals, light is scattered by fluctuation in the director. In contrast, in smectic liquid crystals, light is scattered by fluctuations in both the director and the layer structure [5].

1.2 Uniaxial Nematics

Classical studies of uniaxial nematics often assume that the constituent mesogenic molecules have cylindrical symmetry in keeping with their collective behaviour which often yields a uniaxial nematic phase. In figure 1.2 we show a snapshot of a Monte Carlo simulation which yields a uniaxial nematic phase consisting of cylindrical molecules with the Z axis being the director. The orientation of a molecule in a uniaxial nematic environment can be defined by an angle β between the molecular axis of symmetry and that of the phase which is shown in figure 1.3. The degree of orientational order of the phase should be measured by an average of a function of the angle β. Due to the molecular head-tail symmetry, the order parameter was defined by Tsvetskov [8] as the average of the second-rank Legendre polynomial

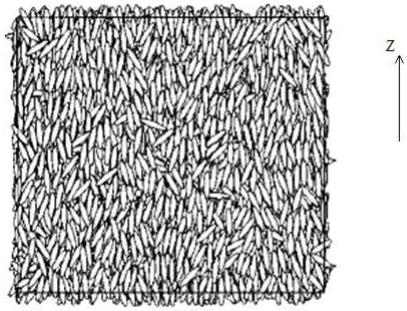

FIGURE 1.2: The molecular organisation in a uniaxial nematic phase composed of ellipsoids of revolution. Reproduced from [3].

$$S = \langle P_2(\cos\beta)\rangle = \langle \frac{3\cos^2\beta - 1}{2}\rangle. \tag{1.2.1}$$

Here, the angular brackets denote the thermodynamic ensemble. This choice for the order parameter also has convenient limiting values. In the isotropic phase since all orientations have equal probability, the molecules are disordered and the value of S is zero. At perfect order, for example, in the crystalline solid, all the symmetry axes of the molecules point in the same direction and so the value of S is 1. In the nematic phase, S depends on the temperature and takes intermediate values between 0 and 1. For typical nematic this order

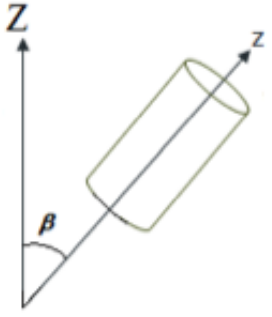

FIGURE 1.3: A cylindrical molecule and its orientation with respect to the laboratory axis.

parameter jumps from 0 to about 0.3 at the isotropic-to-nematic phase transition and continues to increase in the isotropic phase to about 0.8 before crystalised. The discontinuity in the transitional order parameter signifies that the nematic-to-isotropic phase transition is first order.

Theoretical methods for studying thermodynamic phase transition of uniaxial nematic liquid crystals can be broadly divided into two classes: Landau-de Gennes theory and molecular statistical theories [7]. In the Landau-de Gennes theory, the free energy per molecule is postulated to be an expansion of the order parameter with the expansion coefficients that depend on material properties and the temperature, and is usually truncated after fourth or sixth order. By minimising the free energy, the order parameter at a given temperature can be found and hence the transition temperature can be located. Molecular statistical theories clearly have the advantage that molecular shape and symmetry can be taken into account since they are governing factors that determine the phase stability. It seems that the most successful molecular statistical theory is the molecular field theory. This theory was formulated by Maier and Saupe to study a nematic system in which orientational ordering essentially originates from the anisotropic attractive interaction [9, 10]. This approximation is not required in a later reformulation by de Gennes in a variational approach [2]. At the centre of the molecular field theory is the molecular field approximation. The approximation states that each molecule in the system only interacts with a long-range molecular field and ignoring any short-range correlation. The Maier-Saupe theory has successfully described uniaxial nematic-to-isotropic phase transition as well as pretransitional effects and phase behaviour from a qualitative [7] and even semi-quantitative [11] point of view.

Another class of molecular statistical theory for nematic liquid crystal is based on the Onsager theory [2, 7, 10]. In this theory, the hard core short-range repulsive force between rigid rod-like molecules is the only molecular interaction which determines molecular ordering in the nematic phase. The repulsion does not allow the molecule to penetrate each other. The only contribution to the free energy is from the entropy whereas there is no energy contribution [12]. The molecules arrange themselves in order to maximise the entropy, hence minimise the free energy. At low concentration, the elongated molecules tend to pack in a way that their long axes align to form the nematic phase. The Maier-Saupe, reformulated by de Gennes, clearly has an advantage that no assumption need to be made about the nature of the interaction.

1.3 Biaxial Nematics

A weakness of the Maier-Saupe theory is the assumption that constituent molecules are cylindrically symmetric although most nematogenic molecules are intrinsically biaxial as well as flexible. In other words, they are not symmetric around a single axis of rotation. Usually, they give rise to uniaxial phases as a consequence of the rotational disorder around the long molecular axis [13].

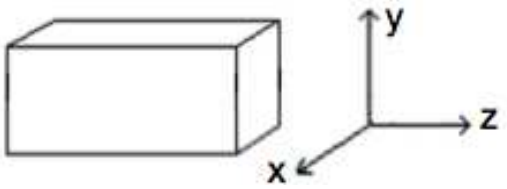

FIGURE 1.4: A D_{2h} molecule with shape of a rectangular parallelepiped.

In 1970, Freiser [14] predicted that a nematic phase which deviates from cylindrical symmetry might be able to form from non-cylindrical molecules. First he considered two identical interacting molecules which are not cylindrical. Their relative orientation is described by three Euler angles. These two molecules then interact via a second-rank effective pair interaction potential which depends on their relative orientation. Freiser then showed that the ground state of this potential corresponds to identical orientation of interacting molecules. He therefore concluded that the ground state of a system of non cylindrical molecules is not uniaxial. In addition, by considering the free energy of the system, he demonstrated that the phase transition from the uniaxial state to the ground state corresponds to the vanishing of the second derivative of the free energy at the minimum. Therefore, the phase transition from the uniaxial state to the ground state is second order. Freiser called this new phase a *biaxial state* to indicate that there are now two axes along which plane polarised light can travel without a change in the state of polarisation. In addition there is a Landau point, that is a second order transition directly from the biaxial nematic phase to the isotropic liquid. Freiser's demonstration of the biaxial nematic phase was further illustrated in his second paper [15].

The simplest example of a biaxial molecule is one whose shape is a rectangular parallelepiped which has D_{2h} symmetry according to Schönflies' notation [16]. In figure 1.4 we show an example of a D_{2h} molecule. The D_{2h} symmetry group has five basic symmetry operations: an identity, a two-fold (principal) axis, two two-fold axes of rotation perpendicular to the principal axis and a horizontal reflection plane perpendicular to the principal axis [16]. If the length is much larger than the breadth and width, then the molecule is calamitic. In the uniaxial phase the longest molecular axis tends to align first. As the system becomes biaxial, the minor axes (width and breadth) tend to align accordingly, giving a phase with physical properties of D_{2h} symmetry. An organisation of a biaxial nematic phase is shown in figure 1.5. A rectangular parallelepiped molecule is discotic if the value of its length is close to one of the minor axis whereas the other minor axis is much smaller. In the uniaxial nematic formed by discotic molecules, the shortest axis tends to align. In the biaxial nematic phase, since all three molecular symmetry axes align, the phase behaviour of calamitic and discotic molecules are the same. This system of parrallelepiped molecules was studied by Straley [17] as an extension of the original Maier-Saupe model. By fixing the molecular length and width and varying its breadth, Straley derived a phase map relating the transition temperature with the molecular breadth which is shown in figure 1.6. In this phase map, a stabilised region of biaxial nematic phase was found. Above this biaxial region is the uniaxial nematic phase which is calamitic (or rod-like) for small values of the molecular breadth and discotic for large values of it. The uniaxial nematic-to-isotropic phase transition is first order, in agreement with experiment whereas

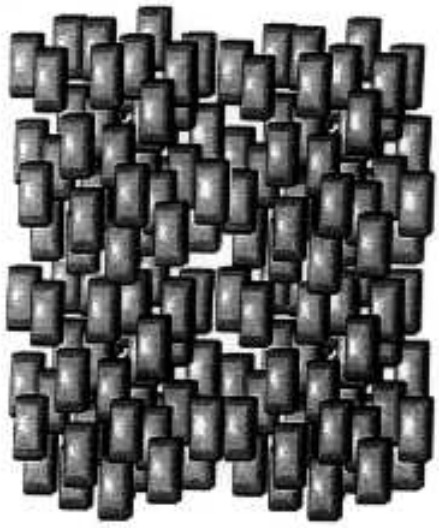

FIGURE 1.5: The molecular organisation in a biaxial nematic phase formed from board-like molecules. Reproduced from [3].

the biaxial nematic-to-uniaxial nematic phase transition is second order, in accord with Freiser's prediction. Moreover, there is a single point of direct second order biaxial nematic-to-isotropic phase transition. This point is called the Landau point and marks the boundary between calamitic and discotic molecules.

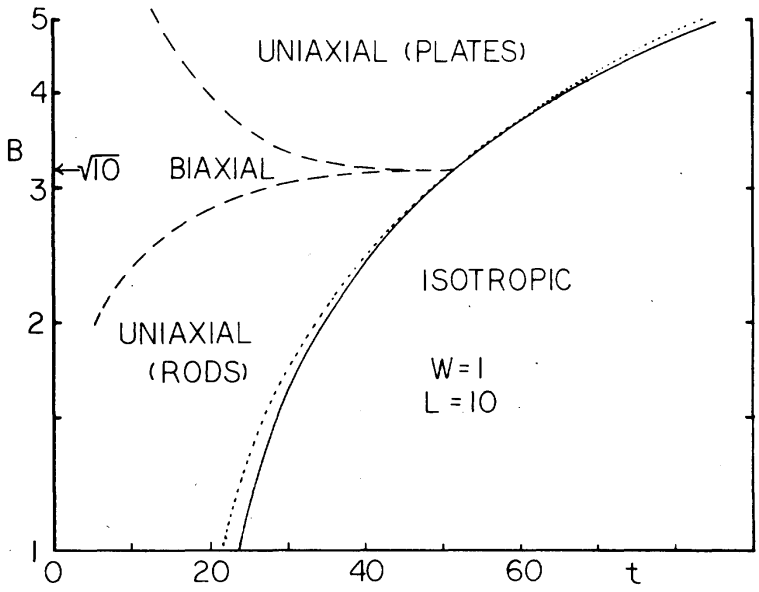

FIGURE 1.6: The phase map for molecules with rectangular parallellepiped shapes as calculated by Straley. Here, B, L and W denote the breadth, length and width of the molecules, respectively while t is the absolute temperature measured in energy units. Reproduced from [17].

Another extension of the Maier-Saupe theory for biaxial nematics was by Boccara, Mejdani and de Seze [18]. They considered a system of asymmetric ellipsoids. An ellipsoid interacts with the molecular field via a potential of mean torque. The deviation of an ellipsoid from cylindrical symmetry is measured by a parameter ϵ. The author then derived a phase map relating the transition temperature with the parameter ϵ. The phase map agreed qualitatively with that by Straley [17]. In their later analogous formulation of the theory, Remler and Haymet [19] also derived another phase map with the same qualitative behaviour. The phase behaviour predicted by Straley [17] was also reproduced using computer simulations [20] and Landau-de Gennes theory [2]. In addition, in an Onsager theory for V-shaped molecules interacting via excluded volume [21], a phase map with the same behaviour was found. In this case the interarm angle represents the molecular biaxiality and the phase behaviour depends on density rather than temperature.

However this behaviour is not unique as demonstrated by recent molecular field calculations and Monte Carlo simulations. These calculations explored different sets of interaction parameters as before [13, 22, 23, 24, 25, 26] and found that the biaxial nematic-to-uniaxial nematic phase transition can be either first or second order. In addition, the Landau point is replaced by a line of either first or second order transition between the biaxial nematic and the isotropic phase. Therefore along both these phase transition lines in the phase map there can be *tricritical points*. A tricritical point is one which marks the boundary between the first and second order transitions. This behaviour was also found in recent Landau-de Gennes calculations [27].

After Freiser's prediction, there has been considerable interests in the creation of compounds,

which might exhibit the biaxial nematic phase. The biaxial nematic phase were later observed in lyotropic [28] and thermotropic polymer liquid crystals [29]. Thermotropic biaxial nematics have also been discovered in a class of supermolecules called *tetrapodes*. A tetrapodal molecule consists of four mesogenic groups connected to a central core through four hydrocarbon chains. The experimental techniques which support the latter discovery are infrared absorbance measurements, together with optical conoscopies and optical textures [30], deuterium nuclear magnetic resonance [31] and dynamic light scattering [32]. However, the low molar mass thermotropic biaxial nematic liquid crystal is much more elusive. One strategy is to design molecules with shape biaxiality. Before 2003, some mesogenic molecules with shape biaxiality such as spoon-like, cross-shaped and bone-shaped [33] were first thought to form biaxial nematic from optical observations but later were proved to be uniaxial nematic by deuterium neulear magnetic resonant experiments [3]. Another strategy was to form mixtures of rod and disc molecules which was also failed since such mixtures are unstable to a phase separation into two regions, one rich in rods and the other rich in discs [34]. To avoid this problem, a rod and a disc units were linked together covalently to form a single molecule. However, systems of such molecules also failed to form a stable biaxial nematic phase [34]. Only in much more recent years does it appear that there is strong evidence of low molar mass thermotropic biaxial nematic. Several systems of V-shaped molecules were claimed to show biaxial nematic phases in which the experimental evidence includes a number of techniques such as X-ray diffraction [35], optical conoscopy, optical textures and deuterium neuclear magnetic resonance [36] as well as Raman scattering [37].

The hunt for thermotropic biaxial nematics is interesting not only because it is an elusive phase of matter that should exist, but also for its potential application in display devices. This is because rotation of the minor directors might be faster than for the major director. This hypothesis has been demonstrated in both electro-optical experiments [38] and molecular dynamic simulations [39] which both show faster response time of the minor directors with respect to the major one. This could produce a display with a fast response and based on in-plane switching [3].

In addition to anisotropy, liquid crystals have other interesting properties when a magnetic field is applied. First, the magnetic field induces some order in the system. Therefore, the isotropic phase becomes the *paranematic* phase with small orientational order. Secondly, recent experimental results by Ostapenko, Wiant, Sprunt, Jákli and Gleeson [40] showed that by applying a magnetic field to a system of biaxial molecules, the transition temperature between the high ordered (nematic) and the low ordered phases (paranematic or isotropic) was increased by one Kelvin. This experimental success is partly attributed to the high magnetic field used in their experiment. The other important factor is the biaxiality of the V-shaped molecules used in their experiment. This latter factor was not explained in details in their paper. In this thesis, we also study the effects of molecular biaxiality on magnetic field induced nematics.

1.4 Biaxial and Uniaxial Smectic A phases

In the last two sections we have discussed nematic liquid crystal phases which have orientational order but no long-range translational order. In contrast, smectic liquid crystals have some long-range translational order. In these phases, the constituent molecules are restricted in two

dimensional layers which are separated with a periodic layer spacing. We are concerned with smectic A phases, in which the long molecular axis is parallel to the normal of the layer on average. In addition, the molecular centres of mass are uniformly distributed in the centres of the layers. In other words, smectic A phases have translational order, together with the orientational order.

In a uniaxial smectic A phase, the symmetry axes of the molecules are ordered parallel to the layer normal. In addition, the molecules rotate freely around the symmetry axis of the phase. The possibility of biaxial ordering in smectic A phases has also been suggested by de Gennes in 1972 [41]. In biaxial *biaxial smectic A* phases, all molecular axes tend to line up. For example, in a biaxial smectic A formed form molecules with D_{2h} symmetry, one symmetry axis of the molecules tends to align along the layer normal whereas the other two symmetry axes align parallel to the layer. Another example is a biaxial smectic A system formed from molecules with C_{2v} symmetry. In this case the molecules are polar along one direction, whereas the other two molecular axes are non-polar. If the polar axes of the molecules point randomly to either side, then the biaxial smectic A phase still has D_{2h} symmetry. If all the polar axis of the molecules tend to point in the same direction, they form a ferroelectric biaxial smectic A phase. If they point to the same direction in one layer but opposite in adjacent layers, then the phase is antiferroelectric. The biaxial smectic A phase, including those with antiferroelectric property has been found in several systems. We review the evidence in chapter 7. In addition, we also review some theoretical models for the biaxial smectic A phase.

1.5 Thesis Plan

Our study concerns with the use of the molecular field approximation for nematogenic and smectogenic systems. One objective is to explain the phenomena observed in experiments and computer simulations of systems made of biaxial molecules. Another is to make numerical predictions about real systems of biaxial molecules. A common problem which occurs throughout chapter 3, 4 and 5 is to locate regions of molecular parameters which can stabilise the biaxial nematic phase. This is with a hope to assist the experimental design of molecules which might be able to form biaxial nematic liquid crystals. In addition, as we already discussed, one chapter is devoted to the study of the magnetic field effects on the uniaxial nematic formed from biaxial molecules. We also extend the molecular field theory to include translational ordering in order to model biaxial and uniaxial smectic A phases.

In Chapter 2 we formaly introduce the molecular field theory according to existing literature. The methods which help to solve the equations from the molecular field theory are also presented. In addition, we give some examples of existing models that are relevant to our discussion in subsequent chapters.

Molecular field theories for biaxial nematics often assume the symmetry of the phase to be D_{2h}. However, in a recent paper by Karahaliou, Vanakaras and Photinos [42], the authors argued that the symmetry of biaxial nematics found in several systems might be C_{2h} instead of D_{2h}. The C_{2h} symmetry group has lower symmetry than D_{2h}. It has only three basic symmetry operations: an identity, a two-fold rotation axis together with a reflection plane perpendicular

to the symmetry axis. In Chapter 3, we develop a molecular field theory for biaxial nematics formed from molecules with C_{2h} symmetry group. The ground state which this system can form is a biaxial nematic phase with C_{2h} point group symmetry, in agreement with the argument in reference [42].

Chapter 4 follows to study a model of V-shaped molecules. The motivation for this work is from experimental evidence. Although there is strong evidence which suggests V-shaped molecules might stabilise biaxial nematic, this evidence seem to disagree with theoretical predictions. One suggestion is that it might be due to a strong tranverse dipole interaction. If this is the case then it would result in a nematic with polarity [43]. By including a tranverse dipolar interaction into the existing molecular field model, we are able to explain this discrepancy between theory and experiment. In addition, we also find that the dipolar interaction indeed stabilises the polar biaxial and polar uniaxial nematic phase.

In Chapter 5 we study nematic liquid crystals formed from liquid crystal dimers. They are mesogenic molecules with two rigid arms conneted by a flexible chain. Due to the flexible chain, a molecule can adopt many conformations, some of which are non cylindrically symmetric. Therefore, we should expect a system of flexible liquid crystal dimers to stabilise a biaxial nematic phase. In addition, the flexibility usually reduce melting temperatue (when a system changes from liquid crystal into solid crystal), thus may increase the chance of forming a biaxial nematic phase. Our model is based on the work by Ferrarini et al. [44] which is a molecular field theory for uniaxial nematic formed from liquid crystal dimers. We extend their model to allow biaxial nematic phase to be formed.

Next, in Chapter 6, we develop a molecular field model which describes a system of biaxial molecules in a uniaxial nematic in the presence of a magnetic field. We discuss three main effects of the applied magnetic field on that system. They have been studied for uniaxial molecules by Wojtowicz and Sheng [45]. We show that the extent of these three effects is different for molecules of different biaxiality in a way that it would be easier to observe these effects for molecules with higher biaxiality. In addition, we make comparisons between our results and those found in the experiments by Ostapenko *et al.* [40].

After that, in chapter 7 we study a model for biaxial smectic A liquid crystals. The existing calculation results for this problem of modelling the biaxial smectic A phase in the literature is still incomplete. One reason is because it involves a large number of order parameters which makes the calculation formidable. An approximation which involves decoupling the order parameters is used in order to reduce this large number of order parameters to make the calculation feasible.

Chapter 2

Background

In this chapter, we aim to explain the mathematical and physical background that is common prerequisite to subsequent chapters. In our work the molecular field theory is used throughout to describe and make predictions about the phase behaviour of nematogenic molecules which can form thermotropic nematic liquid crystals, especially the biaxial phases. In this chapter, we only discuss the molecular field theory for nematic liquid crystals. The molecular field theory in this chapter is extended in chapter 7 to model biaxial smectic A phases. The molecular field theory for nematic liquid crystals is a theory of statistical mechanics which focuses on the difference between isotropic and anisotropic liquids, that is the broken rotational symmetry. This difference is defined by *orientational order parameters* which describe the symmetry of anisotropic phases and molecular ordering. A molecule in the theory is assumed to interact with a mean field generated by all other molecules. There are two major steps in formulating the molecular field theory. The first step is to determine the internal energy of the system. It can be constructed by considering firstly the pair interaction potential which describes the interactions between two neighbouring molecules. This is discussed in section 2.1. To form the internal energy we also need to determine the order parameters of the system which is done using the methods discussed in section 2.2. The second step in formulating the molecular field theory is the application of the molecular field approximation in section 2.3. After introducing the theory for a system with the constituent molecules and the phase of general symmetry, we present some specific examples where the theory has been used to make predictions about nematic behaviour in section 2.4. In section 2.5, we explain the difference between the free energy of a system at equilibrium and a non-equilibrium free energy and a method to determine the non-equilibrium free energy. This method helps us to explain the failure of the classical method of minimising the equilibrium free energy with respect to the order parameters.

2.1 Intermolecular Interactions

The first assumption of the molecular field theory for nematic liquid crystals is about the form of the total internal energy per molecule. The form for this energy may be related to the pair potential which describes the intermolecular interactions between two neighbouring molecules.

The pair potential which we adopt is one which depends on the orientations and symmetries of the two interacting molecules. It seems sensible since nematic phase behaviour is dependent on the rotational ordering of constituent molecules. Consider a general molecule i in three dimensional space which can be asigned a coordinate system (x, y, z) fixed in it. It is a convenient practice to choose these axes to be molecular symmetry axes whenever possible. For a molecule with cylindrical or $D_{\infty h}$ symmetry, the z axis is often taken as the symmetry axis. This $D_{\infty h}$ symmetry point group consists of three basic symmetry operations: an identity, a symmetry axis of infinite rotation and a horizontal reflection plane perpendicular to the symmetry axis [16]. On the other hand, for a molecule with symmetry of a rectangular parallelepiped or D_{2h} symmetry, the (x, y, z) axes are taken along the symmetry axes of the molecule (see figure 1.4) for an example. The molecular orientation with respect to a fixed laboratory axes (X, Y, Z) can be described by three Euler angles $\Omega = (\alpha, \beta, \gamma)$. They are three successive rotations which transform a laboratory into a molecular axis frame. There are several conventions for the Euler angles, of which we use the zyz-convention. In order to transform one coordinate axis system into the other one, there are three successive rotations in the following order. First, a rotation around the z axis by an angle α is taken which gives us the second coordinate system. Then, a rotation by an angle β around the y axis of the second coordinate system is carried out to give the third coordinate system. Finally we need to rotate around the z axis of the third coordinate system by an angle γ to get the new coordinate axis system that we want. In figure 2.1 we

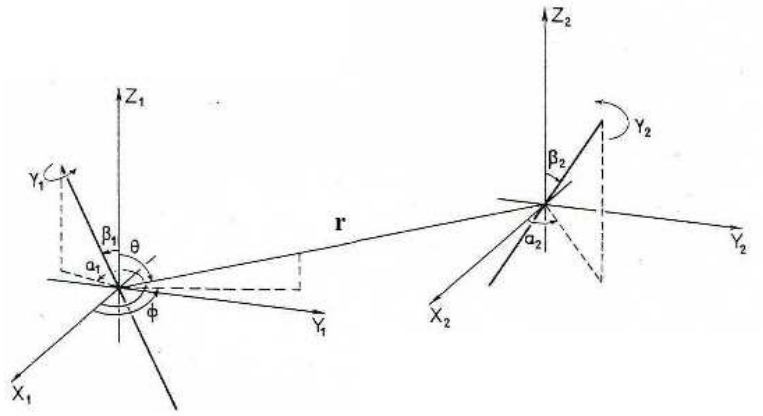

FIGURE 2.1: General definition of angular variables for two molecules which are non-cylindrically symmetric. Reproduced from Stone [46]. For simplicity, the molecules are drawn as lines. Note that here both (X_1, Y_1, Z_1) and (X_2, Y_2, Z_2) denote the laboratory axes. The intermolecular vector connects the centre of molecule 1, with orientation $(\alpha_1, \beta_1, \gamma_1)$, to the centre of molecule 2, with orientation $(\alpha_2, \beta_2, \gamma_2)$. The orientation of the intermolecular vector is defined by two polar angles (θ, ϕ) with respect to the laboratory axes.

give an example of the Euler angles to relate the orientations of the two interacting molecules with a laboratory axis systems $\Omega_1 = (\alpha_1, \beta_1, \gamma_1)$ and $\Omega_2 = (\alpha_2, \beta_2, \gamma_2)$. Now since the pair potential should be a function of molecular orientation, we expand it in a complete set of orthogonal functions spanning the space of the Euler angles. One such set is the Wigner rotation matrices $D^L_{pm}(\Omega)$. A comprehensive account of these functions can be found in reference [47]. The Wigner rotation matrices can also be realised as transformation tensors which are used to transform spherical tensors under the rotation of coordinate axes. A spherical tensor of rank L in a coordinate system T_{Ln} is transformed under the rotation of coordinate axes by the three Euler angles $\Omega = (\alpha, \beta, \gamma)$ into a spherical tensor of the same rank T'_{Lm} in the new coordinate

system according to

$$T'_{Lm} = D^L_{mn}(\Omega) T_{Ln}. \tag{2.1.1}$$

Now we see that the indices m and n represent component indices of Lth-rank tensors T_{Lm}, T_{Ln} and also indices of the transformation matrices $D^L_{mn}(\Omega)$. Therefore $L \geq 0$, $-L \leq m, n \leq L$ and both L, m, n are integers. We give an example of a vector, or first-rank tensor T_{1n} which has three independent components T_{1-1}, T_{10} and T_{11}. This vector is transformed under rotation according to

$$T'_{1m} = D^1_{mn}(\Omega) T_{1n}. \tag{2.1.2}$$

In general, the expressions for the Wigner rotation matrices are given by

$$D^L_{mn}(\Omega) = \mathrm{e}^{-im\alpha} d^L_{mn}(\beta) \mathrm{e}^{-in\gamma}, \tag{2.1.3}$$

where $d^L_{mn}(\beta)$ are the small Wigner rotation matrices. We give some explicit expressions in Appendix A. They can be calculated according to [48]

$$d^L_{mn}(\beta) = \sum_{\chi} C^{Lmn}_{qp} \cos^q(\beta/2) \sin^p(\beta/2). \tag{2.1.4}$$

Here

$$\begin{aligned} q &= 2L + m - n - 2\chi, \\ p &= n - m + 2\chi, \\ C^{Lmn}_{qp} &= (-1)^{\chi} \frac{\{(L+m)!(L-m)!(L+n)!(L-n)!\}^{1/2}}{(L-n-\chi)!(L+m-\chi)!(\chi+n-m)!\chi!}, \end{aligned} \tag{2.1.5}$$

where the sum over χ is taken over such values that the factorials are nonnegative. In addition to the molecular orientation, the pair potential also depends on the intermolecular vector, see figure 2.1. This vector is a two dimensional object and we only need a pair of angles $\omega_r = (\theta\phi)$ to describe it. The intermolecular vector $\mathbf{r}$ joins the centre of the coordinate system (x_1, y_1, z_1) of the first molecule with that of the second one (x_2, y_2, z_2). The angle θ is made up between the intermolecular vector and the laboratory Z axis whereas ϕ is the angle between the projection of the intermolecular vector on the (X, Y) plane and the laboratory X axis. Now the expansion also includes a complete set of orthogonal functions of the angles ω_r. This set can also be formed from the set of Wigner rotation matrices. However, since the intermolecular vector only depends on two Euler angles, the set of orthogonal functions of the angles ω_r can be formed from a subset of Wigner rotation matrices with one index being zero, namely $D^J_{t0}(\omega_r)$. In addition, the pair potential also depends on the separation between interacting molecules. This can be taken into account by multiplying the orientational dependence with the separation dependence terms $u^{mm'nn't}_{LL'J}(r)$. Here the separation is denoted by r and the subscripts as well as superscripts are there to cancel that in the Wigner functions in order for the pair potential to be a scalar. Now we start writing down the form for the pair potential as the product

$$U(\Omega_1, \Omega_2, \omega_r, r) = -\sum u^{mm'nn't}_{LL'J}(r) D^L_{mm'}(\Omega_1) D^{L'}_{nn'}(\Omega_2) D^J_{t0}(\omega_r). \tag{2.1.6}$$

However we must take into account the fact that the pair potential must be invariant under arbitrary rotation of *laboratory* axes. This can be illustrated as follows. The Wigner rotation matrices of a molecule with an orientation (Ω_1) change under rotation by Ω into another orientation (Ω_1') according to

$$D^L_{mn}(\Omega_1') = D^L_{mp}(\Omega) D^L_{pn}(\Omega_1) \tag{2.1.7}$$

Thus the pair potential is changed under rotation by (Ω) to

$$\begin{aligned} U(\Omega_1', \Omega_2', \omega_r, r) \quad &= -\sum u^{mm'nn't}_{LL'J}(r) \left[D^L_{m'p}(\Omega) D^{L'}_{n'p'}(\Omega) D^J_{tP}(\Omega) \right] \\ &\quad \times D^L_{pm}(\Omega_1) D^{L'}_{p'n}(\Omega_2) D^J_{P0}(\omega_r), \end{aligned} \tag{2.1.8}$$

which is different from the original pair potential in general. A correction can be made to allow for the orientational invariance of the pair potential by taking the integrations with respect to the Euler rotation angles Ω over a period of each angle. They are from $-\pi$ to π for β and from 0 to 2π for both α and γ [49].

$$\begin{aligned} U(\Omega_1, \Omega_2, \omega_r, r) = -\sum u^{mm'nn't}_{LL'J}(r) \left[(1/8\pi^2) \int D^L_{m'p}(\Omega) D^{L'}_{n'p'}(\Omega) D^J_{tP}(\Omega) d\Omega \right] \\ \times D^L_{pm}(\Omega_1) D^{L'}_{p'n}(\Omega_2) D^J_{P0}(\omega_r). \end{aligned} \tag{2.1.9}$$

Here the integral element is $d\Omega = \sin\beta d\alpha d\beta d\gamma$. The invariance can be verified as follows. An arbitrary rotation only changes the angles inside the integration. In addition, the Wigner functions are periodic over the integration intervals. Therefore, the pair potential is invariant under the rotation of the laboratory axes. The integral inside the square brackets can be evaluated analytically by the relation

$$\int D^L_{m'p}(\Omega) D^{L'}_{n'p'}(\Omega) {D^J_{-t-P}}^*(\Omega) d\Omega = \frac{8\pi^2}{(-1)^{t-P}} \begin{pmatrix} LL'J \\ m'n't \end{pmatrix} \begin{pmatrix} LL'J \\ pp'P \end{pmatrix}. \tag{2.1.10}$$

where the conjugate of the Wigner rotation matrices is defined by

$${D^J_{-t-P}}^*(\Omega) = (-1)^{P-t} D^J_{tP}(\Omega), \tag{2.1.11}$$

and $\binom{LL'J}{m'n't}$ is the 3j-symbol [47]. These 3j-symbols and the Clebsch-Gordan coefficients which we see later are constants which appear when we multiply Wigner functions and can be used alternatively since they are related [48]. Due to their complex explicit forms we do not include them here but they can be found in the books in reference [47] for the 3j-symbol and reference [50] for the Clebsch-Gordan coefficients. Hence we can rewrite the pair potential in a more compact form

$$U(\Omega_1, \Omega_2, \omega_r, r) = -\sum u^{mn}_{LL'J}(r) S^{mn}_{LL'J}(\Omega_1, \Omega_2, \omega_r). \tag{2.1.12}$$

Now each term in the exansion series of the pair potential is a product of a separation dependence coefficient and an orientational dependence coefficient. Here the separation dependence terms are

$$u^{mn}_{LL'J}(r) = \begin{pmatrix} LL'J \\ m'n't \end{pmatrix} u^{mm'nn't}_{LL'J}(r). \tag{2.1.13}$$

The orientation dependence S-functions are defined by

$$S^{mn}_{LL'J}(\Omega_1,\Omega_2,\omega_r) = (i)^{L-L'-J}\sum \begin{pmatrix} LL'J \\ pp'P \end{pmatrix} D^L_{pm}(\Omega_1)D^{L'}_{p'n}(\Omega_2)D^J_{P0}(\omega_r). \tag{2.1.14}$$

Here the phase factor $(i)^{L-L'-J}$ is added to make $S^{LL'J}_{mn}$ invariant under exchange of the roles of the two molecules [46].

Since the intermolecular vector orientation or a function of it does not occur explicitly in the molecular field theory [51] we take the average over all orientations of the intermolecular vector to get the reduced form of the S functions,

$$S^{mn}_{LL0}(\Omega_1,\Omega_2) = \sum \begin{pmatrix} LL0 \\ p-p0 \end{pmatrix} D^L_{pm}(\Omega_1)D^L_{-pn}(\Omega_2). \tag{2.1.15}$$

The pair potential can now be written as

$$U(\Omega_1,\Omega_2,r) = -\sum (-1)^{L-p} u_{Lmn}(r) D^L_{pm}(\Omega_1)D^L_{-pn}(\Omega_2). \tag{2.1.16}$$

Here the magnitude of the 3j-symbol, $\binom{LL0}{p-p0}$, of $1/(2L+1)^{1/2}$ is used to scale the intermolecular coefficients, $u_{Lmn}(r) = 1/(2L+1)^{1/2} u^{mn}_{LL0}(r)$.

Now we also want the pair potential in (2.1.16) to be invariant under arbitrary rotations of molecular axes. This property of the pair potential defines the structure of the supertensor u_{Lmn}. The Wigner rotation matrices are transformed under the rotation of molecular axes by an angle (Ω) according to

$$\begin{aligned} D^L_{pq}(\Omega'_1) &= \sum_m D^L_{pm}(\Omega_1)D^L_{mq}(\Omega), \\ D^L_{-pq'}(\Omega'_2) &= \sum_n D^L_{-pn}(\Omega_2)D^L_{nq'}(\Omega). \end{aligned} \tag{2.1.17}$$

Hence the pair potential is transformed according to

$$U(\Omega'_1,\Omega'_2) = -\sum (-1)^{L-p} u'_{Lqq'} D^L_{pq}(\Omega'_1)D^L_{-pq'}(\Omega'_2). \tag{2.1.18}$$

Here u_{Lmn} is transformed into $u'_{Lqq'}$. We also omit the separation dependence for simplicity. Now, the original pair potential (2.1.16) can be rewritten as

$$U(\Omega_1,\Omega_2) = -\sum (-1)^{L-p} u_{Lmn}\delta_{mm'}\delta_{nn'} D^L_{pm'}(\Omega_1)D^L_{-pn'}(\Omega_2). \tag{2.1.19}$$

We can expand the Kronecker deltas $\delta_{mm'}$ and $\delta_{nn'}$ by using the *unitary* property of the Wigner functions

$$\begin{aligned} \sum_q D^L_{mq}(\Omega)^* D^L_{m'q}(\Omega) &= \delta_{mm'}, \\ \sum_{q'} D^L_{nq'}(\Omega)^* D^L_{n'q'}(\Omega) &= \delta_{nn'}. \end{aligned} \tag{2.1.20}$$

Therefore,

$$U(\Omega_1,\Omega_2) = -\sum(-1)^{L-p}\left\{\sum_{qq'} D^L_{mq}(\Omega)^* D^L_{nq'}(\Omega)^* u_{Lmn}\right\} D^L_{pq}(\Omega'_1) D^L_{-pq'}(\Omega'_2). \quad (2.1.21)$$

Since the pair potential is invariant under rotations of the molecular axes, the right hand side of equations (2.1.16) and (2.1.21) must be equal. This gives us the expressions of the intermolecular coefficients under the rotation of molecular axes

$$u'_{Lqq'} = \sum_{mn} D^L_{mq}(\Omega)^* D^L_{nq'}(\Omega)^* u_{Lmn}. \quad (2.1.22)$$

Finally, we need to consider how individual molecular symmetry affect the pair potential. It is because a symmetry transformation of the molecule should also leave the value of the pair potential invariant. This is reflected in the intermolecular coefficients u_{Lmn}. A coefficient u_{Lmn} transforms as a tensor of Lth-rank for molecules 1 (with orientation Ω_1) with respect to the first subscript and as a tensor of the same rank for molecules 2 (with orientation Ω_2) with respect to the second subscript. The effect of molecular symmetry on the intermolecular coefficients u_{Lmn} for some symmetry operations is given in table 2.1.

Symmetry Property	Consequence
A. Of the system as a whole	
1. Molecules identical	$u_{Lmn} = u_{Lnm}$
2. Both molecules linear	L even
3. Both molecules have inversion centre	L even
B. Of molecule 1	
(similar rules hold for molecule 2)	
1. Inversion centre I	L even
2. $C_2^{(z)}$ axis	m even
3. σ_h reflection	$m + L$ even
4. Other C_2 rotation	
(a) $C_2^{(x)}$	$u_{Lmn} = (-1)^L u_{L-mn}$
(b) $C_2^{(y)}$	$u_{Lmn} = (-1)^{L+m} u_{L-mn}$
5. σ_v reflection	
(a) σ_v^{xz}	$u_{Lmn} = (-1)^m u_{L-mn}$
(b) σ_v^{yz}	$u_{Lmn} = u_{L-mn}$

TABLE 2.1: Effect of molecular symmetry operations on the the energy expansion (2.1.16) by Stone [46]. The notation is as follows. I stands for the inversion. σ_v^{xy} for a symmetry plane perpendicular to z; $C_2^{(z)}$ for a pi rotation about z.

We note that the quantiy u_{Lmn} is tensorial in the sense that its components transform under rotation with respect to molecular axes. In general, there are three types of rotations. In the first type, the molecular axes are kept fixed with respect to the laboratory axes whereas the molecule is rotated by Ω with respect to the molecular axes, the intermolecular tensor u_{Lmn} transforms according to equation (2.1.22). In the second type of rotation, the molecule is kept fixed but the molecular axes are rotated by Ω with respect to the laboratory axes, the intermolecular

supertensor u_{Lmn} transforms according to

$$u'_{Lqq'} = \sum_{mn} D^L_{mq}(\Omega) D^L_{nq'}(\Omega) u_{Lmn}. \tag{2.1.23}$$

In the third type of rotation, both the molecule and the molecular axes are rotated with respect to the laboratory axes but the relative orientation between them stay fixed. In this case the intermolecular tensor u_{Lmn} does not transform and and its components are constant. The last type of rotation corresponds to the calculation when we take the ensemble average of an angular-dependent quantity, such as an order parameter which we will see later. In this case, the relative orientation between a molecule and its molecular axes is fixed, the constant components of the intermolecular supertensors, u_{Lmn}, can be considered as coefficients which scale the interaction strength.

2.2 Orientational Distribution Functions and Order Parameters

Nematic liquid crystals are characterised by their long-range orientational order and their lack of a long-range translational order. Hence they are described by orientational order parameters. For nematic liquid crystals, we only refer to order parameters as being orientational. Many essential results regarding order parameters have been discussed in details by Zannoni [48] and are repeated in this section. First we consider a molecule with the orientation (Ω) with respect to laboratory frame. The ordering of the molecules in the phase is reflected in the probability to find a molecule in a small orientational volume $f(\Omega)d\Omega$. The function $f(\Omega)$ is called the single particle orientational distribution function. This function belongs to the totally symmetric representation of the symmetry group of the phase. In other words, the symmetry of this function represents the symmetry of the phase. Therefore, an ensemble average of a single particle orientational function $A(\Omega)$ can be written in terms of $f(\Omega)$ as

$$\langle A \rangle = \int_V f(\Omega) A(\Omega) d\Omega. \tag{2.2.1}$$

Since the only information we know about the orientational distribution function is that its variables are the Euler angles $(\Omega) = (\alpha, \beta, \gamma)$, we expand it in a basis of Wigner rotation matrices, a set of complete orthogonal functions spanning the space of the Euler angles

$$f(\Omega) = \sum f_{Lmn} D^L_{mn}(\Omega). \tag{2.2.2}$$

Now multiplying both sides by ${D^L_{mn}}^*(\Omega)$ and integrating over the angles we find

$$f_{Lmn} = \frac{2L+1}{8\pi^2} \langle D^L_{mn} \rangle^*. \tag{2.2.3}$$

Here, the scalar comes from the orthogonality property of the Wigner functions

$$\int D^{L*}_{mn}(\Omega) D^{L'}_{m'n'}(\Omega) d\Omega = \frac{8\pi^2}{2L+1} \delta_{mm'} \delta_{nn'} \delta_{LL'}, \tag{2.2.4}$$

where $\delta_{mm'}$, $\delta_{nn'}$ and $\delta_{LL'}$ are the Kronecker delta functions. In addition, the quantities

$$\langle D^L_{mn} \rangle = \int D^L_{mn}(\Omega) f(\Omega) d\Omega \tag{2.2.5}$$

are the ensemble averages of the Wigner rotation functions. The phase transition of liquid crystals should be described in terms of modifications in the orientational distribution functions. Clearly the parameters which modify this function are the ensemble averages $\langle D^L_{mn} \rangle$. Hence it is natural to define these functions as the order parameters. This choice is also a convenient choice since in our definition for the Euler angles, the Wigner functions $D^L_{mn}(\Omega)$ transform in the laboratory axes as tensors of the Lth-rank with respect to the first subscript and in the molecular axes as tensors of the same rank with respect to the second subscript. Moreover, the orientational distribution function reflects the symmetry of the phase and the molecules. In consequence, we can impose constraints on the order parameters according to molecular and phase symmetry. The effects of molecular and phase symmetry operations on the Wigner rotation matrices are given in Tables 2.2 and 2.3, respectively.

Operator O_M	$O_M \langle D^L_{mn} \rangle$
$I = S_2$	$(-1)^L D^L_{mn}$
$\sigma(xy)$	$(-1)^{L+n} D^L_{mn}$
$\sigma(xz)$	$(-1)^n D^L_{m-n}$
$\sigma(yz)$	D^L_{m-n}
$C_2(z)$	$(-1)^n D^L_{mn}$
$C_2(x)$	$(-1)^L D^L_{m-n}$
$C_2(y)$	$(-1)^{L-n} D^L_{m-n}$

TABLE 2.2: Effect of molecular symmetry operations O_M on the Wigner rotation matrices. The notation is as follows. I stands for the inversion. $\sigma(xy)$ for a symmetry plane perpendicular to z; $C_2(z)$ for a π rotation about z; S_2 for a π roto-reflection where z is the main symmetry axis of the molecule.

Operator O_L	$O_L \langle D^L_{mn} \rangle$
$I = S_2$	$(-1)^L D^L_{mn}$
$\sigma(XY)$	$(-1)^{L+m} D^L_{mn}$
$\sigma(XZ)$	$(-1)^m D^L_{-mn}$
$\sigma(YZ)$	D^L_{-mn}
$C_2(Z)$	$(-1)^m D^L_{mn}$
$C_2(X)$	$(-1)^L D^L_{-mn}$
$C_2(Y)$	$(-1)^{L-m} D^L_{-mn}$

TABLE 2.3: Effect of phase symmetry operations O_L on the Wigner rotation matrices. The notation is as follows. I stands for the inversion. $\sigma(XY)$ for a symmetry plane perpendicular to Z; $C_2(Z)$ for a π rotation about Z; S_2 for a π roto-reflection where Z is the main symmetry axis of the phase.

2.3 Molecular Field Theory

In this section, we derive a thermodynamic theory for nematic liquid crystals with the aim to describe the transitions between the nematic and the isotropic phase and also between different nematic phases. Hence the theory only focuses on the orientational order of the system. A convincing way to derive the theory without making any assumption about the type of molecular interactions is the variational approach by de Gennes in his classic book [2] for cylindrical molecules in uniaxial nematics. This approach can be extended in order to account for biaxial nematics formed from identical constituent molecules of any symmetry. The general procedure has been described in reference [51] and is discussed in details in this section. In the variational approach, the first ingredient we need to construct is the total internal energy per molecule. We recall from section 2.1 that the pair potential describing the interactions between two neighbouring molecules has the form

$$U(\Omega_1, \Omega_2, r) = -\sum (-1)^{L-p} u_{Lmn}(r) D^L_{pm}(\Omega_1) D^L_{-pn}(\Omega_2). \tag{2.3.1}$$

The first assumption we need to make is that the interacting molecules are rigid. This is reasonable for molecules that consist of a single mesogenic group since in this case the flexible chain does not contribute to the ordering in the nematic phase. In the molecular field, a molecule is assumed to interact only with a long-range internal field generated by all other molecules and is independent of any short-range correlations. Quantitative improvement of the theory can be achieved by including short-range correlation effects by using the density functional theory [10] or the two-site cluster theory [52]. Nevertheless, we ignore short-range correlations in this thesis in order to ease computation. In addition, ignoring short-range correlation effects usually still leads to qualitative agreements between theory and Monte Carlo simulation. Therefore we assume the internal energy per molecule to have a form that is analogous to the pair potential

$$\langle U \rangle = -(1/2) \sum (-1)^{L-p} u_{Lmn} \langle D^L_{pm} \rangle \langle D^L_{-pn} \rangle. \tag{2.3.2}$$

This is a quadratic function of the order parameters in equation (2.2.5). The next step is to find the entropy per molecule. This can be derived by considering the total entropy of N molecules [11]

$$S_{\sum} = -k_B \int F_N(\Omega_1, \Omega_2, ..., \Omega_N) \ln F_N(\Omega_1, \Omega_2, ..., \Omega_N) d\Omega_1 d\Omega_2 ... d\Omega_N, \tag{2.3.3}$$

where $F_N(\Omega_1, \Omega_2, ..., \Omega_N)$ is the N body distribution function and k_B denotes the Boltzmann constant. In the molecular field approximation we assume that the behaviour of a molecule depends on the long-range orientational ordering which dominates short-range correlation. In consequence, there is no correlation between individual molecule. Hence we may write the N particle distribution function $F_N(\Omega_1, \Omega_2, ..., \Omega_N)$ as the product of single particle distribution functions [11]

$$F_N(\Omega_1, \Omega_2, ..., \Omega_N) = \prod_{n=1}^{N} f(\Omega_n). \tag{2.3.4}$$

Therefore, the total entropy can be written as the sum of the single particle orientational entropies

$$S_{\sum} = \sum_n S_n, \tag{2.3.5}$$

where

$$S_n = -k_B \int_{\Omega_n} f(\Omega_n) \ln f(\Omega_n) d\Omega_n . \prod_{m \neq n} \int_{\Omega_m} f(\Omega_m) d\Omega_m . \tag{2.3.6}$$

Since the integrations of the distribution functions are equal to unity, all identical molecules have the same single particle orientational distribution which is independent of the behaviour of any other molecule. Therefore, the total entropy per molecule is

$$S = -k_B \int f(\Omega) \ln f(\Omega) d\Omega. \tag{2.3.7}$$

Now we need to find an explicit form for the orientational distribution function in equilibrium. When a thermodynamic system is in the equilibrium state, the *availability* function F has to be minimised [53]. This function is defined such as any change in F depends on changes in the thermodynamic variables

$$dF = dU + p_0 dV - T_0 dS, \tag{2.3.8}$$

where U, V and S are the internal energy, volume and entropy of our system; p_0 and T_0 denote the pressure and temperature of the surroundings which are in contact with our system. In many experiments, the thermodynamic variables which are easier to fix are temperature T and pressure P. In that case the availability function F is equal to the Gibbs free energy G such that

$$dG = dU + p_0 dV - T_0 dS. \tag{2.3.9}$$

Actually, experiments of some liquid crystal systems revealed that the volume change at the phase transition is small, about 0.5 per cent [8]. When this volume change is taken into account to calculate the order parameter at the phase transition using the Gibbs free energy, the order parameter only differs by 1-2 per cent in comparison with the assumption that the volume is constant at the phase transition [8]. Therefore it is often assumed that the thermodynamic variables which are constant at the phase transition are temperature and volume. In this case the availability F is equal to the Helmholtz free energy whose explicit form is simpler than the Gibbs free energy. In effect the Helmholtz free energy is adequate to be used as the thermodynamic potential of the system. This is defined as

$$A = \langle U \rangle - TS, \tag{2.3.10}$$

where T is the absolute temperature. The single particle orientational distribution function at equilibrium can be found by minimising the free energy difference between the nematic and the isotropic phases, subject to two constraints. The first one is that the order parameters are the averages of the Wigner rotation matrices given in equation (2.2.5) and the second one is that the orientational distribution function is normalised

$$\int f(\Omega) d\Omega = 1. \tag{2.3.11}$$

Minimisation of the free energy in equation (2.3.10) with those constraints gives

$$\delta A + \eta \int \delta f(\Omega) d\Omega = 0. \tag{2.3.12}$$

where η denotes the Lagrange multiplier. Taking the variation of the internal energy and the entropy in (2.3.10) with respect to $f(\Omega)$ we get

$$\int \left(-\sum (-1)^{L-p} u_{Lmn} \langle D^L_{pm} \rangle D^L_{-pn}(\Omega) + k_B T + k_B T \ln f(\Omega) + \eta \right) \delta f d\Omega = 0, \tag{2.3.13}$$

which is satisfied for all δf if and only if the integrand vanishes. The orientational distribution function can then be written as

$$f(\Omega) = \frac{\exp\left(\frac{1}{k_B T} \sum u_{Lmn} (-1)^{L-p} \langle D^L_{pm} \rangle D^L_{-pn}(\Omega) \right)}{\exp(1 + \frac{\eta}{k_B T})}. \tag{2.3.14}$$

In order for $f(\Omega)$ to be normalised the denominator has to be the orientational partition function

$$Q = \int_\Omega \exp\left(\frac{1}{k_B T} \sum (-1)^{L-p} u_{Lmn} \langle D^L_{pm} \rangle D^L_{-pn}(\Omega) \right) d\Omega. \tag{2.3.15}$$

Here, the integral element is $d\Omega = \sin\beta d\alpha d\beta d\gamma$ and the integrations are taken from $-\pi$ to π for β and from 0 to 2π for α and γ. From the orientational distribution function, we can find the potential of mean torque $U(\Omega)$, a function which describe the interactions of a molecule at an orientation Ω with the molecular field. From thermal physics, their relation is

$$f(\Omega) = Q^{-1} \exp\left(U(\Omega)/k_B T \right). \tag{2.3.16}$$

Therefore the potential of mean torque is

$$U(\Omega) = -\sum_{L,m,n,p} (-1)^{L-p} u_{Lmn} \langle D^L_{pm} \rangle D^L_{-pn}(\Omega). \tag{2.3.17}$$

The equations of the form as equation (2.2.5) with the potential of mean torque defined as equation (2.3.17) are called the *self-consistency* equations. Now we have derived the thermodynamic equations for nematic states which seem to be adequate to describe any nematic system. However, the free energy defined in (2.3.10) is not very useful to do calculations due to the complex form of the entropy. This can be simplified by substituting the distribution function with the potential of mean torque defined in equation (2.3.17) into equation (2.3.7). This gives

$$S = -k_B \ln Q + \frac{1}{T} \sum_{L,m,n,p} (-1)^{L-p} u_{Lmn} \langle D^L_{pm} \rangle \langle D^L_{-pn} \rangle. \tag{2.3.18}$$

Thus, the free energy can be written in a more convenient form

$$A^* = -\ln Q + \frac{1}{2 k_B T} \sum_{L,m,n,p} (-1)^{L-p} u_{Lmn} \langle D^L_{pm} \rangle \langle D^L_{-pn} \rangle. \tag{2.3.19}$$

where A^* is the scaled free energy $A^* = A/k_BT$. This form can also be realised in another way, by noticing that the first term is the standard formula which relates the Helmholtz free energy to the partition function and the second term is the molecular field correction since the number of molecules is counted twice in the partition function.

2.4 Examples of Uniaxial and Biaxial Nematic Liquid Crystals

2.4.1 Cylindrical Molecules in Uniaxial Nematics

Here we consider some simple examples of nematic liquid crystals before embarking on studying more complex models in subsequent subsections. Not only this is the simplest example, it is also of historical interests since long before a first prediction of biaxial nematic was made, nematic liquid crystals have been known to be uniaxial with cylindrically symmetric physical properties. This is why early theories assumed constituent molecules to be cylindrically symmetric, even though they are not. In order to describe their phase behaviour we need to write down the molecular field theory and then carry out numerical calculations. Both the phase and its constituent molecules have $D_{\infty h}$ symmetry. The non-zero interaction coefficients and order parameters can be found from Tables 2.1, 2.2 and 2.3. By convention, we take the molecular z axis to be the molecular symmetry axis and we take the phase Z axis to be the phase symmetry axis. The only non-zero interaction coefficients are u_{L00} and the non zero order parameters are $\langle D^L_{00}\rangle$. Therefore the potential of mean torque is

$$U(\Omega) = -u_{L00}\langle D^L_{00}\rangle D^L_{00}(\Omega). \tag{2.4.1}$$

Now the Wigner rotation matrices $D^L_{00}(\Omega)$ are the same as the Legendre polynomials $P_L(\beta)$, a complete set of orthogonal functions spanning the basis of the angle β. Thus, the potential of mean torque and hence the distribution functions are functions of β

$$U(\beta) = -u_L\langle P_L\rangle P_L(\beta). \tag{2.4.2}$$

This can be verified physically as follows. Since both the phase and the molecules are cylindrically symmetric, only one angle is required to describe molecular orientation. The the potential of mean torque can be simplified further by noting that experimental evidence revealed that the second-rank order parameter in the system is dominant [51]. Quantitative improvement of the numerical preditions compared to experimental results can be made by including fourth-rank interactions into the potential of mean torque [11]. However, for simplicity we take $L = 2$. The potential of mean toque is then

$$U(\beta) = -u_2\langle P_2\rangle P_2(\beta). \tag{2.4.3}$$

The system now has only one second-rank order parameter

$$S = \langle P_2\rangle = \int \left((3\cos^2\beta - 1)/2\right) f(\beta) d\cos\beta. \tag{2.4.4}$$

Here we note that S is used to denote the uniaxial order parameter in order to conform with the literature. In this section, since we do not discuss the entropy, the notation S should not be confused with the entropy. In consequence, the scaled free energy only depends on the order parameter S

$$A^* = -\ln Q + (T^*)^{-1} S^2, \tag{2.4.5}$$

where $T^* = k_B T / u_{200}$. The behaviour of this system can be found by solving the equation for the order parameter S in equation (2.4.4) graphically. The results are shown as the temperature dependence of the order paramter S and the corresponding scaled free energy difference between the nematic and the isotropic phase in figure 2.2. First we note that the order parameter starts to

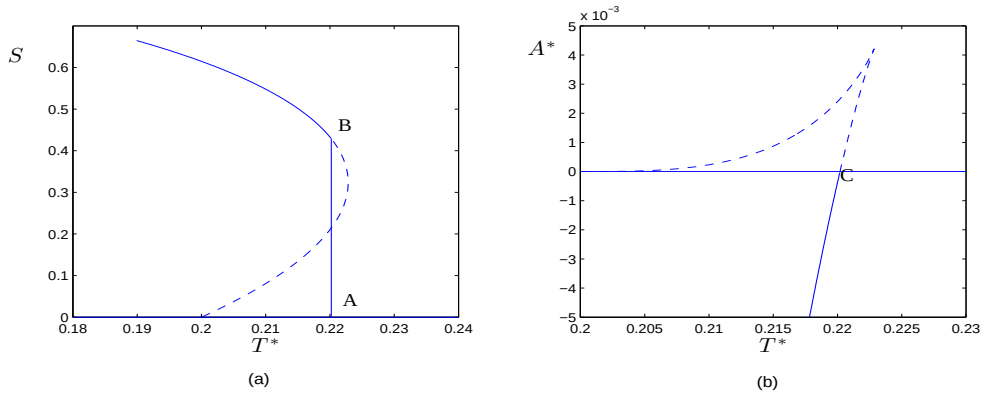

FIGURE 2.2: The dependence of (a) the uniaxial order parameters and (b) the scaled free energy on the scaled temperature for uniaxial molecules in uniaxial nematics.

increase continuously from zero at the scaled temperature of about 0.2. This point is called the *bifurcation point* which can also be found analytically. Since S is small, we can expand the order parameter as a Taylor series upto and including the first order term which does indeed gives $T^* = 0.2$. However, this point is not where the actual phase transition takes place. This is because the part of the order parameter curve from the bifurcation point to the point B corresponds to the positive part of the free energy difference. This means for these parts of the curves, the isotropic phase is more stable than the uniaxial nematic phase. In fact the uniaxial nematic-to-isotropic phase transition happens at point A in the order parameter plot. At this point, the order parameter of the system jumps to about 0.4 at point B and then keep on going to increase. The temperature of the system at points A and B corresponds to that of the free energy at point C. This is where the free energy difference starts to decrease and becomes negative and now the uniaxial nematic phase is more stable than the isotropic phase. The discontinuity in the order parameter and the gradient of the free energy indicates that the transition is first order.

2.4.2 Uniaxial and Biaxial Nematics formed from Orthogonal Parallelepiped Molecules

Uniaxial nematic liquid crystals are formed by the tendency of the alignment of one axis of constituent molecules. If the other axes also have the tendency to align, the rotational symmetry of the cylindrically symmetric phase may be broken and we have a biaxial nematic phase. The lowest symmetry to be broken from cylindrical one which can be described by second-rank

order parameters is the D_{2h} point group symmetry. In this section, we assume that the lowest ordered phase and the constituent molecules have D_{2h} point group symmetry. In order to develop the molecular field theory for this system, first we need to write down the potential of mean torque. Given the success of formulating the molecular field theory for cylindrical molecules in uniaxial nematic by considering only second-rank interactions, we assume that second-rank interactions also make dominant contributions towards the phase behaviour of molecules with D_{2h} symmetry. The number of second-rank order parameters can be restricted to only four due to the molecular and phase symmetry using Tables 2.2 and 2.3

$$\begin{aligned}
&\langle D^2_{00}\rangle,\\
&\langle D^2_{02}\rangle = \langle D^2_{0-2}\rangle,\\
&\langle D^2_{20}\rangle = \langle D^2_{-20}\rangle,\\
&\langle D^2_{22}\rangle = \langle D^2_{2-2}\rangle = \langle D^2_{-22}\rangle = \langle D^2_{-2-2}\rangle.
\end{aligned} \tag{2.4.6}$$

Actually the Wigner functions used to define the order parameters occur in the potential of mean torque as composite functions

$$\begin{aligned}
R_{00}(\Omega) &= D^2_{00}(\Omega),\\
R_{02}(\Omega) &= \left(D^2_{02}(\Omega) + D^2_{0-2}(\Omega)\right)/2,\\
R_{20}(\Omega) &= \left(D^2_{20}(\Omega) + D^2_{-20}(\Omega)\right)/2,\\
R_{22}(\Omega) &= \left(D^2_{22}(\Omega) + D^2_{-22}(\Omega) + D^2_{2-2}(\Omega) + D^2_{-2-2}(\Omega)\right)/2.
\end{aligned} \tag{2.4.7}$$

These functions are also called symmetry adapted basis functions [54]. It is because they are the only combinations whose thermodynamic averages do not vanish. Their explicit forms are

$$\begin{aligned}
R_{00}(\Omega) &= \left(3\cos^2\beta - 1\right)/2,\\
R_{02}(\Omega) &= \sqrt{3/8}\sin^2\beta\cos2\gamma,\\
R_{20}(\Omega) &= \sqrt{3/8}\sin^2\beta\cos2\alpha,\\
R_{22}(\Omega) &= (1/2)\left(1+\cos^2\beta\right)\cos2\gamma\cos2\alpha - \cos\beta\sin2\gamma\sin2\alpha.
\end{aligned} \tag{2.4.8}$$

The order parameters are then defined in terms of these composite functions, they are

$$S = \langle R_{00}\rangle, D = \langle R_{02}\rangle, P = \langle R_{20}\rangle, C = \langle R_{22}\rangle. \tag{2.4.9}$$

It can be seen from their explicit forms that the values of the order parameters are constrained [55]

$$\begin{aligned}
&-(1/2) \le \langle R_{00}\rangle \le 1,\\
&-\left(1/\sqrt{6}\right)(1-\langle R_{00}\rangle) \le \langle R_{02}\rangle \le \left(1/\sqrt{6}\right)(1-\langle R_{00}\rangle),\\
&-\left(1/\sqrt{6}\right)(1-\langle R_{00}\rangle) \le \langle R_{20}\rangle \le \left(1/\sqrt{6}\right)(1-\langle R_{00}\rangle),\\
&-1 \le \langle R_{22}\rangle \le 1.
\end{aligned} \tag{2.4.10}$$

It often assists our understanding to express the order parameters as Cartesian rather than spherical tensors. This can be achieved by defining the ordering supertensor

$$S_{ab}^{AB} = \langle 3l_{Aa}l_{Bb} - \delta_{AB}\delta_{ab}\rangle/2, \tag{2.4.11}$$

where the superscripts A and B can be any of the principal axes X, Y or Z of the phase and the subscripts a and b can be any principal axis x, y or z of the molecules; l_{Aa} denotes the cosine of the angle between axes A and a while δ_{AB} denotes the Kronecker delta. The four order parameters, expressed in Cartesian form are [26]

$$\begin{aligned}
S &= \langle R_{00}\rangle = S_{zz}^{ZZ}, \\
D &= \langle R_{02}\rangle = \frac{S_{xx}^{ZZ} - S_{yy}^{ZZ}}{\sqrt{6}}, \\
P &= \langle R_{20}\rangle = \frac{S_{zz}^{XX} - S_{zz}^{YY}}{\sqrt{6}}, \\
C &= \langle R_{22}\rangle = \frac{(S_{xx}^{XX} - S_{yy}^{XX}) - (S_{xx}^{YY} - S_{yy}^{YY})}{3}.
\end{aligned} \tag{2.4.12}$$

The first order parameter S is that introduced by Tsvetkov. The role of the order parameters can be seen from their relations to the Saupe ordering matrix elements. S and D measure the ordering of the major and minor molecular axes with respect to the major phase axis whereas P and C measure the ordering of the major and minor molecular axes with respect to the minor axes of the phase. Therefore, a uniaxial phase formed from cylindrical molecules can only have one non zero order parameter S. If the uniaxial phase is formed from non-cylindrical molecules there are two order parameters S and D. If the biaxial phase is formed from cylindrical molecules there are also two order parameters S and P. All four order parameters are non-zero in a biaxial nematic phase formed from non-cylindrical molecules.

We have constructed the molecular field theory using the spherical tensor notation. It is because of our familiarity with this notation. In addtion, spherical tensors are easier to transform and manipulate. However, other authors have constructed the theory using Cartesian tensors [13]. Here, we give a method of constructing the order parameters using Cartesian tensors. Let (x, y, z) be three symmetry axes of a molecule of D_{2h} symmetry. The interaction of a molecule with another can be represented by two second-rank, symmetric, tracless tensors

$$\mathbf{q} = \mathbf{z}\otimes\mathbf{z} - (1/3)\mathbf{I}, \tag{2.4.13}$$

and

$$\mathbf{b} = \mathbf{x}\otimes\mathbf{x} - \mathbf{y}\otimes\mathbf{y}. \tag{2.4.14}$$

The tensors $\mathbf{q}$ and $\mathbf{b}$ form an orthogonal basis of a vector space. In addition, we take (X, Y, Z) to be three symmetry axes of the phase which has D_{2h} symmetry. A phase can also be represented by two second-rank, symmetric, tracless tensors

$$\mathbf{e}_q = \mathbf{Z}\otimes\mathbf{Z} - (1/3)\mathbf{I}, \tag{2.4.15}$$

and

$$\mathbf{e}_b = \mathbf{X} \otimes \mathbf{X} - \mathbf{Y} \otimes \mathbf{Y}. \tag{2.4.16}$$

The representations of the tensors $\mathbf{q}$ and $\mathbf{b}$ in the phase axes are given by

$$\mathbf{q}_p = (\mathbf{q} : \mathbf{e}_q)\mathbf{e}_q + (\mathbf{q} : \mathbf{e}_b)\mathbf{e}_b, \tag{2.4.17}$$

and

$$\mathbf{b}_p = (\mathbf{b} : \mathbf{e}_q)\mathbf{e}_q + (\mathbf{b} : \mathbf{e}_b)\mathbf{e}_b. \tag{2.4.18}$$

The phase symmetry can be represented by two macroscopic tensors. They are thermodynamic averages of the molecular tensors

$$\mathbf{Q} = \langle \mathbf{q} \rangle, \tag{2.4.19}$$

and

$$\mathbf{B} = \langle \mathbf{b} \rangle. \tag{2.4.20}$$

The tensors $\mathbf{Q}$ and $\mathbf{B}$ are order parameter tensors. Their representations in the phase axes are given by

$$\mathbf{Q} = S\mathbf{e}_q + P\mathbf{e}_b, \tag{2.4.21}$$

and

$$\mathbf{B} = D\mathbf{e}_q + C\mathbf{e}_b. \tag{2.4.22}$$

Hence, the order parameter tensors $\mathbf{Q}$ and $\mathbf{B}$ depend on four scalar order parameters

$$(2/3)S = \langle \mathbf{q} : \mathbf{e}_q \rangle, \tag{2.4.23}$$

$$\sqrt{8/3}D = \langle \mathbf{b} : \mathbf{e}_q \rangle, \tag{2.4.24}$$

$$\sqrt{8/3}P = \langle \mathbf{q} : \mathbf{e}_b \rangle, \tag{2.4.25}$$

$$2C = \langle \mathbf{b} : \mathbf{e}_b \rangle. \tag{2.4.26}$$

Using the identity $(\mathbf{u} \otimes \mathbf{v}) : (\mathbf{w} \otimes \mathbf{x}) = (\mathbf{u} \cdot \mathbf{x}).(\mathbf{v} \cdot \mathbf{w})$ we see that they agree with equations (2.4.12).

In addition to the restriction of the number of order parameters, the molecular symmetry restricts the number of interaction coefficients according to Table 2.1 from section 2.1 to only three

$$\begin{aligned} &u_{200}, \\ &u_{202} = u_{220} = u_{20-2} = u_{2-20}, \\ &u_{222} = u_{2-22} = u_{22-2} = u_{2-2-2}. \end{aligned} \tag{2.4.27}$$

It is then covenient to scale the interaction coefficients with the anisotropy coefficient u_{200} in order to reduce the number of coefficients in the system from three to two.

$$\gamma = u_{202}/u_{200}, \qquad \lambda = u_{222}/u_{200}. \tag{2.4.28}$$

Now not all values of the biaxiality parameters correspond to stabilised biaxial nematic phases

at the ground state. Hence, the values of γ and λ can be constrained by carrying out a stability analysis of the pair potential using the method discussed in references [13, 55]. First, we consider a pair potential with the interaction coefficients γ and λ without any relation. Next, we consider the ground state of the pair potential which is when two axis sytems of interacting molecules are parallel. Any small perturbation from this ground state should cause the value of the pair potential to increase in order for the biaxial phase to be stabilised. In order for the pair potential to obey this fact, the interaction coefficients must be inside a fanned shaped *stability region*

$$1.5 - |\gamma\sqrt{6}| + \lambda > 0 \qquad \text{and} \qquad \lambda > 0. \tag{2.4.29}$$

In addition, if the molecules are calamitic, or rod-like, any small rotation away from the major axis should cost more energy than one from any minor axes. In this case the interaction coefficients can be restricted to a smaller area called the *essential triangle*

$$1.5 - |\gamma\sqrt{6}| - 3\lambda < 0. \tag{2.4.30}$$

In fact, we only need $\gamma > 0$ since $\gamma < 0$ simply corresponds to a coordinate transformation by exchanging the x and y axes of the molecules. We show both the fanned shaped stability region and the essential triangle in figure 2.3. In fact, any point inside the stability region and outside

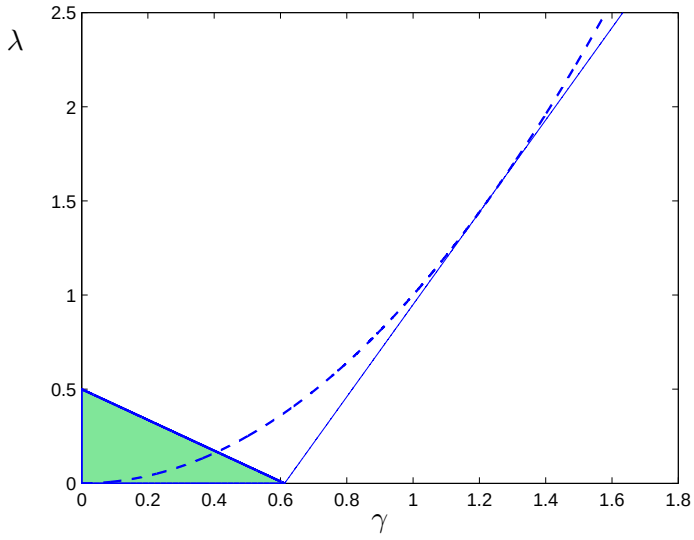

FIGURE 2.3: Constraints for the interaction coefficients γ and λ. The fanned shaped stability region is on the left of the solid line and the essential triangle is shaded. The broken line is the geometric mean parabola. The parabola cuts the triangle boundary at $\gamma = 1/\sqrt{6}$ and is tangential to the boundary of the stability area at $\gamma = \sqrt{3/2}$.

the triangle can be mapped to a point inside the essential triangle by exchanging the molecular axes [55]. The number of parameters can be reduced further from two to only one by using either one of the two approximations discussed in the following subsection. In addition, both approximations help to reduce the number of order parameters from four to only two.

2.4.3 Geometric Mean Approximation

The geometric mean approximation is equivalent to decoupling an intermolecular supertensor into single molecular tensors $u_{2mn} = u_{2m}u_{2n}$. In the essential triangle 2.3, the parameters in this approximation follow the parabola $\lambda = \gamma^2$. Our system now depends on one parameter

$$\gamma = u_{202}/u_{200} = u_{222}/u_{202}. \tag{2.4.31}$$

Now, the potential of mean torque for D_{2h} molecules in nematic phases is consistent with the assumption that dispersion interactions are responsible for the ordering in the system [56]. In addition, the fact that the supertensor can be decoupled into $u_{2mn} = u_{2m}u_{2n}$ is in analogy with the Berthelot combining rule [56]. The Berthelot combining rule is often used to approximate the interaction strength of two different spherical molecules A and B. The intermolecular interaction strength can be written as a product of two single-molecular quantities $\epsilon_{AB} = \epsilon_A\epsilon_B$. In our case, if we denote the single molecular tensors of two different anisotropic molecules A and B as u^A_{2m} and u^B_{2n}, then the interaction tensor is $u^{AB}_{2mn} = u^A_{2m}u^B_{2n}$. If the two molecules are identical, we simply ignore the superscripts. It is also interesting that in this approximation, the number of order parameters is reduced from four to only two

$$\begin{aligned}\langle F_U\rangle &= \langle R_{00}\rangle + 2\gamma\langle R_{02}\rangle,\\ \langle F_B\rangle &= \langle R_{20}\rangle + \gamma\langle R_{22}\rangle.\end{aligned} \tag{2.4.32}$$

These two composite order parameters are adequate to describe the phase behaviour of the system. In the uniaxial nematic phase, only $\langle F_U\rangle$ is non-zero whereas in the biaxial nematic phase, both order parameters are non-zero. In fact, for convenient, we also define the composite angular functions

$$\begin{aligned}F_U(\Omega) &= R_{00}(\Omega) + 2\gamma R_{02}(\Omega),\\ F_B(\Omega) &= R_{20}(\Omega) + \gamma R_{22}(\Omega).\end{aligned} \tag{2.4.33}$$

Hence, the potential of mean torque can be written as

$$U(\Omega) = -u_{200}\left(\langle F_U\rangle F_U(\Omega) + 2\langle F_B\rangle F_B(\Omega)\right). \tag{2.4.34}$$

The parabola of geometric mean approximation $\lambda = \gamma^2$ is always inside the stability region and is tangential to the fanned shaped boundary in figure 2.3 at $\gamma = \sqrt{3/2}$. In addition, the parabola cuts the essential triangle's boundary at $\gamma = 1/\sqrt{6}$. Furthermore, the analysis in reference [55] shows that the values of γ from $1/\sqrt{6}$ to $\sqrt{3/2}$ or those greater than $\sqrt{3/2}$ can be mapped to those inside the essential triangle by exchanging the molecular axes. This mapping provides interchangable results between calamitic and discotic uniaxial nematic phase behaviour since the following reason. The definition of the order parameters assumes the molecules are calamitic where their major axis z align to form the phase axis Z in the uniaxial nematics. However, discotic molecules tend to align one of their short axes to form the phase axis. In this case, the direction of the major molecular axis z is orthogonal to the major phase axis Z on average. Hence, in the uniaxial nematic phase, S takes negative values and there is a false biaxiality with

non-zero values of P. This can be corrected simply by transforming the molecular coordinate axes by exchanging z and y. In the calculations, we choose the values of γ from 0 to $\sqrt{3/2}$ in order to show phase behaviour of both calamitic (rod-like) and discotic (disc-like) molecules.

The graphical method which we have used to find the uniaxial nematic-to-isotropic phase transition temperature is not applicable here. This is because the strength of the two contributions to the molecular field in the biaxial nematic phase depend on different combinations of the order parameters and so varies differently with temperature. One of the more effective methods which we often use is to minimise the free energy with respect to the two order parameters in equation (2.4.35) using a sequential quadratic programming method which is discussed in appendix B. In essence, we need to give the computer program a starting point. The program then uses the algorithm to find an estimate of the solution to desired accuracy using the given starting point. The free energy needs to be minimised is

$$A^* = -\ln Q + \frac{1}{2T^*}\left(\langle F_U\rangle^2 + 2\langle F_B\rangle^2\right). \tag{2.4.35}$$

The efficiency of the minimisation depends heavily on the approximation algorithm for the integration of the partition function. One method is to evaluate it using between 25 and 30 points Gauss-Legendre integration over β and 16 and 25 points trapezoidal rule for the periodic interval of γ and α as suggested by Bisi, Romano and Virga [57]. Direct minimisation of the free energy functional presents several advantages as suggested by Biscarini, Chiccoli, Pasini and Zannoni [52]. First the free energy as a function of the orientational order parameters is concave, with an absolute minimum corresponding to the equilibrium solution. On the contrary, solution of the self-consistency equations (equations which show the order parameters as the orientational averages of Wigner rotation matrices, see equation (2.2.5) for an example) can give unstable or plainly non-physical solutions as well as the stable ones. In Appendix E, we discuss a numerical method to solve the self-consistency equations which will be used in chapter 7. Direct minimisation also requires a smaller number of integrals to be evaluated. The calculation of this set of integrals has to be repeated at every step of an iterative procedure and saving in computer time can be substantial, especially for problems depending on more than one variable. The uniaxial phase is found when the global minimum of the free energy corresponds to non-zero $\langle F_U\rangle$ and the biaxial phase is found when the global minimum of the free energy corresponds non-zero values of $\langle F_U\rangle$ and $\langle F_B\rangle$. In addition, since the values of γ from $1/\sqrt{6}$ to $\sqrt{3/2}$ can be mapped to the region from 0 to $1/\sqrt{6}$ by exchanging the z and the y axes, the values of γ and the transition temperature $T^* = k_BT/u_{200}$ for the latter region can be mapped to the former region according to $(\gamma', T^{*\prime}) = ([(3-\gamma\sqrt{6})/(\sqrt{6}+6\gamma)], 24T^*/(6\gamma+\sqrt{6})^2)$ [20]. Therefore in the calculations for the geometric mean model, the range of γ from 0 to $1/\sqrt{6}$ is essential to carry out the calculations and can be mapped to the range from $1/\sqrt{6}$ to $\sqrt{3/2}$.

To obtain the order of the phase transition from a lower symmetry phase to a phase of higher symmetry, we have determined the order parameters and the scaled temperature both to four decimal places. The phase transition is taken as second order if the order parameters corresponding to the lower symmetry phase changes continuously at the phase transition. In other words, the minimum of the free energy corresponding to the lower symmetry phase is always the global minimum. On the other hand, the order parameters corresponding to the lower symmetry phase changes discontinuously at the first order phase transition. In our methodology it means

that just slightly above the transition temperature we would find a region where there are two minima of the free energy. One minimum corresponding to the lower symmetry phase is the local minimum whereas the other free energy minimum corresponding to the higher symmetry phase is the global minimum.

The phase map in figure 2.4 shows the scaled transition temperature for systems of molecules with different molecular biaxiality γ. The notation is as follows. I, N_U and N_B denote the isotropic, uniaxial nematic and biaxial nematic phase, respectively. This phase map was first revealed by Boccara, Mejdani and Seze [18] and later by Remler and Haymet [19]. The uniax-

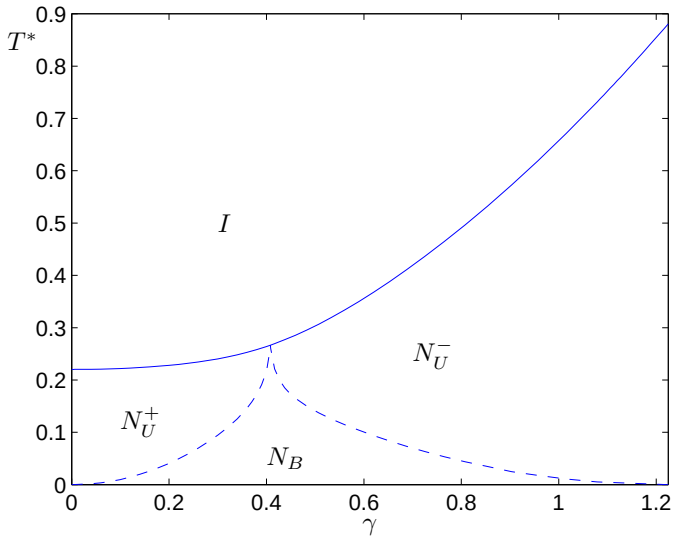

FIGURE 2.4: The phase map for the geometric mean model of biaxial nematics. First order transitions are shown as continuous lines whereas second order transitions are shown as broken lines.

ial nematic-to-isotropic phase transition is first order, indicated by the dicontinuity in the order parameter $\langle F_U \rangle$ at the phase transition. This discontinuity decreases as the biaxiality parameter increases away from 0 and decreases from $\sqrt{3/2}$. In contrast to the first order uniaxial nematic-to-isotropic phase transition, the biaxial nematic-to-uniaxial nematic phase transition is second order and the biaxial order parameter $\langle F_B \rangle$ increases continuously at the phase transition. We notice that, the uniaxial nematic-to-isotropic phase transition temperature increases on increasing γ. The two uniaxial nematic phases which correspond to two ranges of γ are denoted by N_U^+ and N_U^- for calamitic and discotic uniaxial nematic phases, respectively. In calamitic uniaxial nematic the symmetry axis of the phase is formed as the average direction of the major molecular axis. In contrast, in discotic uniaxial nematic, the symmetry axis of the phase is formed by aligning a minor axis of the molecules. Whether a molecular axis is minor or major is determined in the following way. First, a second rank molecular physical property tensor is measured and then diagonalised. The direction corresponds to the largest eigenvalue is the major axis of the molecules whereas the other two axes are minor. Another interesting feature of the phase map is that the biaxial nematic-to-uniaxial nematic phase transition temperature increases for $0 < \gamma < 1/\sqrt{6}$ and decreases for $\gamma > 1/\sqrt{6}$ on increasing γ. The biaxial nematic-to-uniaxial nematic transition lines for two regions of γ meet at a point. This point is where three phases coexist which is called the *triple point*. Furthermore, it is also where the

biaxial nematic phase undergoes a second order phase transition directly to the isotropic phase. This point is called the Landau point. These results show that although molecular anisotropy increases with γ, molecular biaxiality attains its optimum value at $\gamma = 1/\sqrt{6}$, which is also the boundary between calamitic and discotic molecules.

In order to obtain a better understanding, we expand the order parameters as a Taylor series. First we consider the uniaxial nematic-to-isotropic phase transition where the biaxial order parameter vanishes. At the bifurcation point, the uniaxial order parameter $\langle F_U \rangle$ is small. Therefore we can expand the exponentials in the expression of $\langle F_U \rangle$ up to the first order of the Taylor series. The low order limit for the partition function is

$$Q = \int \left(1 + \frac{u_{200}}{k_B T} \langle F_U \rangle (R^2_{00}(\Omega) + 2\gamma R^2_{02}(\Omega))\right) d\Omega = 8\pi^2, \tag{2.4.36}$$

since the integration of both Wigner functions vanish due to their property. The expansion for $\langle F_U \rangle$ then gives

$$\begin{aligned} \langle F_U \rangle &= (8\pi^2)^{-1} \int (R^2_{00}(\Omega) + 2\gamma R^2_{02}(\Omega)) \\ &\quad \times \left(1 + \frac{u_{200}}{k_B T} \langle F_U \rangle (R^2_{00}(\Omega) + 2\gamma R^2_{02}(\Omega))\right) d\Omega \\ &= \frac{u_{200}}{k_B T} \langle F_U \rangle \frac{1 + 2\gamma^2}{5}, \end{aligned} \tag{2.4.37}$$

hence the scaled bifurcation temperature depends linearly on the square of the relative biaxiality parameter γ^2

$$T^* = \frac{1 + 2\gamma^2}{5}. \tag{2.4.38}$$

Therefore, the bifurcation temperature for the uniaxial nematic-to-isotropic phase transition increases on increasing γ. Thus we also expect the actual transition temperature to go up with increasing γ since as we have seen for uniaxial molecules in the uniaxial nematic phase that the difference between the bifurcation temperature and the transition temperature is small. This Taylor expansion can also be applied to the biaxial nematic-to-uniaxial nematic phase transition. Because the biaxial nematic-to-uniaxial nematic phase transition is second order, at the phase transition the order parameter corresponding to the biaxial phase is small whereas that of the uniaxial phase can be sufficiently big. Therefore, it is only necessary to expand the exponential for the biaxial component in the expression of the partition function and the biaxial order parameter $\langle F_B \rangle$. This gives

$$Q = Q_U = \int \exp\left(-\frac{U_U(\Omega)}{k_B T}\right) d\Omega, \tag{2.4.39}$$

$$\begin{aligned} \langle F_B \rangle = Q^{-1} &\int F_B(\Omega) \left\{1 + \frac{u_{200}}{k_B T} 2\langle F_B \rangle F_B(\Omega)\right\} \\ &\times \exp\left(-\frac{U_U(\Omega)}{k_B T}\right) d\Omega. \end{aligned} \tag{2.4.40}$$

where $U_U(\Omega) = -u_{200}\langle F_U\rangle F_U(\Omega)$. Thus the transition temperature can be found by solving

$$\frac{k_BT}{u_{200}} = 2Q^{-1}\int (F_B(\Omega))^2 \exp\left(-\frac{U_U(\Omega)}{k_BT}\right)d\Omega. \tag{2.4.41}$$

Here, $(F_B(\Omega))^2$ can be expressed as a series of the quadratic products of the Wigner rotation matrices, which can be evaluated by

$$D^2_{mn}(\Omega)D^2_{m'n'}(\Omega) = \sum_L C(22L;mm')C(22L;nn')D^L_{m+m',n+n'}(\Omega), \tag{2.4.42}$$

where C$(22L;mm')$ denote the Clebsch-Gordan coefficients. Therefore we have the relation between the biaxial nematic-to-uniaxial nematic phase transition temperature and the order parameters in the isotropic phase (the detailed calculation is given in Appendix C)

$$\begin{aligned}\frac{k_BT}{u_{200}} &= \frac{1+2\gamma^2}{5} + \left(\frac{-2+4\gamma^2}{7}\right)\langle R^2_{00}\rangle + \frac{8}{7}\gamma\langle R^2_{02}\rangle \\ &+ \left(\frac{3+\gamma^2}{35}\right)\langle R^4_{00}\rangle + \frac{2}{7}\sqrt{\frac{3}{5}}\gamma\langle R^4_{02}\rangle + \sqrt{\frac{2}{35}}\gamma^2\langle R^4_{04}\rangle.\end{aligned} \tag{2.4.43}$$

This expression means that the biaxial nematic-to-uniaxial nematic phase transition occurs when the scaled temperature is equal to a combination of the biaxiality parameter γ and the uniaxial second and fouth rank order parameters. In the uniaxial nematic phase, as the temperature is reduced, the order parameters continue to increase until the equality in equation (2.4.43) is satisfied. This is when the biaxial nematic-to-uniaxial nematic phase transition occurs.

The phase map in Figure 2.4 also agrees with a series of Monte Carlo simulations of an analogous pair potential which showed that there exists a second order phase transition from the uniaxial nematic phase to the biaxial nematic phase [58]. These calculations were extended to give a phase map of the dependence of transition temperature on molecular biaxiality [20]. Their phase map shows many qualitative agreements with the molecular field calculations. Thus it validates the molecular field approximation to a certain degree.

2.4.4 Sonnet-Virga-Durand Model

The model adopted by Sonnet, Virga and Durand (SVD model) [13] is an approximate model of biaxial nematics. In this approximation, the biaxiality parameter γ is set equal to zero and λ (see equations (2.4.28)) is varied along the edge of the essential triangle in figure 2.3. Hence, the range for λ is from 0 to 0.5. In this model there are only two order parameters, S and C (see equations (2.4.9)).

The phase map for this model is shown in figure 2.5. Like the geometric mean model, in this case we also find a first order $N_U - I$ transition. Note that in this case, the biaxiality parameter λ does not contribute to the ordering in the uniaxial nematic phase. Therefore, the $N_U - I$ transition temperature is independent of λ. This transition is followed by a $N_B - N_U$ transition at a lower temperature. The $N_B - N_U$ transition is second order for a large range of λ. The $N_B - N_U$ transition temperature increases on increasing λ. In general, this phase transition is

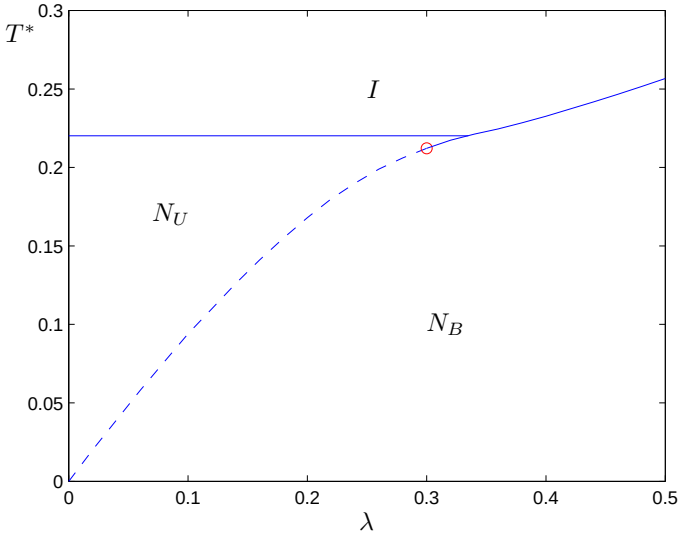

FIGURE 2.5: The phase map for the Sonnet-Virga-Durand model of biaxial nematics. First order transitions are shown as continuous lines whereas second order transitions are shown as a broken line. A tricritical point is shown as a circle.

second order. When λ is big enough (0.3), the $N_B - N_U$ phase transition becomes first order. For λ greater than 0.33, there is a first order phase transition from the biaxial nematic phase directly to the isotropic phase. The stability of the biaxial nematic phase also increase on increasing λ. In the phase map in figure 2.5, we show a tricritical point at $\lambda = 0.3$. In fact, by studying the model for λ greater than 0.5, the authors also found another tricritical point. Above this point, the $N_B - I$ phase transition becomes second order [23]. These results for the approximate model have also been supported by Monte Carlo computer simulations [23]. Analytical methods for locating these tricritical points were also presented in latter publications [22, 24].

2.4.5 Other Model Calculations

Straley was the first to develop a molecular model for biaxial nematics [17]. Others were later developed by Boccara *et al.* [18] and Remler and Haymet [19]. Straley considered some fixed relative orientations of two molecules where the molecular axes are orthogonal. By moving one molecule around the other, the excluded volume of the pair can be found. Then, he calculated the three interaction coefficients in equation (2.4.27) by mapping the pair potential in equation (2.3.1) to the excluded volume between a pair of parallelepiped molecules. Finally, Straley derived a phase map relating the transition temperature with the molecular breadth while fixing the length and width. His phase map showed the same behaviour as those given by Boccara *et al.* [18] and Remler and Haymet [19].

Zheng and Palffy-Muhoray [59] derived a molecular field model analogous to the model of decoupling interaction coefficients (where $u_{2mn} = u_{2m}u_{2n}$). Their coefficients are the three eigenvalues of the molecular polarisability tensors. A phase map relating the scaled temperature with two eigenvalues was presented on a three dimensional diagram. The behaviour of the new phase map is also similar to those by Straley [17], Boccara [18], Remler and Haymet [19]

with the first order uniaxial nematic-to-isotropic phase transition, followed by the second order biaxial nematic-to-uniaxial nematic phase transition. The difference now is that the two regions of rod-like and disc-like uniaxial nematics are separated by a Landau line of second order direct biaxial nematic-to-isotropic phase transitions.

Recent studies showed that the interaction coefficients calculated using the excluded volume model of parallelepipeds by Straley [17] can be mapped to the whole region below the geometric-mean parabola and inside the triangle [60] in figure 2.3. These results are also true for the excluded volume of a more general shape of spherocuboid [60]. A spherocuboid is an object which consists of the volume of a parallelepiped and the volume generated by moving a sphere around it.

The two-parameter model characterised by the essential triangle and described on page 49 has been studied more thoroughly in recent years. In a study, where the molecular field calculations were supported by Monte Carlo simulations [61], the authors investigated the case where both u_{200} and u_{222} are negative and u_{202} vanishes. The same phase sequences were found as in the previous calculations with the biaxial nematic phase stabilised at low temperature for the range of molecular biaxiality studied. However, in this case all phase transitions were second order. In addition, they also calculated a phase map along the line $\lambda = 0$ in the essential triangle in figure 2.3 and found that the biaxial nematic phase cannot be stabilised at low temperature. The latter calculation results agreed with the computer simulations by Luckhurst and Romano [58]. These results mean that in the molecular field theory, the biaxial nematic phase cannot be stabilised by uniaxial molecules. In another set of calculations, Romano [62] set u_{200} to zero and scaled the temperature with u_{222} where the latter is positive. In his molecular field calculations, supported by Monte Carlo simulations, there was a direct second order biaxial nematic-to-isotropic phase transition. These results suggest a dominant contribution of the parameter λ towards the stability of the biaxial nematic phase. Indeed, the calculations by Bisi, Luckhurst and Virga [26] showed that the ratio of the biaxial nematic-to-uniaxial nematic and uniaxial nematic-to-isotropic transition temperatures is almost independent of γ, thus indicating the other as dominant. In addition, bifurcation analysis [24] and detailed calculations [25] of the whole parameter space in the essential triangle revealed that in the region above the geometric mean parabola, there is a line of tricritical points and another line of triple points which meet at the point along the right edge of the triangle. The fact that there is no tricritical point along and below the parabola is in agreement with the previous calculations by Straley [17], Boccara [18], Remler and Haymet [19].

2.5 KKLS Derivation of the Non-equilibrium Free Energy

In section 2.4.3 we discussed the advantages of minimising the equilibrium free energy obtained by de Gennes' variational approach. However, this method has failed in some cases of biaxial nematic phase with D_{2h} symmetry composed of biaxial molecules also with the same symmetry. It was found that, for some combinations of the parameters γ and λ below the geometric mean parabola, the free energy does not have a minimum [25]. Instead, the points which correspond to the solution of the self-consistency equations are saddle points.

To deal with this problem, a group of authors developed a different strategy based on Bogolubov's *minimax principle* [25]. In their method, the molecular field free energy at equilibrium for biaxial molecules with D_{2h} symmetry, A_0, is considered as an approximation to the free energy of the two-particles system, A. The two particles interact via a pair potential which is a function of the molecular tensors in equations (2.4.13) and (2.4.14). The upper and lower bounds for the difference between the molecular field and the two particle free energies are given by the *Bogolubov's inequality*. They found that the pair potential can be considered as a superposition of two molecular interactions, which comes from two independent oscillators in the molecules, represented by two tensors, $\mathbf{q}^+$ and $\mathbf{q}^-$. One interaction is always positive for all values of molecular parameters inside the essential triangle in figure 2.3. The other interaction is positive above the geometric mean parabola whereas negative below the parabola in the essential triangle in figure 2.3. In the molecular field theory, the two oscillators of one molecule are averaged to give the order parameters tensors, $\mathbf{Q}^+$ and $\mathbf{Q}^-$, which are combinations of the two order parameters in equations (2.4.19) and (2.4.20). Using Bogolubov's inequality, the authors demonstrated that the strategy to minimise A_0 for the molecular model below the geometric mean parabola may fail to make A_0 as close as possible to A. Thus a *minimax* strategy was employed for the model below the geometric mean parabola. In this strategy, first A_0 is maximised in $\mathbf{Q}^-$ for fixed $\mathbf{Q}^+$, then the minimum over all $\mathbf{Q}^+$ of the maxima obtained previously is taken. The solution to this method gives the best approximation of A, the two particle free energy. In addition, this method also avoids the problem of the free energy A_0 having saddle points instead of minima.

In this section, we describe a different approach which may be able to explain this contradiction. This approach is a more general view of the molecular field theory given by Katriel, Kventsel, Luckhurst and Sluckin [63], which we call the KKLS theory. We do not reexamine the model of biaxial nematics described in [25] because we only use the two approximations, the geometric mean and the SVD, whose interaction parameters lie on or above the geometric mean parabola. In essence, the KKLS method gives us the dependence of the free energy on the order parameters away from the equilibrium point. In contrast, de Gennes' free energy only gives us the value of the free energy at the equilibrium point and so cannot tell whether the phase is stable or not. In general, we may find the order parameters of a molecular field system by either minimising the equilibrium free energy or solving the self-consistency equations. When the former method does not work, we may use the latter method instead. In contrast to minimising the equilibrium free energy, the method of solving the self-consistency equations always have solutions. In order to know whether the order parameters we get from either method correspond to the minima of the free energy instead of maxima or saddle points, we need to use the KKLS method to derive the non-equilibrium free energy. The KKLS method gives us the more physical free energy surface around the vicinity of the extrema than the equilibrium free energy, thus we can see the nature of the extrema.

2.5.1 Generalised Derivation

This generalised derivation has been used to relate the molecular field theory with Landau-de Gennes theory for biaxial nematic liquid crystals [64]. Here we apply part of their methodology to derive the molecular field theory for a biaxial nematic phase of a general symmetry away

from the equilibrium of the free energy.

The first step in constructing the theory, as for de Gennes' variational method, is to identify the order parameters. They are given in equation (2.2.5). In addition, the internal energy is given in equation (2.3.2). We note that in de Gennes' variational method, we minimise the free energy with respect to the distribution function. In that method, we allow the order parameters to vary with respect to the distribution function $f(\Omega)$ as

$$\delta\langle D^L_{mn}\rangle = \int D^L_{mn}(\Omega)\delta f d\Omega. \tag{2.5.1}$$

Therefore the result gives us an expression of the free energy which is valid at the extrema with respect to both the distribution function and the order parameters. Now we want to find the free energy surface which is also valid away from equilibrium points. To do that we need to consider our system with fixed order parameters. Hence the internal energy is constant for given values of the order parameters. Thus we need to maximise the entropy for given order parameters to find the equilibrium state. We note that a system with maximal entropy is in equilibrium only if the order parameters are kept fixed. When the order parameters are allowed to vary, the order parameters tend to values which minimise the free energy. Therefore, at a given temperature there is only one set of order parameters at equilibrium. Maximising the entropy in equation (2.3.7) with respect to the distribution function $f(\Omega)$ with the constraint given in equations (2.3.11) and keeping the order parameters fixed

$$\delta\langle D^L_{mn}\rangle = \int D^L_{mn}(\Omega)\delta f d\Omega = 0, \tag{2.5.2}$$

we get the distribution function of the form (2.3.16), where the potential of mean torque is

$$U(\Omega) = -k_B T \sum \eta_{Lpm} D^L_{pm}(\Omega). \tag{2.5.3}$$

Here, the Lagrangian multipliers η_{Lpm} are introduced to satisfy the constraint (2.2.5). The entropy can now be rewritten as

$$S = -k_B \left(\sum \eta_{Lpm} \langle D^L_{pm}\rangle - \log Q \right). \tag{2.5.4}$$

Hence, we can construct the non-equilibrium free energy from equation (2.3.10) from the entropy with the internal energy given in equation (2.3.2). This non-equilibrium free energy gives us physical values of the free energy at any values of the order parameters, unlike de Gennes' free energy. In addition, the value of the order parameters at equilibrium minimises the free energy.

2.5.2 Uniaxial Nematics formed from Uniaxial Molecules

We give a comparison of the free energies in the de Gennes and KKLS theories by looking at the simplest case for a uniaxial nematic phase formed from uniaxial molecules. First, we construct the KKLS theory for this case. In keeping with the classical notation, in this case we call the order parameter as S, which should not be confused with the entropy. The distribution function

can be found by maximising the entropy in equation (2.3.7) with the constraint in equation (2.5.2)

$$f(\beta) = Q^{-1} \exp\left(\eta P_2(\cos\beta)\right), \tag{2.5.5}$$

where the partition function is

$$Q(\eta) = \int \exp\left(\eta P_2(\cos\beta)\right) d\cos\beta. \tag{2.5.6}$$

Hence, the order parameter introduced by Tvetskov is

$$S(\eta) = Q^{-1} \int P_2(\cos\beta) \exp\left(\eta P_2(\cos\beta)\right) d\cos\beta. \tag{2.5.7}$$

In addition, the internal energy is taken to be

$$U = -(1/2) u_{200} S^2, \tag{2.5.8}$$

and so the free energy is

$$A = -(1/2) u_{200} S^2 + k_B T(\eta S - \log Q). \tag{2.5.9}$$

The free energy can be thought of as a function of η since both the order parameter S and the partition function Q are functions of η,

$$A(\eta) = -(1/2) u_{200} S(\eta)^2 + k_B T(\eta S(\eta) - \log Q(\eta)). \tag{2.5.10}$$

In order to find the order parameter at equilibrium, we need to minimise the free energy in equation (2.5.10) with respect to η where $S(\eta)$ is given in (2.5.7) in order to get η at equilibrium. Then, we substitute this value of η into (2.5.7) to get the value of the order parameter at equilibrium. To ilustrate the difference between the two free energies, we give the plots of the two free energies at the scaled temperature $T^* = 0.2$ in figure 2.6. In order to construct the plot for the KKLS free energy, first we pick a range of values for η according to the following consideration. The range of values for S is from 0 to 1 whereas the range of values for T^* which we are interested in is from 0.01 to about 0.2. In addition, at the equilibrium point, we know that $\eta = S/T^*$. Thus the range of values which we can choose for η is from 0 to 100. Then, we calculate the KKLS free energy according to equation (2.5.10) and the order parameter S according to equation (2.5.7). The dependence of de Gennes' free energy on the order parameter was computed using equation (2.4.5). Finally, we plot the values of the KKLS free energy against the corresponding order parameter. We see that both free energies in figure 2.6 have the same minimum at $S = 0.6148$ and the same local maximum at $S = 0$. However, their values for the same S are different away from the extrema. In this case, the KKLS free energy surface has physical significance since it corresponds to maximum entropy. In the comparison we just see, both free energies have the same minimum. In section 7.3.1, we give an example that the two theories give different results in a molecular field theory for uniaxial smectic A phase.

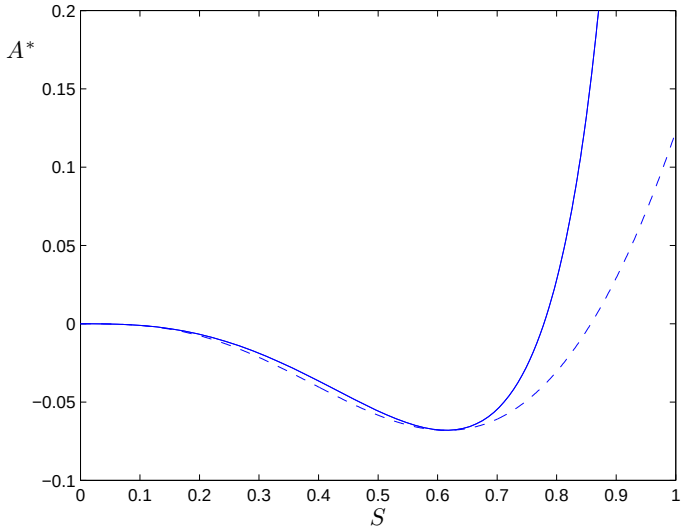

FIGURE 2.6: The dependence of the free energy for uniaxial molecules in uniaxial nematics on the order parameter S at the scaled temperature $T^* = 0.2$. The continuous line shows the numerical results using KKLS formulation whereas the broken line is done using the de-Gennes formulation, equation (2.4.5).

2.6 Conclusions

In this chapter we have reviewed a derivation for the molecular field theory for nematic liquid crystals at equilibrium based on de Gennes' variational method. In essence, we assume that a molecule only interact with a mean field of all other molecules in the system and we ignore any short-range correlation. This mean field is generated by pair-wise intermolecular interactions. In addition, we ignore volume change at the phase transition and we use the Helmholtz free energy instead of the Gibbs free energy. Then we discussed some examples when the molecular field theory is used to describe the uniaxial nematic and biaxial nematic phases of D_{2h} symmetry. In general, we can minimise the Helmholtz free energy to determine the order parameters at equilibrium. This allows us to find the transition temperature as a function of the molecular parameters. We also note that the method of minimising the equilibrium Helmholtz free energy sometimes fails. It is because the equilibrium Helmholtz free energy as a function of the order parameters only holds at equilibrium and gives a physically wrong surface around the equilibrium. Away from equilibrium, the physical value of the Helmholtz free energy should be described by the KKLS method.

Chapter 3

Biaxial Nematics formed from Molecules with C_{2h} Symmetry

This chapter consists of a collaborative project with Prof. S. Naemura and Dr. S. Turzi. The theory was developed jointly. I carried out the calculation and provided the solutions. Prof. Naemura suggested the possibility of an axial first-rank order parameter. This was demonstrated by Dr. Turzi using Cartesian tensor notation which confirmed my calculation.

Most theoretical studies on biaxial nematic liquid crystals have assumed that the constituent molecules and the phase have orthorombic D_{2h} symmetry. Straley [17], in his paper stated this explicitly. In other papers, it is implied implicitly. An example is the seminal paper by Freiser [15]. In his paper, Freiser separated each intermolecular tensor into a product of single molecular tensors. As we will see later, this is equivalent to having a model of molecules with D_{2h} symmetry. A recent analysis of experimental results by Karahaliou, Vanakaras and Photinos [42] showed that the symmetry of the biaxial nematics might be C_{2h} instead of the usually assumed D_{2h}. In fact, the notion of biaxial nematics which have lower symmetry than D_{2h} has been suggested for a long time before this analysis. In this chapter, we develop a molecular field theory for biaxial nematics of C_{2h} symmetry formed from molecules of the same symmetry. The theory is a contribution towards our study of biaxial nematic liquid crystals. In section 3.1 we review some related works which have discussed the possibility of low symmetry biaxial nematics. After that, we produce a molecular field theory for biaxial nematics composed of molecules with C_{2h} symmetry in section 3.2. In order to facilitate the calculations, we use an approximate model. This is discussed in section 3.3. Our approximate model is an extension of that for biaxial nematics composed of D_{2h} symmetry which we reviewed in section 2.4.4. The numerical predictions for the approximate model are presented in section 3.4.

3.1 Related Works

3.1.1 Experimental Studies

In this section, we summarise the paper by Karahaliou, Vanakaras and Photinos [42]. In this paper, the authors discussed recent experimental evidence for biaxial nematics and concluded that the phase symmetry for these systems is more likely to be C_{2h} rather than D_{2h}.

Recent experimental evidence showed that V-shaped molecules [35, 36, 37] and tetrapodes [30, 31, 32] are the most likely candidates for biaxial nematics. An analysis of this experimental evidence by Karahaliou *et al.* [42] showed that the symmetry of the biaxial nematics might be C_{2h} instead of the usually assumed D_{2h}. In contrast, it was claimed by Karahaliou *et al.* [42] that experimental evidence for lyotropic [28] and polymeric systems [29] shows that indeed they have D_{2h} symmetry. In the study by Karahaliou *et al.* [42], phase symmetries are restricted to achiral, apolar that can be characterised by second-rank ordering tensors; they are: triclinic C_i, monoclinic C_{2h} and orthorhombic D_{2h} point groups. The major difference between the three phases is the number of common principal axis for all second-rank macroscopic physical properties.

In a phase with C_i point group symmetry, there is no principal axis dictated by symmetry. Therefore, there is no common principal axes for all second-rank macroscopic physical property tensors. In constrast, the number of principal axes dictated by symmetry in the C_{2h} and D_{2h} phase are one and three, respectively. They correspond to the numbers of principal axes common to all second-rank macroscopic physical property tensors. In their paper, Karahaliou *et al.* discussed the two methods that can be used to determine second-rank orientational order parameters characterising the ordered phase: namely deuterium nuclear magnetic resonance (NMR) and polarised infrared spectroscopy (IR).

In their discussion of NMR experiments, first the authors introduced a second-rank symmetric and traceless tensor ($G^{(i)}_{AB}$) which describes the orientational averaging of the field gradient associated with the molecular site i. This tensor relates the principal axes of the electric field gradient tensor with a space fixed frame ($\mathbf{A}$ and $\mathbf{B}$). The tensor $G^{(i)}_{AB}$ can be split into two independent components, a primary order component $S^{(i)}$ and the biaxiality parameter $\eta^{(i)}$. Since the $G^{(i)}_{AB}$ tensor is related to the quadrupolar splittings, which are measurable, the primary component and the biaxiality parameter can be calculated from the two extrema of the quadrupolar splittings. These two extrema correspond to different orientations of the magnetic field along the principal axes of the $G^{(i)}_{AB}$ tensor.

In a real NMR experiment, one of the axes of the liquid crystal sample is aligned with the magnetic field of the NMR spectrometer. In addition, the other two axes are aligned using an electric field. Therefore, the space fixed frame can be chosen to be the magnetic susceptibility frame of the phase (χ^m_{AB}). This allows us to measure the components of the quadrupolar splittings parallel and perpendicular to the magnetic field. The $G^{(i)}_{A_M B_M}$ tensor, expressed in this frame, can also be split into two independent components, $S^{(i)}_M$ and $\eta^{(i)}_M$, which are measurable quantities. It is because they can be related to the quadrupolar splittings components along and perpendicular to the magnetic field which are measurable. The authors called these components the *apparent*

parameters.

The final step in an NMR study is to calculate the primary order component $S^{(i)}$ and the biaxiality parameter $\eta^{(i)}$ from the apparent parameters $S_M^{(i)}$ and $\eta_M^{(i)}$. Their relations are different for nematics with different symmetry. For a nematic phase with D_{2h} symmetry, the electric field gradient tensor and the magnetic susceptibility tensor have the same principal axis frames. As a consequence, the three principal axes of the apparent parameters align with those of the principal component and the biaxiality parameter. Therefore their relations only involve diagonal components of $G^{(i)}_{A_M B_M}$. In contrast, in the monoclinic C_{2h} and triclinic C_i phases, their principal axis frame are different and therefore the relations between the apparent and the true parameters also depend on the off-diagonal elements of $G^{(i)}_{A_M B_M}$.

In analysing recent NMR experiments, the authors are concerned with monoclinic liquid crystals in which the maximum magnetic energy axis coincides with the symmetry axis of the phase and its effect on the evaluation of the true parameters $S_M^{(i)}$ and $\eta_M^{(i)}$. For nematics with triclinic symmetry or monoclinic liquid crystals in which the maximum magnetic energy axis does not coincide with a symmetry axis of the phase, different NMR techniques would be required. For liquid crystals with monoclinic symmetry, the authors derived relations between the apparent and the true parameters and draw the following conclusions. First, a large apparent biaxiality can be obtained even if the proper biaxiality is negligible and a negligible apparent biaxiality can be measured even if the proper biaxiality is large. Secondly, since the angle between the non-principal axis of the electric field gradient tensor and that of the magnetic susceptibility tensor vary with temperature, the values of the apparent parameters may exhibit an anomalous temperature dependence.

The discussion of the IR method is analogous to that of NMR experiments. The difference is now the absorption of the IR beam is measured which gives information on the absorbance tensor instead of the electric field gradient tensor. In addition, the order parameters are measured by the positions of the peaks in NMR experiments whereas they are measured by the intensities of the peaks in IR experiments.

After setting up the theory, the authors discussed recent experimental results. They argued that the order parameters obtained for tetrapodes using NMR and IR methods violate the relation between the principal component and the biaxiality parameter. Hence the order parameters obtained were only apparent and did not represent true order parameters. On the other hand, the NMR experimental results for V-shaped molecules was too limited to do any analysis. The authors pointed out that, in the results for V-shaped molecules using polarised Raman scattering, the second-rank order parameters also violate the relation between the principal component and the biaxiality parameter. This discrepancy can also be removed on relaxing the assumption of D_{2h} symmetry. Finally, the authors remarked that, it is more accurate to assign these experimental systems with the monoclinic symmetry over the triclinic symmetry since the nematic phases in the experiments have at least one plane of symmetry.

3.1.2 Molecular Field Theories

The first prediction of a biaxial nematic phase was by Freiser [14] in 1970. By considering a molecular field theory for rigid non-cylindrically symmetric mesogenic molecules, the author demonstrated that the ground state of such system is a biaxial nematic phase. However the symmetry of this biaxial nematic phase was not stated explicitly although implicitly it may be understood that this phase possess D_{2h} symmetry.

Straley [17] in 1974 provided a molecular field model for nematic liquid crystals composed of D_{2h} molecules. By fixing the molecular length and width and varying its breath, a range of molecular biaxialities was investigated. The lowest nematic state can be formed in this case is the biaxial nematic phase with D_{2h} symmetry. In the conclusion, Straley pointed out the possibility that generalisation of nematic liquid crystals formed from less symmetric particles might be necessary in order to describe biaxial phases of lower and special symmetry.

Gorkunov, Osipov, Kocot and Vij [65] developed a molecular model for tetrapodes in 2010. A tetrapodal molecule was modelled as composed of four uniaxial mesogenic groups. All the symmetry axes of the mesogenic groups are parallel. The lines joining the centres of mass form a rectangle. In addition, they are coplanar with the symmetry axes of the mesogenic groups. The symmetry axes are not parallel with the lines joining the centres of the mesogenic groups. The resulting molecules have C_{2h} symmetry and the angle α between a mesogenic group's symmetry axis and a line joining two mesogenic groups' centres characterises the degree of deviation from D_{2h} symmetry. The intermolecular potential was expanded in powers of three molecular tensors. Six intermolecular coefficients were needed in the expansion. These six coefficients were calculated by mapping the potential with the Gay-Berne interaction of two molecules. It was found that the three coefficients which characterse the deviation from D_{2h} to C_{2h} symmetry are small and thus have been ignored in the molecular field calculation. In the full model, the three molecular tensors give rise to six order parameters. However, when the small intermolecular coefficients are ignored, only four order parameters were retained. Thus their molecular field calculations were essentially for D_{2h} biaxial nematics formed from D_{2h} molecules. By increasing the elongation of the mesogenic groups and α, the stability of the biaxial nematic phase increases. This suggests an increase in the effective molecular biaxiality.

Another molecular field theory was developed by Osipov and Gorkunov [66] in 2010 to model ferroelectricity in low-symmetry biaxial nematic liquid crystals. A molecule was first modelled as having C_{2h} symmetry. A molecule thus have three molecular tensors instead of two for molecules with D_{2h} symmetry. These three tensors are averaged to give eight order parameters in a phase with C_{2h} symmetry. They are seven second-rank order parameters and one first-rank pseudo order parameter. Three of seven second-rank order parameters characterise the low-symmetry biaxial nematic phase with C_{2h} symmetry. When the molecules become chiral, which is characterised by a pseudoscalar, the system can have a spontaneous polarisation. A pseudoscalar is a constant with respect to rotations of molecular axes but changes sign on inversion of molecular axes, which describe the handedness of a molecule. This polarisation is a coupling between the pseudoscalar, the pseudovector order parameter and a second-rank order parameter which characterise the C_{2h} phase. Hence this polarisation is not directly determined by a dipolar interaction. Instead it is induced by the rotation of the axes of the tensor order parameter characterising the C_{2h} phase with respect to the primary nematic director.

3.1.3 Topological Theories of Defects

Mermin in 1979 [67], while reviewing a topological theory of defects, which includes defects in nematic liquid crystals, remarked that there is no particular reason why the point group D_{2h} should be singled out for special attention for biaxial nematics. The author demonstrated that uniaxial nematics can have topologically stable point defects with strengths of ± 1 and $\pm 1/2$ and topologically stable line defects with strengths of only $\pm 1/2$. In contrast, biaxial nematics do not have a topologically stable point defect since they have discrete rotational point group symmetry. Moreover, line defects for biaxial nematics of different symmetry may be different. The author only discussed the case of biaxial nematics with D_{2h} point group symmetry. In this case, we can have topologically stable line defects with strengths of both ± 1 and $\pm 1/2$, as opposed to uniaxial nematics. These results are in agreement with a review of experimental methods to characterise thermotropic biaxial nematic phases by Galerne [68]. Thus disclinations of strength 1 are topologically stable in the biaxial nematic phase which is contrary to the uniaxial nematic phase where they excape to the third dimension. In principle, these defects can be observed experimentally by looking at nematic textures through an optical microscope.

3.1.4 Theories of Hydrodynamics

Symmetries of biaxial nematic liquid crystals were also considered from a point of view of a nonlinear hydrodynamic theory of static and dynamic behaviour in biaxial nematic liquid crystals by Liu in 1981 [69]. The author regarded a biaxial nematic as a liquid crystal system that breaks all three rotational symmetries but none of the translational ones. This is in contrast with uniaxial nematics where only two rotational symmetries are broken. This description allows a rich variety of biaxial nematics. In addition to the classical orthorhombic D_{2h} system, biaxial nematics can have other different symmetries such as triclinic (C_1, C_i), hexagonal (D_{6h}, C_{6v}, C_{6h}, C_6, D_6, D_{3h}, C_{3h}), cubic (T, T_h, O, T_d, O_h) and even those that are forbidden in the lattice such as icosahedral symmetry. These systems obey hydrodynamic equations of identical structure since they break the same continuous symmetries. Thus they have the same variables and are characterised by equal number of propagating and diffusive modes. On the other hand, their discrete symmetries determine the number of independent elastic and transport coefficients. This decides whether certain modes are coupled or not. In general, there is no one-to-one correspondence between the symmetry groups and the sets of hydrodynamic equations. This is because the tensors that appear in the equations are of finite rank which cannot distinguish phases with symmetries that allow non-vanishing higher rank tensors. Thus some biaxial nematics (such as icosahedral and hexagonal) may be called "quasi-isotropic nematics" since their elastic and transport tensors mimic isotropic behaviour. The equations were solved for two special cases: orthorhombic and quasi-isotropic nematics. It was found that in both cases, there is always a purely diffusive mode, in addition to sound and heat diffusions. In quasi-isotropic nematics, it is the longitudinal rotation angle that diffuse whereas in orthorhombic nematics, this diffusive mode involves a linear combination of both longitudinal and transverse angles. In contrast, in uniaxial nematics, the only pure diffusion is the longitudinal rotation when the wavevector is perpendicular to the director.

In another hydrodynamic theory of biaxial nematic, Kini in 1984 [70] derived the expressions

for the elastic free energy density, viscous stress and flexoelectric polarisation for monoclinic (C_2, C_{2h}, C_s) and triclinic (C_1, C_i) symmetry classes of biaxial nematics. This was an extension of the work by Saupe for orthorhombic nematics (D_2, D_{2h}, C_{2v}). These three different biaxial nematics are represented by different number of elastic constants, viscosity coefficients, surface terms and flexoelectric coefficients and so their explicit expressions for the free energy density, viscous stress and surface terms are dissimilar.

3.1.5 Phenomenological Theories

The first notion of nematic phases with different symmetries seems to have been given by Boccara [71] in 1973. The author predicted a list of the possible "anisotropic liquid phases which can appear as a result of the violation of the rotational invariance of the isotropic liquid". In other words, he considered possible nematic phases with different rotational symmetries as well as inversion symmetry. The list of nematic symmetries considered has C_n, C_{nv}, D_n, C_{nh}, D_{nh}, S_{2n} and D_{nd} for integer number n. Therefore, a tensor which represents a physical property of a nematic phase needs to transform according to an irreducible representation of the orthogonal group $O(3)$. The group $O(3)$ is the direct product of $SO(3)$ and C_i since the inversion commutes with any rotation. To each irreducible representation D^L of $SO(3)$ corresponds two irreducible representations D^L_+ and D^L_- of $O(3)$, where L is an integer. Tensors which transform like D^L_+ do not change sign on inversion whereas those transforming like D^L_- do change sign on inversion. Tensors of odd rank are proper if they transform according to D^L_- and improper if they transform according to D^L_+. In contrast, tensors of even rank are proper if they transform according to D^L_+ and improper if they transform according to D^L_-. Using character theory, the author calculated the number of independent components of an irreducible proper tensor of rank L for given symmetry groups of nematic phases. As an example consider a second-rank tensor, there are two independent components for the groups D_2 and D_{2h} and three independent components for C_{2h} group. The difference is because a nematic phase with C_{2h} symmetry has only one principal axis defined by symmetry whereas the other two axes are not defined and so it still has one off diagonal element.

Goshen et al. [72] in 1975 discussed liquid crystals with rotational and also translational symmetries. The translational symmetries are considered in order to describe liquid crystal phases with tranlational order such that smectic phases. In addition to those given by Boccara, he also added other possible phase symmetries such as tetrahedral T and octahedral O nematic liquid crystals.

Lubensky and Radzihovsky [73] proposed a Landau theory of the nematic phases and the transitions between them. When formulating the orientational order parameters the V-shaped or bent-core molecules were taken to have C_{2v} point group symmetry. Thus for the uniaxial nematic with $D_{\infty h}$ symmetry just a single quadratic order parameter is needed. However, for this phase to undergo a transition to a uniaxial polar nematic with $C_{\infty v}$ symmetry a polar or vector order parameter is required together with a third-rank tensor. This third-rank tensor is introduced because it is essential for the description of the spontaneously ordered chiral phases with point group symmetries D_2 and C_2. A chiral liquid crystal phase is a liquid crystal phase with the director forming a twisted structure. The set of three order parameters, first, second and third

rank, is able to describe a host of nematic phases which also includes those with point group symmetries D_{3h}, C_{3v}, D_{2d} and C_{1h}. Also of relevance are the tensor order parameters which are needed to create these order parameters from phases with higher symmetry. Of particular interest for the bent-core mesogens is the transition from a biaxial nematic with D_{2h} symmetry to an achiral nematic with symmetry D_2 where the mesophase is expected to separate into domains of opposite handedness separated by domain walls that will coarsen over time. The extensive and detailed analysis presented by Lubensky and Rodzihovsky [73] is aided by the use of pictorial representations to show the idealised organisation in the different phases and their change at the phase transitions.

Recent results on the symmetries of nematic liquid crystals were presented in two publications by Mettout [74, 75]. In the first paper [74] the author formulated a phenomenological theory for nematic liquid crystals formed from bent-core molecules. The theory revolves around the expansion of the orientational distribution function in a basis of Wigner rotation matrices. The coefficients of the expansion are components of order parameter tensors. It was argued that two second-rank order parameter tensor are required to describe the phase behaviour of bent-core molecules. They are $\langle D^2_{p0}\rangle$ and $\langle D^2_{p2}\rangle + \langle D^2_{p-2}\rangle$. In contrast, we only need one order parameter tensor for uniaxial molecules which is $\langle D^2_{p0}\rangle$. In the uniaxial phase, the two tensors required for bent-core molecules are $\langle D^2_{00}\rangle$ and $\langle D^2_{02}\rangle + \langle D^2_{0-2}\rangle$. They are cylindrically symmetric with respect to the director and they have the same principal axis. In the biaxial D_{2h} phase, the two second-rank tensors have the same eigenframe. However, in the C_{2h} phase only one direction of the two eigenframes are the same whilst in C_i phase none of the directions of the eigenframes coincides.

In his later paper, Mettout [75] studied the effect of molecular symmetry on macroscopic properties of nematic phases. His paper concerned the relation between three types of symmetries: molecular symmetry, $G_{\rm mol}$, macroscopic phase symmetry, $G_{\rm nem}$, and the *effective symmetry* of the molecules in the ordered phases, $G_{\rm eff}$. At frequencies smaller than the molecular rotation frequency, the behaviour of the system is determined only by $G_{\rm nem}$ and $G_{\rm eff}$. The effective symmetry of a molecule is determined by the behaviour of that molecule in the phase. As an example consider a system whose $G_{\rm mol}$ is characterised by a major rotation axis of order greater than 2. All these molecules yield the same effective cylindrical symmetry in both the uniaxial and the biaxial phase with D_{2h} symmetry. It is because these phases only permit order parameter tensors of second-rank whereas higher rank tensors are needed to describe $G_{\rm mol}$. The discussion on the relation between macroscopic and molecular symmetries allows the author to determine stable nematic phases which can be stabilised by given molecular symmetries, with given rank and parity of order parameter tensors. Of relevant to our work is the results which show the number of independent tensors needed to characterise nematic systems based on molecular and phase symmetries. These results are different from Boccara [71] in that there are two types of tensors. The first is defined by the symmetry of the phase which is called an *external* tensor. The second is determined by the symmetry of the molecules which is called an *internal* tensor. Since internal and external transformations commute, the number of order parameters required for a given rank is a product of the number of internal and external tensors for that rank. An example of this can be found in a biaxial nematic phase of D_{2h} symmetry formed from identical molecules also have D_{2h} symmetry. In this case, there are two internal and two external tensors. Thus the total number of order parameters is four. They are S, D, P and C, as we have seen in

equations (2.4.12).

3.2 Molecular Field Theory

In this section, we develop a molecular field theory for biaxial nematics composed of molecules with C_{2h} symmetry. It might be expected that a system of such molecules is able to form biaxial nematics with either D_{2h} or C_{2h} symmetry. In figure 3.1 we show the idealised organisation of

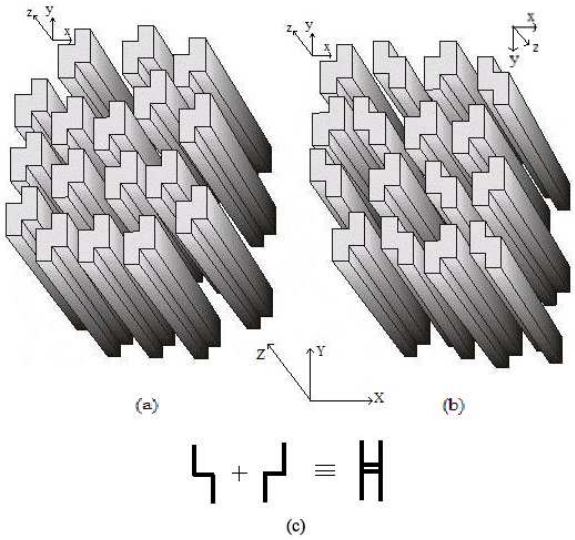

FIGURE 3.1: A sketch of the idealised organisation of elongated molecules with C_{2h} point group symmetry in a biaxial nematic phase with (a) C_{2h} symmetry and (b) D_{2h} symmetry. The coordinate systems are whose for the phase (XYZ) and for the molecule (xyz). (c) The cross-sections of the average molecular structure formed by combining two molecular orientations.

molecules with C_{2h} point group symmetry in the C_{2h} and D_{2h} biaxial nematic phases. The key feature in these sketches is the orientation of the constituent molecules and not their translational distribution. Following the ideas of Lubensky and Radzihovsky [73] we consider an average structure for the molecules in the different phases. Thus in the D_{2h} biaxial nematic phase there are two types of molecule related by a 180^{o} rotation about the molecular x-axis, which is called internal rotation by Mettout [74]. The addition of these two gives a structure with D_{2h} point group symmetry having an H-shaped cross section in the (xy) plane (see figure 3.1(c)).

Our notation for the biaxial nematic phases in this section is different from the classical notation. Instead of writing N_B with a superscript which denotes the phase symmetry, we write the biaxial phases as ND_{2h} and NC_{2h}. It is because the symmetry characterises the biaxiality of the phases and thus the subscript B is redundant.

3.2.1 Interaction Coefficients

A molecule with C_{2h} symmetry is less symmetric than one with D_{2h} symmetry. In other words, it has a smaller number of basic symmetry operations which can reduce the number of interaction

coefficients. Therefore, we expect that there are more interaction coefficients to describe the interactions of molecules with C_{2h} symmetry than those with D_{2h} symmetry. In fact, the same argument can be applied to the order parameters. In our system of biaxial nematics formed from molecules with C_{2h} symmetry, there are more order parameters than one from molecules with D_{2h} symmetry. The coefficients required to describe the interactions of identical molecules with C_{2h} symmetry can be found according to Table 2.1. There are six of them in total:

$$
\begin{aligned}
&(1)\ u_{200},\\
&\left.\begin{aligned}(2)\ u_{202} &= u_{220},\\ (3)\ u_{20-2} &= u_{2-20},\end{aligned}\right\}\ \text{These components are related by } u^*_{202} = u_{20-2} \text{ and } u^*_{220} = u_{2-20}.\\
&\left.\begin{aligned}(4)\ &u_{222},\\ (5)\ &u_{2-2-2},\end{aligned}\right\}\ \text{These components are related by } u^*_{222} = u_{2-2-2}.\\
&(6)\ u_{22-2} = u_{2-22}.
\end{aligned}
$$

As the molecular symmetry becomes D_{2h}, all the components become real and so the components (2) and (3) are equal and the components (4) and (5) are also equal. We may define system parameters as combinations of those coefficients in a way that can distinguish between the two biaxial molecules with two different symmetries C_{2h} and D_{2h} as follows

$$
\begin{aligned}
\gamma_s &= (u_{220} + u_{2-20})/2u_{200},\\
\gamma_a &= (u_{220} - u_{2-20})/2iu_{200},\\
\lambda_s &= (\mathrm{Re}u_{222} + u_{2-22})/2u_{200},\\
\lambda_a &= (\mathrm{Re}u_{222} - u_{2-22})/2u_{200},\\
\lambda_0 &= (u_{222} - u_{2-2-2})/2iu_{200},
\end{aligned}
\tag{3.2.1}
$$

Thus, a molecule with C_{2h} symmetry differs from one with D_{2h} symmetry by the non vanishing values of the coefficients γ_a, λ_a and λ_0.

It should be noted that not all parameterisation methods for molecules with D_{2h} symmetry can be used for those with C_{2h} symmetry. One example is the separability approximation $u_{2mn} = u_{2m}u_{2n}$ which decomposes an intermolecular supertensor u_{2mn} into single molecular tensors u_{2m}. This is because we can always find a principal axis system which makes $u_{2\pm1} = 0$, so that the interaction would behave like that for D_{2h} molecules. Therefore we conclude that all molecular models which require the separability approximation, such as the surface tensor [76, 77] or the additive tensor [44, 78] models cannot be used in this case. We review both models in chapter 4 when we calculate the interaction tensors for V-shaped molecules. A possibility for parameterising the intermolecular coefficients for C_{2h} molecules is by calculating the excluded volume of molecules which are made up of touching spheres to form the desired symmetry [79, 80]. Another model for calculating the intermolecular coefficients for molecules with C_{2h} symmetry was carried out by Gorkunov, Osipov, Kocot and Vij [65] in an attempt to model tetrapodal molecules. The pair potential was fitted to the values of the Gay-Berne inter-

action potential between a pair of molecules at every relative orientation in order to calculate the intermolecular coefficients. The Gay-Berne interaction potential is a more realistic pair potential since it takes into account both attractive and repulsive forces explicitly. The excluded volume and Gay-Berne interaction fiitting are possible for our future research.

3.2.2 Order Parameters

The number of second-rank order parameters for molecules with C_{2h} symmetry in the three nematic phases can be found according to tables 2.2 and 2.3. Thus in the uniaxial phase with $D_{\infty h}$ symmetry, there are three order parameters: $\langle D^2_{00}\rangle$, $\langle D^2_{02}\rangle$ and $\langle D^2_{0-2}\rangle$. The last two order parameters are complex conjugates of one another. As the system goes into the biaxial phase with C_{2h} symmetry, there are six more second-rank order parameters $\langle D^2_{20}\rangle$, $\langle D^2_{-20}\rangle$, $\langle D^2_{22}\rangle$, $\langle D^2_{-2-2}\rangle$, $\langle D^2_{-22}\rangle$ and $\langle D^2_{2-2}\rangle$. These order parametes are related by the conjugate relations $\langle D^2_{-m-n}\rangle = \langle D^2_{mn}\rangle^*$. In the D_{2h} phase some of the order parameters become equal, namely, $\langle D^2_{-mn}\rangle = \langle D^2_{mn}\rangle$. It is therefore more convenient to define the order parameters as linear combinations of those averages of the Wigner rotation matrices such as some vanish at the NC_{2h}-to-ND_{2h} phase transition. Therefore in the uniaxial phase, there are three order parameters

$$\langle R_{00}\rangle = \langle D^2_{00}\rangle, \tag{3.2.2}$$

$$\langle R_{02}\rangle = \left(\langle D^2_{02}\rangle + \langle D^2_{0-2}\rangle\right)/2, \tag{3.2.3}$$

$$\langle I_{02}\rangle = \left(\langle D^2_{02}\rangle - \langle D^2_{0-2}\rangle\right)/2i. \tag{3.2.4}$$

As the system becomes more ordered, it may take a transition into the nematic phase with D_{2h} symmetry, there are now three more order parameters

$$\langle R_{20}\rangle = \left(\langle D^2_{20}\rangle + \langle D^2_{-20}\rangle\right)/2, \tag{3.2.5}$$

$$\begin{aligned}\langle R^s_{22}\rangle = &\left[\left(\langle D^2_{22}\rangle + \langle D^2_{-2-2}\rangle\right)\right.\\ &\left.+\left(\langle D^2_{-22}\rangle + \langle D^2_{2-2}\rangle\right)\right]/2,\end{aligned} \tag{3.2.6}$$

$$\begin{aligned}\langle I^s_{22}\rangle = &\left[\left(\langle D^2_{22}\rangle - \langle D^2_{-2-2}\rangle\right)\right.\\ &\left.+\left(\langle D^2_{-22}\rangle - \langle D^2_{2-2}\rangle\right)\right]/2i.\end{aligned} \tag{3.2.7}$$

And for the biaxial nematic with C_{2h} symmetry, there are nine second-rank order parameters. Three of them characterise this new phase and join the existing six

$$\langle I_{20}\rangle = \left(\langle D^2_{20}\rangle - \langle D^2_{-20}\rangle\right)/2i, \tag{3.2.8}$$

$$\begin{aligned}\langle R^a_{22}\rangle = &\left[\left(\langle D^2_{22}\rangle + \langle D^2_{-2-2}\rangle\right)\right.\\ &\left.-\left(\langle D^2_{-22}\rangle + \langle D^2_{2-2}\rangle\right)\right]/2,\end{aligned} \tag{3.2.9}$$

$$\langle I^a_{22}\rangle = \left[\left(\langle D^2_{22}\rangle - \langle D^2_{-2-2}\rangle\right) - \left(\langle D^2_{-22}\rangle - \langle D^2_{2-2}\rangle\right)\right]/2i. \tag{3.2.10}$$

As usual, the Cartesian representation of the order parameters gives us the direct information on the ordering of molecular axes. The nine order parameters can be related to the Saupe ordering matrices (see equation (2.4.11)) by

$$\langle R_{00}\rangle = S^{ZZ}_{zz}, \tag{3.2.11}$$

$$\langle R_{02}\rangle = \frac{1}{\sqrt{6}}\left(S^{ZZ}_{xx} - S^{ZZ}_{yy}\right), \tag{3.2.12}$$

$$\langle I_{02}\rangle = \sqrt{\frac{2}{3}} S^{ZZ}_{xy}, \tag{3.2.13}$$

and

$$\langle R_{20}\rangle = \frac{1}{\sqrt{6}}\left(S^{XX}_{zz} - S^{YY}_{zz}\right), \tag{3.2.14}$$

$$\langle R^s_{22}\rangle = \frac{1}{3}\left[\left(S^{XX}_{xx} - S^{YY}_{xx}\right) - \left(S^{XX}_{yy} - S^{YY}_{yy}\right)\right], \tag{3.2.15}$$

$$\langle I^s_{22}\rangle = \frac{2}{3}\left(S^{XX}_{xy} - S^{YY}_{xy}\right), \tag{3.2.16}$$

and

$$\langle I_{20}\rangle = -\sqrt{\frac{2}{3}} S^{XY}_{zz}, \tag{3.2.17}$$

$$\langle R^a_{22}\rangle = \frac{2}{3}\left(S^{XY}_{xy} + S^{YX}_{xy}\right), \tag{3.2.18}$$

$$\langle I^a_{22}\rangle = -\frac{2}{3}\left(S^{XY}_{xx} - S^{XY}_{yy}\right). \tag{3.2.19}$$

Hence, the C_{2h} ordering in the molecules and the phase are represented by the Cartesian super matrices S^{AB}_{xy} and S^{XY}_{ab}, respectively, where $\{A, B\}$ can be any of $\{X, Y, Z\}$ and $\{a, b\}$ any of $\{x, y, z\}$. In addition to the nine second-rank order parameters, there is another rank one order parameter with pseudo character. It is in keeping with the calculations by Mettout [75] about the number of order parameter tensors using character theory. This first-rank order parameter can be seen clearly by considering the Cartesian ordering tensors (2.4.11). If we define z to be the C_2 rotation axis in the molecule and Z that in the phase then the ordering supermatrix has

the form

$$\mathbf{S} = \begin{pmatrix} S_{xx}^{XX} & S_{xx}^{XY} & 0 & S_{xy}^{XX} & S_{xy}^{XY} & 0 & 0 & 0 & 0 \\ S_{xx}^{YX} & S_{xx}^{YY} & 0 & S_{xy}^{YX} & S_{xy}^{YY} & 0 & 0 & 0 & 0 \\ 0 & 0 & S_{xx}^{ZZ} & 0 & 0 & S_{xy}^{ZZ} & 0 & 0 & 0 \\ S_{yx}^{XX} & S_{yx}^{XY} & 0 & S_{yy}^{XX} & S_{yy}^{XY} & 0 & 0 & 0 & 0 \\ S_{yx}^{YX} & S_{yx}^{YY} & 0 & S_{yy}^{YX} & S_{yy}^{YY} & 0 & 0 & 0 & 0 \\ 0 & 0 & S_{yx}^{ZZ} & 0 & 0 & S_{yy}^{ZZ} & 0 & 0 & 0 \\ 0 & 0 & 0 & 0 & 0 & 0 & S_{zz}^{XX} & S_{zz}^{XY} & 0 \\ 0 & 0 & 0 & 0 & 0 & 0 & S_{zz}^{YX} & S_{zz}^{YY} & 0 \\ 0 & 0 & 0 & 0 & 0 & 0 & 0 & 0 & S_{zz}^{ZZ} \end{pmatrix}. \quad (3.2.20)$$

By using the Cartesian tensor notation to describe the ordering of the phase, we can see more easily the effects of the molecular and phase symmetries. If the constituent molecules have D_{2h} symmetry, the molecular axes are defined which are the three molecular symmetry axes. Thus we would not have the off-diagonal tensor S_{xy}^{AB}. For C_{2h} molecules, only one molecular axis is defined by symmetry, which in this case is taken to be z. Since the other axes are not defined, although each tensor of the form S_{ab}^{AB} can be diagonalised with respect to the molecular axes, their principal axis frames only have one common axis, z. Similarly, in a phase with D_{2h} symmetry, the phase symmetry axes are defined and there is no off-diagonal tensor S_{ab}^{XY}. For the C_{2h} phase, only the Z axis is defined. Therefore, when we diagonalise the tensors S_{ab}^{AB} with respect to the phase axes, their principal axis frames only have one common axis, Z.

It is clear that the diagonal submatrices S_{aa}^{AB} are symmetric about their diagonals. In marked contrast, the two off-diagonal submatrices S_{xy}^{AB} and S_{yx}^{AB} are not symmetric about their diagonals. We can write the non-symmetric matrix as the sum of an anti-symmetric matrix and a

symmetric one

$$\begin{pmatrix} S_{xy}^{XX} & S_{xy}^{XY} & 0 \\ S_{xy}^{YX} & S_{xy}^{YY} & 0 \\ 0 & 0 & S_{xy}^{ZZ} \end{pmatrix} \equiv \begin{pmatrix} 0 & (S_{xy}^{XY} - S_{xy}^{YX})/2 & 0 \\ -(S_{xy}^{XY} - S_{xy}^{YX})/2 & 0 & 0 \\ 0 & 0 & 0 \end{pmatrix} + \begin{pmatrix} S_{xy}^{XX} & (S_{xy}^{XY} + S_{xy}^{YX})/2 & 0 \\ (S_{xy}^{XY} + S_{xy}^{YX})/2 & S_{xy}^{YY} & 0 \\ 0 & 0 & S_{xy}^{ZZ} \end{pmatrix}. \tag{3.2.21}$$

Now the anti-symmetric supermatrix contains just a single element

$$S_{xy}^{XY} - S_{xy}^{YX} = (3/2)\langle(\mathbf{x}\cdot\mathbf{X})(\mathbf{y}\cdot\mathbf{Y}) - (\mathbf{x}\cdot\mathbf{Y})(\mathbf{y}\cdot\mathbf{X})\rangle, \tag{3.2.22}$$

and use of the Binet-Cauchy identity [81] allows this to be written as

$$S_{xy}^{XY} - S_{xy}^{YX} = (3/2)\langle(\mathbf{x}\wedge\mathbf{y})\cdot(\mathbf{X}\wedge\mathbf{Y})\rangle. \tag{3.2.23}$$

The two cross products define, in a sense, the axes $\mathbf{z}$ and $\mathbf{Z}$ in the molecular and phase frames, respectively. There is, however, a fundamental difference between these and the conventional axes, $\mathbf{z}$ and $\mathbf{Z}$, which are polar vectors, that is they change sign under inversion through the centre of symmetry of the respective coordinate system. In contrast the vectors defined by the cross products are axial or pseudovectors, that is they do not change sign under inversion. To distinguish between these two classes of vector we add a tilde to the pseudovectors so that the independent element of the anti-symmetric supermatrix is given by

$$S_{xy}^{XY} - S_{xy}^{YX} = (3/2)\langle\tilde{\mathbf{z}}\cdot\tilde{\mathbf{Z}}\rangle. \tag{3.2.24}$$

Since neither $\tilde{\mathbf{z}}$ nor $\tilde{\mathbf{Z}}$ changes sign when inverted through the centre of symmetry of their respective frames this means that the order parameter $(S_{xy}^{XY} - S_{xy}^{YX})$ is invariant under inversion and does not vanish for a molecule with C_{2h} point group symmetry in a phase having the same symmetry. This contrasts with the behaviour of the analogous order parameter $\langle\mathbf{z}\cdot\mathbf{Z}\rangle$ defined in terms of the axes in the molecular and phase frames. These are conventional vectors and so change sign when the respective system, molecule or phase, is inverted through the centre of symmetry. In consequence, the polar order parameter $\langle\mathbf{z}\cdot\mathbf{Z}\rangle$ changes sign and so must vanish in the C_{2h} phase, unlike the pseudovector order parameter, $\langle\tilde{\mathbf{z}}\cdot\tilde{\mathbf{Z}}\rangle$.

We have introduced these order parameters using the Cartesian language since this leads logically to the definition of the pseudovector order parameter. However, this and the polar order parameter can also be written in terms of Wigner functions. Thus

$$\langle\mathbf{z}\cdot\mathbf{Z}\rangle = \langle D_{00}^{1}\rangle, \tag{3.2.25}$$

and

$$\langle \tilde{\mathbf{z}} \cdot \tilde{\mathbf{Z}} \rangle = \langle \tilde{D}^1_{00} \rangle, \tag{3.2.26}$$

where the tilde again indicates the definition in terms of pseudovectors for the molecule and for the phase. The consequence of this is that $\langle D^1_{00} \rangle$ changes sign on inverting through the centre of symmetry in the C_{2h} phase and so this polar order parameter vanishes. This contrasts with the behaviour of the pseudovector order parameter $\langle \tilde{D}^1_{00} \rangle$ which does not change sign on inversion and so does not vanish in a C_{2h} phase composed of molecules with the same symmetry.

3.2.3 Potential of Mean Torque

The potential of mean torque is constructed according to equation (2.3.2). For the NC_{2h} phase composed of molecules with C_{2h} symmetry, it can be written in terms of the combined interaction coefficients and order parameters. Given a large number of intermolecular coefficients and order parameters, the potential of mean torque has a complex form which can be conveniently split into three parts

$$U(\Omega) = U_U(\Omega) + U_{D_{2h}}(\Omega) + U_{C_{2h}}(\Omega), \tag{3.2.27}$$

where the individual terms responsible for driving the appearance of the three nematic phases, N_U, ND_{2h} and NC_{2h} are

$$\begin{aligned} U_U(\Omega) = -\big[&(\langle R_{00}\rangle + 2\gamma_s\langle R_{02}\rangle - 2\gamma_a\langle I_{02}\rangle)\, R_{00}(\Omega) \\ &+ (2\gamma_s\langle R_{00}\rangle + 4\lambda_s\langle R_{02}\rangle - 2\lambda_0\langle I_{02}\rangle)\, R_{02}(\Omega) \\ &+ (-2\gamma_a\langle R_{00}\rangle - 2\lambda_0\langle R_{02}\rangle - 4\lambda_a\langle I_{02}\rangle)\, I_{02}(\Omega)\big], \end{aligned} \tag{3.2.28}$$

$$\begin{aligned} U_{D_{2h}}(\Omega) = -2\big[&(\langle R_{20}\rangle + \gamma_s\langle R^s_{22}\rangle - \gamma_a\langle I^s_{22}\rangle)\, R_{20}(\Omega) \\ &+ (\gamma_s\langle R_{20}\rangle + \lambda_s\langle R^s_{22}\rangle - (1/2)\lambda_0\langle I^s_{22}\rangle)\, R^s_{22}(\Omega) \\ &+ (-\gamma_a\langle R_{20}\rangle - (1/2)\lambda_0\langle R^s_{22}\rangle - \lambda_a\langle I^s_{22}\rangle)\, I^s_{22}(\Omega)\big], \end{aligned} \tag{3.2.29}$$

$$\begin{aligned} U_{C_{2h}}(\Omega) = -2\big[&(\langle I_{20}\rangle + \gamma_s\langle I^a_{22}\rangle + \gamma_a\langle R^a_{22}\rangle)\, I_{20}(\Omega) \\ &+ (\gamma_a\langle I_{20}\rangle + (1/2)\lambda_0\langle I^a_{22}\rangle - \lambda_a\langle R^a_{22}\rangle)\, R^a_{22}(\Omega) \\ &+ (\gamma_s\langle I_{20}\rangle + \lambda_s\langle I^a_{22}\rangle + (1/2)\lambda_0\langle R^a_{22}\rangle)\, I^a_{22}(\Omega)\big]. \end{aligned} \tag{3.2.30}$$

Here, some explicit formulae for the angular dependent terms are given in equation (2.4.8) with

$R^s_{22}(\Omega) = R_{22}(\Omega)$. In addition, the explicit formulae for the new angular dependent terms are

$$
\begin{aligned}
I_{02}(\Omega) &= -\sqrt{\frac{3}{2}}\sin^2\beta\sin 2\gamma, \\
I_{20}(\Omega) &= -\sqrt{\frac{3}{2}}\sin^2\beta\sin 2\alpha, \\
R^s_{22}(\Omega) &= \frac{1}{2}\left(1+\cos^2\beta\right)\cos 2\gamma\cos 2\alpha - \cos\beta\sin 2\gamma\sin 2\alpha, \\
I^s_{22}(\Omega) &= -\frac{1}{2}\left(1+\cos^2\beta\right)\sin 2\gamma\cos 2\alpha - \cos\beta\cos 2\gamma\sin 2\alpha, \\
R^a_{22}(\Omega) &= -\frac{1}{2}\left(1+\cos^2\beta\right)\sin 2\gamma\sin 2\alpha + \cos\beta\cos 2\gamma\cos 2\alpha, \\
I^a_{22}(\Omega) &= -\frac{1}{2}\left(1+\cos^2\beta\right)\cos 2\gamma\sin 2\alpha - \cos\beta\sin 2\gamma\cos 2\alpha.
\end{aligned}
\tag{3.2.31}
$$

We note that our definitions of the order parameters and angular functions are different from Osipov *et al.* [65] and Gorkunov *et al.* [66]. In Osipov *et al.* [65], where they considered D_{2h} phase formed from C_{2h} molecules, the major molecular axis z is not the symmetry axis, instead, the symmetry axis is a minor axis. In Gorkunov *et al.*'s theory for C_{2h} phase formed from C_{2h} molecules [66], both the major molecular axis z and the major phase axis Z are not the symmetry axes of the molecule and the phase, respectively. In contrast, in our model, both the major axes are also the symmetry axes.

3.3 Approximate Model

Now we see that our system depends on six interaction coefficients and nine order parameters. These large numbers present a challenging problem. First of all, it is a challenge in choosing the values for these interaction coefficients. Secondly, minimising the free energy with respect to nine order parameters is a formidable task. In order to simplify the problem, we use an approximate model which is analogous to that used in the calculation for biaxial nematics formed from molecules with D_{2h} symmetry by Sonnet *et al.* [13]. We note from the Cartesian representations of the order parameters for D_{2h} molecules in D_{2h} phase in equations (2.4.12). At ground state, the order parameters S and C are non zero whereas the other order parameters, D and P vanish. Thus, in their model, Sonnet *et al.* [13] set the order parameters D and P to zero. In addition, they set the coefficient γ which scale these order parameters in the potential of mean torque to zero. Thus, we see from the order parameters for C_{2h} molecules in equations (2.4.12) and from (3.2.11) to (3.2.19), the order parameters which tend to zero at perfect order are $\langle R_{02}\rangle$, $\langle R_{20}\rangle$, $\langle I_{02}\rangle$, $\langle I_{20}\rangle$, $\langle I^s_{22}\rangle$ and $\langle I^a_{22}\rangle$. In our approximate model, we set these order parameters together with the interaction coefficients γ_s, γ_a and λ_0 to zero. Now our model depends on three order parameters $\langle R_{00}\rangle$, $\langle R^s_{22}\rangle$, $\langle R^a_{22}\rangle$ and two interaction coefficients λ_s and λ_a. We will see later that this dramatic approximation can still retain some essential physics. It is because it is still able to stabilise the three nematic phases: uniaxial, biaxial phase with D_{2h} symmetry and another biaxial nematic phase with C_{2h} symmetry. In the next section we use the stability analysis to

find the range of values for the parameters λ_s and λ_a which can stabilise the biaxial nematic phase with C_{2h} symmetry at the ground state.

3.3.1 Stability Analysis

The pair potential for the truncated model can be written in terms of the products of the molecular vectors as

$$\begin{aligned} U_{ij}(\mathbf{x}_1,\mathbf{y}_1,\mathbf{z}_1,\mathbf{x}_2,\mathbf{y}_2,\mathbf{z}_2) = -u_{200}\left\{(3(\mathbf{z}_1.\mathbf{z}_2)^2-1)/2\right. \\ + \lambda_s\left[(\mathbf{x}_1.\mathbf{x}_2)^2+(\mathbf{y}_1.\mathbf{y}_2)^2-(\mathbf{x}_1.\mathbf{y}_2)^2-(\mathbf{y}_1.\mathbf{x}_2)^2\right] \\ \left. + 2\lambda_a\left[(\mathbf{x}_1.\mathbf{x}_2).(\mathbf{y}_1.\mathbf{y}_2)+(\mathbf{x}_1.\mathbf{y}_2).(\mathbf{y}_1.\mathbf{x}_2)\right]\right\}. \end{aligned} \tag{3.3.1}$$

We consider a rotation $\mathbf{R}$ around an arbitrary axis $\mathbf{a}=(a_1,a_2,a_3)^T$ about an angle θ that takes the first molecule into the second [55] (see Appendix D)

$$\mathbf{R} = \mathbf{e}^{\theta\mathbf{A}}, \tag{3.3.2}$$

where $\mathbf{A}$ is the skew-symmetric tensor associated with $\mathbf{a}$

$$\mathbf{A} = \begin{pmatrix} 0 & -a_3 & a_2 \\ a_3 & 0 & -a_1 \\ -a_2 & a_1 & 0 \end{pmatrix}$$

Consider the case that these two molecules are so nearly parallel to one another that the terms $O(\theta^3)$ are negligible in the rotation that takes the first molecule into the second. Thus

$$\mathbf{R} = \mathbf{I} + \theta\mathbf{A} + (1/2)\theta^2\mathbf{A}^2. \tag{3.3.3}$$

Expanding the pair potential in terms of θ up to second order we find that the energy difference between the pair potential and the ground state (the state of complete alignment of the two molecules where $\theta = 0$) is

$$\delta U(\Omega) = -u_{200}\theta^2\left[(1.5+\lambda_s+\lambda_a)\,a_1^2+(1.5+\lambda_s+\lambda_a)\,a_2^2+4\,(\lambda_s+\lambda_a)\,a_3^2\right]. \tag{3.3.4}$$

Any small rotation away from the state of complete alignment of two molecules should be unstable and the pair energy is increased. Therefore the incremental energy should be positive which gives us the following *stability region*

$$\lambda_s + \lambda_a > 0. \tag{3.3.5}$$

3.3.2 Equilibrium Free Energy

The approximate potential of mean torque can be written as

$$U_{\mathrm{trun}}(\Omega)/u_{200} = -\left[\langle R_{00}\rangle R_{00}(\Omega) + 2\lambda_s\langle R^s_{22}\rangle R^s_{22}(\Omega) + 2\lambda_a\langle R^a_{22}\rangle R^a_{22}(\Omega)\right]. \tag{3.3.6}$$

The Helmholtz free energy associated with this takes the form

$$A^* = (1/2)T^{*-1}\left(\langle R_{00}\rangle^2 + 2\lambda_s\langle R^s_{22}\rangle^2 + 2\lambda_a\langle R^a_{22}\rangle^2\right) - \ln Q, \tag{3.3.7}$$

where the partition function is given by

$$Q = \int \exp\left(-U^*_{\text{trun}}(\Omega)/T^*\right) d\Omega, \tag{3.3.8}$$

It should be noted that, in this approximation, there are strictly only three order parameters, namely $\langle R_{00}\rangle$, $\langle R^s_{22}\rangle$ and $\langle R^a_{22}\rangle$. This is because there are special symmetry operations of this model which make the other order parameters vanish while leving the distribution function invariant. The order parameters $\langle R_{02}\rangle$, $\langle I_{02}\rangle$, $\langle R_{20}\rangle$ and $\langle I_{20}\rangle$ vanish due to the symmetry operation $C_4(z)C_4(Z)$. In addition, the order parameters $\langle I^s_{22}\rangle$ and $\langle I^a_{22}\rangle$ vanish due to the symmetry operation $C_2(x)C_2(X)$.

3.4 Calculations and Results

3.4.1 Phase Behaviour

In keeping with the calculations by Sonnet, Virga and Durand [13], we choose the parameter λ_s to be within their investigated range which is from 0 to 0.5. Hence we fix λ_s to 0.2, 0.3 and 0.4 and vary λ_a to calculate three phase maps describing the phase behaviour of our system. The three phase maps are shown in figures 3.2.

In figure 3.2(a) we show a phase map for $\lambda_s = 0.2$. We see that the transition temperatures for $ND_{2h} - N_U$ and $N_U - I$ are both independent of the parameter λ_a. This is because in the truncated approximate model λ_a does not contribute to the ordering of the phases ND_{2h} and N_U. In contrast, the NC_{2h} phase becomes more stable upon increasing λ_a. At λ_a equals 0.2, the ND_{2h} phase region disappears and now there is a direct $NC_{2h} - N_U$ transition. It is interesting that as λ_a is greater than 0.2, there is a new phase. This new phase, first separates NC_{2h} from N_U and later from the isotropic phase. This new phase is characterised by the non zero values of the order parameters $\langle R_{00}\rangle$ and $\langle R^a_{22}\rangle$ whereas $\langle R^s_{22}\rangle$ vanishes. What we have found is not expected since it does not fit in with our previous understanding of the three nematic phases N_U, ND_{2h} and NC_{2h}. That is, the ND_{2h} phase should be characterised by the order parameters $\langle R_{00}\rangle$ and $\langle R^s_{22}\rangle$ whereas the NC_{2h} phase should be characterised by all three order parameters. In figure 3.2 we denote this new phase as $ND_{2h}(\perp)$ and the convensional nematic phase with D_{2h} symmetry as $ND_{2h}(||)$ due to subsequent identification of the new nematic phase. For now as the phase has not been identified, we refer to it as the N_{B-} phase. We come back to the identification of this phase later in this section. In analogy with the results by Sonnet *et al.* [13], the $ND_{2h} - N_U$ transition is second order and the $N_U - I$ transition is first order and the order of the phase transitions are also independent of the parameter λ_a. In addition, both the $NC_{2h} - ND_{2h}$ and $NC_{2h} - N_{B-}$ transitions are second order. For small values of λ_a, the $N_{B-} - N_U$ phase transition is second order. At $\lambda_a = 0.3$, there is a tricritical point. For λ_a greater than that, the $N_{B-} - N_U$ is first order. Finally, the $N_{B-} - I$ phase transition is

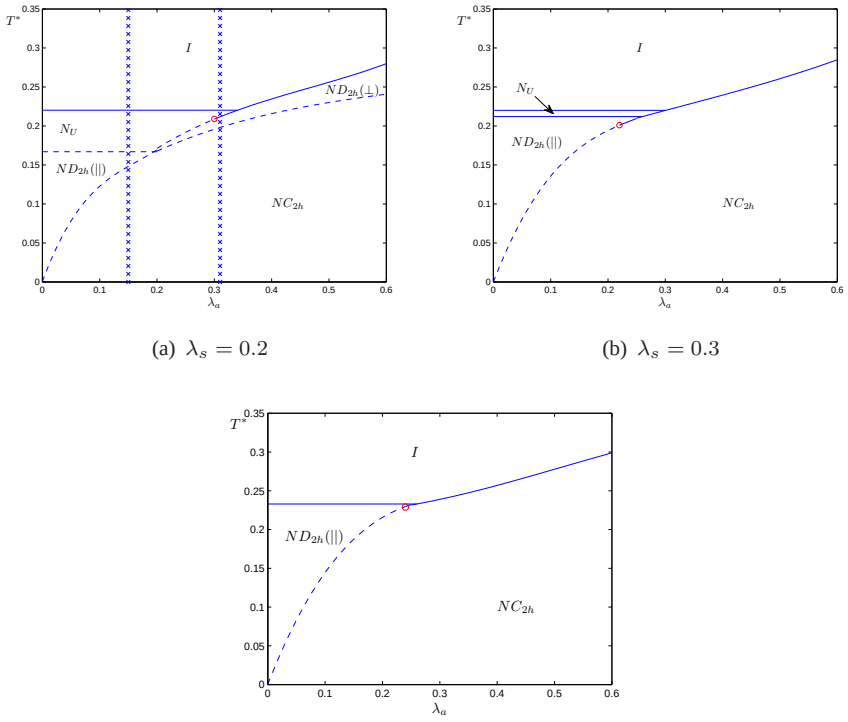

(a) $\lambda_s = 0.2$ (b) $\lambda_s = 0.3$

(c) $\lambda_s = 0.4$

FIGURE 3.2: The phase map predicted by the truncated model potential (see equation (3.3.6)) for a nematogen composed of biaxial molecules with C_{2h} symmetry; the phase behaviour is shown as a function of the relative biaxiality coefficient λ_a, with λ_s of (a) 0.2, (b) 0.3 and (c) 0.4. The phase labelled in the text as N_{B-} is here indicated by $ND_{2h}(\perp)$ given its subsequent identification. The dashed line indicates second order phase transitions and solid lines denote first order phase transitions; a circle shows a tricritical point. The vertical crosses indicate the temperature over which the order parameters shown in figure 3.3 were calculated.

first order. This is in analogy with the approximate model by Sonnet *et al.* [13] that the biaxial nematic-to-isotropic phase transition is first order for a long range of temperature.

Next, we show the phase map for $\lambda_s = 0.3$ in figure 3.2(b). We see now that the extent of the N_U phase is much narrower. It is because the strength of the biaxial interaction is higher which pushes the biaxial nematic boundary up. Moreover, the biaxial interaction does not contribute to the uniaxial ordering and so it does not influence the uniaxial nematic-to-isotropic phase transition temperature. In addition, the $ND_{2h} - N_U$ phase transition is first order, in contrast with that for $\lambda_s = 0.2$, which is second order. This indicates a tricritical behaviour. Here we do not find the N_{B-} phase. The reason might be that the larger value for λ_s of 0.3 drives the appearance of $\langle R^s_{22} \rangle$, thus inhibiting the formation of the N_{B-} phase. We find a tricritical point along the $NC_{2h} - ND_{2h}$ phase boundary at $\lambda_a = 0.22$, separating a second order transition from a first order one along the $NC_{2h} - ND_{2h}$ transition line. In this case we find that the biaxial nematic NC_{2h}-to-isotropic phase transition is first order.

We have also explored another region of the phase map by setting $\lambda_s = 0.4$. According to the calculations of Sonnet *et al.* [13] with $\lambda_a = 0$, the system exhibits a first order transition directly from the isotropic phase to the ND_{2h} phase. As λ_a increases from zero the $ND_{2h} - I$ transition

temperature does not change. On the other hand, first the $NC_{2h} - ND_{2h}$ then the $NC_{2h} - I$ phase transitions grow with λ_a. Again, we do not find the N_{B-} phase for this value of λ_s which we have found for λ_s of 0.2. A tricritical point is found in this case along the $NC_{2h} - ND_{2h}$ transition line at $\lambda_a = 0.24$. Moreover, the $NC_{2h} - I$ phase transition is also first order, in similarity with what we have found for a smaller value for λ_s of 0.3.

3.4.2 Identifying The N_{B-} Nematic Phase

In order to identify the N_{B-} biaxial nematic phase, we plot the dependence of the order parameter on the scaled temperature for $\lambda_s = 0.2$ in figure 3.3. In figure 3.3(a) we show temperature dependence of the order parameters for $\lambda_a = 0.15$ where we expect the phase sequence $NC_{2h} - ND_{2h} - N_U - I$. As we lower the temperature, first there appears a jump in the order parameter $\langle R_{00} \rangle$, indicating a first order $N_U - I$ transition, as expected. Next, the order param-

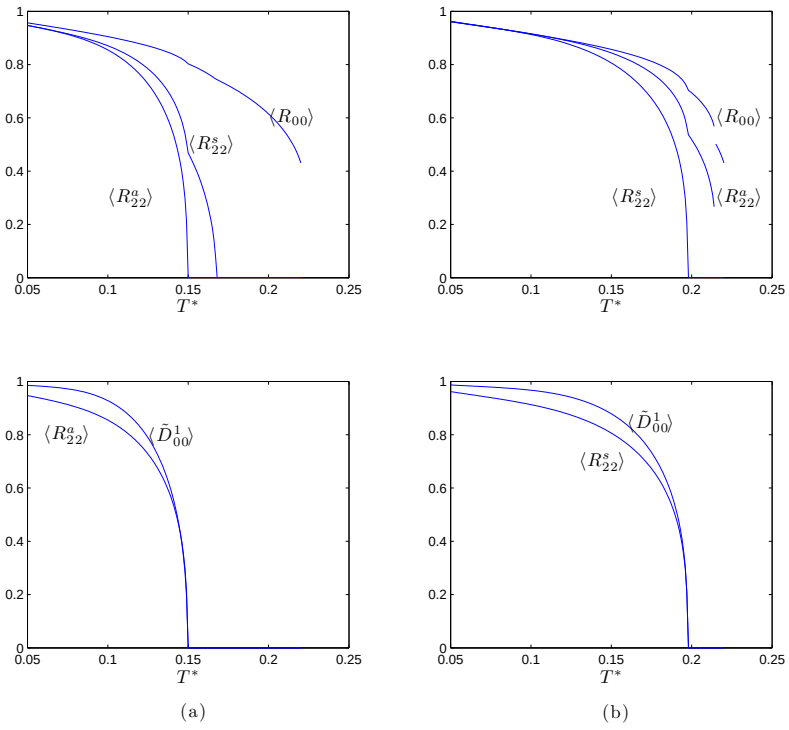

FIGURE 3.3: The dependence of the three order parameters $\langle R_{00} \rangle$, $\langle R^s_{22} \rangle$ and $\langle R^a_{22} \rangle$ calculated with $\lambda_s = 0.2$ and (a) $\lambda_a = 0.15$ and (b) $\lambda_a = 0.31$ on the scaled temperature T^*. In addition the temperature variation of the pseudovector based order parameter, $\langle \tilde{D}^1_{00} \rangle$, is shown in comparison with (a) $\langle R^a_{22} \rangle$ and (b) $\langle R^s_{22} \rangle$.

eter $\langle R^s_{22} \rangle$ increases gradually from zero, indicating a second order $ND_{2h} - N_U$ transition. We also note a slight increase in the rate of change of $\langle R_{00} \rangle$ at the phase transition. As the temperature is lowered further, the order parameter $\langle R^a_{22} \rangle$ increases steeply but continuously from zero, indicating also a second order $NC_{2h} - ND_{2h}$ transition. The order parameters $\langle R_{00} \rangle$ and $\langle R^s_{22} \rangle$ also increase continuously at the phase transition. In addition to the second-rank order parameters, we also calculate the pseudovector order parameter $\langle \tilde{D}^1_{00} \rangle$. As we expect, this order parameter vanishes in the N_U and ND_{2h} phases and gradually increases in the NC_{2h} phase.

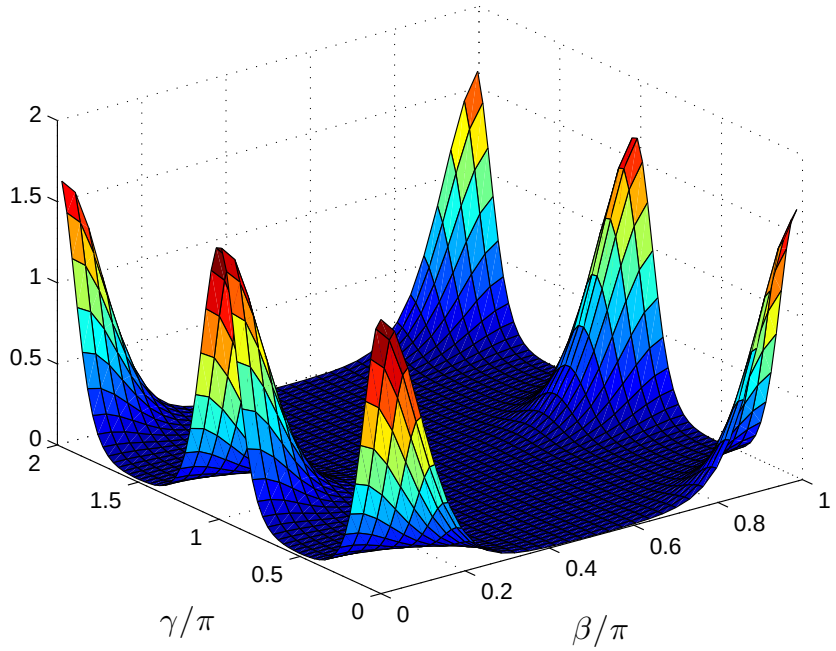

FIGURE 3.4: Distribution function of the $ND_{2h}(||)$ phase as a function of the Euler angles β and γ when α is set equal to zero at $\lambda_s = 0.4$, $\lambda_a = 0.2$ and the scaled temperature $T^* = 0.22$.

Now we move to figure 3.3(b) where we find the new, unidentified phase at $\lambda_a = 0.31$. First, we find that the order parameter $\langle R_{00} \rangle$ jumps at the $N_U - I$. As we lower the temperature, both $\langle R_{00} \rangle$ and $\langle R^a_{22} \rangle$ increase discontinuously, indicating a first order transition to the new phase. At the transition to the NC_{2h} phase, the order parameter $\langle R^s_{22} \rangle$ increases continuously and joins with the other two, indicating a second order transition. What is important here is the pseudovector order parameter only becomes non-zero in the NC_{2h} phase where the other three order parameters are non-zero. Thus the phase with only $\langle R_{00} \rangle$ and $\langle R^a_{22} \rangle$ non-zero is not NC_{2h}.

In order to determine the symmetry of the N_{B-} phase, we plot the singlet distribution function for the nematic phases: $ND_{2h}(||)$, N_{B-}, NC_{2h}. In figure 3.4 we show the distribution function of the nematic phase with D_{2h} symmetry. The distribution function is shown as a function of the Euler angles γ and β when the angle α is set equal to zero. Here we see that the distribution function is maximised when the angles β and γ are multiples of π. It is when the molecular axes (x, y, z) are parallel or antiparallel with those of the phase axes (X, Y, Z).

Now we look at the distribution function for the C_{2h} phase in figure 3.5. The distribution function is maximised at $\beta = 0$ and when γ is a multiple of π, indicating that the x and y axes are parallel and antiparallel with the X and Y axes of the phase. This is because Z is a two-fold rotation axis of the phase. However now we do not see the same maxima when $\beta = \pi$ since in this case the X and Y axes are not two-fold rotation axes.

In figure 3.6 we plot the distribution function for the N_{B-} phase. This phase still has the maxima at $\beta = 0$ and γ is a multiple of π. However, at the maxima with $\beta = \pi$, γ is shifted by $\pi/2$ in comparison with that for $\beta = 0$. To investigate this further, we plot the distribution function as a function of the angles β and γ when α is set equal to $\pi/4$ in figure 3.7. We see now that

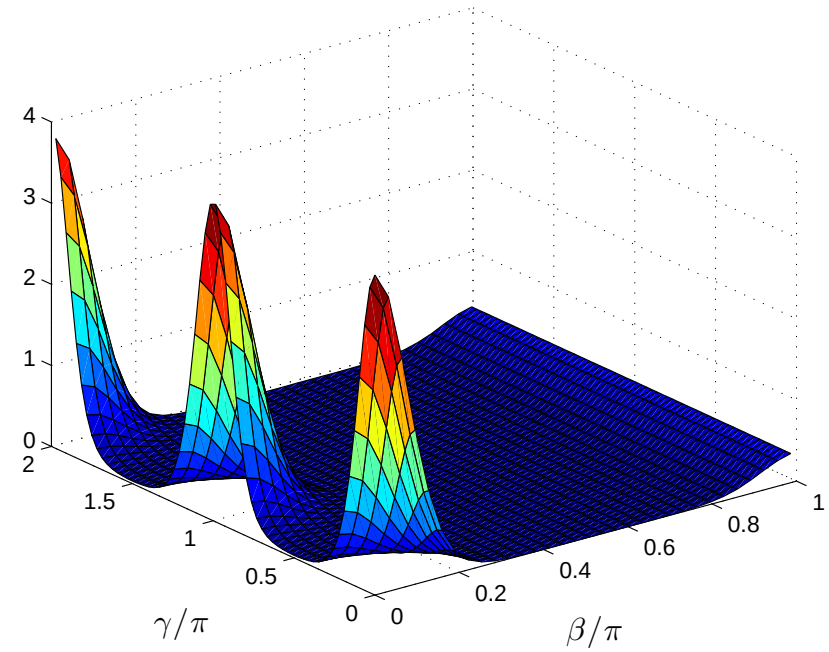

FIGURE 3.5: Distribution function of the NC_{2h} phase as a function of the Euler angles β and γ when α is set equal to zero at $\lambda_s = 0.2$, $\lambda_a = 0.2$ and the scaled temperature $T^* = 0.165$.

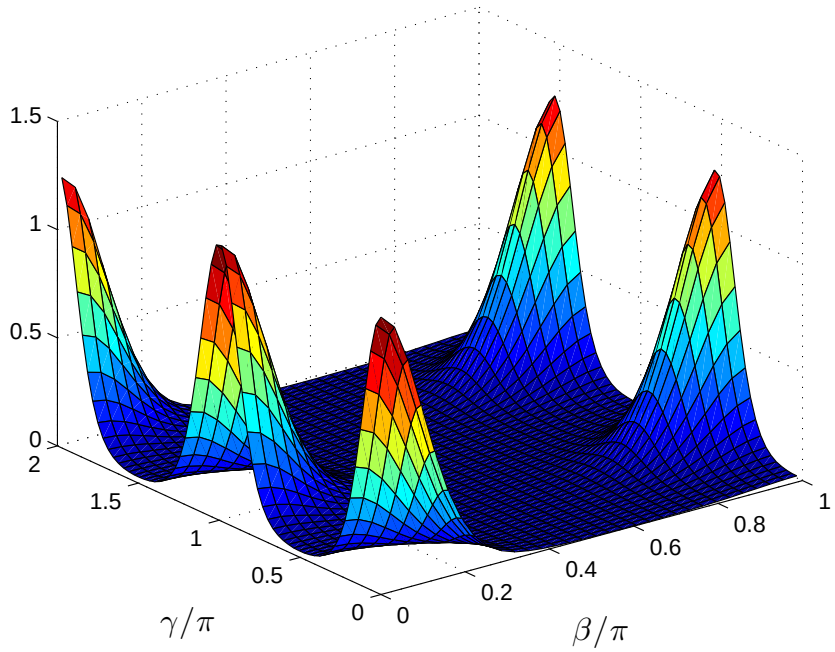

FIGURE 3.6: Distribution function of the $ND_{2h}(\perp)$ (N_{B-}) phase as a function of the Euler angles β and γ when α is set equal to zero at $\lambda_s = 0.2$, $\lambda_a = 0.4$ and the scaled temperature $T^* = 0.23$.

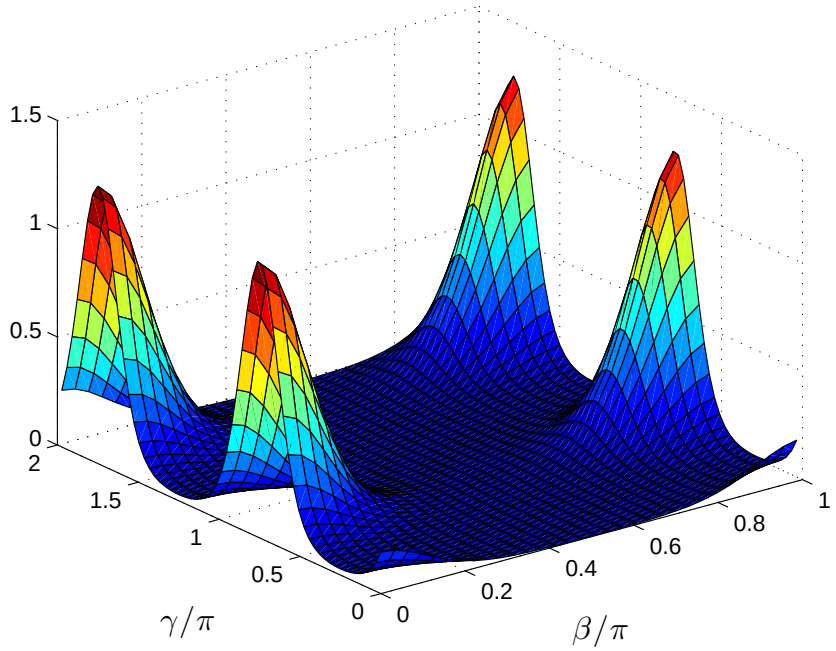

FIGURE 3.7: Distribution function of the $ND_{2h}(\perp)$ (N_{B-}) phase as a function of the Euler angles β and γ when α is set equal to $\pi/4$ at $\lambda_s = 0.2$, $\lambda_a = 0.4$ and the scaled temperature $T^* = 0.23$.

the values of γ at the maxima for $\beta = \pi$ are the same as those for $\beta = 0$. However, the values of γ at the maxima are now at multiples of π minus $\pi/4$. This suggests to us that a coordinate transformation of $\alpha + \pi/4$ and $\gamma - \pi/4$ would make the distribution of the N_{B-} phase the same as the ND_{2h} phase. In fact these transformations lead to a remarkable change in the functions defining the two order parameters. Thus

$$R^a_{22}(\alpha, \beta, \gamma) \xrightarrow[\text{rotations}]{\pi/4} R^s_{22}(\alpha', \beta, \gamma') \tag{3.4.1}$$

$$R^s_{22}(\alpha, \beta, \gamma) \xrightarrow[\text{rotations}]{\pi/4} R^a_{22}(\alpha', \beta, \gamma') \tag{3.4.2}$$

where the two rotations take place about the z and Z axes. The results of the transformation to the new molecular and phase frames interchanges the order parameters $\langle R^s_{22} \rangle$ and $\langle R^a_{22} \rangle$ so that in the new frames $\langle R^s_{22} \rangle$ is non-zero and now it is $\langle R^a_{22} \rangle$ that vanishes. This is what we expect for a biaxial nematic phase with D_{2h} point group symmetry. To distinguish between the two ND_{2h} phases we have added the symbols ($\parallel$) and ($\perp$) to indicate whether the molecular minor axes are parallel or perpendicular in the biaxial nematic phase. In fact we should find the effect of the coordinate transformation on the interaction parameters λ_s and λ_a. Using equation (2.1.22), the coefficients u_{Lmn} transform under $\pm\pi/4$ rotation of molecular axes according to

$$u'_{Lmn} = \mathrm{e}^{\pm(m+n)\pi/4} u_{Lmn}. \tag{3.4.3}$$

Therefore the coefficient λ_s is mapped to $-\lambda_a$ and λ_a is mapped to $-\lambda_s$. Our study of the distribution function shows that an idealised picture of this phase at perfect order should look

like that in figure 3.8.

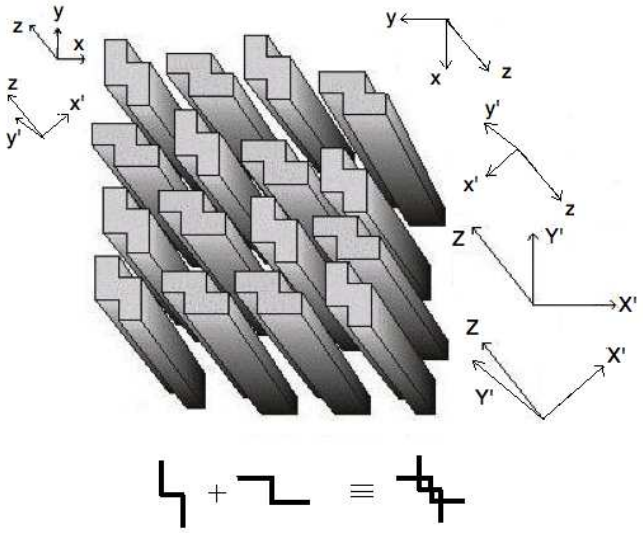

FIGURE 3.8: A sketch of the idealised organisation of molecules with C_{2h} point group symmetry in the biaxial nematic phase, $ND_{2h}(\perp)$, in which the minor axes of half the molecules tend to be perpendicular to those of the other half. The axis systems, (x' y' z) and (X' Y' Z), show the symmetry axes for this idealised ND_{2h} phase and the molecules forming it. The cross-section of the average structure obtained by merging molecules in which the x axes are orthogonal is also shown.

3.5 Conclusions

In this chapter, we have developed a molecular field theory to investigate biaxial nematics formed from molecules with C_{2h} symmetry. Thus the ground state of our system also has the same symmetry with the constituent molecules. This theory has a significantly larger number of order parameters and interaction coefficients in comparison with that for molecules and phases with D_{2h} symmetry. There are nine second-rank order parameters and six interaction coefficients in total. In addition, we also have a first-rank order parameter. In order to facilitate the calculations, we use an approximate model. In this model, the number of interaction coefficients is reduced to only two and the number of order parameters to three. This dramatic approximation still retains the essential physics and is able to describe a rich phase behaviour. In addition to the isotropic and uniaxial nematic phase, there are two biaxial nematic phase with D_{2h} symmetry. These two biaxial nematic phases are characterised by the alignment of the molecular axes. In the $D_{2h}(||)$ phase, the molecular axes tend to be parallel. This is in constrast with the $D_{2h}(\perp)$ where the molecular axes tend to be perpendicular. Moreover, we have found a biaxial nematic phase with C_{2h} symmetry at the ground state. This has the same symmetry with that of the constituent molecules.

The approximate model, even though takes a dramatic approximation, still retain much of the essential physics. It is expected that our calculation results for this model would help the interpretation of experimental studies of mesogens thought to form the biaxial nematic phase with C_{2h} symmetry. It seems that there are many facets of this model which merit further investigation.

Chapter 4

Polar Nematic Liquid Crystals formed from V-shaped molecules

Recent experimental evidence suggests that a class of V-shaped molecules might be a promising candidate for low molar thermotropic biaxial nematic liquid crystals [35, 36, 37]. Those molecules are made by linking two rod-like mesogenic groups through a central unit, which results in a rigid V-shaped core, with flexible hydrocarbon chains at both ends. They are also known as bent-core, banana-like, or boomerang-like [43]. Various experiments on those V-shaped molecules with the interarm angle of 140^{o} using different techniques, namely polarised microscopy, conoscopy, ^{2}H NMR spectroscopy [36], X-ray diffraction [35] and Raman scattering [37] have revealed the existence of a rich biaxial nematic phase with a first order direct transition to the isotropic phase. On the other hand, the molecular field theory and Monte Carlo simulations have shown that the biaxial nematic phase can only be formed at very low temperature for V-shaped molecules with that value of the interarm angle [3, 82]. Our interest in studying the dipolar interactions of V-shaped molecules stems from this disagreement between the theoretical and the experimental results.

An explanation to the disagreement between the theoretical predictions and the experimental results that has been proposed is that the molecular field theory and Monte Carlo simulations neglect a large molecular electrostatic dipolar interaction which may be present in the emprirical systems. In consequence, this could stabilise the formation of the biaxial nematic phase for large bend angles [36]. In addition to stabilising the biaxial nematic phase, we expect the dipolar interactions to stabilise the novel nematic phases with polar character [33].

In section 4.1 we discuss some related works which include dipolar interactions in the study of nematic liquid crystals. We review the classical molecular field theory for V-shaped molecules without dipolar interactions in 4.2. Then, in section 4.3 we extend the molecular field theory to include dipolar interactions. Next, in section 4.4 we describe our calculation results for the latter case. Two new major effects have been found by adding dipolar interactions into the theory. First, the biaxial nematic phase can be formed at high temperature for molecules with large interarm angle. These results agree with the Monte Carlo simulations and partly explain the disagreement between theoretical predictions and experimental results. Secondly, the polar uni-

axial and biaxial nematic phases can be stabilised which have not been confirmed in experiment. Finally, we conclude this chapter in section 4.5.

4.1 Related Works

The hypothesis of a large transverse dipolar interaction of V-shaped molecules has been examined by Bates [83] in a series of Monte Carlo simulations. In these simulations, two neighbouring molecules interact via a pair potential which depends on their relative orientation. The model pair potential consists of the normal second-rank interactions for V-shaped molecules [82] plus a (first-rank) dipolar interactions. Each molecular dipole points along the y axis in Figure 4.1.

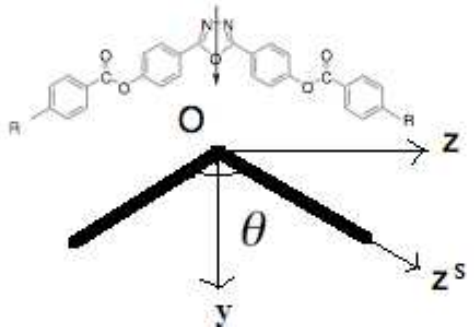

FIGURE 4.1: The coordinate axes labeled for a V-shaped molecules.

The nature of this dipolar interaction is not purely electrostatic but may include other types of intermolecular forces such as *steric* interaction. The steric interaction happens when two molecules are brought too close, the electron clouds overlap. Since more than one electrons cannot occupy the same quantum state due to *Pauli's exclusion principle*, there are repulsive forces between two molecules. The steric dipolar interaction is expected since interacting molecules have polar shapes. The temperature and hence the dipole strength are scaled with the second-rank tensor component along the z^s axis of an arm (analogous to u_{200}). The scaled dipole strength is called κ. The simulation results were given in four phase maps reproduced in figure 4.6. These show the dependence of the scaled transition temperature on the interarm angle from 100^{o} to 130^{o}. These figures correspond to four values of κ, namely 0, 0.2, 0.5 and 1.0. The first diagram in figure 4.6(a) shows a classical behaviour for systems without dipolar interaction as we have discussed in Chapter 2 with a Landau point joining the phase boundaries. As the dipole strength is increased to 0.2, with the corresponding phase map shown in figure 4.6(b), the biaxial nematic-to-uniaxial nematic transition temperature for θ near the tetrahedral angle as well as the biaxial nematic-to-isotropic phase transition at the Landau point are unchanged. However for values of the interarm angle that are not close to the Landau point, the biaxial nematic-to-uniaxial nematic transition temperature is increased. The phase map for $\kappa = 0.5$ is shown in figure 4.6(c). In this case, we still see a Landau point but now most of the $N_B - N_U$ phase boundary is raised in comparison with the classical case where dipolar interactions are not included. The last diagram in figure 4.6(d) shows the results for $\kappa = 1.0$. Now it is interesting that the Landau point is replaced by a line of first order direct biaxial nematic-to-isotropic phase transitions over a large range of the interarm angle from 107^{o} to 122^{o}. Below 107^{o} there is a narrow stripe of uniaxial nematic phase between the isotropic phase and the biaxial nematic phase. In conclusion, the simulations show that the biaxial nematic phase is more stabilised with stronger transverse dipolar interaction. In addition, there is a direct first order biaxial nematic-to-isotropic phase transition at high temperature for large interarm angles. The last result is somehow in agreement with the experimental evidences.

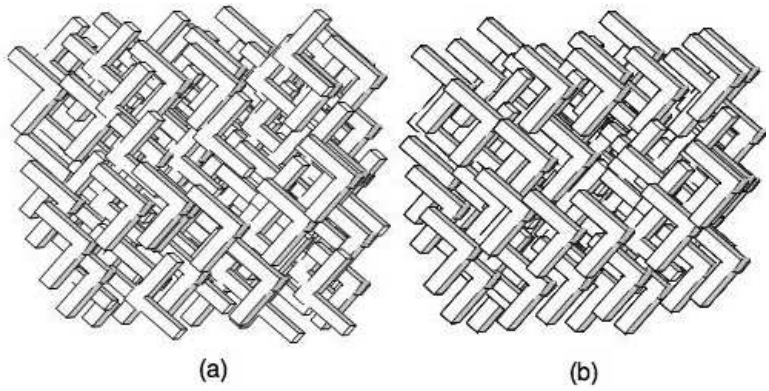

FIGURE 4.2: Idealised visualisations of (a) non-polar and (b) polar biaxial nematic phase formed from V-shaped molecules.

In comparison to the results by Bates [83] was the more recent calculations by Grzybowski and Longa [84]. Their calculations were of a low density approximation of the local density functional theory based on the Gay-Berne pair potential. This is a more realistic interaction potential compared to that used by Bates [83]. This is because the Gay-Berne model takes into account both attractive and repulsive interactions and is dependent on the intermolecular vector. Without the dipolar interaction, the model showed a similar phase map with the Landau point at 107° interarm angle. On increasing the dipole strength, the Landau point is shifted towards lower value of interarm angle. In contrast to this, as we have discussed, the model by Bates [83] predicts that the Landau point is broadened into a Landau line. Moreover, in the calculations by Grzybowski *et al.* [84], the biaxial nematic-to-uniaxial nematic transition temperature increases on increasing dipolar interaction strength for sufficiently large interarm angle ($\theta > 110^{\circ}$). This result supports the existence of the dipolar interaction in the system such that for large interarm angle the biaxial nematic phase is stabilised by dipolar interactions.

The existence of polar nematic phases has not been reported in the Monte Carlo simulations by Bates [83] and the density functional theory by Grzybowski and Longa [84]. A sketch of a polar and a non-polar phase is shown in figure 4.2. Phase polarity has been found in many liquid crystals, including nematics made of lyotropic system and thermotropic nematic polymer liquid crystals [85, 86, 87]. Even polar thermotropic biaxial nematic polymer liquid crystals have been found [87]. However, there has not been any hard evidence which suggests the existence of a polar low-molar thermotropic nematic liquid crystals although recent electro-optical experimental results have suggested that it might be possible [38]. The usefulness of polar low-molar thermotropic nematic liquid crystals has been discussed in reference [88]: "these materials might have useful technological applications due to their envisaged easy and fast response to an external electric field, coupled to fluidity and self-healing ability typical of nematics that is crucial to their use in electro-optical devices".

Despite the fact that polar biaxial nematic phases have not been found in real low-molar thermotropic systems, theoretical studies and computer simulations have shown that it should be possible for them to exist: "there is no fundamental reason that these ferroelectric phases should not exist" [89]. The possibility of a polar uniaxial nematic phase have been studied by several authors using a standard molecular field theory [89, 90], a two side cluster molecular field theory and Monte Carlo simulations [52] for dipolar anisotropic molecules and molecular dy-

namic simulations for dipolar spheres [91]. Their results suggest that the polar uniaxial nematic phase can be stabilised for a range of dipolar interaction strength. The polar uniaxial nematic phase can take a transition to the non-polar uniaxial nematic phase, followed by the uniaxial nematic-to-isotropic phase transition. Alternatively, there might be a direct polar uniaxial nematic-to-isotropic phase transition. In one case where the coupling between first and second rank interactions was allowed, the author found a tricritical point along the polar nematic-to-uniaxial nematic phase transition line [89]. In another model of polar uniaxial nematics using the two side cluster molecular field theory, two tricritical points were detected, one along the polar uniaxial nematic-to-non-polar uniaxial nematic and the other along the polar uniaxial nematic-to-isotropic phase boundaries [52].

The first theory which described the coesistence of biaxiality and polarity in thermotropic nematic liquid crystals seems to have been a Landau-de Gennes theory for a system of polymeric molecules of symmetry C_s by Mettout, Toledano, Takezoe and Watanabe [92]. The C_s group is a symmetry group with only an identity and a reflection plane. This work was stimulated by experimental evidence which found a polar biaxial nematic phase exhibiting in thermotropic polymer liquid crystals [87] although the mathematical structure is indistinguishable between polymeric and low molar mass systems. First, the authors only allowed for first-rank interaction while ignoring second and higher rank interactions. They found two nematic phases by varying the coefficients in the Landau-de Gennes free energy expansion: the isotropic phase, the polar uniaxial nematic phase (with $C_{\infty v}$ symmetry) and the polar biaxial nematic phase (with C_s symmetry). Here, the $C_{\infty v}$ symmetry group consists of an infinite rotation axis and a reflection plane with the axis of rotation lies in it, together with an identity. These results mean that the biaxial nematic phase can be stabilised only by one symmetry breaking mechanism which is molecular polarity. When the authors include second-rank interactions, they found a phase map with richer phase behaviour, including nematic phases with different symmetries as before, namely $D_{\infty h}$, $C_{\infty h}$, D_{2h}, C_{2v}, C_s and C_1. Since these symmetry groups are not relevant to our model we do not discuss them in detail. Their definition can be found in the book in reference [16]. Hence it seems that a biaxial nematic phase with symmetry other than C_s requires contributions from either only second-rank interaction or a combination of both first and second rank interactions. In the simulations by Bates the constituent molecules have C_{2v} symmetry and so by including both first and second rank interactions, we expect the system would be able to form polar nematics.

It is worth noting that in some calculations for the excluded volume of V-shaped molecules consisting of touching spheres [93, 80], the configuration where the dipoles are antiparallel is more favoured than when they are parallel. It is because in the former the excluded volume is smaller and the molecules tend to arrange in this way to minimise their excluded volume. These results also agreed with the calculations for an orientation-dependent second virial coefficient [80]. The authors found that, for a variety of shapes, this coefficient is smaller when the dipoles are parallel than when they are antiparallel. This also suggests that antiparallel configuration is favoured by steric interactions. Therefore it seems that, in order for the polar phase to be stabilised, electrostatic dipolar interactions need to be dominant. Another important results is from the electro-optical experiments for the two single systems of V-shaped molecules made up of ODBP-Ph-C7 and ODBP-Ph-O-C12. It was found that, the response time for short axis switching of ODBP-Ph-C7 is linear with respect to the applied electric field whereas for ODBP-Ph-O-C12 it is quadratic [38]. According to the authors it is indicative that the system

of ODBP-Ph-C7 has a macroscopic dipole, hence might be a polar biaxial nematic. In contrast, atomistic simulations of ODBP-Ph-C7 by Peláez and Wilson [94] showed the formation of small ferroelectric ordered domains in the biaxial nematic phase at the same temperature range as in the experiments. We note that, the biaxial nematic formed from ODBP-Ph-O-C12 still exists at high temperature without a macroscopic dipole may be stabilised by local ordering of molecular dipoles. Nevertheless, we treat the dipolar interaction in a general way and neglect the nature of the interaction. In addition, we ignore short-range correlations for simplicity.

4.2 V-shaped Molecules in Non-polar Nematics

In addition to molecules with D_{2h} symmetry, those with C_{2v} symmetry can also form biaxial nematics where the phase behaviour can be described by second rank order parameters. One type of molecules with this symmetry is V-shaped molecules or often known as bent-core molecules. Some V-shaped molecules are promising candidates which can stabilise biaxial nematics since there are empirical evidence which strongly supported that they may form such phase [35, 36, 37]. Before discussing the molecular field model for polar biaxial nematics, here we review a model for biaxial nematics with D_{2h} symmetry, formed from V-shaped molecules without dipolar interactions. The equations of the molecular field theory for nematic phases with D_{2h} symmetry formed from V shaped molecules arising from second-rank interactions are exactly the same as that for D_{2h} molecules in section 2.4.2. Moreover, in this case, we can relate the intermolecular interaction coefficients, u_{2mn}, to the geometry of the constituent V-shaped molecules. We should note that since the constituent V-shaped molecules have polar shape, the nematic phase may also be polar due to the dipolar interactions between the molecules. However in this section we only consider second-rank interactions, we assume that only non-polar phases are formed. In fact, the phase polarity only manifests in odd rank order parameters. In modelling the interactions of V-shaped molecules, we use the the geometric mean approximation. If we assume the arms are cylindrically symmetric, then the biaxiality γ only depends on the interarm angle. This relation has been worked out by Ferrarini, Luckhurst, Nordio and Roskilly [78] using a model called the additive tensor model. This is because a molecular tensor is the sum of the tensors of the segments which make up of the molecule. In our case, the segments are the mesogenic arms.

It should be noted that there are other molecular interaction models which we can use. One example is the surface tensor model, also presented by the same group of authors [76, 77]. In this model, a molecule is depicted as overlapping spheres and the single molecular tensor components are equated to the integrations of the relevant spherical harmonics over the molecular surface. Using this more elaborate model, the authors also predicted transitional behaviour as found for the additive tensor model [44]. Another possibility is to model a V-shaped molecule as consists touching spheres and the intermolecular interaction coefficients can be calculated from the excluded volume of two molecules [80]. Both the surface tensor and the excluded volume models are much more computationally demanding than the additive tensor model.

The decoupling approximation allows us to calculate the combined intermolecular tensor u_{2mn} as $u_{2mn} = u_{2m}u_{2n}$. The single molecular tensor u_{2m} can be related to the molecular geometry. In a V-shaped molecule, the two arms are identical and cylindrically symmetric and hence their

interaction tensors are uniaxial with only one component u^s_{20}. Here, we use the superscript s to denote that it is a tensor component of an arm instead of the molecule. This segmental arm tensor takes a value in the molecular axis representation by a spherical transformation

$$u^s_{2m} = \sum_m C_{2m}(\omega_s) u'^s_{20}. \tag{4.2.1}$$

Here, $C_{2m}(\omega_s)$ are the modified spherical harmonics. In addition, $\omega_s = (\alpha_s \beta_s)$ denotes the relative orientation of the arm with respect to the molecular axis frame. Here, the spherical harmonics coincide with the Wigner rotation matrices where one of the indices is zero.

$$C_{Lm}(\omega_s) = d^L_{0m}(\beta_s) e^{-im\alpha_s}. \tag{4.2.2}$$

Now, the molecular second-rank tensor is the addition of the segmental tensors in the molecular axis representation

$$u_{2m} = \sum_s C_{2m}(\omega_s) u'^s_{20}. \tag{4.2.3}$$

The spherical harmonics can be expressed in terms of the interarm angles as follows. If we let O be the point where the arms are connected, then Oz^s points along the symmetrical axis of one of the rods. The molecular axes are defined in the way as shown in figure 4.3, namely Ox is the bisector of the interarm angles and Oz is in the same plane as the arms. Thus, $\beta = \angle z O z^s$ and $\alpha = 0$. Therefore, the spherical harmonics become

$$\begin{aligned} C_{20}(\omega_s) &= \frac{1 - 3\cos\theta}{4}, \\ C_{22}(\omega_s) &= \frac{1}{4}\sqrt{\frac{3}{2}}(1 + \cos\theta), \end{aligned} \tag{4.2.4}$$

Therefore the second-rank molecular interaction tensor components are

$$\begin{aligned} u_{20} &= u^s_{20}\left(\frac{1 - 3\cos\theta}{2}\right), \\ u_{22} &= u^s_{20}\sqrt{(3/8)}(1 + \cos\theta). \end{aligned} \tag{4.2.5}$$

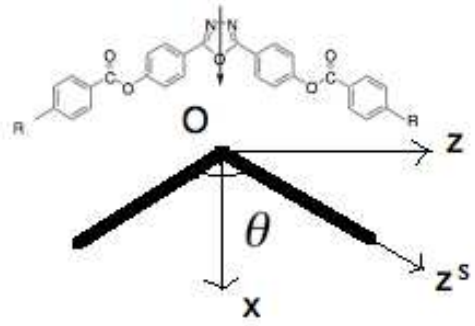

FIGURE 4.3: The coordinate axes labeled for a V-shaped molecule.

The biaxiality parameter γ is simply u_{22}/u_{20}. In addition, we scale the temperature with the anisotropy of an arm, u^{ss}_{200}. The phase map for this system can be found easily simply by converting values of γ in the phase map in figure 2.4 to θ according to equation (4.2.5). The results are shown in figure 4.4. These results were revealed by Luckhurst [3] for a smaller range of the interarm angle θ from 90^o to 180^o which shows that the most biaxial molecule is the one with the tetrahedral interarm angle ($\theta = 109.5^o$). The phase map in figure 4.4 also shows another point which corresponds to the optimum biaxiality at the complement of the tetrahedral angle. Thus, there are now two Landau Triple points in the phase map. Molecules with the interarm angles of 0^o, 90^o and 180^o are uniaxial. In addition, the

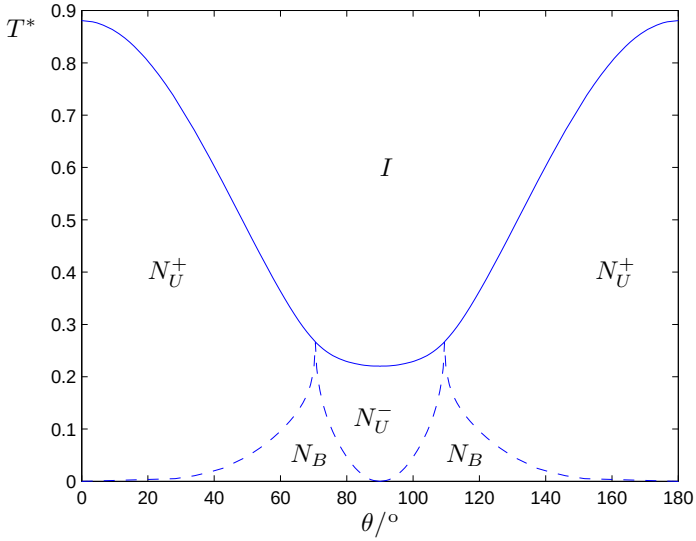

FIGURE 4.4: The dependence of the scaled transition temperature on the interarm angle of V-shaped molecules.

molecule with $90^{\rm o}$ interarm angle is discotic whereas the other two are calamitic. The results for $90^{\rm o} \leq \theta \leq 180^{\rm o}$ agree qualitatively with the Monte Carlo simulations of analogous pair potential [82].

4.3 V-shaped Molecules in Polar Nematics

In the last section, we discussed the molecular field theory for non-polar uniaxial and biaxial nematic phase formed from V-shaped molecules. In this section we add a first-rank or dipolar interaction with a transverse dipole in the direction of the bisector of two segmental arms. In this case, the results we obtain for calamitic and discotic molecules cannot be exchanged as before.

First, we consider a calamitic system which is for $109.5^{\rm o} < \theta < 180^{\rm o}$. We take x to be the axis perpendicular to the molecular plane, y to be the bisector of the arms and z to be in the direction perpendicular to y and in the molecular plane. In this notation, we expect the major molecular axis z to align in the nematic phase to form the main director whereas the other axes align in the biaxial nematic phase to form the minor directors. In addition, the transverse dipole points along the minor axis y. Now the molecules have C_{2v} symmetry and we expect that the lowest symmetry of the phase is also C_{2v}, with Z being the major axis of the phase. In addition, the dipole of the phase points along the minor director Y. The molecular symmetry operations are a two-fold rotation about y and two reflection planes, (xy) and (yz). Likewise, the phase symmetry operations of the C_{2v} phase are a two-fold rotation about Y and two reflection planes, (XY) and (YZ). Therefore, from table 2.1, there is a first-rank interaction coefficient in addition to the second-rank ones

$$u_{111} = u_{1-11} = u_{1-1-1} = u_{11-1}. \tag{4.3.1}$$

In addition, from tables 2.2 and 2.3 in section 2.2, there is also a first-rank order parameter

$$\langle D^1_{11}\rangle = \langle D^1_{-11}\rangle = \langle D^1_{-1-1}\rangle = \langle D^1_{1-1}\rangle. \tag{4.3.2}$$

Hence, the potential of mean torque can be constructed according to equation (2.3.17)

$$U(\Omega) = -u_{200}\left(\kappa\langle F_P\rangle F_P(\Omega) + \langle F_U\rangle F_U(\Omega) + 2\langle F_B\rangle F_B(\Omega)\right), \tag{4.3.3}$$

Here, $\kappa = u_{111}/u_{200}$. The definitions of the composite order parameters and angular functions are given in equations (2.4.32) and (2.4.33). In addition,

$$F_P(\Omega) = (1/2)\left(D^1_{11}(\Omega) + D^1_{-11}(\Omega) + D^1_{-1-1}(\Omega) + D^1_{1-1}(\Omega)\right), \tag{4.3.4}$$

and

$$\langle F_P\rangle = \langle \mathbf{y}.\mathbf{Y}\rangle = \langle \cos\gamma\cos\alpha - \cos\beta\sin\gamma\sin\alpha\rangle. \tag{4.3.5}$$

In this formulation, the dependence of the magnitude of the biaxiality parameter γ on the inter-arm angle is still the same as that for non-polar molecules which we have discussed in section 4.2. However, the axis labels for x and y in this case are exchanged with respect to those in section 4.2. Thus the sign of γ is reversed. The reason for this exchange is to facilitate the calculations. The function $\mathbf{y}.\mathbf{Y}$ is periodic over the interval 0 to π for α and γ whereas the equivalent period for $\mathbf{x}.\mathbf{X}$ is from 0 to 2π. The scaled Helmholtz free energy is

$$A^* = -\ln Q + \frac{1}{2T^*}\left(\kappa\langle F_P\rangle^2 + \langle F_U\rangle^2 + 2\langle F_B\rangle^2\right). \tag{4.3.6}$$

We note that the value of κ_B used by Bates [83] is scaled with u^{ss}_{200} of an arm whereas we scale κ with the intermolecular coefficient u_{200}. Hence in order to compare these two sets of results, we need to make a transformation according to

$$\kappa = \frac{4\kappa_B}{(1-3\cos\theta)^2}, \tag{4.3.7}$$

while the comparison for the interaction strength is

$$u_{200} = u^{ss}_{200}\left(\frac{1-3\cos\theta}{2}\right)^2. \tag{4.3.8}$$

Moreover, in the simulations, a molecule interacts with six nearest neighbours. This number of neighbours is often called *coordination number*. The molecular field results for the transition temperature need to be multiplied by this coordination number in order to compare to those obtained from the simulations.

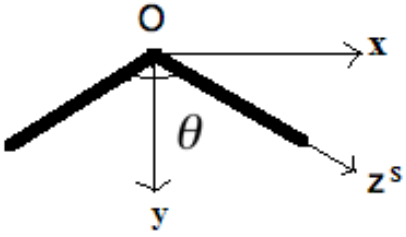

FIGURE 4.5: The coordinate axes labeled for a discotic V-shaped molecules.

Now we consider a discotic molecule with the interarm angle in the range $90^o < \theta < 109.5^o$. We take the molecular axes as follows. We take z to be

perpendicular to the molecular plane, y to be the bisector of the arms and x to be perpendicular to both z and y and in the molecular plane. In this notation, we expect the molecules to align their z axis to form the director Z in uniaxial discotic nematic phases. The transverse dipole still points along the y axis. In this case, the interaction coefficients for the molecules are given by

$$\begin{aligned} u_{20} &= -u_{20}^{s}, \\ u_{22} &= -u_{20}^{s}\sqrt{(3/2)}\cos\theta. \end{aligned} \tag{4.3.9}$$

In addition, the value of κ in comparison with that used by Bates is

$$\kappa = \kappa_B. \tag{4.3.10}$$

4.4 Calculations and Results

Since the potential of mean torque in our theoretical model is analogous to the pair potential used by Bates, we perform analogous calculations for the same values of κ_B, namely 0, 0.2, 0.5 and 1.0. For each value of κ_B the dependence of the transition temperature on the interarm angle is calculated by minimising the equilibrium free energy with respect to the three order parameters using the methods described in Chapter 2. The results are given in figure 4.7. The results which show the phase behaviour of V-shaped molecules without dipolar interaction (for $\kappa_B = 0$) are discussed in detail in section 4.2 and are reproduced in Figure 4.7(a). We see that the results are good qualitative agreement with the simulation. We recall that there is a unique Landau point at which the isotropic phase undergoes a second order transition directly to the biaxial nematic. In addition, as the angle deviates from the tetrahedral value, the biaxial nematic rapidly becomes less stable.

If we include a small dipolar interaction ($\kappa_B = 0.2$, figure 4.7(b)) we see that the biaxial nematic-to-uniaxial nematic transition temperature is increased for a sufficient deviation of the interarm angle from the optimum value. In addition, as might be expected, we have found a region of polar biaxial nematic, N_B^P. Above this region, the non-polar uniaxial and biaxial nematic phases and the Landau point at the tetrahedral angle still remain. For the interarm angle θ from about 106° to about 116° excluding the Landau point, we see a rich behaviour $N_B^P - N_B - N_U - I$ whereas for the interarm angle outside that region we do not see the non-polar biaxial nematic phase. These results are in good agreement with the simulations by Bates. However in our calculations, the reason for the biaxial nematic phase to be stabilised is because of the formation of the polar biaxial nematic phase. In addition, the first order uniaxial nematic-to-isotropic phase transition is unaffected. It is because the polar biaxial phase is formed at a lower transition temperature. Hence the dipolar interaction strength which depends explicitly on the ordering of the molecular dipoles does not make any contribution to the transition at higher temperature. We also see that for $106^{\circ} < \theta < 116^{\circ}$, the polar biaxial nematic phase is formed at lower temperature than the non-polar biaxial nematic phase. Therefore, it does not affect the second order non-polar biaxial nematic-to-uniaxial nematic phase transition and the Landau point for the same reason. In general, the $N_B^P - N_B$ phase transition is second order. For $101^{\circ} < \theta < 107^{\circ}$ and $114^{\circ} < \theta < 127^{\circ}$, both the $N_B^P - N_B$ and $N_B^P - N_U$ transitions are

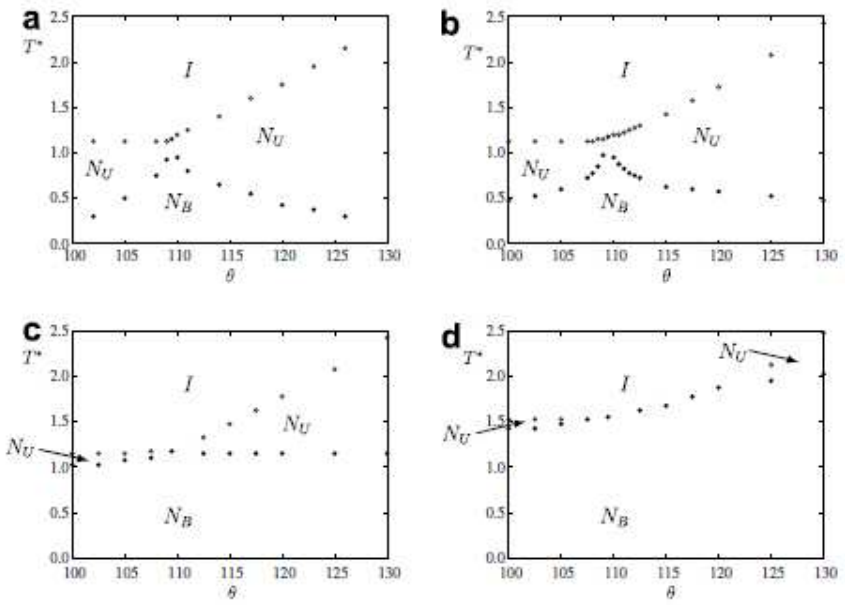

FIGURE 4.6: The phase maps as a function of the scaled temperature and bend angle for bent-core molecules with transverse dipoles (a) $\kappa = 0.0$, (b) 0.2, (c) 0.5 and (d) 1.0 as predicted by the Monte Carlo simulations by Bates. Reproduced from [82].

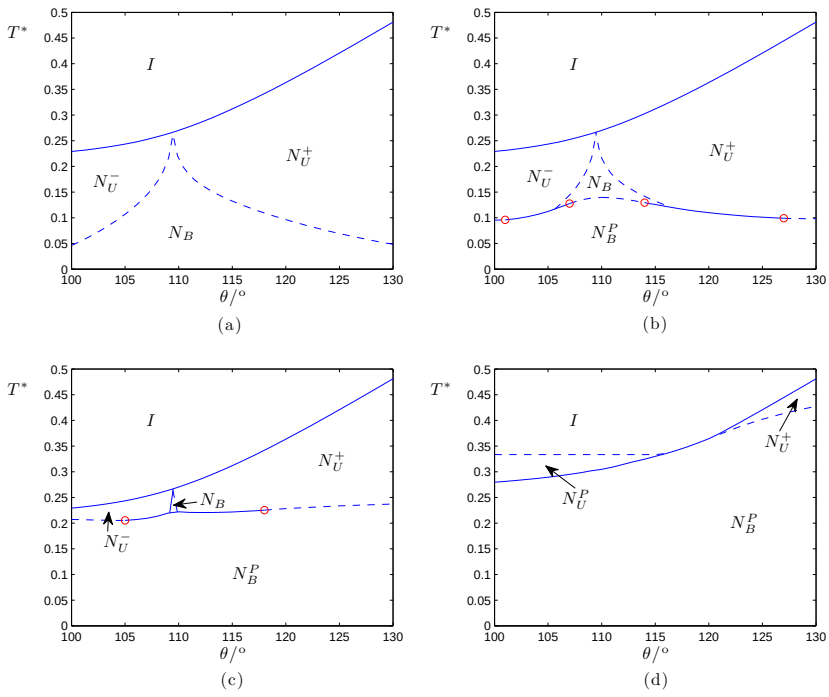

FIGURE 4.7: Phase maps for polar V-shaped molecules with dipole strength (a) $\kappa_B = 0$, (b) $\kappa_B = 0.2$, (c) $\kappa_B = 0.5$ and (d) $\kappa_B = 1.0$ which are predicted by our molecular field theory. First order transitions are shown as continuous lines whereas second order transitions are shown as broken lines. Tricritical points are shown as circles.

first order. For θ smaller than $101^{\rm o}$ or larger than $127^{\rm o}$, the $N_B^P - N_U$ is second order. Hence there are four tricritical points.

As the value of κ_B is increased to 0.5 in figure 4.7(c), the polar biaxial nematic phase becomes more stable. Further, the uniaxial nematics remain non-polar but less extensive in the phase map. Likewise, the extent of the non-polar biaxial nematic is also small. Regardless of phase polarity then our results are in good agreement with the simulations in which the region of discotic uniaxial nematic liquid crystal is narrow. Moreover, the biaxial-to-uniaxial nematic phase transition only changes slightly with the scaled temperature for large values of the interarm angles. We found that, for $105^{\rm o} < \theta < 118^{\rm o}$, both the $N_B^P - N_B$ and $N_B^P - N_U$ transitions are first order. For θ outside that region, the $N_B^P - N_U$ transition is second order.

Finally we show the calculation results for $\kappa_B = 1$ in figure 4.7(d). Again we see some good qualitative agreements with the Monte Carlo simulations. We find two narrow regions of uniaxial nematics. They are connected by a line of first order polar biaxial nematic-to-isotropic phase transitions for θ from $116^{\rm o}$ to $122^{\rm o}$. One difference between our results and the simulations is that one of the uniaxial phases is polar. We denote this polar uniaxial nematic phase by N_U^P. Another difference is the extent of the polar uniaxial nematic phase in our calculations is larger than the simulation. Below the uniaxial nematic phases, there exists a very large region of biaxial nematics. In our calculations, this region of biaxial nematics is polar, in contrast with the simulation. For $\theta > 122^{\rm o}$, the $N_B^P - N_U$ phase transition is second order and is below the first order $N_U - I$ transition. The latter transition is unaffected by the strength of the dipolar interaction. For $\theta < 116^{\rm o}$, the $N_B^P - N_U^P$ transition is first order. This is followed by a second order polar uniaxial nematic-to-isotropic phase transition.

In the case where the uniaxial nematic phase is polar, the dipolar interaction is strong enough that the ordering axis is along the bisector of the arms. In this case the major order parameter is measured along the bisector. Therefore in order to facilitate the calculations, we need to exchange the molecular axes y and z. It is then more convenient to locate the first order phase transition $N_B^P - N_I^P$. In this case the molecular tensor components are

$$\begin{aligned} u_{20} &= u_{20}^s \left(\frac{1 + 3\cos\theta}{2} \right), \\ u_{22} &= u_{20}^s \sqrt{(3/8)} (\cos\theta - 1). \end{aligned} \tag{4.4.1}$$

We also calculate the order parameters for the arms in order to make comparison with the results by Bates. These results by Bates are shown in figure 4.8. These order paramters are defined in the coordinate axes of an arm. The arm order parameters can be found simply by transforming the molecular order parameters from the representation in the molecular coordinate axes to their representation in the axes of an arm according to the transformation rule

$$S_{aa}^{AA} = \sum_b (l_{ab}^{AA})^2 S_{bb}^{AA}, \tag{4.4.2}$$

where a and b can be x, y and z and A can be X, Y, Z. For the case where z is the long axis, this gives us

$$S_{aa}^{AA} = \cos^2(\theta/2) S_{yy}^{AA} + \sin^2(\theta/2) S_{zz}^{AA}. \tag{4.4.3}$$

When z is along the dipole, we get a different expression

$$S_{aa}^{AA} = \cos^2(\theta/2) S_{zz}^{AA} + \sin^2(\theta/2) S_{yy}^{AA}. \tag{4.4.4}$$

The results for the arm order parameters are given in figure 4.9. In figure 4.9(a) we show the results for the system without dipolar interaction. In the isotropic phase, all components of the order parameter tensor for the arms are zero. As the temperature is lowered, the order parameters increase discontinuously to a non zero values with $S_{aa}^{XX} = S_{aa}^{YY} = (-1/2) S_{aa}^{ZZ}$, indicating the uniaxial phase with z being the ordering axis. As we lower the temperature the components S_{aa}^{XX} and S_{aa}^{YY} gradually become different although they remain negative and smaller than S_{aa}^{ZZ}, indicating a biaxial phase. Next we introduce a small dipolar interaction $\kappa_B = 0.2$ which is shown in figure 4.9(b): we can still see the $N_U - I$ and $N_B - N_U$ phase transitions at the same temperatures as before. In addition, now we find that at lower temperatures, the components S_{aa}^{XX} and S_{aa}^{YY} changes discontinuously. At the same temperature, the polar order parameter also becomes non zero, indicating a first order $N_B^P - N_B$ phase transition. Now we increase the dipolar interaction slightly to $\kappa_B = 0.5$ in figure 4.9(c), the $N_U - I$ phase transition is still the same as before with z being the major axis. Here the non-polar biaxial nematic is not found and instead the order parameters S_{aa}^{XX} and S_{aa}^{YY} change with a slight jump at the $N_B^P - N_U$ phase transition. This is also accompanied by a jump in the polar order parameter. We note that the discontinuities in the order parameters at both phase transitions are more pronounced than in the simulation. The final values of $\kappa_B = 1.0$ is shown in figure 4.9(d). As the temperature is decreased in the isotropic phase, we see a vanishingly small region where both the polar and the second rank order parameters are non zero, indicating a second order phase transition to the polar uniaxial nematic phase. As the temperature is lowered, all order parameters increase discontinuously. In addition, the order parameters of the arms do not follow the relation $S_{aa}^{XX} = S_{aa}^{YY} = (-1/2) S_{aa}^{ZZ}$. This indicates a polar biaxial nematic phase.

Now our molecular field theory for V-shaped molecules is verified by its agreements with the Monte Carlo simulations by Bates [83]. Here we use the molecular field theory to make comparisons with experimental results for V-shaped molecules with interarm angle of 140°. Hence, we fix the interarm angle to 140° in the calculations and we vary the dipolar interaction strength κ_B. In choosing the range of value for κ_B, we note from figures 4.7 that, for $\kappa_B = 1$, we do not see the biaxial nematic-to-isotropic phase transition at $\theta = 130^\circ$. Hence, for $\theta = 140^\circ$ we expect that the dipole strength $\kappa_B = 1$ is not enough to cause a direct biaxial nematic-to-isotropic phase transition. Therefore, we choose the value of κ_B greater than one to do the calculations. Figure 4.10 shows the phase map for $\theta = 140^\circ$ and we vary κ_B from 1 to 2. We see that, as κ_B increases, the $N_U^+ - I$ transition temperature does not change. It is simply because in our model, the polar interaction only influences the ordering in the polar phase. Indeed, we see that the stability of the biaxial and uniaxial nematic phases increase with κ_B. It is important to note that, between the non-polar uniaxial nematic and the polar uniaxial nematic regions, there is a region of first order direct biaxial nematic-to-isotropic phase transitions. This region exists for κ_B from 1.53 to 1.77. Therefore we conclude that, the dipolar interaction strength for the compounds ODBP-Ph-C7 and ODBP-Ph-O-C12 used in the experiment would be from $1.53 u_{200}$ to $1.77 u_{200}$ where u_{200} is the anisotropic interaction of an arm.

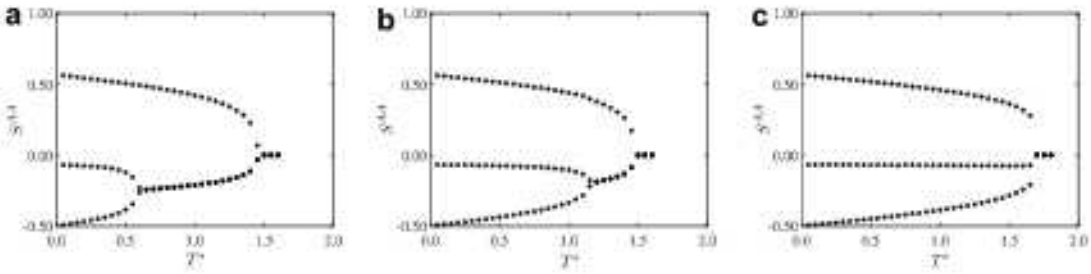

FIGURE 4.8: The dependence of the Cartesian tensor components of the order parameter tensor for the mesogenic arms for $\theta = 115^{o}$ and (a) $\kappa_B = 0$, (b) $\kappa_B = 0.5$ and (c) $\kappa_B = 1.0$ as predicted by the Monte Carlo simulations by Bates. Reproduced from [82].

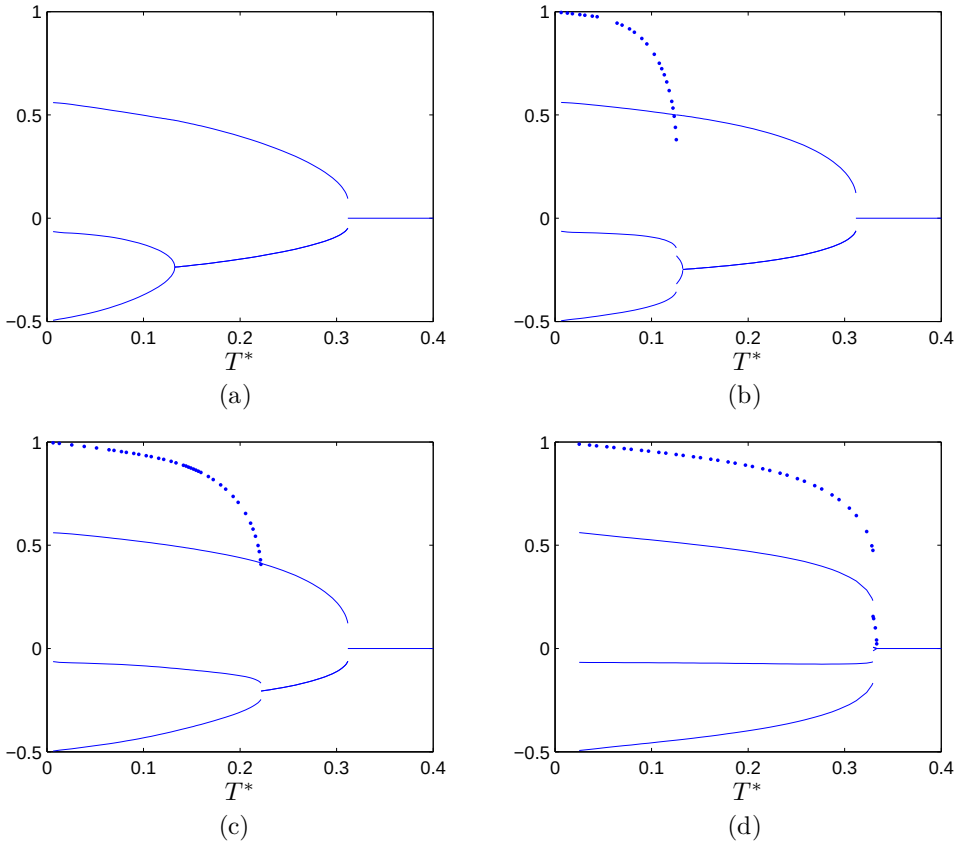

FIGURE 4.9: The continuous lines show the temperature dependence of the Cartesian tensor components of the second-rank order parameter tensor for the mesogenic arms for $\theta = 115^{o}$ and (a) $\kappa_B = 0$, (b) $\kappa_B = 0.2$, (c) $\kappa_B = 0.5$ and (d) $\kappa_B = 1.0$. The dotted lines show the temperature dependence of the polar order parameter.

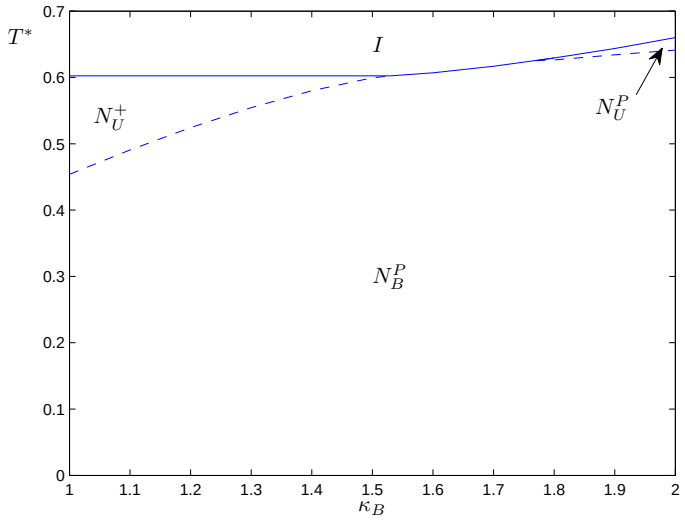

FIGURE 4.10: The dependence of the scaled transition temperature T^* on the dipolar interaction strength κ_B when the interarm angle is fixed at $140°$.

4.5 Conclusions

Our work in this chapter sets out to provide a possible explanation to the disagreement between theoretical predictions and recent experimental evidence regarding the biaxial nematic phase formed from V-shaped molecules [35, 36, 37]. A possible explanation is that there is a transverse dipolar interaction which is often ignored in the molecular field theory and Monte Carlo simulations which usually are only concerned with second-rank interactions. Bates supported this hypothesis by performing Monte Carlo simulations of V-shaped molecules with dipolar interaction [83] as well as the classical second-rank interactions. His results agree with experimental evidence. In addition to explaining the disagreement, the existence of dipolar interaction also suggest that the biaxial nematic phase formed from V-shaped molecules might be a polar phase.

We have modified the classical molecular field theory to include dipolar interaction and the formation of the novel polar uniaxial and biaxial nematic liquid crystal phases. The choice of the dipolar interaction strength as well as the interarm angle of V-shaped molecules in our calculations is the same as the Monte Carlo simulations by Bates [83]. Our calculation results are shown in four phase maps analogous to that found by Bates [83] which shows remarkable agreements. However, there is a significant difference between our results and Bates [83]: in Bates' calculations the polar phase is not observed. This may be due to local ordering of the dipoles in the simulation which destroy macroscopic long-range polar order. On the other hand, the molecular field theory does not take into account local ordering, so that it may stabilise an unstable polar phase. In essence, our results strengthen the hypothesis that the disagreement between theoretical predictions and experimental results is due to the existence of a large transverse dipolar interaction. In addition, we find that the transverse dipolar interactions helps to stabilise the novel polar biaxial nematic and polar uniaxial nematic phases which to our knowledge have not been experimentally confirmed in any small molar mass system.

Chapter 5

Uniaxial and Biaxial Nematics formed from Flexible Molecules

Flexible molecules are those which can change their shapes. An example of flexible molecules is liquid crystal dimers. These molecules are made by linking two mesogenic groups together with an alkyl chain which is called a spacer. They are one of the candidates for stabilising biaxial nematic phases. Due to their flexible hydrocarbon link, the molecules are flexible which can take many geometric shapes, or conformations. Some conformations have biaxial shapes and their presence can drive the formation of biaxial nematics. In addition, modelling liquid crystal dimers would be a first step towards modelling more complex molecules which have been found to form biaxial nematics.

In section 5.1 we describe some related works on modelling liquid crystal dimers. A molecular field theory for biaxial nematics formed from flexible molecules for a general system has been developed by Luckhurst [51]. We take a few steps in reintroducing the theory and applying it to model a two-conformers system in order to explore the mutual influences of molecular flexibility and phase biaxiality. In section 5.2 we apply the theory to model a non-exchanging binary mixture of linear and bent conformers. We also calculate a phase map to investigate the dependence of the phase behaviour on the mole fractions of the conformers. In section 5.3, we include the molecular flexibility in the theory and hence allow the conformers to interconvert. In that section, first we keep the approximation used by Ferrarini, Luckhurst, Nordio and Roskilly [44] that the mole fractions are independent of the temperature in order to make comparisons with their results. After that, we allow the mole fractions to change with the temperature in order to study a more physical system. Indeed, we find that the biaxial nematic phase is stabilised in both systems when the conformational or internal energy of the bent conformer is sufficiently lower than that of the linear conformer.

5.1 Related Works

Liquid crystal dimers often exhibit the interesting even-odd effect at the uniaxial nematic-to-isotropic phase transition [44]. First, the uniaxial nematic-to-isotropic transition temperature is

higher for even dimers (dimers with an even number of carbon atoms in the spacer) than for odd dimers (dimers with an odd number of carbon atoms in the spacer) and this difference decreases on increasing spacer length. Secondly, the entropy of transition for odd dimers is significantly lower than for even dimers and is independent of the spacer length for those with less than twelve methylene groups.

An early molecular field theory for liquid crystal dimers has been developed to understand this effect by Ferrarini *et al.* [44]. It is known that the bonds between the carbon atoms in the hydrocarbon chain and those between the first carbon atom in the link and the mesogenic groups can rotate around. Consequently, a molecule can take many different conformations with different angles between the mesogenic groups. We call molecules which adopt the same conformation *conformers*. In the theory by Ferrarini *et al.* [44], a dimer consists of two connecting identical cylindrically symmetric mesogenic arms and the interaction of the hydrocarbon chain is ignored. A conformation is defined by the angle between the arms of the molecules. The many conformations of a molecule is replaced by only two, one is linear with one arm form 180^{o} with the other, the other is bent with the tetrahedral interarm angle (109.45^{o}). These two conformations may be regarded as the most stable forms since they have the lowest conformational energies. In addition, the all-trans conformation has the lowest energy of all and so it gives the most stable conformation of all. In this conformation, all the carbon-carbon bonds in the spacer are coplanar and every pair of adjacent bonds makes up a tetrahedral angle. From figure 5.1 we see that the all-trans conformation for an odd dimer is bent whereas it is linear for an even dimer. Hence, for even dimers, the linear conformer have a lower internal energy and so is more stable than the bent conformer. In contrast, for odd dimers the situation is reversed. In the theory by Ferrarini *et al.* [44], the difference in the mole fractions of the linear and the bent conformer was attributed to the difference in their internal energy and the order of the phase. In order to facilitate their calculations, the internal energy difference was assumed to be independent of the temperature. In other words, the mole fractions are constant in the isotropic phase and only change in the ordered phase. It was found that, due to the presence of a greater number of the lower anisotropy bent conformer in odd dimers than even dimers, the transition temperature for odd dimers is less than that for even dimers. In addition, at the transition to the nematic phase the onset of orientational order increases the concentration of the linear conformer. For odd dimers, this increse is continuous. In contrast, for even dimers, most bent molecules are converted to linear which causes a discontinous change in the conformational entropy. This leads to a much larger increase in the transitional entropy for even dimers compared to odd dimers.

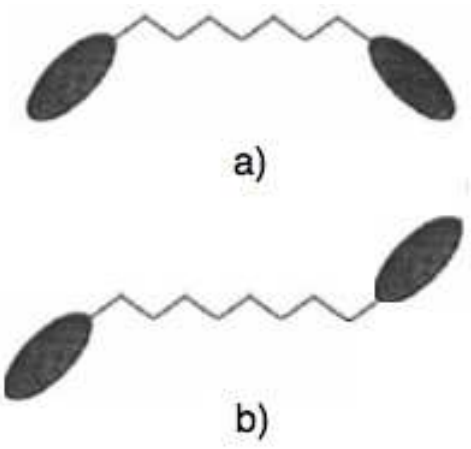

FIGURE 5.1: A sketch of Liquid Crystals with a) odd-spacer and b) even-spacer. Reproduced from [44].

These qualitative features of the model have also been confirmed by Monte Carlo simulations of analogous pair potential for even [95] and odd dimers [96].

In the calculations by Ferrarini *et al.* [44], the additive tensor model was used in order to calculate a single molecular interaction tensor. The intermolecular coefficients are calculated as the products of the components of the single molecular tensor of two interacting molecules. It is worth mentioning that this model has also been used to investigate the dependence of the transitional properties of liquid crystal dimers on the geometry of bent conformer. Depending on the link between the mesogenic units and the flexible chain, the angle of the bent conformer may be different. Thus the transitional order parameter and entropy changes can differ depending on the interarm angle of the bent conformer [78].

The motivation for us to study liquid crystal dimers is to investigate how the molecular flexibility and different conformations affect the stability of thermotropic biaxial nematics and how the onset of the nematic phases influence the stability of the conformers. The presence of the bent conformer leads to the expectation that liquid crystal dimers might be able to form biaxial nematics: biaxial conformers have biaxial shapes and previous studies have related their phase behaviour with their interarm angles. Moreover, among recent evidence for biaxial nematics include systems which are formed from flexible molecules. They are liquid crystal polymers and tetrapodes [30, 31, 32]. The molecular flexibility may be a contribution towards forming the biaxial nematics. In addition, modelling such system for a biaxial nematic phase is a challenging task due to the biaxial nature of board-like units and flexibility of hydrocarbon chains. This has been done for a simpler system of uniaxial nematic formed from tetrapodes [97]. Our work on liquid crystal dimers to investigate the effect of flexibility on nematic stability would be a first step towards modelling the more complex systems. Since the two-conformers model has been used to successfully explain the even-odd effect by Ferrarini *et al.* [44], we use the same model, extending it to allow a biaxial nematic phase to be formed.

The additive tensor model can be improved by allowing the interarm angle to adopt a continuous range of values rather than just two. This addition of conformations produced quantitatively different results and it gives a more realistic conformational distribution [95, 96]. When a continuous range of conformations is allowed, the molecular shape, and hence, its anisotropy and biaxiality follow a statistical distribution. A molecular field study by Longa, Pajak and Wydro [98] related the stability of the biaxial nematic phase with the first two moments of the molecular shape Gaussian distribution in the isotropic phase. They found that, generally, the transition between the isotropic and the nematic phase occurs at higher temperatures when the change in the molecular shape is allowed. In addition, in their phase map, a Landau point is split into two triple points connected by a line of first-order transitions between the isotropic and the biaxial nematic phases. On the other hand, in one case which corresponds to a particular set of values for the moments of the molecular shape distribution, the biaxial nematic phase is destabilised. Bates [99] carried out a series of Monte Carlo simulations on how flexibility influences the stability of biaxial nematic phases of V-shaped molecules. In his simulations, the contituent molecules are allowed to change their orientations as well as their interarm angles. In addition to the Lewohl-Lasher potential, Bates added a bending potential which the square of the difference between the bend angle and a preferred angle, multiplied by a bending force constant. The resulting conformational distribution is then Gaussian with the mean value at the tetrahedral angle. It was found that the molecular flexibility has interesting effects on the original phase map of V-shaped molecules without the bending potential [82]. In general, the biaxial nematic phase becomes less stable compared to non-flexible molecules. Moreover, the author also derived phase maps

relating the scaled temperature with the scaled force constant.

In our first attempt to model molecular flexibility in biaxial nematic systems, we use the additive tensor model for its simplicity and adequacy for describing the essential physics of real systems of liquid crystal dimers.

5.2 Binary Mixture of Non-exchanging Linear and Bent Molecules

The first step in extending the molecular field theory for biaxial nematics to include molecular flexibility with two conformers is to study a binary mixture of non exchanging molecules. This binary mixture has only two components. The molecules are made by joining two identical cylindrically symmetric arms. In the linear molecule, the arms are antiparallel which make an interarm angle of 180^{o} whereas the interarm angle of the bent molecule is tetrahedral ($\cos^{-1}(-1/3)$ or 109.45^{o}).

We ignore the possibility of the formation of biphasing regions since this section is only an intermediate step towards studying the exchanging systems. The exchanging systems clearly do not form biphasing regions. This can be verified by the *Gibbs phase rule* which can be used to determine whether it is possible to have regions of coexisting phases in equilibrium. Under constant pressure, the Gibbs phase rule is $F = C - P + 1$, where *F* is the degree of freedom of the system, *C* is the number of components in the system and *P* is the number of coexisting phases in equilibrium. In this binary mixture there are two components so $C = 2$. For example consider a region of single phase or $P = 1$, thus $F = 2$ and so there are two degrees of freedom: the temperature and the composition in the isotropic phase. Now we consider if the biphasing region exists in this binary system, in this case we still have $C = 2$ but now $P = 2$ so $F = 1$. This can be verified that, the system only depends on the temperature since the composition is now determined by the *lever rule*. Therefore, the system has only one degree of freedom. Therefore a region of two phases in coexistence in equilibrium can be formed. Now we consider a single system of exchanging conformers with only one component, $C = 1$. In the single phase region, $P = 1$ and so $F = 1$ and that single degree of freedom is the temperature. Suppose now two phases can coexist in equilibrium then $P = 2$ but we still have $C = 1$ and therefore F must be zero. This means that we have to fix both the temperature and the composition in order to have two phases in coexistence. Therefore the a biphasing region cannot be formed.

5.2.1 Multicomponent Mixture

In this subsection, we discuss a molecular field theory for a nematic mixture with an arbitrary number of components. Liquid crystal mixtures are interesting in their own rights and the molecular field theory have been used to study several systems. One example is the binary mixture of symmetric, rod-like molecules [100]. In another example, a molecular field theory has been used to study binary mixture of linear and bent V-shaped molecules in the uniaxial nematic phase [44]. The latter example was studied as a first step towards modelling flexible molecules. We discuss the molecular field theory for flexible molecules in the next section.

The total internal energy per molecule of a multicomponent mixture is analogous to that for a system of identical molecules where only pairwise interactions between molecules is allowed

$$\langle U\rangle = -(1/2)\sum x_j x_k u^{kj}_{Lmn}\langle D^L_{pm}\rangle_k \langle D^L_{-pn}\rangle_j. \tag{5.2.1}$$

where x_j and $\langle D^L_{-pn}\rangle_j$ denote the mole fraction and the order parameters of component j, respectively. In addition, u^{kj}_{Lmn} denotes the interaction supertensors between molecules j and k. The entropy per particle has linear contributions from the components for an ideal mixture in the molecular field approximation

$$S_j = -k_B \sum x_j \int f_j(\Omega)\ln f_j(\Omega) d\Omega. \tag{5.2.2}$$

Here, k_B is the Boltzmann constant and $f_j(\Omega)$ denotes the orientational distribution function of component j. The sum of all the entropy per particle gives the total entropy of the multicomponent system. From the internal energy and the entropy we can form the Helmholtz free energy for the system using equation (2.3.10). The variation of the free energy in terms of the orientational distribution functions for all components is taken subject to two constraints. The first one is that these orientational distribution functions are normalised and the second one is that they are averages of the Wigner rotation matrices. Therefore,

$$\int \left\{ -x_j \sum_j \left(x_k \sum u^{kj}_{Lmn}\langle D^L_{pm}\rangle_k D^L_{-pn}(\Omega) + k_B T + k_B T \ln f_j(\Omega)\right) + \eta_j/x_j \right\} d\Omega = 0. \tag{5.2.3}$$

The solution of this equation gives the orientational distribution function of the *j* component

$$f_j(\Omega) = \frac{\exp\left(\frac{1}{k_B T}\sum x_k u^{kj}_{Lmn}\langle D^L_{pm}\rangle_k D^L_{-pn}(\Omega)\right)}{\exp(1+\frac{\eta_j}{x_j k_B T})}. \tag{5.2.4}$$

For normalisation of the distribution function, the denominator must be the partition function of the *j* conponent. Therefore, the potential of mean torque is

$$U_j(\Omega) = -\sum x_k u^{kj}_{Lmn}\langle D^L_{pm}\rangle_k D^L_{-pn}(\Omega). \tag{5.2.5}$$

Now we can derive the more explicit free energy at equilibrium. Taking the average of $\ln f_j(\Omega)$ for component *j* we find

$$x_j k_B T \int f_j(\Omega)\ln f_j(\Omega) d\Omega + x_j\langle U_j\rangle = -x_j\langle U_j\rangle - x_j k_B T \ln Q_j \tag{5.2.6}$$

Hence, the free energy can be written as

$$\frac{A}{k_B T} = -\frac{\langle U\rangle}{k_B T} - \sum_j x_j \ln Q_j. \tag{5.2.7}$$

5.2.2 Binary Mixture

In the last subsection, we have developed a molecular field theory for a general multicomponent system. In this subsection, we apply this theory to study a binary mixture of linear and bent molecules. The potential of mean torque responsible for the ordering of component j is

$$U_j(\Omega) = -\sum_{m,n,p} \left(x_j u_{2mn}^{jj} \langle D_{pm}^2 \rangle^j + x_k u_{2mn}^{kj} \langle D_{pm}^2 \rangle^k \right) D_{-pn}^2(\Omega), \tag{5.2.8}$$

where j and k can either be linear, l, or bent component, b. We assume the gound state biaxial nematic phase has D_{2h} symmetry. In order to reduce the number of parameters we use the decoupling approximation $u_{2mn}^{jk} = u_{2m}^{j} u_{2n}^{k}$. In addition, we define the biaxiality parameters γ_j of molecule j and the relative anisotropy ϵ_{kj} of molecules k and j as

$$\gamma_j = u_{22}^j / u_{20}^j \qquad \epsilon_{kj} = u_{20}^k / u_{20}^j. \tag{5.2.9}$$

The biaxiality parameters and relative anisotropy of the linear and bent molecules can be found using a method introduced for modeling V-shaped molecules without dipolar interactions which we have discussed in section 4.2

$$\gamma_l = 0 \qquad \gamma_b = 1/\sqrt{6} \qquad \epsilon_{lb} = 2. \tag{5.2.10}$$

These results mean the anisotropy of a linear molecule is double that of a bent molecule. In addition, while linear molecules are uniaxial, bent molecules have optimal biaxiality. That is $\gamma_b = 1/\sqrt{6}$ corresponds to the largest biaxial region in figure 2.4. The explicit expressions of the potentials of mean torque for linear and bent molecules are

$$U_l(\Omega) = -4u_{200} \left[\langle F_U \rangle R_{00}(\Omega) + 2\langle F_B \rangle R_{20}(\Omega) \right], \tag{5.2.11}$$

$$\begin{aligned} U_b(\Omega) = -2u_{200} \Big[& \langle F_U \rangle \left(R_{00}(\Omega) + 2/\sqrt{6} R_{02}(\Omega) \right) \\ & + 2\langle F_B \rangle \left(R_{20}(\Omega) + 1/\sqrt{6} R_{22}(\Omega) \right) \Big]. \end{aligned} \tag{5.2.12}$$

The molar Helmholtz free energy for the mixture at equilibrium is

$$A^* = -(x_l \ln Q_l + x_b \ln Q_b) + \frac{1}{T^*} 2 \left(\langle F_U \rangle^2 + 2\langle F_B \rangle^2 \right). \tag{5.2.13}$$

Here, the temperature is scaled with the interaction coefficient of an arm $T^* = k_B T / u_{200}$, where $u_{200} = u_{200}^{bb}$; $\langle F_U \rangle$ and $\langle F_B \rangle$ are the averages of the composite order parameters of the linear and bent molecules

$$\begin{aligned} \langle F_U \rangle &= x_l \langle F_U \rangle_l + (1/2) x_b \langle F_U \rangle_b, \\ \langle F_B \rangle &= x_l \langle F_B \rangle_l + (1/2) x_b \langle F_B \rangle_b. \end{aligned} \tag{5.2.14}$$

Here, the composite order parameters for each component are defined as

$$\langle F_U\rangle_l = \langle R^2_{00}\rangle_l, \qquad \langle F_U\rangle_b = \langle R^2_{00}\rangle_b + 2/\sqrt{6}\langle R^2_{02}\rangle_b,$$
$$\langle F_B\rangle_l = \langle R^2_{20}\rangle_l, \qquad \langle F_B\rangle_b = \langle R^2_{20}\rangle_b + 1/\sqrt{6}\langle R^2_{22}\rangle_b. \tag{5.2.15}$$

The model turns out to be simple within the geometric mean approximation since it only depends on two composite order parameters, $\langle F_U\rangle$ and $\langle F_B\rangle$ which characterise the ordering of the phase. This is clearly the advantage of the geometric mean approximation which facilitates the calculations. The order parameters are determined by minimising the free energy by the method discussed in chapter 2.

5.2.3 Calculations and Results

The calculation results are presented in a phase map in figure 5.2 which shows the dependence of the transition temperature on the mole fraction of bent molecules. The biaxial nematic phase

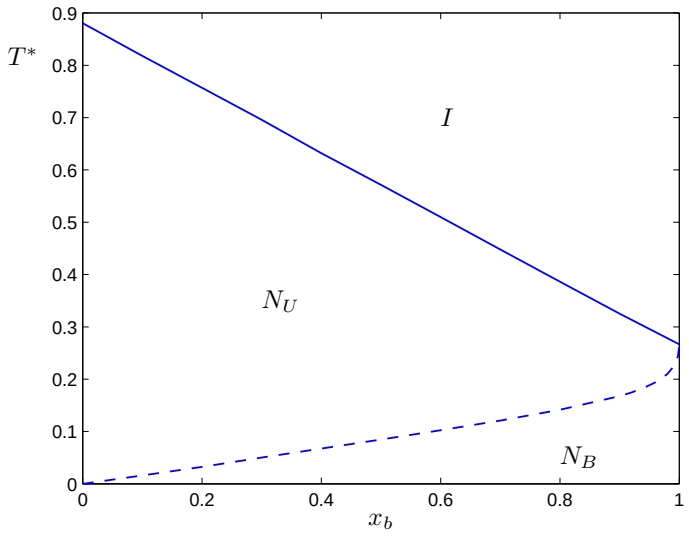

FIGURE 5.2: The phase map for binary mixture of non-flexible linear and bent molecules. First order transitions are shown as continuous lines whereas second order transitions are shown as broken lines.

N_B is found when both the order parameters, $\langle F_U\rangle$ and $\langle F_B\rangle$, are non zero. At the biaxial nematic-to-uniaxial nematic phase transition, the biaxial order parameter, $\langle F_B\rangle$, vanishes but the uniaxial order parameter, $\langle F_U\rangle$, still remains non-zero. When the system goes into the isotropic phase, the global minimum of the free energy is where both order parameters vanish. From the phase map we see that the uniaxial nematic-to-isotropic phase transition temperature decreases almost linearly on increasing the mole fraction of bent molecules x_b. In contrast, the biaxial nematic-to-uniaxial nematic phase transition temperature increases on increasing x_b. In addition, the biaxial nematic-to-uniaxial nematic transitions is almost linear in composition at first but then bends upward to form the Landau point of continuous direct transition between the biaxial nematic and the isotropic phase. This behaviour is clearly due to the presence of more

biaxial (bent) molecules which increases the biaxial nematic-to-uniaxial nematic transition temperature. The uniaxial nematic-to-isotropic phase transition is first order, with the discontinuity in the transitional order parameter decreasing on increasing mole fraction of bent molecules. On the other hand, the biaxial nematic-to-isotropic phase transition is continuous, or second order.

The linear dependence of the uniaxial nematic-to-isotropic transition temperature on the mole fraction can be understood if we first expand the uniaxial order parameters of the linear and bent molecules as a Taylor series in terms of the uniaxial order parameter $\langle F_U \rangle$. The rotational partition functions are both $8\pi^2$. The order parameters are given by

$$\begin{aligned} \langle F_U \rangle_l &= (8\pi^2)^{-1} 4 (T^*)^{-1} \langle F_U \rangle \int (C_{20}(\omega))^2 \, d\Omega, \\ \langle F_U \rangle_b &= (8\pi^2)^{-1} 2 (T^*)^{-1} \langle F_U \rangle \int \Big(C_{20}(\omega) + 2/\sqrt{6} C_{22}(\omega) \Big)^2 \, d\Omega. \end{aligned} \tag{5.2.16}$$

The integrations can be evaluated from

$$\int (C_{20}(\omega))^2 \, d\Omega = (8\pi^2)/5, \qquad \int (C_{22}(\omega))^2 \, d\Omega = (8\pi^2)/10. \tag{5.2.17}$$

Therefore, the bifurcation temperature is

$$T^*_{\text{mixt}} = (6 - 4x_b^0)/15 + O(\langle F_U \rangle). \tag{5.2.18}$$

This bifurcation temperature is a good approximation of the temperature at which the order parameters start to bifurcate. It is not the transition temperature since there is a first order phase transition at higher temperature and so the bifurcation temperature already corresponds to an ordered phase (see chapter 2). However, the difference between the transition temperature and the bifurcation temperature is small compared to the transition temperature. In consequence, since the bifurcation point depends linearly on the mole fraction we may expect the uniaxial nematic-to-isotropic transition line to be close to linearity. The linear dependence might be analogous to a binary mixture of uniaxial molecules of different anisotropy [101]. In this system, the interaction strength between two different molecules, ϵ_{AB}, is the geometric mean of that between two identical molecules, ϵ_{AA} and ϵ_{BB}. Actually, this system does exhibit a negligible deviation from linearity, about one per cent of the transition temperature. In addition, this deviation is magnified when the interaction coefficients do not follow the geometric mean rule [100]. Another result worth noting in our case is that the uniaxial nematic-to-isotropic transition temperature decreases on increasing mole fraction of bent molecules. This is not surprising: bent molecules are less anisotropic and their presence in the system depresses the transition temperature.

Since the biaxial nematic-to-uniaxial nematic phase transition is second order, the biaxial order parameter $\langle F_B \rangle$ increases continuously at the phase transition. Therefore, we can obtain a better understanding of the system by expanding the expressions for the biaxial order parameters of

the two components as a Taylor series

$$
\begin{aligned}
Q_l = Q_U^l &= \int \exp\left(4T^{*-1}\langle F_U\rangle R_{00}(\Omega)\right)d\Omega,\\
Q_b = Q_U^b &= \int \exp\left[2T^{*-1}\langle F_U\rangle\left(R_{00}(\Omega)+\left(2/\sqrt{6}\right)R_{02}(\Omega)\right)\right]d\Omega,\\
\langle F_B\rangle_l &= \left(8/T^{*-1}\right)\langle F_B\rangle {Q_U^l}^{-1}\int \left(R_{20}(\Omega)\right)^2\exp\left(4T^{*-1}\langle F_U\rangle R_{00}(\Omega)\right)d\Omega,\\
\langle F_B\rangle_b &= \left(4/T^{*-1}\right)\langle F_B\rangle {Q_U^b}^{-1}\int \left(R_{20}(\Omega)+\left(1/\sqrt{6}\right)R_{22}(\Omega)\right)^2\\
&\times\exp\left[2T^{*-1}\langle F_U\rangle\left(R_{00}(\Omega)+\left(2/\sqrt{6}\right)R_{02}(\Omega)\right)\right]d\Omega.
\end{aligned}
\tag{5.2.19}
$$

Therefore the biaxial nematic-to-uniaxial nematic transition temperature is given by (see Appendix C)

$$T^*_{\text{mixt}} = 4(1-x_b)\tau_l + x_b\tau_b + O(\langle F_B\rangle). \tag{5.2.20}$$

where

$$
\begin{aligned}
\tau_j = \frac{1+2\gamma_j^2}{5} &+ \left(\frac{-2+4\gamma_j^2}{7}\right)\langle R_{00}^2\rangle_j + \frac{8}{7}\gamma_j\langle R_{02}^2\rangle_j\\
&+ \left(\frac{3+\gamma_j^2}{35}\right)\langle R_{00}^4\rangle_j + \frac{2}{7}\sqrt{\frac{3}{5}}\gamma_j\langle R_{02}^4\rangle_j + \sqrt{\frac{2}{35}}\gamma_j^2\langle R_{04}^4\rangle_j.
\end{aligned}
\tag{5.2.21}
$$

It can be seen that τ_l and τ_b would be the transition temperatures of single systems made up of either molecules in the absence of the other component. It is interesting to notice that in figure 5.2 the uniaxial nematic-to-isotropic phase transition temperature is linearly dependent on the composition of the system whereas that of the biaxial nematic-to-uniaxial nematic phase transition is bent and asymmetric towards high mole fraction of bent molecules. We see that if the order parameters in equation (5.2.21) of molecule l are independent of the order parameters of molecule b and vice versa then in place of τ_l and τ_b would be the scaled transition temperature of molecules l and b in the absence of the other component, respectively. These values of τ_l and τ_b would be independent of the mole fraction and hence the transition temperature of the mixture would be linear with respect to the mole fraction. However, the presence of the bent molecules in the system reduces the order parameters for the linear molecules, hence τ_l is lower than the transition temperature for the single system of linear molecules. In contrast the presence of the linear molecules increases the order parameters for the bent molecules, therefore τ_b is higher than the transition temperature for the single system of bent molecules. In addition, from the expression for the transition temperature we see that the contribution from τ_l is four times that of τ_b. Consequently, a decrease in τ_l dominates an increase in τ_b which causes a negative deviation from linearity in the biaxial nematic-to-uniaxial nematic transition temperature. In addition, the asymmetry in the curve is more gradual towards the linear molecule, the more anisotropic nematogen. The smaller perturbation of the behaviour of the linear component by the bent component may be understood in terms of the smaller order of the bent component due to its smaller anisotropy and its biaxiality.

5.3 System of Exchanging Linear and Bent Conformers

In the last section we saw that the uniaxial nematic-to-isotropic phase transition temperature of a binary mixture of linear and bent molecules decreases continuously on increasing the mole fraction of bent molecules. These results can partly explain the even-odd effect: liquid crystals formed from odd dimers have more bent molecules than those formed from even dimers. However, the agreement between this model and the experiments is not desirable because in the experiments the transitional entropy change at the phase transition is significantly larger for even dimers than for odd dimers. On the other hand, the transitional entropy change for the non-exchanging mixture model decreases continuously on increasing the mole fraction of the bent conformer [44]. Thus, the non-exchanging mixture does not capture the essential physics of the empirical systems. An improvement of the existing non-exchanging mixture model can be made by including the coupling between the conformational distribution and the long range orientational order [44]. The coupling results in the more elongated conformers being favoured over the bent ones within the uniaxial nematic liquid crystal phase. Hence, in this section we allow the conformers to interconvert. We consider a simple model of V-shaped liquid crystal in which the constituent molecules can adopt one of two conformations, linear and bent.

5.3.1 Multiple Conformer System

In the last section, we have discussed an application of the molecular field theory in studying multicomponent mixtures. In these mixtures, the components are non-exchanging and their mole fractions are fixed. In this thesis, studying mixtures is an intermediate step towards studying flexible molecules. Real liquid crystals are usually flexible. That is, a molecule may adopt many different shapes or conformations. Each conformer can be considered as a component in the system. However, in this case, one conformer may convert to another depending on the thermodynamic properies and the ordering of the system. Thus there are two main differences between a system of flexible molecules and a multicomponent mixture. First, the mole fractions of all conformers in the system of flexible molecules can change according to thermodynamic variables and the molecular ordering. Secondly, in a system of flexible molecules, the conformational energy also contributes towards the total energy, in addition to the anisotropic energy. The molecular field theory for flexible molecules has been developed by Luckhurst [51]. In this subsection we reintroduce this theory for an arbitrary number of conformers.

The thermodynamic anisotropic internal energy of a system with many conformers is identical to that for a mixture of non-exchanging components

$$\langle U_{\rm anis}\rangle = -(1/2)\sum x_k x_j u^{kj}_{Lmn}\langle D^L_{pm}\rangle_k\langle D^L_{-pn}\rangle_j, \tag{5.3.1}$$

where x_j is the mole fraction of conformer *j* and u^{jk}_{Lmn} denote the tensorial interaction coefficients between two conformers, *j* and *k*. The difference between this case and the non-exchanging system is that the mole fraction in this case is a function of the temperature and the ordering of the system. In addition to this orientational internal energy there is a contribution from the conformational energy $u^j_{\rm conf}$ and the additional scalar interaction, u^{kj}_0 between two non-identical molecules. Hence we need to take into account the combined conformational

energy which can be assumed to take the form [51]

$$\tilde{u}^j_{\rm conf} = u^j_{\rm conf} + u^{jk}_0. \tag{5.3.2}$$

The additional internal energy is then

$$\langle U_{\rm conf}\rangle = \sum x_j \tilde{u}^j_{\rm conf}. \tag{5.3.3}$$

Hence the total internal energy per particle is

$$\langle U\rangle = \langle U_{\rm anis}\rangle + \langle U_{\rm conf}\rangle. \tag{5.3.4}$$

The total entropy has a contribution from the orientational entropy. The orientational entropy has the same form as the non-exchanging mixture. In addition, there is an entropy of mixing since the mole fractions x_j change with the orientational order of the nematic phase. Thus the total entropy is

$$S = -k_B \sum \left\{ x_j \int f_j(\Omega) \ln f_j(\Omega) d\Omega + x_j \ln x_j \right\}. \tag{5.3.5}$$

In order to find the orientational and conformational distributions, we take the variation of the free energy with respect to both distribution functions, subject to the order parameters are equal to the averages of the Wigner functions and that the distributions are normalised

$$\int f(\Omega) d\Omega = 1, \tag{5.3.6}$$

$$\langle D^L_{pm}\rangle_j = \int D^L_{pm}(\Omega) f_j(\Omega) d\Omega,$$

$$\sum x_j = 1. \tag{5.3.7}$$

The variation of the free energy gives

$$\begin{aligned} \delta A = \sum_j \int \Big\{ & -\sum x_k x_j u^{kj}_{Lmn} \langle D^L_{pm}\rangle_k D^L_{-pn}(\Omega) \\ & + k_B T x_j \left(1 + \ln f_j(\Omega)\right) + \eta_j \Big\} \delta f_j(\Omega) d\Omega \\ & + \sum_j \Big\{ -\sum x_k u^{kj}_{Lmn} \langle D^L_{pm}\rangle_k \langle D^L_{-pn}\rangle_j + \tilde{u}^j_{\rm conf} \\ & + k_B T \sum_j \int f_j(\Omega) \ln f_j(\Omega) d\Omega + k_B T (\ln x_j + 1) + \beta_j \Big\} \delta x_j = 0. \end{aligned} \tag{5.3.8}$$

where γ_i and β_i are the undetermined Lagrange multipliers. For δA to be zero, the expressions inside the curly brackets must vanish simultaneously. Solving for the first expression to vanish, we get

$$f_j(\Omega) = \frac{\exp\left(\frac{1}{k_B T} \sum x_k u^{kj}_{Lmn} \langle D^L_{pm}\rangle_k D^L_{-pn}(\Omega)\right)}{\exp(1 + \frac{\eta_j}{x_j k_B T})}. \tag{5.3.9}$$

And so the denominator must be the partition function for the orientational distribution to nor-

malise. Thus, the potential of mean torque for molecule j is

$$U_j(\Omega) = -\sum x_k u^{kj}_{Lmn} \langle D^L_{pm} \rangle_k D^L_{-pn}(\Omega). \tag{5.3.10}$$

In order to find the conformational distribution, first we notice that by taking the average of $\ln f_j(\Omega)$ for conformer *j*, we have

$$-\sum x_k u^{kj}_{Lmn} \langle D^L_{pm} \rangle_k \langle D^L_{-pn} \rangle_j + k_B T \int f_j(\Omega) \ln f_j(\Omega) d\Omega = -k_B T \ln Q_j. \tag{5.3.11}$$

Substitute this into the free energy in equation (5.3.8) we have

$$-k_B T \ln Q_j + \tilde{u}^j_{\text{conf}} + k_B T(\ln x_j + 1) + \beta_j = 0. \tag{5.3.12}$$

Therefore, the conformational distribution is

$$x_j = \frac{Q_j \exp(-(1/k_B T)\tilde{u}^j_{\text{conf}})}{\exp(1 + \beta_j / k_B T)}. \tag{5.3.13}$$

In order to normalise the conformational distribution function, the denominator must be the conformational-orientational partition function

$$Z = \sum_k \exp\left(-\tilde{u}^k_{\text{conf}} / k_B T\right) Q_k, \tag{5.3.14}$$

Hence, the conformational distribution is

$$x_j = Z^{-1} Q_j \exp(-\tilde{u}^j_{\text{conf}} / k_B T). \tag{5.3.15}$$

Now we find the more explicit form for the free energy at equilibrium. Taking the logarithm of $f_j(\Omega)$ and then take the orientational average, we get

$$k_B T \int f_j(\Omega) \ln f_j(\Omega) d\Omega = -2\langle U_{\text{anis}} \rangle - k_B T \ln Q_j \tag{5.3.16}$$

Now we take the logarithm for x_j

$$k_B T \ln x_j = -\tilde{u}^j_{\text{conf}} + k_B T \ln Q_j - k_B T \ln Z. \tag{5.3.17}$$

Adding these two expressions we get the simple form for the free energy

$$A = -\langle U_{\text{anis}} \rangle - k_B T \ln Z. \tag{5.3.18}$$

5.3.2 Two Conformer System

We see that the expressions for the potential of mean torque for the exchanging system is the same as that for the non-exchanging mixture. However the mole fractions of the two conformers

are related to their internal energy difference $\Delta E = \tilde{u}^l_{\rm conf} - \tilde{u}^b_{\rm conf}$ between them by

$$x_b^0 = \exp\left(\Delta E/k_BT\right)/\left[1 + \exp\left(\Delta E/k_BT\right)\right]. \tag{5.3.19}$$

Here, the superscript zero is used to denote the value in the isotropic phase. In the nematic phase, the mole fraction of the bent conformer is given by

$$x_b = \exp\left(\Delta E/k_BT\right)Q_b/\left[Q_b + \exp\left(\Delta E/k_BT\right)Q_l\right]. \tag{5.3.20}$$

We note that, $x_l + x_b = 1$. This expression for the mole fraction is valid provided the internal energy difference ΔE is independent of the orientation of the molecules with respect to the director. The mole fraction or conformational distribution of the bent conformer can change in the mesophase according to

$$x_b = x_b^0 Q_b \left[x_b^0 Q_b + x_l^0 Q_l\right]^{-1}. \tag{5.3.21}$$

Moreover the scaled free energy in this case is different from the non-exchanging mixture since in our system the conformers can interexchange

$$A^* = -\ln\left(Q_l + (x_b^0/x_l^0)Q_b\right) + \frac{1}{T^*}2\left(\langle F_U\rangle^2 + 2\langle F_B\rangle^2\right). \tag{5.3.22}$$

5.3.3 Calculations and Results

Most of the findings for the uniaxial nematic-to-isotropic transition for exchanging linear and bent molecules have been presented by Ferrarini *et al.* [44] for several mole fractions of the bent conformer in the isotropic phase. We extend their calculations to produce a phase map shown in figure 5.3 of the scaled transition temperature versus the mole fraction of the bent conformer in the isotropic phase. In their calculations, it was assumed that ΔE and hence the istropic composition and the Boltzmann factor $\exp(-\Delta E/k_BT)$ are held constant which ignores the small temperature dependence resulting from $1/k_BT$, but facilitates the calculations. The exchanging system agrees with the non-exchanging mixture and the experiments (as reviewed by Ferrarini *et al.* [44]) that the uniaxial nematic-to-isotropic transition temperature decreases on increasing the mole fraction of the bent conformer. In addition, the transitional order parameters and entropy also increases continuously on increasing the mole fraction of the bent conformer. When the mole fraction of the bent conformer is sufficiently large at 0.97, there is a discontinuity in the dependence of the transitional order parameter on the mole fractions. This happens since, the nematic phase consists of many bent molecules has a very low order. Thus the ordering is not enough to convert a significant amount of bent molecules into linear. These results can explain the even-odd effect which we have discussed in the Introduction of this chapter. In this model, the mole fractions the bent conformer of even dimers are less than 0.97 whereas those of odd dimers are greater than 0.97. Moreover, odd dimer, there are two phase transitions as we show in figure 5.4(a). As we lower the temperature from the isotropic phase, first the system undergoes a second order phase transition into the uniaxial nematic phase. The bent conformer also convert into linear continuously. This is because the system is mostly bent. The uniaxial nematic phase composed of most bent molecules is weakly ordered. Therefore, the energy difference between

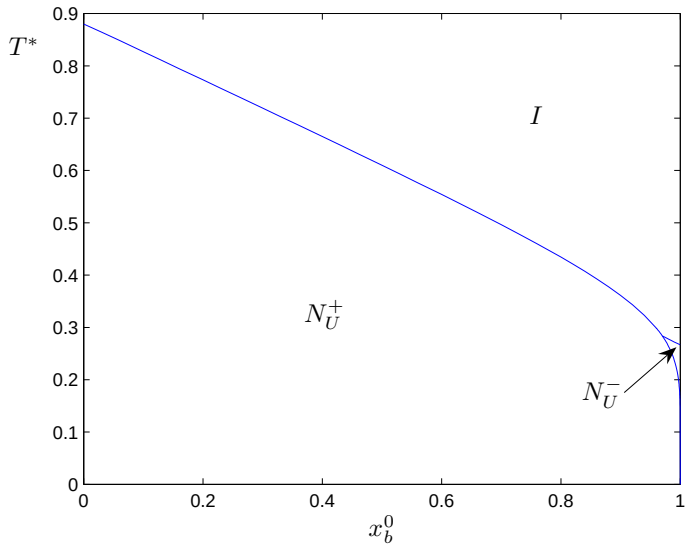

FIGURE 5.3: The dependence of the scaled transition temperature on the mole fraction of the bent molecules in the isotropic phase in exchanging system. First order transitions are shown as continuous lines whereas second order transitions are shown as broken lines.

the isotropic and the uniaxial nematic phase is not enough to cause a large change in the composition. As we lower the temperature, the system undergoes a first order transition into another uniaxial nematic phase. This new uniaxial nematic phase consists of mostly linear conformer since the majority of bent conformer convert into linear. In the phase map we use N_U^+ and N_U^- to denote nematic phase rich in linear and bent conformers, which respectively are analogous to nematic phases formed from calamitic and discotic molecules.

We also see from the phase map in figure 5.3 that for $x_b^0 < 0.97$, there is a positive deviation from linearity in the uniaxial nematic-to-isotropic phase transition temperature. In addition, this transition temperature is higher than that for the non-exchanging binary mixture. We may understand this difference by considering the two contributions to the total free energy from the anisotropic free energy and the conformational free energy. At the uniaxial nematic-to-isotropic phase transition, for $x_b^0 < 0.97$, the anisotropic free energy of the uniaxial nematic phase is positive. Therefore, in the non-exchanging mixture, the transition takes place at a lower temperature when it becomes zero. However, the conformational free energy of the nematic phase is less than in the isotropic phase due to large changes in the mole fractions at the phase transition. In addition, the difference in the conformational free energy is greater than the anisotropic free energy. Therefore, the total free energy of the uniaxial nematic phase is less than the isotropic phase which causes the phase transition at a higher scaled temperature than the non-exchanging mixture. When the mole fraction of the bent conformer is equal to 0.97, at the phase transition, both the anisotropic free energy and the conformational free energy differences are zero and so the transition temperature for this exchanging system is equal to that for the corresponding non-exchanging system. In addition, the conformational free energy difference is just enough to cause large changes in the mole fractions at the phase transition. Clearly for a system with a small amount of the linear conformer ($x_l^0 < 0.97$), just below the uniaxial nematic-to-isotropic phase transition temperature, the conformational free energy of the nematic system rich in linear conformer is greater than that for the system rich in bent conformer. As we lower the temper-

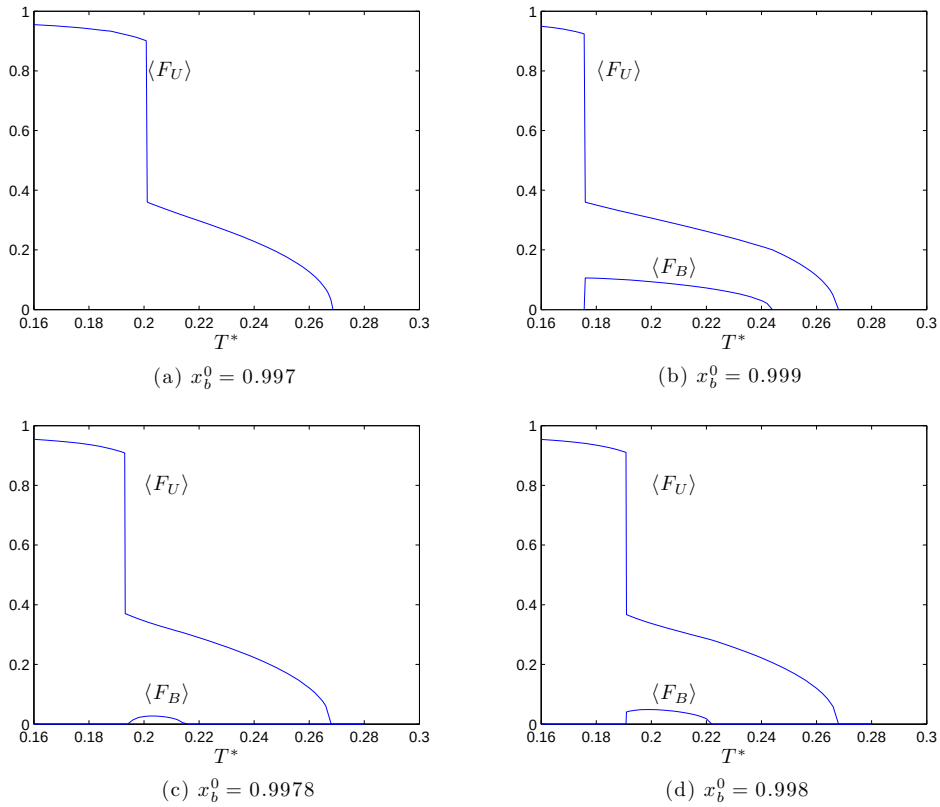

(a) $x_b^0 = 0.997$ (b) $x_b^0 = 0.999$

(c) $x_b^0 = 0.9978$ (d) $x_b^0 = 0.998$

FIGURE 5.4: The dependence of the order parameters on the scaled temperature for the exchanging system.

ature, the system becomes more and more ordered. The anisotropic free energy gets smaller. Until it compensates for the conformational free energy difference then most bent conformer convert to linear conformer and we see a first order jump in the uniaxial order parameter. This is an illustration that the uniaxial nematic phase favours the more anisotropic (linear) conformer. It is also important to note that in the regime of the uniaxial nematic formed mostly of bent molecules, the presence of a large amount of bent molecules leads us to believe that it might be possible for a biaxial nematic phase to form. In addition, since the uniaxial nematic phase favours the more uniaxial (linear) conformers, we may expect that the biaxial nematic phase would favour the more biaxial (bent) conformers.

Indeed we find a small island of biaxial nematic phase in the regime rich in bent conformer. It is shown in the magnification of the phase map in figure 5.5. In contrast to the first order uniaxial nematic composed of mostly linear molecules (N_U^+) to biaxial nematic (N_B) phase transition, the transition from biaxial nematic to uniaxial nematic phase consists of mostly bent conformer (N_U^-) is continuous, the changes in the mole fraction is also continuous. Generally, this second order transition temperature increases on increasing the mole fraction of the bent conformer x_b^0 in the isotropic phase. This behaviour is analogous to the non-exchanging mixture since adding more biaxial (bent) molecules into our system increases the biaxial nematic-to-uniaxial nematic transition temperature. The difference between this exchanging system with the non-

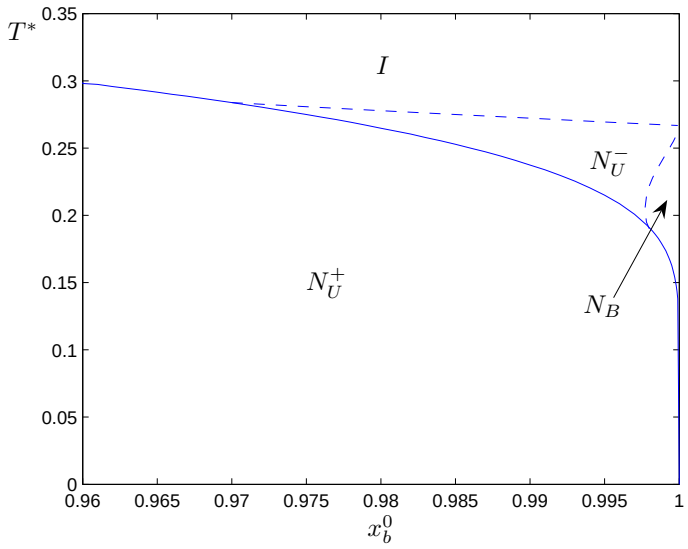

FIGURE 5.5: The dependence of the scaled transition temperature on the mole fraction of the bent molecules in the isotropic phase in the exchanging system. First order transitions are shown as continuous lines whereas second order transitions are shown as broken lines.

exchanging one is that firstly the $N_U^- - N_B$ transition temperature of the exchanging system is lower for the same mole fraction of bent molecules compared to the non-exchanging system. It is simply because in the uniaxial nematic phase, more bent conformer convert into linear, which depresses the transition temperature. Secondly, for a vanishingly small interval of x_b^0 we find that the biaxial nematic phase undergoes a second order reentrant transition back into the uniaxial nematic phase which consists mostly of bent conformer (N_U^-) before a first order $N_U^+ - N_U^-$ transition. This behaviour is shown in figure 5.4(c) which gives the order parameters for $x_b^0 = 0.9978$. In order to understand this behaviour, we need to see how the mole fractions change in the biaxial nematic phase. In figure 5.6 we show an example of how the mole fractions change with temperature for $x_l^0 = 0.001$. It is clear that even in the biaxial nematic phase, the bent molecules still convert into the linear one, although the rate of conversion would be faster if we do not allow the biaxial phase to form. This has a negative impact on the biaxial order parameter and causes the biaxial order to decrease gradually and the system reenters the uniaxial nematic. In contrast, for larger values of x_b^0, the biaxial nematic phase reenters directly to the uniaxial nematic phase which consists mostly of linear conformer. This is shown in figures 5.4(b) and 5.4(d). It is because when most of bent molecules convert to linear, the ordering in the system is governed by the uniaxial linear conformer. The system simply does not have enough bent molecules to order biaxially.

So far in the calculations we make the assumption that the mole fractions of linear and bent molecules in our exchanging system is invariant in the isotropic phase. In other words, the ratio of the conformational energy difference and the temperature $\Delta E/k_BT$ is constant. This assumption clearly allow us to extend the previous calculations by Ferrarini *et al.* [44], allowing the biaxial nematic phase to form. In addition, we can now understand that the biaxial ordering of the system still favours the less biaxial component. When we include the explicit temperature dependence of the mole fraction, the two effects intervene and it is not easy to make that conclusion. The other advantage of this assumption is that the mole fractions only range from

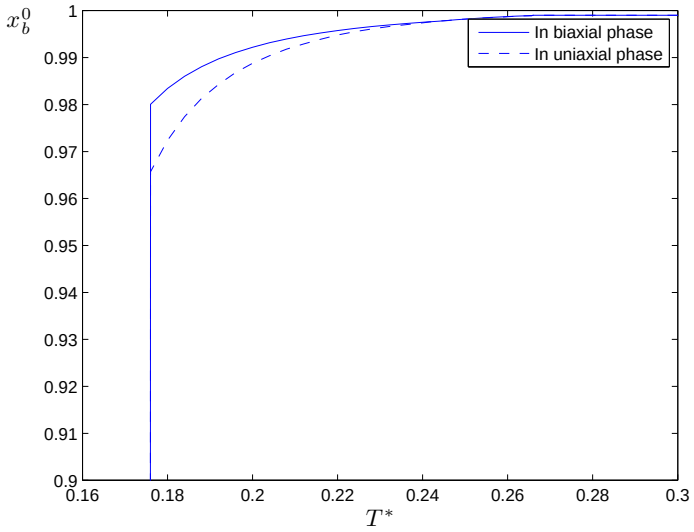

FIGURE 5.6: The dependence of the mole fraction of the bent conformer on the scaled temperature for $x_l^0 = 0.001$. The continuous line shows the value when we allow the biaxial nematic to form. The broken line shows the value when we do not allow the biaxial nematic to form.

0 to 1 whereas the conformational energy different ΔE can take any real value. Hence, it is much more difficult to find an essential range for ΔE to perform the calculations. This assumption, however, is clearly unphysical since the conformational energy difference is a molecular property and should be constant with respect to the temperature and the order of the system.

It is then essential to remove this assumption and calculate a phase map of temperature and the conformational energy difference. For convenience we scale the conformational energy difference with the anisotropy of an arm $\Delta E^* = \Delta E/u_{200}$. In order to find an essential interval for ΔE^*, we convert the phase map of the dependence of the transition temperature on the mole fraction in the isotropic phase into a phase map of the dependence of the transition temperature on the ratio $\Delta E/k_BT = \Delta E^*/T^*$ which is shown in figure 5.7. Clearly in order to see the biaxial nematic phase ΔE^* must be positive. In addition, at $\Delta E^*/T^* = 7$ and $T^* = 0.2$ the system is biaxial. Hence it seems that the essential interval for ΔE^* is from 0 to about 1.4. Based on this premise, we have constructed a phase map of the transition temperature with ΔE^* in figure 5.8. This new phase map still retains some features of the old phase map. Here the negative value of the conformational energy difference ΔE^* means that the linear conformer is more stable in the isotropic phase, hence it is analogous to the calculations where the isotropic mole fraction of the bent conformer $x_b^0 < 0.5$ and is fixed. In contrast, the positive value of ΔE^* corresponds to $x_b^0 > 0.5$ and the bent conformer is more stable. The even-odd effect can then be explained in the same way as that suggested by Ferrarini *et al.* [44]. Thus, the values of ΔE^* for odd dimers are greater than 0.96 whereas for even dimers they are less than 0.96. We also see that the $N_U^- - I$ transition temperature decreases whereas the $N_B - N_U^-$ transition temperature increases as the value of ΔE^* goes up. This is because there are more bent conformer at the phase transition for larger values of ΔE^* and that the bent conformer is less anisotropic and more biaxial compared to the linear one. However, there are differences between this representation of the results and that when we fix the value of the ratio $\Delta E^*/T^*$. First of all, the biaxial nematic phase does not undergo a reentrant transition into

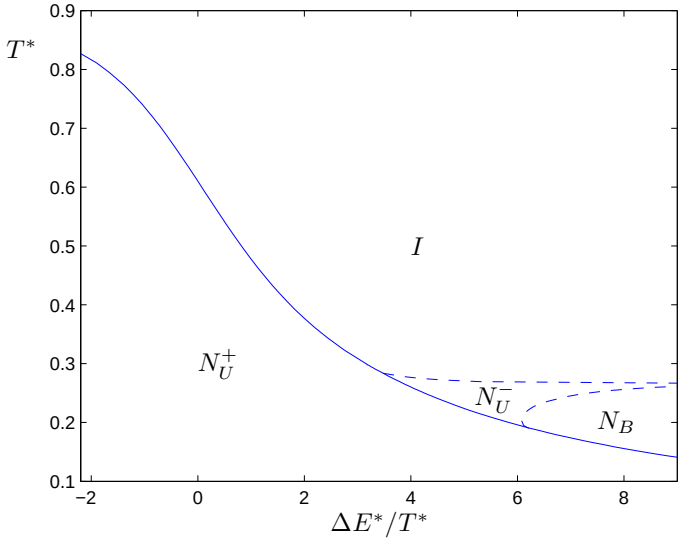

FIGURE 5.7: The dependence of the scaled transition temperature on the ratio $\Delta E^*/T^*$. First order transitions are shown as continuous lines whereas second order transitions are shown as broken lines.

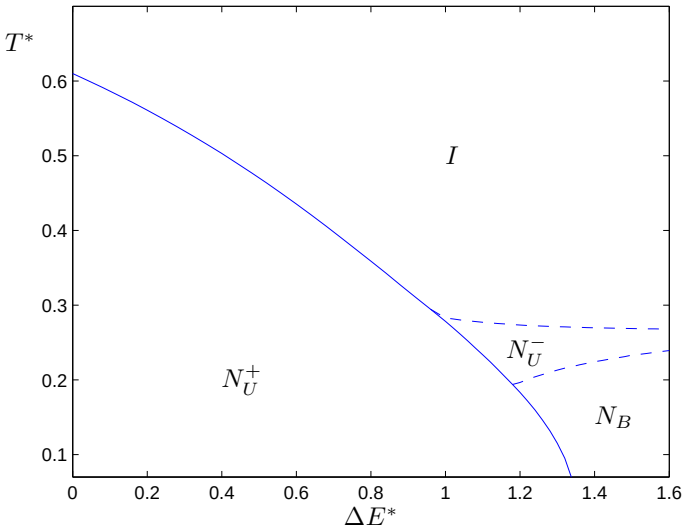

FIGURE 5.8: The dependence of the scaled transition temperature on the conformational energy difference ΔE^*. First order transitions are shown as continuous lines whereas second order transitions are shown as broken lines.

the discotic uniaxial nematic phase composes of mostly bent conformer as we have seen when we fix $x_b^0 = 0.9978$. This might be because, in the ordered phase, the effect of increasing the mole fraction of the linear conformer by ordering the phase is countered by the bent conformer being more favoured with decreasing temperature. Therefore the mole fraction of the linear conformer does not increase to a value large enough to cause the reentrant transition. Secondly, for sufficiently large conformational energy difference ΔE^*, greater than about 1.4, the biaxial nematic phase is stable and the system does not undergo a transition into the calamitic uniaxial nematic consists of mostly linear molecules. This can also be explained due to the increase in mole fraction of the bent conformer on decreasing the temperature. In contrast, it is decreased

by the ordering of the system. It may be that for large values of ΔE^*, the overall effect is that the ordering of the system is not enough in order to force the bent conformer to convert into linear in order for the biaxial nematic phase to undergo a transition into the calamitic uniaxial nematic phase.

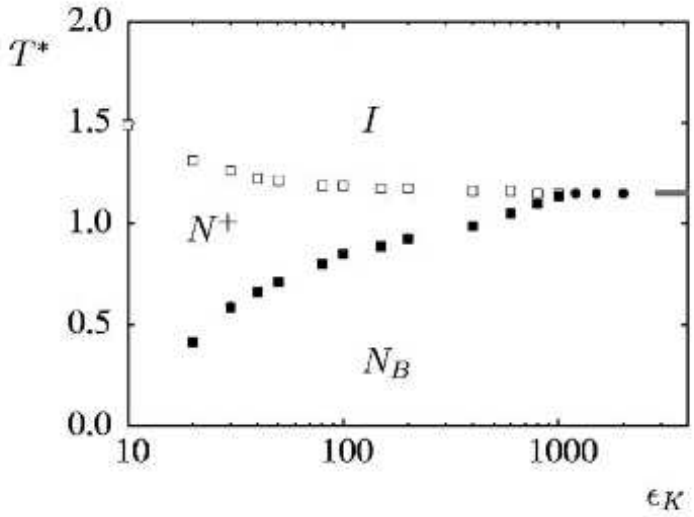

FIGURE 5.9: The dependence of the scaled transition temperature on the bending force constant in Bates's calculations. Reproduced from [99].

It is of interest to make comparisons between our molecular field calculations and the Monte Carlo simulations by Bates [99] which is shown in figure 5.9. Although our theory was developed originally for uniaxial nematics by Ferrarini *et al.* [44] to explain the even-odd effect found in liquid crystal dimers, it can be thought of as a model two extreme conformers of V-shaped molecules. In this case, contacts can be between our theory and Bates' Monte Carlo simulation. We should note a fundamental difference between our model and Bates' model. The conformational distribution is discrete in our model whereas it is continous in Bates' model. In addition, the difference between the parameters should be noted. In our case, ΔE^* is the scaled energy difference between the two extreme conformers. In comparison, ϵ_K in the simulations is the bending force constant. It multiplies the square of the difference between the interarm angle and the preferred angle, which in this case takes the tetrahedral value. Therefore direct comparisons of the two models cannot be made. However, we can still see the effects of making the model continuous on our model. There are several similarities between the two phase maps. First, we see that the nematic-to-isotropic phase transition temperature decreases on increasing ΔE^* in our model and ϵ_K in Bates' model. Secondly, the biaxial nematic phase is destabilised as ΔE^* and ϵ_K decrease. It can be understood that the smaller value of the energy difference in our model and the bending force constant in Bates' model means that the tetrahedral molecules are easier to bend. Therefore a system with smaller ΔE^* or ϵ_K has a larger mole fraction of molecules which deviate from the tetrahedral value. This leads to the system becomes more anisotropic and less biaxial. Thirdly, the uniaxial nematic-to-isotropic and biaxial nematic-to-uniaxial nematic transition lines approach each other asymptotically. It is because as the energy difference or the bending force constant becomes large, the molecules become more and more rigid and the mole fractions of those conformers whose interarm angles deviate from the tetrahedral value become small. Therefore, the phase behaviour is more independent of the energy

difference. As ΔE^* and ϵ_K tend to infinity, there should be a direct biaxial nematic to isotropic phase transition, in keeping with molecular field calculations and Monte Carlo simulation results for rigid tetrahedral V-shaped molecules. Moreover, there is a major difference between our calculations and Bates' simulation results. We notice that in our calculations, there is a first order transition from a uniaxial nematic composed mostly of linear molecules to a uniaxial nematic composed mostly of bent molecules which was not observed in the simulation. It may be explained that in the simulation, there was a continuous range of conformation, thus allowing the conformers to convert continuously, favouring a second order phase transition.

5.4 Conclusions

The exchanging system of linear and bent molecules studied in this chapter is an idealised model for a liquid crystal dimer. In our model, the many conformations that can be adopted by a liquid crystal dimer is replaced by just two, one is linear and the other is bent. This model has been used by Ferrarini *et al.* [44] to explain various properties of the characteristic even-odd effect exhibited by liquid crystal dimers in uniaxial nematics. Our theory is an extension of that to allow biaxial nematics based on the work by Luckhurst [51]. Indeed we find a stabilised biaxial nematic region for sufficiently large conformational energy difference between the linear and the bent conformer. Therefore in order to see the biaxial nematic phase in the experiment we need odd spacer liquid crystal dimers whose conformational energy difference between the linear and the bent conformers is sufficiently large. In addition, we find that the ordering of both the uniaxial and the biaxial nematic phases stabilise the more anisotropic, less biaxial linear conformer. This is in contrast to our expectation that biaxial ordering would stabilise the more biaxial conformer.

Chapter 6

Magnetic Field Induced Uniaxial Nematic Liquid Crystals for Biaxial Molecules

In this chapter, we formulate a molecular field theory for magnetic field induced uniaxial nematic liquid crystals formed from biaxial molecules. Since we only consider uniaxial nematics, we refer to it as the nematic phase in this chapter. Our work is inspired by recent experimental results on magnetic field induced nematic phase for a system of V-shaped molecules by Ostapenko, Wiant, Sprunt, Jákli and Gleeson [40]. In section 6.1, we discuss some theoretical and experimental works on the effect of a magnetic field on the phase behaviour of nematogen. Next, in section 6.2, we discuss the molecular field theory and the Landau-KKLS theory for biaxial molecules in the presence of a magnetic field. The calculation results are presented in sections 6.3 and 6.4.

Under non-zero magnetic field strength, both the Landau-de Gennes and the molecular field theory for uniaxial nematics predict that there are three effects. First, for temperature greater than the clearing point, a *paranematic* phase with small nematic ordering is induced. The second effect is that the first order phase transition temperature from the more ordered phase to the less ordered phase is shifted towards higher temperature. This is called the *Cotton-Mouton effect* if the field is magnetic and the *Kerr effect* if the field is electric. Finally, there is a *critical field* strength, above which there is no clear transition between the paranematic and the nematic phases.

6.1 Related Works

All the three field induced effects have been observed experimentally for a system of rod-like molecules in electric field [102] . In contrast, early experimental studies for rod-like molecules using magnetic field only discovered the Cotton-Mouton effect [103] and an increase in the

transition temperature of only a few milli-Kelvin [104]. Only in recent years, both the Cotton-Mouton effect [105] and significant increases in the transition temperature [40] due to magnetic field have been observed for V-shaped molecules. In their experimental studies, Ostapenko et al. [40] discovered two of the three effects predicted by theory. First, the magnetic field induces a small nematic ordering in the isotropic phase, which forms the paranematic phase. Secondly, the paranematic-to-nematic phase transition was measured using several experimental techniques. By varying the magnetic field from 0 to 31 Tesla, the authors observed a magnetic field induced first order phase transition in a thermotropic liquid crystals. The transition temperature increases on increasing the field strength. The success of this experiment was attributed to two factors. The first was that a strong magnetic field was available. The second factor was that the system under study was formed from V-shaped molecules. The second factor was explained by the authors within the framework of the Landau-de Gennes theory. In this theory, the coefficient B in the Landau expansion multiplies the cubic of the order parameter. This coefficient controls the strength of the first order transition.The authors argued that, in their system of V-shaped molecules, the coefficient B is small. Therefore, the magnetic field required to observe the field dependence of the transition temperature for bent-core nematics should be significantly smaller than for calamitic nematics. In this chapter, we demonstrate that the coefficient B can be related to molecular biaxiality. Since V-shaped molecules are highly biaxial, the coefficient B for this case is significantly smaller than for calamitic molecules. This becomes apparent when we relate the parameters in the molecular field theory to the coefficients in the Landau-de Gennes expansion using the method in reference [64].

The mathematical structure for electric field and magnetic field induced nematic phase are analogous. A molecular field theory which described the effects of electric field on the nematic-to-isotropic phase transition was developed by Hanus [106]. This was an extension of the Maier-Saupe theory for uniaxial nematics to include a strong external electric field. Three effects analogous to magnetic field induced nematics were observed. The first of those was the optical Kerr effect. In this effect, the electric field induces a small nematic order in the isotropic phase. This small order causes a small birefringence, which depends on the square of the applied electric field. In addition, analogous to the magnetic field induced nematics, the coefficient which multiplies the square of the electric field is $(T - T_{bf})^{-1}$. Here, T is the temperature at which the birefringence is measured and T_{bf} is the bifurcation temperature. The other two effects are also analogous to those predicted for magnetic field: the first order transition temperature between the high and low order phases increases on increasing the applied magnetic field strength and the existence of the critical field strength.

Wojtowicz and Sheng [45] extended the Maier-Saupe theory to investigate the magnetic field effects on nematic liquid crystals. In addition to the three main effects which we discussed before, there are three other interesting results associated with the transitional and critical order parameter and temperature. They are, the parabolic coexistence curve, the law of rectilinear diameter and the cubic power law. We discuss them when we repeat this calculations in the next section. In addition, we extend their calculations to deal with biaxial molecules.

These results for magentic field induced effects using the molecular field theory have also been confirmed by other methods. Luckhurst and Simpson [107] carried out a series of Monte Carlo simulations for a system of magnetic field induced nematics with the magnetic field strength greater than the critical field strength. In these calculations, the molecules were confined in a

simple cubic lattice and neighbouring molecules interact via an orientational dependence pair potential in addition to the interaction of the molecules with the field. These calculations showed a qualitative agreement with the molecular field theory, presented in the same paper. Since their calculations is done above the critical field, the system did not exhibit a phase transition. A more recent series of simulations was by Warsono, Abraha, Yusuf and Nurwantoro [108]. In these simulations, the molecules are also confined in a cubic lattice. In addition, each molecule is modelled as a three dimensional spin which can only point along six directions on the lattice axes. In these simple calculations, the authors were able to produce two of the three effects, namely the magnetic field induced nematic-to-isotropic phase transition and the critical field. Palffy-Muhoray and Dunmur [109] studied the effect of field induced nematic liquid crystals for uniaxial molecules using both the molecular field theory and the Landau-de Gennes theory. The molecular field free energy was expanded upto fourth order of the order parameter invariants. It was found that, in general, the free energy expansions in two theories differ. It was because the coefficients in the molecular field free energy expansion depends on the field strength, in contrast with those in the Landau-de Gennes theory. This causes the bifurcation temperature T^* in the molecular field theory to depend on the field strength. The authors removed this dependence and studied the common free energy. The direction of the field vector in the principle axis system which minimises the free energy is along one of the principle axes. The effects of the applied magnetic field on the phase behaviour were studied for materials with positive and negative diamagnetic anisotropy. For positive materials, the solution with the director parallel to the field is always energetically favourable. In contrast, for negative materials, the director tends to align perpendicular to the field in the nematic phase and parallel to the field in the paranematic phase.

6.2 Molecular Field Theory and Landau-KKLS Theory

6.2.1 Molecular Field Theory

As usual, the first step in formulating the molecular field theory is to construct the internal energy. In this case, it consists of two parts

$$U = U_U + U_H. \tag{6.2.1}$$

The first part, U_U, is generated by the pairwise intermolecular interactions in the uniaxial nematic phase formed from biaxial molecules. It can be constructed by considering the internal energy (2.3.2) for a general system of biaxial molecules in biaxial nematic. In this case, the nematic phase is uniaxial, the index p which represents the phase symmetry should be set equal to zero. The remaining Wigner functions $D^2_{0m}(\Omega)$, where $(\Omega) = (\alpha, \beta, \gamma)$, are identical to the spherical harmonics $C_{2m}(\omega)$, where $(\omega) = (\beta, \gamma)$. Hence,

$$U_U = -(1/2) \sum u_{2mn} \langle C_{2m} \rangle \langle C_{2n} \rangle. \tag{6.2.2}$$

The second part, U_H, is generated by the interaction of the molecules with the applied magnetic field. In order to construct this energy, we assume that the director is parallel to the field. This is in agreement with the calculations by Palffy-Muhoray and Dunmur which showed that in this

orientation of the director, the free energy is minimised [109] . Hence, U_H can be written as

$$U_H = -(3/2)B^2\chi^p_{20}, \tag{6.2.3}$$

where B is the magnetic flux density and χ^p_{20} is the material susceptibility tensor per molecule. The magnetic interaction has this form because if we define B_{2m} as a second-rank tensor such that $U_H = -B_{20}\chi^p_{20}$, then

$$B_{20} = (1/2)\left(2B_{ZZ} - (B_{XX} + B_{YY})\right) = (3/2)B_{ZZ} = (3/2)B^2. \tag{6.2.4}$$

Here, we use the fact that the second-rank tensor $\mathbf{B}$ is traceless $B_{XX} + B_{YY} + B_{ZZ} = 0$. In addition, χ^p_{20} can be related to the molecular susceptibility tensor, χ_{2n}, by

$$\chi^p_{20} = \chi_{2n}\langle C_{2n}\rangle. \tag{6.2.5}$$

Hence,

$$U_H = -\sum(3/2)B^2\chi_{2n}\langle C_{2n}\rangle. \tag{6.2.6}$$

Now we can construct the Helmholtz free energy according to equation (2.3.10) subject to two constraints in order to find the distribution function at equilibrium. The first one is that the distribution function is normalised. The second one is that the order parameters are the convolutions of the modified spherical harmonics with the distribution function

$$\langle C_{2m}\rangle = \int C_{2m}(\omega)f(\omega)d\omega. \tag{6.2.7}$$

The minimisation gives

$$\int\left(-\sum u_{2mn}\langle C_{2m}\rangle C_{2n}(\omega) - (3/2)B^2\chi_{2n}C_{2n}(\omega) + k_BT(\ln f(\omega) + 1) + \eta\right)d\omega = 0. \tag{6.2.8}$$

Solving this equation gives us the functional form of the distribution function at equilibrium. From that we can find the potential of mean torque

$$U(\omega) = -\left(\sum u_{2mn}\langle C_{2m}\rangle C_{2n}(\omega) + (3/2)B^2\chi_{2n}C_{2n}(\omega)\right) \tag{6.2.9}$$

In order to reduce the number of parameters, we use the geometric mean approximation. Hence, the molecular interaction part only depends on one biaxiality parameter. For the field interaction part, we see that there could be two parameters. They are related to the two components of the molecular magnetic susceptibility tensor, χ_{2n}. However, in order to simplify the problem, we assume that $\chi_{22} = \gamma\chi_{20}$. The field interaction part now only depends on γ and one more parameter, namely $\delta_{20} = (3/2)B^2\chi_{20}/u_{200}$. The potential of mean torque now becomes

$$U(\Omega) = -u_{200}\left(\langle F_U\rangle + \delta_{20}\right)\left(C_{20}(\Omega) + 2\gamma ReC_{22}(\Omega)\right). \tag{6.2.10}$$

In order to simplify the numerical calculations, we can write the partition function in terms of

the zeroth order Bessel function of the first kind

$$Q = 2\pi \int_0^{\pi} \exp[(1/T^*)\left(\langle F_U\rangle + \delta_{20}\right) d_{20}^2(\beta)]\mathrm{I}_0\left(\gamma\left(1/T^*\right)\left(\langle F_U\rangle + \delta_{20}\right) 2d_{22}^2(\beta)\right)\sin\beta d\beta. \tag{6.2.11}$$

Here,

$$I_n(a) = \frac{1}{\pi}\int_0^{\pi} \cos\left(n\theta\right)\exp\left(a\cos\theta\right)d\theta. \tag{6.2.12}$$

Finally, the equilibrium orientational Helmholtz free energy is

$$A/k_{\mathrm{B}}T = -\ln Q + \left(1/2T^*\right)\langle F_U\rangle^2. \tag{6.2.13}$$

6.2.2 Landau-KKLS Theory

The Landau-de Gennes theory has also beeen used to explain the effects of magnetic and electric fields on nematogens. This theory has the advantage over the molecular field theory of its simplicity. As we can see in Appendix F.1 that for the Landau-de Gennes expansion up to the fourth order of the order parameter, all results are analytical. However, the classical Landau-de Gennes theory does not relate the coefficients in the free energy expansion to the molecular biaxiality. One method which was employed to do that is to derive the Landau expansion from the non-equilibrium free energy in the molecular field theory [63, 64]. We discuss the non-equilibrium free energy in section 2.5. This method was at first employed for uniaxial molecules in uniaxial nematic phase [63]. Later, it was extended for various other systems, including biaxial molecule in uniaxial nematics in zero field [64]. Here we extend this method to derive the Landau-de Gennes expansion from the molecular field theory for uniaxial nematics in the presence of a magnetic field.

Here, we argue that in the Landau-KKLS theory, the contribution of the field interaction to the free energy expansion only comes from the internal energy and does not come from the expansion of the partition function. First of all, maximising the entropy using the method which we have discussed in section 2.5.1 gives us the partition function of the form

$$Z(\eta) = \int \exp(\eta F_U(\omega))d\omega. \tag{6.2.14}$$

Now the non-equilibrium order parameter can be written as

$$\langle F_U\rangle = Z(\eta)^{-1}\int F_U(\omega)\exp(\eta F_U(\omega))d\omega. \tag{6.2.15}$$

The next step in the Landau-KKLS theory is to invert this function to get η as a function of $\langle F_U\rangle$. Then, the partition function becomes a function of the order parameter $\langle F_U\rangle$. We can see that this procedure does not involve the dependence on the field. We note that if the field is electric instead of magnetic then the entropy in the non-equilibrium free energy may still have contribution from the external field. For example, in a similar system the electric field does induce a macroscopic polarisation. As a result the entropy should be maximised with two constraints which correspond to the polar first-rank and non-polar second-rank order parameters. In this case the entropy does depend on the field [110]. On the other hand, magnetic field

does not induce polar order and the interaction between magnetic dipoles is negligibly small. Therefore in our calculation, the only contribution of the field to the non-equilibrium free energy is from the internal energy. Consequently, we do not need to redo the whole procedure in order to derive the Landau-KKLS theory. We only need to add the field contribution in the internal energy to the free energy in zero field in reference [64] in order to get the following Landau-KKLS expansion

$$A/u_{200} = (3/4)a(T^* - T^*_{\rm bf})\langle F_U\rangle^2 + (1/4)bT^*\langle F_U\rangle^3 + (9/16)C\langle F_U\rangle^4 - \delta_{20}\langle F_U\rangle. \quad (6.2.16)$$

Here,

$$\begin{aligned} T^*_{\rm bf} &= \left(1+2\gamma^2\right)/5, \\ a &= \frac{10}{3(1+2\gamma^2)}, \\ b &= -\left(\frac{100}{21}\right)\frac{\left(1-6\gamma^2\right)}{\left(1+2\gamma^2\right)^3}, \\ C &= \left(\frac{400}{1764}\right)\frac{\left(56\gamma^6+444\gamma^4-78\gamma^2+17\right)\theta_C}{\left(1+2\gamma^2\right)^5}, \end{aligned} \quad (6.2.17)$$

Here, we note that the Landau-KKLS expansion differs from the original Landau-de Gennes expansion in that the coefficient which multiply the cubic term is temperature dependent. We call the latter the *pure Landau* theory, as opposed to the *Landau-KKLS* theory. A direct contact can be made between the Landau-KKLS and the pure Landau theories by replacing the temperature dependent of the coefficient which multiplies the cubic term with a constant which we shall call θ_B. In other words, we replace bT^* by $B = b\theta_B$. Solving this system is the same as solving the Landau-de Gennes theory for uniaxial nematics which has been reviewed in reference [111] and which is rediscussed in Appendix F.1.

6.3 Field Induced Phase Transition

6.3.1 Molecular Field Theory

First, we discuss the pretransitional behaviour of the system. The application of a magnetic field induces a small order in the isotropic phase. This new phase is called the paranematic phase. As the temperature is lowered, the order parameter increases and there might be a transition between the nematic and the paranematic phase. We can get the induced order parameter in the paranematic phase by expanding the exponential in the partition function in terms of the order parameter $\langle F_U\rangle$ upto first order. The dependence of the order parameter on the field strength in the paranematic phase is

$$\langle F_U\rangle = \frac{(2\gamma^2+1)\delta_{20}}{5(T^* - T^*_{\rm bf})}. \quad (6.3.1)$$

Hence, we see that at a fixed temperature in the paranematic phase, the induced order parameter increases quadratically with the magnetic flux density, B.

The second effect due to the field is the induced transition temperature. We find the nematic-to-paranematic phase transition temperature by studying the dependence of the order parameter on the scaled temperature for a fixed value of the scaled magnetic flux density δ_{20} and molecular biaxiality, γ. The nematic-to-paranematic transition temperature is located when there is a jump in the order parameter. In figures 6.1, we show the dependence of the order parameter $\langle F_U \rangle$ on the scaled temperature for different values of δ_{20} and γ. The value of γ is kept fixed in each figure. We see that, when the field strength is zero, δ_{20} is zero, the first order transition is essentially between the uniaxial nematic and the isotropic phase. This phase transition temperature increases as we increase γ, in agreement with figure 2.4. As δ_{20} increases, the jump in the order parameter gets smaller. When this gap just starts to be zero then we reached a critical point. For the field strength higher than the critical value, the nematic phase and the paranematic phase are no longer distinguishable. For each value of γ, the values which we use for δ_{20} are equally spaced. In addition, the transition temperatures found for those values of δ_{20} are also equally spaced, as can be seen from the vertical lines connecting the two curves in the two phases. Therefore, the scaled transition temperature increases linearly with B^2 for a fixed value of γ.

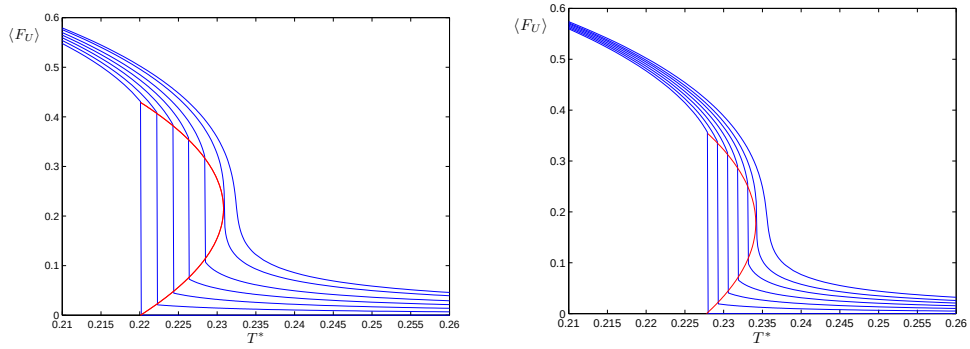

(a) $\gamma = 0$ (b) $\gamma = 0.2$

(c) $\gamma = 0.3$ (d) $\gamma = 0.36$

FIGURE 6.1: The dependence of the combined order parameter $\langle F_U \rangle$ on the scaled temperature as the field strength is varied for different values of the biaxiality parameter γ. The order parameters at the phase transition follows parabolic coexistent curves of the form $(\langle F_U \rangle_N - \langle F_U \rangle_c)^2 = \alpha(T^* - T_c^*)$ where α is a constant. The values of α in these case are: (a) 4.295, (b) 5, (c)6.065, (d) 6.763. The values of δ_{20} used in these case are: (a) [0:0.002:0.008 0.01046 0.012], (b) [0:0.001:0.004 0.00490 0.006], (c) [0 .0005 .00108 .0015] and (d) [0 .000111 .00025]. Here, we use $0 : a : b$ to denote an array of parameters from 0 to b with regular spacing a.

In their calculations for the field induced uniaxial nematic-to-isotropic phase transition, Wojtowicz and Sheng [45] reported that at the transition, the coexistent values for $\langle F_U \rangle$ in the nematic and the paranematic phases follow a quadratic curve. Let us call the value of $\langle F_U \rangle$ at the nematic phase $\langle F_U \rangle_N$ and that at the paranematic phase $\langle F_U \rangle_P$. In order to find a coexistent parabola for a value of γ, first we fit a parabola through the data points, which are $\langle F_U \rangle_N$ and $\langle F_U \rangle_P$ for different values of δ_{20}. The parabolae are plotted as red curves in figures 6.1. Then we take the value of the critical order parameter and scaled temperature at the base of the parabola. After that we fit a line through the data $(\langle F_U \rangle_N - \langle F_U \rangle_c)^2$ against $(T^* - T_c^*)$. Here, we use $\langle F_U \rangle_c$ to denote the value of the order parameter at the phase transition at the critical field. The gradient of the line gives us the relation between the two quantities $(\langle F_U \rangle_N - \langle F_U \rangle_c)^2 = \alpha(T^* - T_c^*)$. For $\gamma = 0$ we found $\alpha = 4.295$. This implies the relation $(S_N - S_P)^2 = 17.18.(T^* - T_c^*)$. We note that the previous calculations by Wojtowicz and Sheng [45] gave the constant in the latter relation equals to 16.45. As we explain later in this chapter, the estimation of T_c^* has some limitations which prevents us from achieving more accuracy. Our results for δ_{20}^c and T_c^* are slightly different from Wojtowicz and Sheng [45]. Our estimated values for δ_{20}^c and T_c^* in zero field are 0.01046 and 0.23094, respectively. In comparison, the estimated values for by Wojtowicz and Sheng [45] is 0.01044 and 0.23092, respectively. The differences between the two calculations may not seem very large. However, they may introduce a larger relative difference when we estimate the constant α, as we have seen.

We see that as γ increases, the difference between the zero field transition temperature and the critical transition temperature (at the critical field) gets smaller. There are two reasons for that as we can conclude from figures 6.1. The first reason is the value of $\langle F_U \rangle$ at the phase transition in zero field gets smaller as γ increases due to an increase in molecular biaxiality. The second reason is that the parabola is less curved as γ increases. The cause for this second reason is unknown. Consequently, the point from the transition temperature in zero field to the bottom of the parabola, which is the critical point, gets smaller as γ increases.

In figure 6.2 we show the dependence of the scaled transition temperature on the scaled magnetic flux density δ_{20} for different values of the biaxiality parameter γ. The curve for each value of γ is linear, in keeping with the results we showed in figure 6.1. The bottom line in figure 6.2 depicts the dependence of T_{NP}^* on δ_{20} for uniaxial molecules. As the value of γ goes up, T_{NI}^* increases, as expected for the nematic to paranematic transition for biaxial molecules. This is in accord with the phase map in figure 2.4 and the order parameter plots in figure 6.1.

We can see that the critical temperature and the slopes of the lines in figure 6.2 also increases on increasing γ. The latter implies that for the same applied field, the difference between the field induced transition temperature and the nematic-to-isotropic transition temperature in zero field for biaxial molecules is larger than that for uniaxial molecules. This is as expected since experimental results [40] have shown that a significant increase of the field induced transition temperature has only been observed in V-shaped molecules rather than rod-like molecules. In other words, while an increase in the transition temperature due to applied field for rod like molecules may be insignificant, it can be significant for biaxial molecules. One interesting feature we also need to mention is that the critical field strength gets smaller as γ increases. This is because the gap between the zero field transition temperature and the critical temperature gets smaller as γ increases, hence a smaller field strength is required to induce the transition temperature up to the critical point. Consequently, for a system of highly biaxial molecules,

it only requires a much smaller applied field to observe the critical point than for a system of rod-like molecules.

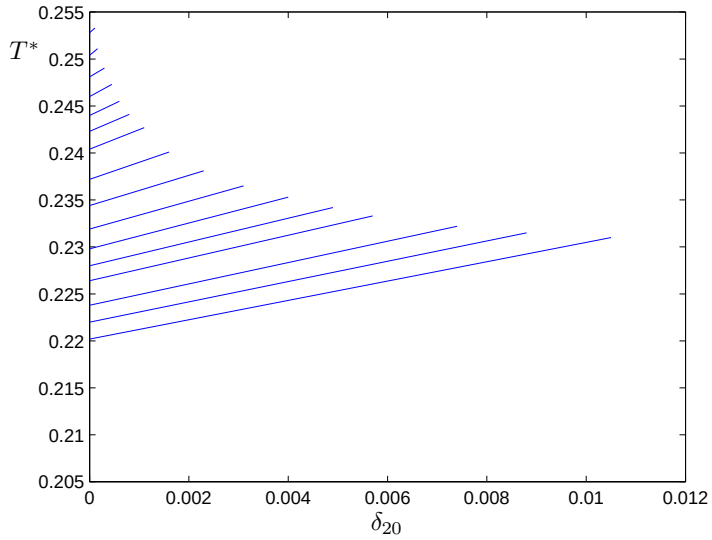

FIGURE 6.2: The dependence of the transition temperature on the scaled magnetic flux density δ_{20} as the biaxiality γ increases. The values of γ, from bottom to top, are: 0, 0.1, 0.14, 0.18, 0.2, 0.22, 0.24, 0.26, 0.28, 0.3, 0.31, 0.31, 0.32, 0.33, 0.34, 0.35, 0.36.

Here, we can to make a contact to the experimental results by Ostapenko et al. [40]. In their experimental result, the ratio

$$\frac{T_{NP} - T_{bf}}{T_{cp} - T_{bf}} \tag{6.3.2}$$

approaches 2.4 at the highest field strength. Here, T_{cp} denotes the nematic-to-isotropic phase transition in zero field, T_{NP} denotes the field induced transition and T_{bf} denotes the bifurcation temperature. However, the magnetic field used in their experiment has not reached the critical value. Therefore, we would expect the ratio

$$\frac{T_c - T_{bf}}{T_{cp} - T_{bf}}, \tag{6.3.3}$$

where T_c denotes the critical temperature, to be greater than 2.4 for their compound. In contrast, in our calculations this ratio is almost constant as we vary the biaxiality parameter γ and roughly equals to 1.5, in agreement with their prediction using the Landau-de Gennes theory. This disagreement may be due to the poor estimation of T_{bf} in the molecular field theory. The estimated value of T_{bf} can be improved by using the two-site cluster theory [112]. Therefore, in making comparisons with their results, we do not use the ratio $(T_c - T_{bf})/(T_{cp} - T_{bf})$. Instead, we rely on the ratios of the three scaled temperature T_c^*, T_{cp}^* and T_{bf}^*. We note that this comparison is imperfect since the experiment has not reached the critical field. We assume $T_{NP}(H_{max})$ which is the induced transition temperature at the highest value of the magnetic field strength H used in the experiment to be the critical temperature. In addition, the values for the temperature in the calculations are in scaled unit, in contrast with those in the experiment which are in degree Kelvin. The latter difference can be removed by taking the ratios T_{bf}^*/T_{cp}^*, T_c^*/T_{cp}^* and T_{bf}^*/T_c^* and compare them with the associated experimental values. In the experiment, $T_{cp} = 363.1K$.

We take the lower bound for T_c at $T_{N-P}(H_{max})$ to be $363.77K$. This gives us $T_{bf} = 362.82$. In figure 6.3, we show the calculated values for these three ratios from the molecular field theory. As γ decreases, the gaps between the ratios also decrease. In addition, the three ratios tend to one as γ gets larger. This is as we expect since for $\gamma = 1/\sqrt{6}$, the uniaxial nematic-to-isotropic phase transition is second order and therefore the three temperatures should be equal. In the figure, we also show the value for the three ratios from the experiment at $\gamma = 0.37$. Here we see that, according to the plot, $\gamma = 0.37$ is the best approximated value for the V-shaped molecules used in the experiment by Ostapenko et al. [40]. From equation (4.2.5), we can calculate the interarm angle of their V-shaped molecules which is $101.59°$.

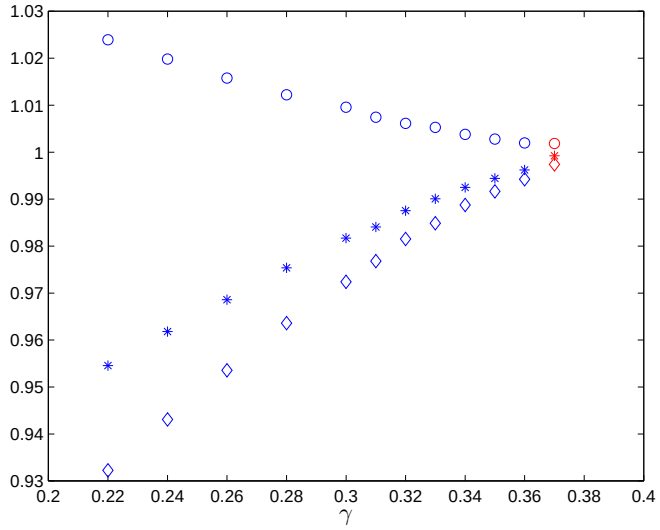

FIGURE 6.3: The data in blue are the dependence of the temperature ratios on the biaxiality parameter γ as predicted by the molecular field theory, $\circ$ T_c^*/T_{cp}^*, $*$ T_{bf}^*/T_{cp}^* and $\diamond$ T_{bf}^*/T_c^*. The data in red are the associated experimental results, plotted at $\gamma = 0.37$.

6.3.2 Landau-KKLS Theory

In addition to the molecular field theory, we can also use the Landau theory to predict the pre-transitional behaviour. In the paranematic phase, we assume that the order parameter $\langle F_U \rangle$ is small. Hence, the free energy only depends on the quadratic of $\langle F_U \rangle$ (see equation (6.2.16)). In this case, the pure Landau theory and the Landau-KKLS theory are the same. It is because the two theories are the same up to second order. The value of $\langle F_U \rangle$ in the paranematic phase is given by

$$\langle F_U \rangle = \frac{(2\gamma^2 + 1)\delta_{20}}{5(T^* - T_{bf}^*)}. \tag{6.3.4}$$

We see that this result agrees with the molecular field theory.

First, we discuss the solutions for the pure Landau theory because it is more analytical. We discuss the details of the calculations in Appendix F.1. The transition temperature for each

value of the magnetic flux density is given by

$$T^*(\delta_{20}) = T^*_{bf} + \frac{B^2}{27aC}\left(1 + \frac{\delta_{20}}{2\delta^c_{20}}\right). \tag{6.3.5}$$

In this case, it is clear that the transition temperature increases linearly with δ_{20}. Here, the critical field is

$$\delta^c_{20} = -\frac{B^3}{324C^2}. \tag{6.3.6}$$

Due to the complex forms of B and C (see equations (6.2.17)), it is not obvious that δ_{20} gets smaller as γ increases. However, it is clear that, at $\gamma = 1/\sqrt{6}$, B vanishes whereas C does not. Hence δ^c_{20} vanishes at $\gamma = 1/\sqrt{6}$. This is in keeping with the fact that at $\gamma = 1/\sqrt{6}$, the nematic-to-isotropic phase transition is the second order, hence the critical temperature is the same as the nematic-to-isotropic transition temperature. Therefore the critical field is zero in this case.

In addition, the coexistent values of order parameter at the phase transition is

$$Q_{N,P} = Q_c\left(1 \pm \sqrt{1 - \frac{\delta_{20}}{\delta^c_{20}}}\right). \tag{6.3.7}$$

Clearly, they follow the parabola

$$(Q_{N,P} - Q_c)^2 = Q_c^2\left(1 - \frac{\delta_{20}}{\delta^c_{20}}\right). \tag{6.3.8}$$

This is a qualitative agreement with the molecular field theory in figures 6.1.

For the Landau-KKLS theory, simple analytical solutions for the transition temperature and the transitional order parameter for non-zero field cannot be obtained. However, we can still find the expressions for the critical field and critical transition temperature. We discussed these solutions in Appendix F.2. The critical temperature is given by

$$T^*_c = \frac{1}{2}\left(\frac{18aC}{b^2} - \sqrt{\left(\frac{18aC}{b^2}\right)^2 - 4T^*_{\mathrm{bf}}\frac{18aC}{b^2}}\right). \tag{6.3.9}$$

The critical field is dependent on the critical temperature

$$\delta^c_{20} = -\frac{1}{324}\frac{b^3T^{*3}_c}{C^2}. \tag{6.3.10}$$

First we set θ_C to 0.45 as this value gives phase maps which are in good agreement with the molecular field theory in the geometric mean and Sonnet-Virga-Durand limits [64]. Our preliminary calculations has shown that the transition temperature also increases linearly with the applied field. Hence, in representing the phase maps, we only calculate the transition temperature at zero and critical field and connect them to get the phase maps. In figure 6.4(a), we show the phase map for the Landau-KKLS theory with the regularisation parameter $\theta_C = 0.45$. We see that these results disagree dramatically with the molecular field calculations in figure 6.2. The critical field is only ten per cent of the molecular field results. One reason is because when

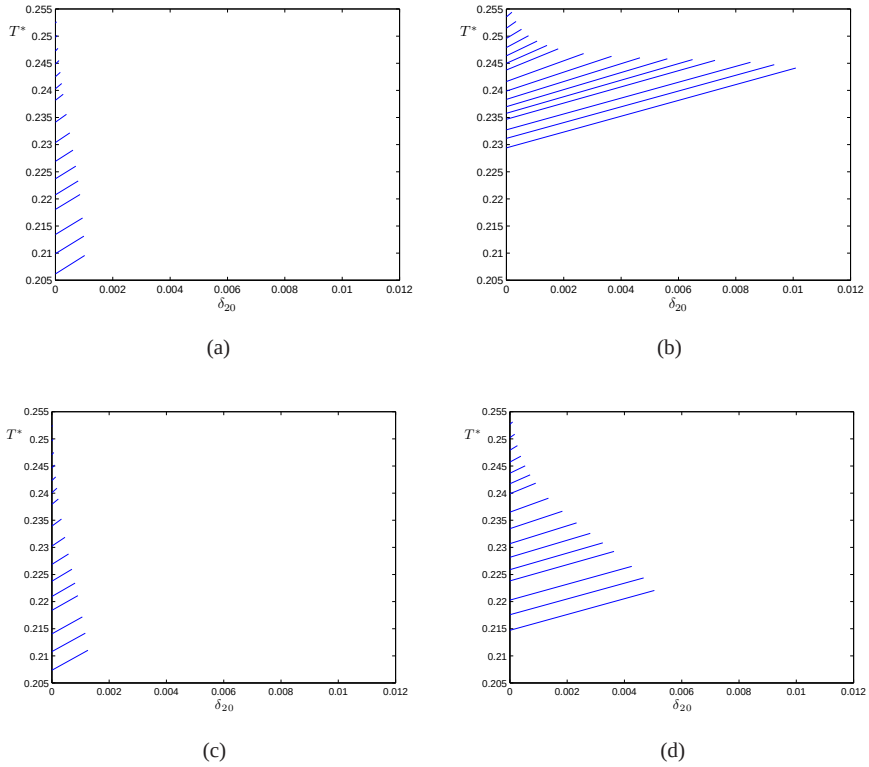

FIGURE 6.4: The dependence of the scaled transition temperature on the scaled magnetic flux density δ_{20} for different values of the biaxiality parameter γ for (a) the Landau-KKLS theory with $\theta_C = 0.45$ and for the pure Landau theory with (b) $\theta_B = \theta_C = 0.45$, (c) $\theta_B = 0.225$ and $\theta_C = 0.45$ and (d) $\theta_B = \theta_C = 0.225$. The values of γ, from bottom to top lines: 0, 0.1, 0.14, 0.18, 0.2, 0.22, 0.24, 0.26, 0.28, 0.3, 0.31, 0.32, 0.33, 0.34 0.35 and 0.36.

we set $\theta_C = 0.45$, the order parameter at the phase transition is much smaller compared to the molecular field theory [64]. In marked contrast, when we set both θ_B and θ_C to 0.45 for the pure Landau theory as in figure 6.4(b), the predicted critical field is in better agreement with the molecular field theory. Now we note that the value of the critical field in the Landau-KKLS theory depends on the cube of the critical temperature T_c^* whereas that value in the pure Landau theory depends on the cube of θ_B. The value of T_c^* is about 0.22 and does not change very much with γ, this is only half the value which we have set for θ_B in the pure Landau theory (0.45). Hence the pure Landau theory should produce similar results to the Landau-KKLS theory in figure 6.4(a) if we set $\theta_B = 0.225$ and keeping $\theta_C = 0.45$. Indeed it is true and the results are shown in figure 6.4(c). In fact, in order to compare the pure Landau theory with the Landau-KKLS theory, it might be best to keep $\theta_B = 0.225$ in the pure Landau theory since it is close to the range of T_c^* in the Landau-de Gennes theory. In this case, a better approximation might be achieved by setting both θ_B and θ_C to 0.225 in the pure Landau theory since that value is close to the temperature range which the transition takes place. We show these results in figure 6.4(d). Now, compared to the molecular field theory, we get a good agreement on the nematic-to-isotropic transition temperature and the agreement on the critical field is much better than in figure 6.4(c).

In order to make further decision about which values of the parameters (θ_B, θ_C) in the pure

Landau theory would be in better agreement with the molecular field theory, we compare the phase maps and the dependence of the transitional order parameter on γ. The plots are shown in figures 6.5. It is clear that if we use the transitional order parameter as a deciding factor then we may use one of the two sets θ_B = θ_C since they give better agreements with the molecular field theory. Furthermore, the shape of the phase map for θ_B = $\theta_C = 0.225$ gives a better agreement with the molecular field theory than θ_B = $\theta_C = 0.45$. Therefore it is a better parameter set. Note that this is also what we have decided based on figures 6.4.

In keeping with the parameter set which we have chosen for the pure Landau theory, we take $\theta_C = 0.225$ in the Landau-KKLS theory. We know that the small temperature range of T_c^* for the Landau-KKLS theory is similar to fixing θ_B at 0.225 in the pure Landau theory. We plot the dependence of the transitional order parameter and transition temperature for the Landau-KKLS theory with θ_C is set equal to 0.225 in figure 6.6. As we expect, the agreement with the pure Landau theory with $\theta_B = \theta_C = 0.225$ is very good. In addition, we show the phase map for the Landau-KKLS theory with $\theta_C = 0.225$ in figure 6.7. Again, the similarity between this and figure 6.4(d) is remarkable.

6.4 Critical-point Exponent

In their paper, Wojtowicz and Sheng [45] looked for the critical-point exponent β, such that at $\delta_{20} = \delta_{20}^c$,

$$\beta = \lim_{T^* \to T_c^*} \frac{\log\left(T_c^* - T^*\right)}{\log\left(\langle F_U \rangle - \langle F_U \rangle_c\right)}. \tag{6.4.1}$$

They claimed that the critical-point exponent is $\beta = 3$ for the two cases, $T^* < T_c^*$ and $T^* > T_c^*$. However, the authors did not explain the details of their calculations. Here, we present our method to estimate β for different values of the biaxiality parameter γ. The first step to calculate the critical exponent is to estimate T_c^* and $\langle F_U \rangle_c$ as accurately as possible. We estimate T_c^* by plotting $\langle F_U \rangle$ against δ_{20}. When we see an interval of δ_{20} where the transition changes from first to second order, we perform more calculations in that interval, with a smaller range of T^* around T_c^*. This process is repeated until we reach a desired accuracy. Note that in practice we can only be certain about T_c^* up to four decimal places, because as we get closer to δ_{20}^c, the phase transition becomes less noticeable. The second step is to find $\langle F_U \rangle_c$. We can estimate it as $\langle F_U \rangle_{NI}/2$ where $\langle F_U \rangle_{NI}$ is the nematic-to-isotropic phase transition in zero field. This is in keeping with the quadratic behaviour in figures 6.1. In the third step, we produce the plot of $\log\left(T^* - T_c^*\right)$ against $\log\left(\langle F_U \rangle - \langle F_U \rangle_c\right)$. We take T^* as close as possible to T_c^* in order for the plot of the data is visibly straight. Then we fit a line through the data points. The slope of the line gives us the exponent.

We note that there is a limitation in these calculations for the molecular field theory. The method we use to estimate the critical temperature only accurate up to four decimal places. Hence, if we get too close to the critical temperature (between 0.00005 and 0.0001 near the estimated value for T_c), the relative error of the difference between a temperature and the critical temperature would be larger. Consequently, the log-log plot does not produce a straight line for such data. However as we will see, with the Landau theory, the convergence of the critical exponent can be slow and we may need to get closer to T_c to estimate it more accurately. In table 6.1, we show

our estimated values for the critical-point exponent β for the two theories where T^* is greater or less than T_c^*, for the molecular field theory. We also show the estimated values for T_c^* and δ_{20}^c. In addition, the intervals of T^* which we use in the calculations are also shown. We see that, for $T^* < T_c^*$, the estimated exponent is less than 3. In contrast, for $T^* > T_c^*$, it is greater than 3. An common feature is that as γ increases, the estimated values of β gets further away from 3. For $\gamma = 0.36$ and $T^* > T_c^*$, we see that the deviation of β is quite dramatic. Its value of 3.886 is now closer to 4 than 3. The reason for those deviation might be because of the slow convergence of the series expansion of $T_c^* - T^*$ in terms of $\langle F_U \rangle - \langle F_U \rangle_c$. However, we cannot get any closer to the critical temperature without introducing a significant error and we do not have an analytical value for β for the molecular field theory.

			$T^* < T_c^*$		$T^* > T_c^*$	
γ	T_c^*	δ_{20}^c	ΔT^*	β	ΔT^*	β
0	0.23094	0.01046	[0.2307, 0.2309]	2.739	[0.231, 0.2312]	3.252
0.2	0.234265	0.0049	[0.232, 0.2342]	2.718	[0.2343, 0.235]	3.372
0.3	0.24261	0.00109	[0.242, 0.2425]	2.657	[0.24265, 0.243]	3.369
0.36	.2533	0.000111	[.2534, .2535]	2.533	[0.25335, 0.2534]	3.886

TABLE 6.1: Table for the critical exponent β at the critical field δ_{20}^c for the molecular field theory. T_c^* denotes the critical temperature. ΔT^* denotes the temperature range which we use to estimate β. For $T^* < T_c^*$, $\beta = \log(T_c^* - T^*)/\log(\langle F_U \rangle_c - \langle F_U \rangle)$. For $T^* > T_c^*$, $\beta = \log(T^* - T_c^*)/\log(\langle F_U \rangle - \langle F_U \rangle_c)$.

One way to understand this problem better is to use the pure Landau theory. In this theory, we have analytical results for both $\langle F_U \rangle_c$ and T_c^*. Hence, in the calculations we can get as close to T_c^* as we want. In addition, the pure Landau theory has an advantage over the Landau-KKLS theory in this case because we now have an analytical value for β. For the pure Landau theory, we proved in Appendix F.1 that the critical-point exponent is cubic. In addition, at the critical field, the order parameter is the solution of the cubic equation

$$\frac{3}{2}C(\langle F_U \rangle - \langle F_U \rangle_c)^3 = a\langle F_U \rangle (T_c^* - T^*). \tag{6.4.2}$$

In table 6.2, we give the estimated values for β. In this case, as T_c^* is known exactly, we can use its value in the calculations. We use 100 points in each case within $[T_c^* - 0.001, T_c^*]$ and $[T_c^*, T_c^* + 0.001]$. Here, we observe the same behaviour as we saw for the molecular field theory that the critical exponent gets further away from 3 as we increase γ. In general, the values of β is closer to 3 than the molecular field theory. However, the error between the estimated values for β reported in the table and the analytical value is still large. In order to test if the source of error really comes from the convergence, we do the same calculations. This time we use a smaller interval around the critical point as $T_c^* \pm 0.0001$. The results are shown in table 6.3. We see that the improvement in the estimated values for β is remarkable. Hence, we conclude that the error in the estimated values for β comes from the slow convergence of the polynomial expansion. As the smaller interval around T_c^* is used in the calculations, the estimated values for the critical-point exponent β gets closer to the true value, which is 3. This is in agreement with the value of the critical-point exponent reported in the calculations by Wojtowicz and Sheng [45].

			$T^* < T_c^*$		$T^* > T_c^*$	
γ	T_c^*	δ_{20}^c	ΔT^*	β	ΔT^*	β
0	0.222059	0.0050461	$[T_c^* - 0.001, T_c^*]$	2.819	$[T_c^*, T_c^* + 0.001]$	3.24
0.2	0.230842	0.0032462	$[T_c^* - 0.001, T_c^*]$	2.797	$[T_c^*, T_c^* + 0.001]$	3.28
0.3	0.241827	0.0009033	$[T_c^* - 0.001, T_c^*]$	2.7	$[T_c^*, T_c^* + 0.001]$	3.407
0.36	0.253122	0.00009647	$[T_c^* - 0.001, T_c^*]$	2.617	$[T_c^*, T_c^* + 0.001]$	3.484

TABLE 6.2: Table for the critical exponent β at the critical field δ_{20}^c for the pure Landau theory. T_c^* denotes the critical temperature. ΔT^* denotes the temperature range which we use to estimate β. For $T^* < T_c^*$, $\beta = \log(T_c^* - T^*)/\log(\langle F_U\rangle_c - \langle F_U\rangle)$. For $T^* > T_c^*$, $\beta = \log(T^* - T_c^*)/\log(\langle F_U\rangle - \langle F_U\rangle_c)$.

			$T^* < T_c^*$		$T^* > T_c^*$	
γ	T_c^*	δ_{20}^c	ΔT^*	β	ΔT^*	β
0	0.222059	0.0050461	$[T_c^* - 0.0001, T_c^*]$	2.937	$[T_c^*, T_c^* + 0.0001]$	3.071
0.2	0.230842	0.0032462	$[T_c^* - 0.0001, T_c^*]$	2.93	$[T_c^*, T_c^* + 0.0001]$	3.092
0.3	0.241827	0.0009033	$[T_c^* - 0.0001, T_c^*]$	2.906	$[T_c^*, T_c^* + 0.0001]$	3.118
0.36	0.253122	0.00009647	$[T_c^* - 0.0001, T_c^*]$	2.856	$[T_c^*, T_c^* + 0.0001]$	3.242

TABLE 6.3: Table for the critical exponent β at the critical field δ_{20}^c for the pure Landau theory. T_c^* denotes the critical temperature. ΔT^* denotes the temperature range which we use to estimate β. For $T^* < T_c^*$, $\beta = \log(T_c^* - T^*)/\log(\langle F_U\rangle_c - \langle F_U\rangle)$. For $T^* > T_c^*$, $\beta = \log(T^* - T_c^*)/\log(\langle F_U\rangle - \langle F_U\rangle_c)$.

6.5 Conclusions

In this chapter, we applied the molecular field theory to study the effects of magnetic field on a system of biaxial molecules in uniaxial nematic. We are motivated by recent experimental success in observing a significant increase in the uniaxial nematic-to-isotropic phase transition temperature due to the magnetic field. Their experimental success was attributed to a high magnetic field strength used in the experiment. Using the molecular field theory, we have shown that for the same applied magnetic field strength, the gap between the field induced transition temperature and the transition temperature at zero field increases on increasing the biaxiality parameter. Hence we conclude that the experimental successes can also be attributed to the high molecular biaxiality of the V-shaped molecules. Our theory also predicts that the transitional order parameter follows a quadratic curve, in analogy with previous calculations for uniaxial molecules. In addition, we have calculated the critical field strength, above which the nematic and paranematic phases are indistinguishable. We have also studied the Landau theory and the Landau-KKLS theory which make the same qualitative predictions with the molecular field theory.

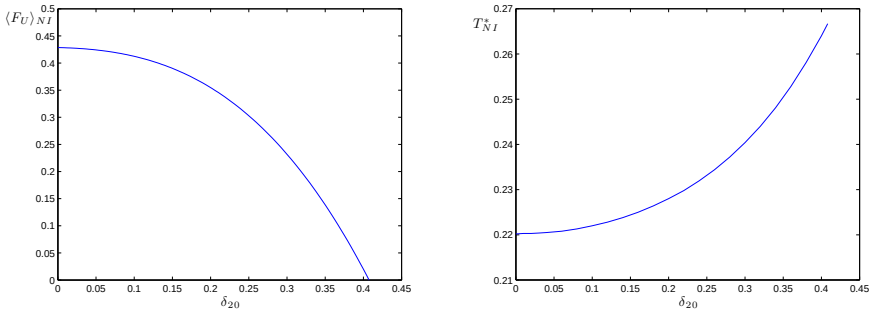

(a)

(b)

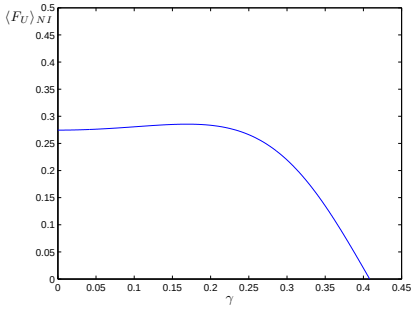

(c)

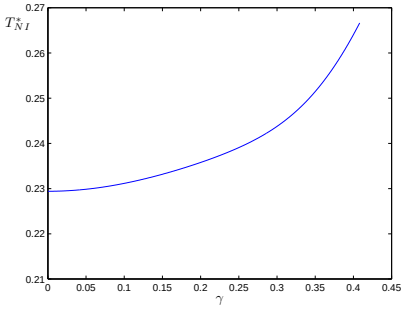

(d)

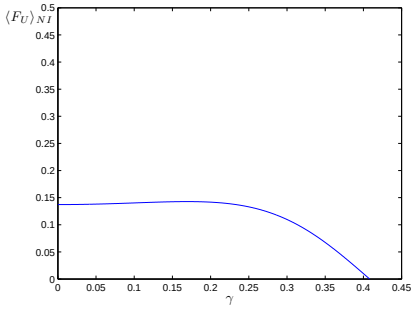

(e)

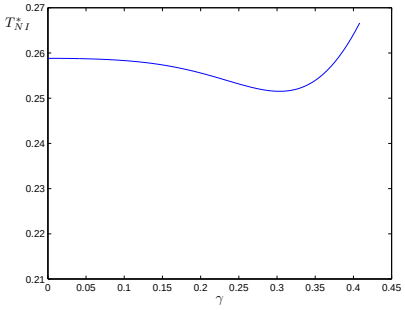

(f)

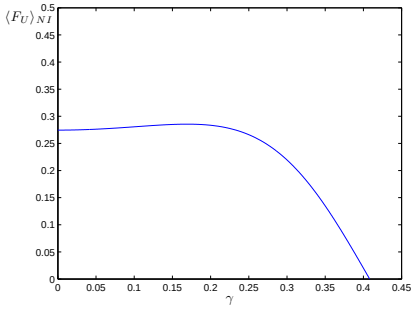

(g)

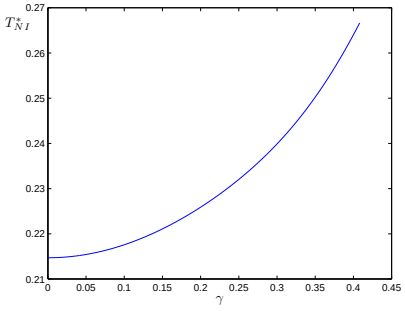

(h)

FIGURE 6.5: The dependence of the transitional order parameter and transition temperature for various models: (a) and (b) are the results for the molecular field theory, the rest of the plots are for the pure Landau theory, with different values for the regularisation parameters: (c) and (d) are for $\theta_B = \theta_C = 0.45$, (e) and (f) are for $\theta_B = 0.225$ and $\theta_C = 0.45$, (g) and (h) are for $\theta_B = \theta_C = 0.225$.

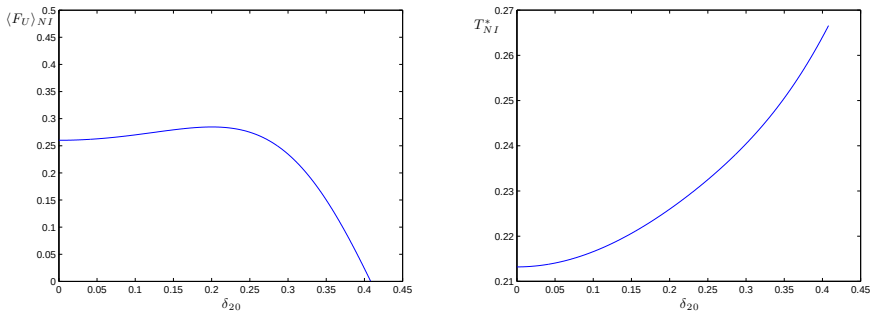

(a) (b)

FIGURE 6.6: The dependence of the transitional order parameter and transition temperature for the Landau-KKLS theory with θ_C is set equal to 0.225.

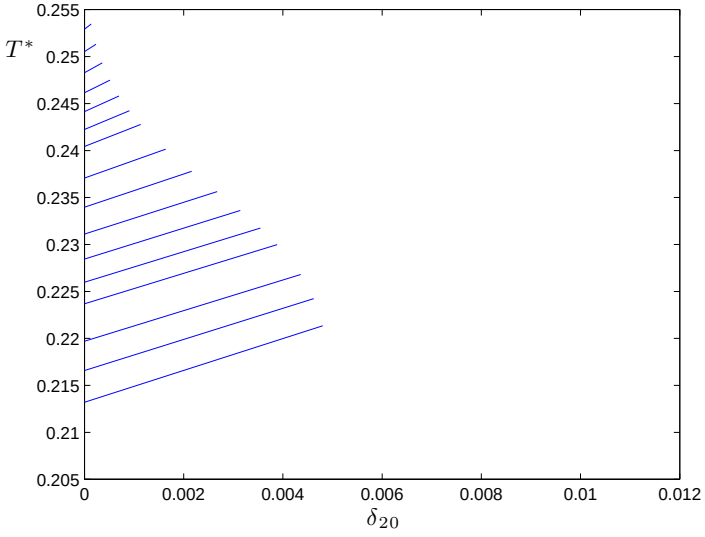

FIGURE 6.7: The dependence of the transition temperature on the scaled magnetic flux density δ_{20} for the Landau-KKLS theory with θ_C as the biaxiality γ increases. The values of γ, from bottom to top, are: 0, 0.1, 0.14, 0.18, 0.2, 0.22, 0.24, 0.26, 0.28, 0.3, 0.31, 0.31, 0.32, 0.33, 0.34, 0.35, 0.36.

Chapter 7

Biaxial Smectic A Phases

In this chapter, we study a molecular field theory for biaxial smectic A phases of D_{2h} symmetry which are formed from molecules also of D_{2h} symmetry. After reviewing some related works in section 7.1, we discuss the molecular field theory in section 7.2. The calculation results for the molecular field theory are presented in sections 7.3 and 7.4.

7.1 Related Works

The first prediction of biaxial smectic A phases seems to have been by de Gennes [41]. The structure of biaxial smectic A phases were later analysed by Brand, Cladis and Pleiner [113, 114]. A biaxial smectic A phase formed from board-like molecules has D_{2h} symmetry whereas one formed from V-shaped molecules can have C_{2v} symmetry [113]. An idealisation of the structure of the former phase is shown in figure 7.1 (a). The latter is a ferroelectric phase without chiral molecules and its idealised structure is shown in figure 7.1 (b). The authors also mentioned the possibility of a biaxial smectic A phase with C_{2v} symmetry, but with antiferroelectric order. In addition, they discussed the possibility that the biaxial smectic A-to-biaxial nematic phase transition can be continuous. The symmetry of biaxial smectic A phases were discussed further in a later publication by the same group of authors [114]. The authors started with a biaxial smectic A phase with D_{2h} symmetry. By adding a polar direction in the planes of smectic layers, a biaxial smectic A phase with C_{2v} symmetry is formed. When a second polar direction is added in the planes of smectic layers, a biaxial smectic A phase with a very low symmetry (C_{1h}) is formed. The symmetry group C_{1h} consists of two basic symmetry operations: a reflection plane and an identity. The next and final step is to add a third polar direction perpendicular to the layers and we have a phase with no symmetry (C_1).

Biaxial smectic A phases have been found in several low-molar mass system over 20 years since its first theoretical prediction by de Gennes. The common experimental techniques which support the identification of biaxial smectic A phases are optical textures, conoscopic studies and X-ray diffraction measurements. In 2001, Hegmann, Kain, Diele, Pelzl and Tschierske [115] studied a mixture of a board-like mesogen and a board like non-mesogenic molecule. Their experimental evidence by texture observations and X-ray diffraction studies strongly supported

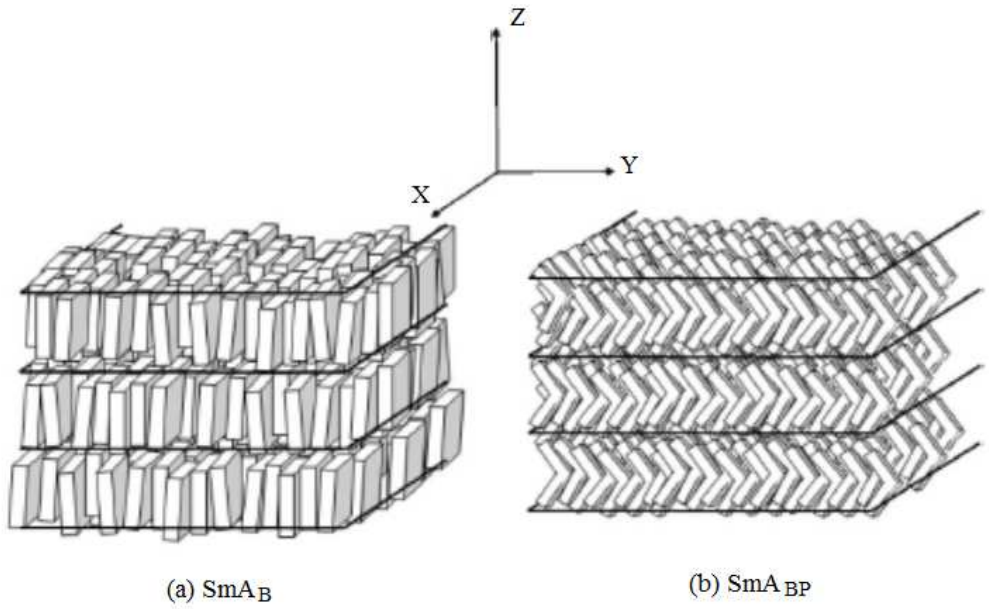

FIGURE 7.1: Sketches of the idealised structures of the biaxial smectic A phases: (a) Non-polar biaxial smectic A phase formed from board-like molecules and (b) Polar biaxial smectic A phase formed from V-shaped molecules. Reproduced from [41].

that the biaxial smectic A phase was stabilised. This evidence was further supported by scanning transmission X-ray microscopy in 2007 by Kaznacheev and Hegmann [116]. A study of rigid, symmetric V-shaped molecules in 2001, using the same techniques as Hegmann *et al.* [115] also found a stabilised biaxial smectic A phase [117]. In this case the V-shaped molecules exhibit a phase sequence $\mathrm{SmA}_B - \mathrm{SmA}_U - I$. In addition, electro-optical measurement showed that the biaxial smectic A phase is ani-ferroelectric. The same experimental methods were applied to show that liquid crystal dimers also can form biaxial smectic A. In one case, a dimer is made up of a rod-like and a V-shaped mesogenic units [118] and linked by a flexible spacer. In another case, a dimer is made up of two different rod-like mesogenic groups with a flexible spacer linking them [119]. In the former case, the dimers exhibit the phase sequence $\mathrm{SmA}_B - N_B - I$. In contrast, the phase sequence in the latter case is $\mathrm{SmA}_B - \mathrm{SmA}_U - I$. Biaxial smectic A phase has also been found in a system of rigid, asymmetric V-shaped molecules using the aforementioned experimental techniques, together with differential scanning calorimetry, with the phase sequence $\mathrm{SmA}_B - \mathrm{SmA}_U - I$ [120]. In a later publication [121], using electro-optical experiment, the authors showed that this biaxial smectic A phase is antiferroelectric.

The molecular field theory have also been used to describe biaxial smectic A phases. One example is a theory developed by Matsushita in 1981 [122]. This was an extension of a two order parameters theory for biaxial nematic to include smectic ordering. In this model, there are two interaction parameters, one is the molecular biaxiality and the other controls the smectic interaction strength. Additionally, there are four order parameters. Two of them are pure orientational order parameters and are non-zero in both the nematic and the smectic A phases. The other two order parameters are mixed orientational-translational order parameters and are non-zero only in the smectic A phases. With these four order parameters, the author was able

to produce a rich phase behaviour. In principle, there are five phases: isotropic, uniaxial and biaxial nematics, uniaxial and biaxial smectics A. Moreover, there are three phase sequences: $\mathrm{SmA}_U - N_U - I$, $\mathrm{SmA}_B - \mathrm{SmA}_U - N_U - I$ and $\mathrm{SmA}_B - N_U - I$. Over the range of molecular biaxiality under their study, the biaxial nematic phase was not found. Thus it may suggest that the biaxial smectic A phase is easier to form than the biaxial nematic phase. Another molecular field theory for biaxial smectic A phases was by Teixeira, Osipov and Luckhurst in 2006 [41]. This theory is more general than that by Matsushita [122] in that they include all four orientational order parameters in the nematic phase. In the biaxial smectic A phase, they are joined by four mixed orientational-translational order parameters and one pure translational order parameter. The authors then studied a model in perfect uniaxial order, which left only three order parameters: one orientational biaxial, one mixed biaxial and one pure translational. Bifurcation analyses were performed to investigate the stability of the uniaxial nematic phase with respect to the other phases: biaxial nematic, uniaxial smectic A and biaxial smectic A. Depending on the combinations of the interaction parameters, the uniaxial nematic phase can go through a phase transition into one of these three phases. Furthermore, the authors studied a model of parallelepiped molecules. The interaction parameters were related to the molecular dimensions. Hence the stability of the uniaxial nematic phase with respect to the other three aforementioned phases were also related to the molecular dimensions.

Monte Carlo simulations also predicted the existence of the biaxial smectic A phases. In one series of simulations, an off-lattice system of identical molecules interacting via the Gay-Berne potential was studied by Berardi and Zannoni [123]. In this model, the molecular biaxiality has contributions from both the molecular shape and interaction. Both the biaxial nematic and biaxial smectic A phases were stabilised. In addition, their stability depends on the combination of the molecular shaped and interaction. In these simulations, only the transition from the uniaxial and biaxial nematic phases to the biaxial smectic A phase was found. In another set of simulations, supported by Onsager's molecular theory, Vanakaras, Bates and Photinos [124] studied a hard particle model. In this model, the major molecular axis were assumed to line up. Therefore they only investigated the stability of the uniaxial nematic phase against the other liquid crystal phases, namely biaxial nematic and biaxial and uniaxial smectics. In their phase map of transitional density against the aspect ratio of molecular breadth and width, all these four phases were found. The authors also performed simulations for binary mixtures of rod-like molecules with the same biaxiality but different anisotropy. They found that the biaxial smectic A phase was destabilised and hence the biaxial nematic phase was stabilised.

There are theoretical grounds to expect the existence of these phases. First, it is for the same reason that we expect the biaxial nematic phase to exist. The constituent molecules are biaxial. Their biaxiality has been demonstrated in a molecular field theory by Averyanov and Primak [125]. It is an extention of the molecular field theory for uniaxial molecules: in uniaxial smectic A by McMillan [126] to include molecular biaxiality, although the phase was still uniaxial. In this case, the molecular biaxiality was important in explaining the weakness of the first order nematic-isotropic transition for real mesogenic compounds. We expect that the molecular biaxiality also help to stabilise the biaxial smectic A phase at ground state. Secondly, it was suggested by Texeira *et al.* [41] that biaxial smectic A phases should be easier to form than biaxial nematic phases. The reason is there are two ways to stabilise a biaxial phase. One of them is to design molecules with high biaxiality. However, we see from the phase map in figure 2.4 that this

strategy is difficult to achieve since the molecular biaxiality needs to be in a very narrow range around the optimum biaxiality. The second strategy is to have a large value of the order parameter S that describe the ordering of the major molecular axis in order to allow a more effective anisotropic interaction between the minor axes [41]. However, for nematic phases this can be achieved only for low molecular biaxiality where the biaxial nematic phases are formed at very low temperature. At low temperature, the smectic or even crystal phase can be more stable than the biaxial nematic phase, which is why it is difficult to observe the latter phase. In contrast, the influence of the molecular biaxiality on the major order parameter on the smectic A-nematic phase transition may not be so large. It is because the major order parameter is coupled to the translational order of the smectic A phase. Therefore it can increase significantly in the smectic A-nematic phase transition, especially if the phase transition is first order. This effect can be even more favourable if the system undergoes a transition directly from the isotropic phase to the smectic A phase.

Due to the success of the molecular field theory in modelling the uniaxial and biaxial nematic phases, we extend this theory to model the biaxial smectic A phases. In our model, we use the strategy suggested by Teixeira *et al.* in their paper's Appendix [41]. That is, we use the approximation by Kventsel, Luckhurst and Zewdie [127]. This approximation was developed as an alternative to the McMillan theory [6, 126] in modelling the uniaxial smectic A phase. We also use the geometric mean and SVD approximation for the orientational interaction parameters together with the KLZ approximation. When we use these approximations for biaxial smectic A systems, the number of order parameters is reduced significantly, thus our calculations are facilitated. Thus, the complex system of biaxial smectic A phase can be described by an elegant model with only three order parameters: one orientational uniaxial, one orientational biaxial and one pure translational.

7.2 Molecular Field Theories

7.2.1 Classical Molecular Field Model

In this subsection, we discussed the molecular field theory for a biaxial smectic A phase of general symmetry which is formed from molecules of general symmetry. This theory was developed by Teixeira *et al.* [41]. The first step in constructing the molecular field theory for biaxial smectic A phases is to identify the order parameters which describe the ordering of the system. The smectic A phases can be described by three types of order parameters. The first type consists of the pure orientational order parameters

$$\langle D^L_{mn} \rangle = \int \int D^L_{mn}(\Omega) f(Z, \Omega) dZ d\Omega. \tag{7.2.1}$$

The other two types of order parameters incorporate translational ordering in the system. Suppose that the molecular centres of mass sit on planes parallel to the $X - Y$ plane of the phase and intersecting the Z axis of the phase at nd where n is an integer. We call d the smectic layer spacing. Regarding translational ordering, the system is mostly ordered when the molecules are with their centres of mass lying in one of the planes and least ordered when the molecular

centres of mass lying in the middle of any two adjacent planes. In addition, the molecules prefer to sit as near the planes as possible. Thus, there is a molecular density wave in the Z direction. The function which has these properties is $\cos(2\pi Z/d)$. The second type of order parameters is the average of that function. This forms a pure translational order parameter.

$$\tau = \int\int \cos(2\pi Z/d) f(Z,\Omega) dZ d\Omega, \tag{7.2.2}$$

The third type of order parameters are the averages of the products of the density wave with the Wigner rotation matrices. They form the mixed orientational-translational order parameters,

$$\sigma^L_{mn} = \int\int \cos(2\pi Z/d) D^L_{mn}(\Omega) f(Z,\Omega) dZ d\Omega. \tag{7.2.3}$$

The next step in constructing our theory is to form the internal energy of the system from the invariant combinations of the order parameters

$$\langle U\rangle = -(1/2)\left(u_0\tau^2 + \sum u_{Lmn}\langle D^L_{pm}\rangle\langle D^L_{-pn}\rangle + \sum u'_{Lmn}\sigma_{Lpm}\sigma_{L-pn}\right). \tag{7.2.4}$$

The singlet distribution function $f(Z,\Omega)$ is a function of both the Euler angles Ω and the position of the centre of mass of the molecule with respect to the phase axis Z. Hence, the integrations in the entropy has to be taken over both the orientation and the position of the molecule.

$$S = -k_B \int\int f(Z,\Omega)\ln f(Z,\Omega) dZ d\Omega. \tag{7.2.5}$$

The free energy can be formed from equation (2.3.10). In order to find the distribution function, we minimise the free energy, subject to the constraints of the order parameters in equations (7.2.1), (7.2.2) and (7.2.3), together with the nomalisation condition

$$\int\int f(Z,\Omega) dZ d\Omega = 1. \tag{7.2.6}$$

The resulting distribution function is given by

$$f(Z,\Omega) = Q^{-1}\exp\left(U(Z,\Omega)/k_BT\right), \tag{7.2.7}$$

where the potential of mean torque can be written as

$$\begin{aligned} U(Z,\Omega) = -\Big(&u_0\tau\cos(2\pi Z/d) + \sum u_{Lmn}\langle D^L_{pm}\rangle D^L_{-pn}(\Omega) \\ &+ \sum u'_{Lmn}\sigma_{Lpm}\cos(2\pi Z/d) D^L_{-pn}(\Omega)\Big). \end{aligned} \tag{7.2.8}$$

Hence, the free energy at equilibrium can be written as

$$A = -k_BT\log Q + (1/2)\left(u_0\tau^2 + \sum u_{Lmn}\langle D^L_{pm}\rangle\langle D^L_{-pn}\rangle + \sum u'_{Lmn}\sigma_{Lpm}\sigma_{L-pn}\right). \tag{7.2.9}$$

7.2.2 Kventsel-Luckhurst-Zewdie Decoupling Approximation

The Kventsel-Luckhurst-Zewdie (KLZ) approximation [127] can be used to reduce the number of order parameters. This is especially essential in biaxial smectic A phases. For example, we consider the biaxial smectic A phase with D_{2h} symmetry which is formed from molecules also have the same symmetry. The classical model discussed in the last subsection gives us one pure translational, four orientational and four mixed order parameters, giving totally nine order parameters. On the other hand, using the KLZ approximation, each mixed order parameter can be written as a product of an orientational order parameter and the translational one. Hence there are only five order parameters when we use the KLZ decoupling approximation. This is certainly of great help in doing the calculations. In general, the KLZ approximation can be written as [41]

$$\sigma_{Lpm} = \tau \langle D^L_{pm} \rangle. \tag{7.2.10}$$

This approximation has to be used before we construct the internal energy. The reason was discussed when the KLZ approximation was first introduced [127] for uniaxial molecules: in uniaxial smectic A phases "the distribution function cannot be factorised if the decoupling approximation is introduced at a later stage in the McMillan theory". We will see that, the factorisation of the partition function makes the calculations a lot simpler since one partition function is simply the Bessel function of the second kind of zeroth order. The new internal energy in the KLZ approximation is

$$\langle U \rangle = -(1/2) \left(u_0 \tau^2 + \sum u_{Lmn} \langle D^L_{pm} \rangle \langle D^L_{-pn} \rangle + \sum u'_{Lmn} \tau^2 \langle D^L_{pm} \rangle \langle D^L_{-pn} \rangle \right). \tag{7.2.11}$$

The distribution function for this approximation can be found by minimising the new free energy with respect to the same constraints in subsection 7.2.1. We get the potential of mean torque

$$\begin{aligned} U(Z, \Omega) = -\Big\{ \Big(u_0 + \sum u'_{2mn} \langle D^L_{pm} \rangle \langle D^L_{-pn} \rangle \Big) \tau \cos(2\pi Z/d) \\ + \sum \left(u_{Lmn} + u'_{Lmn} \tau^2 \right) \langle D^L_{pm} \rangle D^L_{-pn}(\Omega) \Big\}. \end{aligned} \tag{7.2.12}$$

Hence, the free energy at equilibrium is

$$A = -k_B T \log Q + (1/2) \left(u_0 \tau^2 + \sum u_{Lmn} \langle D^L_{pm} \rangle \langle D^L_{-pn} \rangle + 3 \sum u'_{Lmn} \tau^2 \langle D^L_{pm} \rangle \langle D^L_{-pn} \rangle \right). \tag{7.2.13}$$

We can further facilitate the calculations by factorising the partition function as a function of the translational and the orientational partition functions

$$Q = Q_Z Q_\Omega. \tag{7.2.14}$$

Where the orientational partition function is

$$Q_\Omega = \int \exp \left(\frac{1}{k_B T} \sum (u_{Lmn} + u'_{Lmn} \tau^2) \langle D^L_{pm} \rangle D^L_{-pn}(\Omega) \right) d\Omega. \tag{7.2.15}$$

And the translational partition function is

$$Q_Z = dI_0\left(\frac{1}{k_BT}(u_0 + \sum u'_{Lmn}\langle D^L_{pm}\rangle\langle D^L_{-pm}\rangle)\tau\right). \tag{7.2.16}$$

Here, $I_n(a)$ is the Bessel function of the first kind which is shown in equation (6.2.12).

We will see later that, within the KLZ decoupling approximation and for some interaction parameters, the equilibrium free energy does not have minima which correspond to the solutions of the self-consistency equations. Therefore, we resort to the method of solving the self-consistency equations. In order to make comparisons between the equilibrium and non-equilibrium free energy surfaces, here we introduce the KKLS free energy for biaxial smectic A phases. This is analogous to the derivation for biaxial nematics which we have discussed in section 2.5. We note that in this case the integration is taken over both the orientation and the position in the Z direction. The non-equilibrium potential of mean torque is

$$U(Z,\Omega) = -k_BT\left(\eta_0\cos(2\pi Z/d) + \sum \eta_{Lpm}D^L_{pm}(\Omega)\right). \tag{7.2.17}$$

In addition, the entropy can be written as

$$S = -k_B\left(\eta_0\tau + \sum \eta_{Lpm}\langle D^L_{pm}\rangle - \log Q\right). \tag{7.2.18}$$

Hence, we can construct the non-equilibrium free energy from equation (2.3.10).

In order to simplify the problem, we use the approximation $u'_{Lmn} = \alpha u_{Lmn}$. We note that, this approximation preserves the rotational invariance of the total internal energy. We also set δ as $\delta = u_0/(u_{200}\alpha)$. The stability analysis in Appendix G can give us a rough estimate of when the method of minimising the equilibrium free energy fails to work. We examine three models: uniaxial smectic A formed from uniaxial molecules, biaxial smectic A with KLZ-GM (KLZ and geometric mean) approximation and biaxial smectic A with KLZ-SVD (KLZ and Sonnet-Virga-Durand) approximation. In all three cases, we have kept $\delta = 0$ and have found that for $\alpha > 1/3$ the classical method of minimising the equilibrium free energy fails, regardless of the biaxiality parameters.

7.3 Uniaxial Smectic A Phases formed from Uniaxial Molecules

7.3.1 McMillan and KLZ Theories

Here, we briefly discuss the two theories for uniaxial smectic A formed from uniaxial molecules as an example before discussing the more complicated system of biaxial smectic A. First, we consider the McMillan theory. The internal energy is given by

$$U = -(1/2)\left(u_0\tau^2 + u_{200}S^2 + u'_{200}\sigma^2_{200}\right). \tag{7.3.1}$$

In addition, the potential of mean torque is

$$U(Z,\Omega) = -\left(u_0\tau\cos\left(2\pi Z/d\right) + u_{200}SP_2(\cos\beta) + u'_{200}\sigma_{200}P_2(\cos\beta)\cos\left(2\pi Z/d\right)\right). \tag{7.3.2}$$

And the equilibrium free energy is given by

$$A = -k_BT\log Q + (1/2)(u_0\tau^2 + u_{200}S^2 + u'_{200}\sigma^2_{200}). \tag{7.3.3}$$

It was mentioned by McMillan that [6, 126] a model for uniaxial smectic A phases by Kobayashi had been developed earlier. In this model, only the pure translational interaction term was added to the Maier-Saupe theory. In contrast, in McMillan's first paper on modelling these phases [6], he only added the mixed interaction term to the Maier-Saupe theory. In his later paper, he included both the pure translational and the mixed interaction term to the Maier-Saupe theory. Hence the pure order parameter τ is the density wave amplitude, and the mixed order parameter σ is required to model the coupling between the translational and orientational order. The addition of the pure translational interaction term was needed to reduce the values of the order parameter, entropy and heat capacity at the phase transition in order to reach better quantitative agreements with experimental results. The theory in the later paper by McMillan which includes both the pure-translational and the mixed interaction terms are also referred to as the McMillan-Kobayashi theory by some authors [7, 10]. In addition, as mentioned by Osipov [10], a limitation of this theory is that it does not allow the determination of the smectic period in a self-consistent way.

In the McMillan theory, the order parameters only involve the first order term in the Fourier series, $\cos\left(n2\pi Z/d\right)$, where n is zero or ±1. However, the symmetry of smectic A phases permits other higher order terms in the Fourier series, namely for $|n| > 1$ [128]. The effects of these higher order terms has been investigated, for example by Marguta, Martín del Río and de Miguel [128]. In their calculations, the Fourier series of up to $n = 5$ was included. They found that, although there are some quantitative differences to the McMillan theory, the inclusion of these higher order Fourier terms does not solve the inconsistencies between the McMillan theory and experiments in the values of the order parameter, entropy and heat capacity at the phase transition. Therefore using the first order Fourier term to construct the order parameters is sufficient within the molecular field approximation.

In order to apply the KLZ theory, the decoupling approximation need to be introduced when we formulate the internal energy. The decoupling approximation is $\sigma_{200} = S\tau$. Hence the internal energy is given by

$$\langle U\rangle = -(1/2)\left(u_0\tau^2 + u_{200}S^2 + u'_{200}\tau^2S^2\right). \tag{7.3.4}$$

In addition, the potential of mean torque is

$$U(Z,\beta) = -\left((u_0 + u'_{200}S^2)\tau\cos\left(2\pi Z/d\right) + (u_{200} + u'_{200}\tau^2)SP_2(\cos\beta)\right). \tag{7.3.5}$$

The free energy at equilibrium can be written as

$$A = -k_BT\log Q + (1/2)(u_0\tau^2 + u_{200}S^2 + 3u'_{200}\tau^2S^2). \tag{7.3.6}$$

The partition function can also be decoupled into an orientational and a translational part in the

form (7.2.14). The orientational part is

$$Q_\beta = \int \exp\left(\frac{1}{k_B T}(u_{200} + u'_{200}\tau^2) S P_2(\cos\beta)\right) d\cos\beta, \tag{7.3.7}$$

and the translational part is

$$Q_Z = I_0\left(\frac{1}{k_B T}(u_0 + u'_{200} S^2)\tau\right). \tag{7.3.8}$$

The detailed comparisons of the two theories have been performed when the KLZ approximation was first introduced in reference [127].

In order to reduce the number of parameters in the model, we scale the temperature with the anisotropy of the molecules, $T^* = k_B T/u_{200}$. We keep the original notation by McMillan [126] to scale the mixed interaction parameter, $u'_{200} = \alpha u_{200}$, and the pure one, $u_0 = \delta\alpha u_{200}$. The parameter α can be thought of as dependent on a factor which governs the stability of the smectic A phase, such as the chain length of the molecules. The constant δ is only a proportionality constant. This is to make sure that when the chain length varies, both the pure translational and the mixed interactions also changes accordingly. Since setting the value of δ to non zero does not change the qualitative behaviour of the McMillan model [126] according to a calculation by the author, we keep $\delta = 0$ in the following calculations.

7.3.2 Failures of Minimising the Equilibrium Free Energy

The method which we usually used to solve the molecular field theories which is to minimise the equilibrium free energy obtained by the variational derivation by de Gennes fails to work here. While this method work for small values of the parameter α, for large value of α and at some low temperature, the free energy behaves unexpectedly. As an example, we take the parameter set $\delta = 0$, $\alpha = 0.5$ at the scaled temperature $T^* = 0.08$. The minimisation of the equilibrium free energy gives a solution $S = 0.9828$ and $\tau = 0.8165$, which is shown as a red cross in figure 7.2(a). At a lower temperature $T^* = 0.05$, the solution which corresponds to the minimum of the equilibrium free energy is invalid with $S = 1.0438$ and $\tau = 0.8165$. Now we need to check whether this anomalous behaviour also occurs in the self-consistency equations

$$S = Q_\beta^{-1} \int P_2(\cos\beta) \exp\left(T^{*-1}(1 + \alpha\tau^2) S P_2(\cos\beta)\right) d\cos\beta, \tag{7.3.9}$$

$$\tau = Q_Z^{-1} I_1\left(T^{*-1}(\delta + \alpha S^2)\tau\right). \tag{7.3.10}$$

Solving these self-consistency equations gives us a different solution $S = 0.9375$ and $\tau = 0.8909$ at $T^* = 0.08$. This solution of the self-consistency equations can be seen, as a red dot, in the contour plot for the free energy in figure 7.2(a) as a saddle point rather than a minimum. In this case, minimising the non-equilibrium free energy gives us the same solution as solving the self-consistency equations, in marked contrast with the classical approach of minimising the equilibrium free energy. The contour plot for the KKLS free energy is shown in figure 7.2(b). The minimum of this free energy is also shown as a red dot which is well-behaved and at the

same location as the solution of the self-consistency equations. The suscess of the KKLS theory in this case can be considered as an explanation for the failure of the old method of minimising the equilibrium free energy. For completeness, we show the equations of the KKLS theory below. In the calculations, we solve the self-consistency equations instead of minimising the KKLS free energy. It is because near a first order phase transition, we may have more than one local minima and we need to compare the corresponding values of the free energy to find the global minimum. In minimising the KKLS free energy, we cannot guess the values of the Lagrangians which correspond to different minima in order to start the minimisation algorithm. The self-consistency equations are solved using the MATLAB function *fsolve*. This function implements the Trust-Region dogleg algorithm, which is an improvement of Newton's method in solving non-linear equations. We discuss the function fsolve in Appendix E. In essence, we give the computer program a starting point. The computer program then looks for an estimate of a solution to a desired accuracy using the given starting point for the search. After solving the self-consistency equations, we check the solutions against the KKLS free energy at selected values of the parameter α and scaled temperature to make sure it does give a minimum of the free energy. This method of calculations is also employed to solve the self-consistency equations of biaxial smectic A phases.

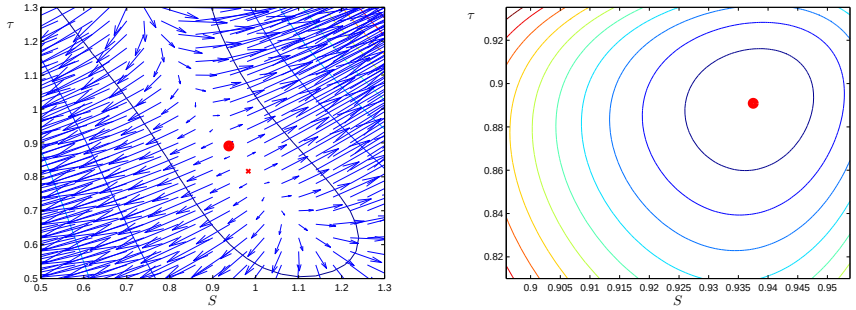

(a) Equilibrium free energy.

(b) KKLS free energy

FIGURE 7.2: The contour plots for the equilibrium and non-equilibrium KKLS free energies as functions of two order parameters, S and τ, for $\delta = 0$ and $\alpha = 0.5$ at the scaled temperature $T^* = 0.08$.

The KKLS theory is given as follows. First, we maximise the entropy, subject to the order parameters and the normalisation to get the distribution function

$$f(Z,\beta) = Q^{-1} \exp\left(\eta_z \cos\left(2\pi Z/d\right) + \eta_\beta P_2(\cos\beta)\right). \tag{7.3.11}$$

Here,

$$Q(\eta_z,\eta_\beta) = \int\int \exp\left(\eta_z \cos\left(2\pi Z/d\right) + \eta_\beta P_2(\cos\beta)\right) dZ d\cos\beta. \tag{7.3.12}$$

Therefore, the order parameters are given by

$$S(\eta_z,\eta_\beta) = Q^{-1} \int\int P_2(\cos\beta) \exp\left(\eta_z \cos\left(2\pi Z/d\right) + \eta_\beta P_2(\cos\beta)\right) dZ d\cos\beta, \tag{7.3.13}$$

$$\tau(\eta_z, \eta_\beta) = Q^{-1} \int \int \cos(2\pi Z/d) \exp(\eta_z \cos(2\pi Z/d) + \eta_\beta P_2(\cos\beta)) dZ d\cos\beta. \quad (7.3.14)$$

In addition, the internal energy is given by

$$U = -(1/2)\left(u_0\tau^2 + u_{200}S^2 + u'_{200}\tau^2 S^2\right). \quad (7.3.15)$$

Finally, we can construct the non-equilibrium KKLS free energy from equation (2.3.10) to give

$$A^* = -(1/2)T^{-1}\left(u_0\tau^2 + u_{200}S^2 + u'_{200}\tau^2 S^2\right) + (\eta_z\tau + \eta_\beta S) - \log(Q(\eta_z, \eta_\beta))). \quad (7.3.16)$$

7.3.3 Calculations and Results

In figure 7.3, we show the phase map for the KLZ theory, where δ is set equal to zero. The KLZ approximation produces the same qualitative features as the original McMillan theory [6]. All the three phases are shown in the phase map: isotropic, uniaxial nematic and uniaxial smectic A. The stability of the three phases is changed by varying the smectic interaction strength, α. As α increases, first the nematic-to-isotropic transition temperature is constant. It is because in the KLZ theory and also in the McMillan theory, the smectic interaction strength does not affect the molecular ordering in the nematic phase. In contrast, the stability of the uniaxial smectic A phase increases as we increase α. First the $\mathrm{SmA}_U - N_U$, then the $\mathrm{SmA}_U - I$ transition temperature goes up on increasing α. We see that, for small value of α, the $\mathrm{SmA}_U - N_U$ transition is second order. This behaviour changes at $\alpha = 0.52$ where it becomes first order. In comparison, both the $N_U - I$ and the $\mathrm{SmA}_U - I$ transition are first order for all the investigated range of α. Finally, all three phases coexist at a triple point. There is a major quantitative disagreement between the KLZ theory and the McMillan theory when we set δ to zero: the location of the tricritical point is lower in the KLZ theory compared to the McMillan theory. The tricritical temperature of the KLZ theory is $0.71T_{NI}$ whereas in the McMillan theory it is $0.85T_{NI}$. This value for the tricritical point predicted by the KLZ theory according to our calculations is in agreement with the original calculations by Kventsel, Luckhurst and Zewdie (KLZ) [127]. They also found that, as λ increases where α is kept fixed, the value of the tricritical temperature tends closer to T_{NI}. Nevertheless, both the KLZ and the McMillan theories describe correctly the qualitative behaviour of a system forming the uniaxial smectic A phase and can be used interchangeably. The KLZ theory has an advantage that we now also have the information on the pure translational order parameter. In contrast, in order to have this order parameter in the McMillan theory we need to set δ to a non-zero value and the theory would become more complex with three order parameters.

7.4 Biaxial Smectics A Phases

In this section we study the molecular field theory for biaxial smectic A phases. We take the assumption that both the phase and the molecular symmetries are D_{2h}.

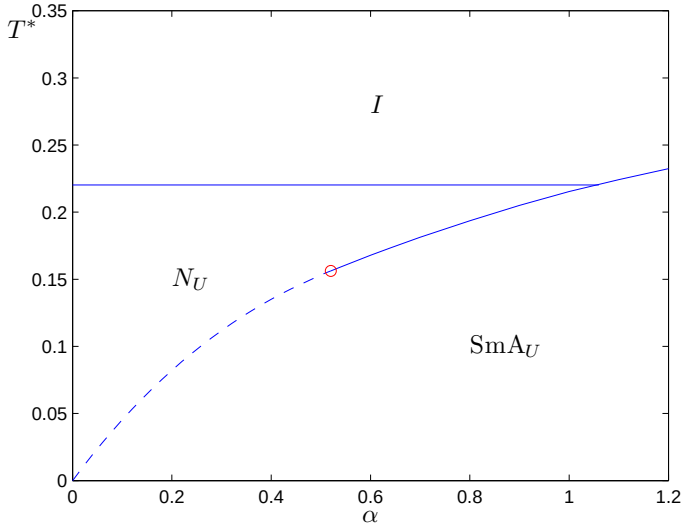

FIGURE 7.3: The dependence of the scaled transition temperature on the smectic interaction parameter, α, for the KLZ theory with $\delta = 0$. Continous lines denote first order phase transitions whereas broken lines denote second order transitions. The tricritical point is marked by a circle.

7.4.1 Approximations for The Interaction Parameters

In addition to the KLZ approximation for the order parameters, we can either use the geometric mean approximation as in section 2.4.3 or the SVD approximation as in section 2.4.4 for the orientational interaction parameters. These latter approximations for the orientational interaction parameters can help to reduce the number of orientational order parameters from four to only two. If we use the SVD approximation, the potential of mean torque is given by

$$U(Z,\Omega) = -u_{200}\left\{\left(\alpha(\langle R_{00}^2\rangle^2 + 2\lambda\langle R_{22}^2\rangle^2)\right)\tau\cos\left(2\pi Z/d\right) + \left(1+\alpha\tau^2\right)\left(\langle R_{00}^2\rangle R_{00}^2(\Omega) + 2\lambda\langle R_{22}^2\rangle R_{22}^2(\Omega)\right)\right\}. \tag{7.4.1}$$

In addition, the equilibrium free energy can be written as

$$A^* = -\log Q + (1/(2T^*))\left\{(\langle R_{00}^2\rangle^2 + 2\lambda\langle R_{22}^2\rangle^2)(1+3\alpha\tau^2)\right\}. \tag{7.4.2}$$

In order to find the stable state of the system at a given scaled temperature, we solve the following self-consistency equations

$$\langle R_{00}^2\rangle = Q_\Omega^{-1}\int R_{00}^2(\Omega)\exp\left(T^{*-1}(1+\alpha\tau^2)\left(\langle R_{00}^2\rangle R_{00}^2(\Omega) + 2\lambda\langle R_{22}^2\rangle R_{22}^2(\Omega)\right)\right)d\Omega, \tag{7.4.3}$$

$$\langle R_{22}^2\rangle = Q_\Omega^{-1}\int R_{22}^2(\Omega)\exp\left(T^{*-1}(1+\alpha\tau^2)\left(\langle R_{00}^2\rangle R_{00}^2(\Omega) + 2\lambda\langle R_{22}^2\rangle R_{22}^2(\Omega)\right)\right)d\Omega, \tag{7.4.4}$$

$$\tau = Q_Z^{-1} I_1\left(T^{*-1}\left(\alpha(\langle R_{00}^2\rangle^2 + 2\lambda\langle R_{22}^2\rangle^2)\right)\tau\right). \tag{7.4.5}$$

Here, the orientational and translational partition functions are given by

$$Q_\Omega = \int \exp\left(T^{*-1}(1+\alpha\tau^2)\left(\langle R^2_{00}\rangle R^2_{00}(\Omega) + 2\lambda\langle R^2_{22}\rangle R^2_{22}(\Omega)\right)\right)d\Omega, \tag{7.4.6}$$

$$Q_Z = I_0\left(T^{*-1}\left(\alpha(\langle R^2_{00}\rangle^2 + 2\lambda\langle R^2_{22}\rangle^2)\right)\tau\right). \tag{7.4.7}$$

If we use the geometric mean approximation, the potential of mean torque is given by

$$\begin{aligned} U(Z,\Omega) = -u_{200}\Big\{&\left(\alpha(\langle F_U\rangle^2 + 2\langle F_B\rangle^2)\right)\tau\cos(2\pi Z/d) \\ &+ (1+\alpha\tau^2)\left(\langle F_U\rangle F_U(\Omega) + 2\langle F_B\rangle F_B(\Omega)\right)\Big\}. \end{aligned} \tag{7.4.8}$$

In addition, the free energy is given by

$$A^* = -\log Q + (1/(2T^*))\left\{(\langle F_U\rangle^2 + 2\langle F_B\rangle^2)(1+3\alpha\tau^2)\right\}. \tag{7.4.9}$$

The self-consistency equations for this case are

$$\langle F_U\rangle = Q_\Omega^{-1}\int F_U(\Omega)\exp\left(T^{*-1}(1+\alpha\tau^2)\left(\langle F_U\rangle F_U(\Omega) + 2\langle F_B\rangle F_B(\Omega)\right)\right)d\Omega, \tag{7.4.10}$$

$$\langle F_B\rangle = Q_\Omega^{-1}\int F_B(\Omega)\exp\left(T^{*-1}(1+\alpha\tau^2)\left(\langle F_U\rangle F_U(\Omega) + 2\langle F_B\rangle F_B(\Omega)\right)\right)d\Omega, \tag{7.4.11}$$

$$\tau = Q_Z^{-1} I_1\left(T^{*-1}\left(\alpha(\langle F_U\rangle^2 + 2\langle F_B\rangle^2)\right)\tau\right), \tag{7.4.12}$$

where the orientational and translational partition functions are

$$Q_\Omega = \int \exp\left(T^{*-1}(1+\alpha\tau^2)\left(\langle F_U\rangle F_U(\Omega) + 2\langle F_B\rangle F_B(\Omega)\right)\right)d\Omega, \tag{7.4.13}$$

$$Q_Z = I_0\left(T^{*-1}\left(\alpha(\langle F_U\rangle^2 + 2\langle F_B\rangle^2)\right)\tau\right), \tag{7.4.14}$$

7.4.2 Calculations and Results

Figure 7.4 shows four phase maps for the KLZ-SVD approximation in which we fix the value of α in each phase map and vary the biaxiality λ. In figure 7.4(a) we show the phase map for $\alpha = 0$. This is in fact the same phase map presented by Sonnet *et al.* [13] which we have described in section 2.4.4. We recall that as the biaxiality λ increases, the $N_B - N_U$ transition temperature also goes up. In addition, for large values of λ, there is a line of first order $N_B - I$ transitions. Next, in figure 7.4(b), the value of α is set equal to 0.3. Now the upper boundaries of the nematic phases, the order of the phase transitions and the location of the tricritical point at high temperature are not affected by increasing α from 0 to 0.3. It is because the smectic A phases are formed at low temperature and in our theory, the smectic interaction strength α does not affect nematic ordering. In addition, the ground states of the system at low temperature are the smectic A phases instead of the nematic phases as we have seen in figure 7.4(a). We also see that the $\mathrm{SmA}_U - N_U$ transition temperature is independent of λ, in comparison with the

$N_U - I$ transition. It is because, in the SVD approximation, the potentials of mean torque in the uniaxial nematic and uniaxial smectic A phases do not depend on λ, therefore the ordering in these phases is independent of λ. In contrast, the biaxiality parameter λ does appear in the potentials of mean torque for the biaxial nematic and smectic A phases and hence they are more stable on increasing λ. For small λ, the SmA_B phase exists at lower temperature than the SmA_U phase. For large value of λ, the SmA_U region vanishes and there is a direct transition, first from SmA_B to N_U, and then from SmA_B to N_B. All phase transitions to the smectic A phases are second order. The phase map for $\alpha = 0.9$ is shown in figure 7.4(c). The $\mathrm{SmA}_U - N_U$ and $N_U - I$ transition temperatures are also independent of the biaxiality λ. We see that, the N_U region now becomes much narrower and the $\mathrm{SmA}_U - N_U$ transition is now first order, in agreement with the KLZ theory in figure 7.3. In addition, we see that now the N_B region vanishes and is replaced by the SmA_B region. The $\mathrm{SmA}_B - \mathrm{SmA}_U$ transition is mainly second order, with only a small region of it being first order, indicating a tricritical point in between the two regions. As λ increases, the stability of the SmA_B phase also goes up, as we would expect. Moreover, the phase sequence changes from $\mathrm{SmA}_B - \mathrm{SmA}_U$ to $\mathrm{SmA}_B - N_U$ and then $\mathrm{SmA}_B - I$. We calculate a phase map for $\alpha = 1.2$ which we show in figure 7.4(d). Now there exists only three phases: isotropic, uniaxial smectic A and biaxial smectic A. The vanishing of the uniaxial nematic phase is in agreement with figure 7.3. The stability of the SmA_B phase also increases with λ and the phase sequence changes from $\mathrm{SmA}_B - \mathrm{SmA}_U - I$ to directly from SmA_B to the isotropic phase. While the $\mathrm{SmA}_B - \mathrm{SmA}_U$ transition is second order, the $\mathrm{SmA}_B - I$ transition is first order. It is curious that in this case we do not find a tricritical point along the $\mathrm{SmA}_B - \mathrm{SmA}_U$ transition line. It may be explained that, as the transition is directly from the isotropic to the uniaxial smectic A phase, the ordering of the major axis is already high at the phase transition. It would then be easier for the minor axes to align and the biaxial ordering is formed at a high temperature, thus blocking a first order transition from uniaxial to biaxial phase at a lower temperature. Hence a first order $\mathrm{SmA}_B - \mathrm{SmA}_U$ transition does not exist in this case.

Figures 7.5 show five phase maps for the KLZ-GM approximation in which we fix α in each phase map and vary the biaxiality γ. The phase map for $\alpha = 0$ is essentially the phase map for the geometric mean approximation for biaxial nematics which we have described in section 2.4.4 and is reproduced in figure 7.5(a). We recall that the stability of both the uniaxial and biaxial nematic phases increase on increasing γ until they reach the Landau triple point at $\gamma = 1/\sqrt{6}$. The phase map repeats itself for larger values of γ and is not shown here. As α is set equal to 0.3, the behaviour of the nematic phases at high temperature is not affected, as shown in figure 7.5(b). The explanation is analogous to the KLZ-SVD approximation. At low temperature, the smectic A phases are stabilised. It is curious that, even though the biaxiality γ does appear in the potentials of mean torque for the uniaxial nematic and smectic A phases, the $\mathrm{SmA}_U - N_U$ transition temperature decreases very slightly as γ increases. In contrast, the stability of the SmA_B phase goes up significantly as γ increases. In addition, the phase transition changes from $\mathrm{SmA}_B - \mathrm{SmA}_U$ to $\mathrm{SmA}_B - N_U$ and then to $\mathrm{SmA}_B - N_B$, in comparison with the KLZ-SVD model in figure 7.4(b). Moreover, all phase transitions, except for the $N_U - I$ transition, are second order. Next, we show the phase map for $\alpha = 0.9$ in figure 7.5(c). Now the extent of the nematic phases are much smaller. In addition, the $\mathrm{SmA}_U - N_U$ transition is first order, in agreement with the KLZ theory in figure 7.3 for $\gamma = 0$. The stability of the SmA_B phase increases as γ goes up. The $\mathrm{SmA}_B - \mathrm{SmA}_U$ transition is still second order. In contrast, the

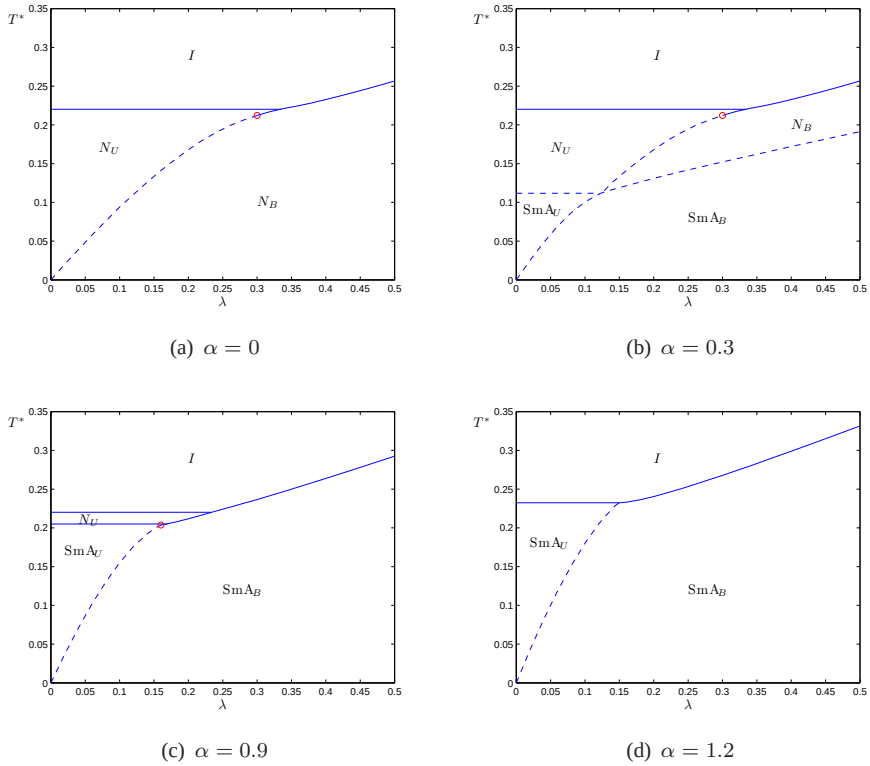

(a) $\alpha = 0$ (b) $\alpha = 0.3$

(c) $\alpha = 0.9$ (d) $\alpha = 1.2$

FIGURE 7.4: The dependence of the scaled transition temperature on the biaxiality λ for the KLZ-SVD approximation when α is fixed. Continous lines denote first order phase transitions whereas broken lines denote second order transitions. The tricritical point is marked by a red circle.

$\mathrm{SmA}_B - N_B$ and $\mathrm{SmA}_B - N_U$ are first order. For $\alpha = 1.2$, the phase map is shown in figure 7.5(d), the phase behaviour does not change in a significant way. The nematic phase regions now become much narrower, whereas the smectic A phase regions become larger. In addtion, there is a line of direct transitions from the SmA_U to the isotropic phase, in agreement with the KLZ theory in figure 7.3 for $\gamma = 0$. It is also curious that the stability of the biaxial smectic A phase does not change in a significant way as we increase α, especially for small values of γ. Now in the KLZ-GM approximation, we have not seen a direct transition from the isotropic phase to the biaxial smectic A phase for α as large as 1.2. Since we find that the stability of the smectic A phases increase as α increases, we would expect that the direct $\mathrm{SmA}_B - I$ can be found for larger values of α. Thus we increase α to 1.5 and the phase map is shown in figure 7.5(e). Indeed we find a direct $\mathrm{SmA}_B - I$ phase transition. Additionally, the qualitative phase behaviour we find for this case is analogous to the KLZ-SVD approximation for a smaller α of 1.2 in figure 7.5(d).

In order to illustrate the significance of the smectic interaction on the stability of the biaxial phases, we fix the biaxiality parameters and plot the dependence of the scaled transition temperature T^* on the smectic parameter α. In figures 7.6(a) and 7.6(b), we show these phase maps for the KLZ-SVD and KLZ-GM approximation, respectively. The values of the biaxiality parameters are chosen so that the biaxial nematic-to-uniaxial nematic transition temperature is not too high. Thus we choose $\lambda = 0.1$ and $\gamma = 0.3$ for the KLZ-SVD and KLZ-GM approximations,

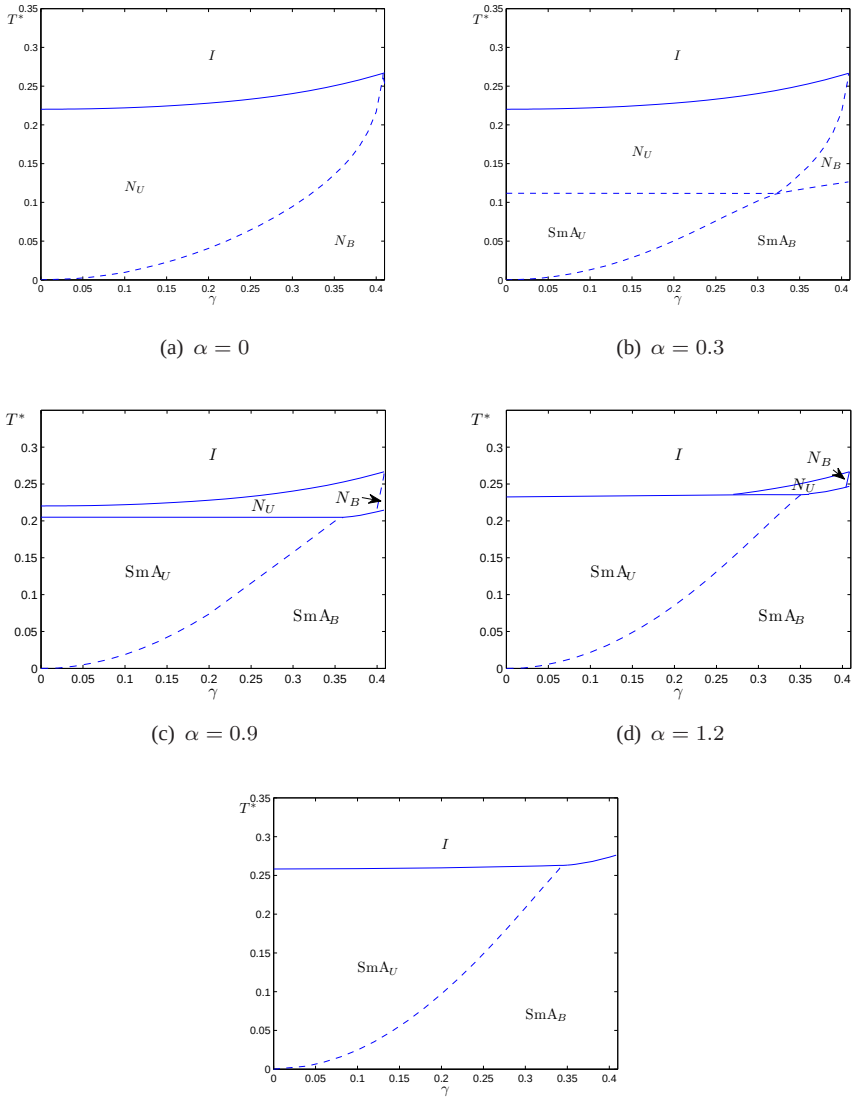

(a) $\alpha = 0$ (b) $\alpha = 0.3$

(c) $\alpha = 0.9$ (d) $\alpha = 1.2$

(e) $\alpha = 1.5$

FIGURE 7.5: The dependence of the scaled transition temperature on the biaxiality γ for the KLZ-GM approximation when α is fixed. Continous lines denote first order phase transitions whereas broken lines denote second order transitions. The tricritical point is marked by a red circle.

respectively. We see that, the qualitative behaviour of the two cases is the same. For small values of α, the $N_U - I$ and $N_B - N_U$ transition temperatures are independent of α. This is simply because in our theory, α does not influence the ordering in the nematic phases. As the temperature is lowered, there is a second order phase transition from the biaxial nematic to the biaxial smectic A phase. As α increases, the $\mathrm{SmA}_B - N_B$ transition temperature increases. For large values of α, the biaxial nematic phase disapears. Instead, the uniaxial nematic phase goes directly into the uniaxial smectic A phase. It is followed by a second order transition into the biaxial smectic A phase at a lower temperature. In addition, we find a tricritical point along the $\mathrm{SmA}_U - N_U$ transition line at 0.52 for both approximations. It is also interesting to observe that the $\mathrm{SmA}_B - \mathrm{SmA}_U$ transition temperature increases almost linearly with α.

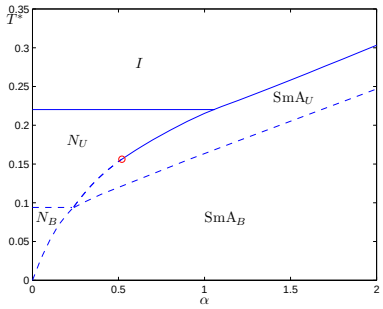

(a) KLZ-SVD approximation

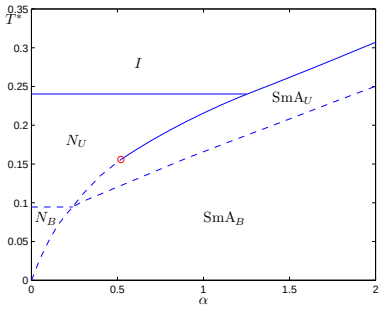

(b) KLZ-GM approximation

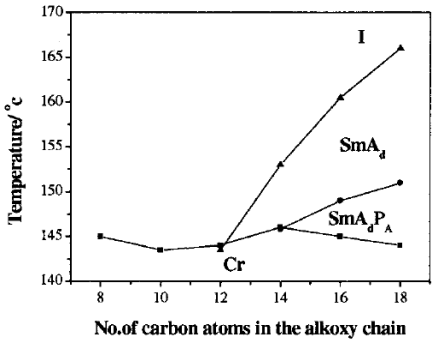

(c) Experimental results. Reproduced from [121]

FIGURE 7.6: Figures (a) and (b) depict the dependence of the scaled transition temperature on the smectic interaction parameter α for the KLZ-SVD approximation with $\lambda = 0.1$ and the KLZ-GM approximations for $\gamma = 0.3$. Figure (c) plots the dependence of the transition temperature on the number of carbon atoms in the flexible chain of a V-shaped molecules in an experiment reported in reference [121]. The smectic A phases in figure (c) are antiferroelectric; SmA_d is uniaxial whereas $\mathrm{SmA}_d P_A$ is biaxial, Cr stands for the crystal phase.

The parameter α in the molecular field theory can be related to the chain length of the compounds used in the experiments of biaxial smectic A phases for rigid V-shaped molecules [120, 121]. We can take a simple assumption that α is proportional to the chain length. In this case the molecular field and the experimental results agree qualitatively. We can make this comparison by looking at the two phase maps from the molecular field theory in figures 7.6(a) and 7.6(b) and the phase map from an experiment of V-shaped molecules [121] in figure 7.6(c). Both the biaxial smectic A-to-uniaxial smectic A and uniaxial smectic A-to-isotropic phase transition temperatures increase with the number of carbon atoms in the flexible chain. In agreement, both these phase transition temperatures go up with the parameter α in the molecular field theory.

We see from figures 7.6(a) and 7.6(b) that, for a small biaxiality, the biaxial nematic phase is formed at a low temperature. At that low temperature, a real system may already form a smectic or crystal phase. However, for large smectic interactions, the biaxial smectic A phase can form at high temperature, even for those small biaxiality that we studied. Therefore, the phase maps in figure 7.6 demonstrate that the biaxial smectic A phase is easier to form than the biaxial nematic phase.

7.5 Conclusions

In this chapter, we have developed a molecular field theory for biaxial smectic A phases. Our theory is an extension of the molecular field theory for uniaxial smectic A phases by Kventsel, Luckhurst and Zewdie, or KLZ theory. The KLZ theory is an alternative of a classical molecular field theory for uniaxial smectic A phases by McMillan. These two theories are in good qualitative agreement. One important approximation in the KLZ theory which we adopt is the decoupling approximation which allows us to write each mixed orientational-translational order parameters as a product of an orientational order parameter and the translational order parameter. In addition, we can use either the approximation proposed by Sonnet, Virga and Durand or the geometric mean approximation to reduce the number of orientational order parameters and interaction coefficients. Using these approximations, we can reduce the total number of order parameters from nine to only three. Thus the calculations are facilitated considerably. The calculation results for this model reveal that the method of minimising the equilibrium free energy sometimes fails to produce a desired solution. This can be explained by considering the non-equilibrium free energy in the KKLS theory. We check that minimising the non-equilibrium free energy does indeed give a desired solution. Using a combination of the two methods and by solving the self-consistency equations, we find that the stability of the biaxial and uniaxial smectic A phases increase as we increase the smectic interaction. Even for a small molecular biaxiality, a system with high smectic interaction strength can still form a biaxial smectic A phase at high temperature. In contrast, for the same biaxiality, a system with no smectic interaction needs to go to a very low temperature to form a biaxial nematic phase. Additionally, our results can be made contact with experimental results by other groups by assumming that the smectic interaction parameter is proportional to the chain length of the constituent molecules. These experimental results also shows that the stability of the biaxial and uniaxial smectic A phases increases with the chain length. Therefore, we conclude that, with the same molecular biaxiality, it is easier to form macroscopic biaxial ordering in the smectic A phases than in the nematic phases.

Chapter 8

Summary and Future Directions

8.1 Summary

In this thesis we have used the molecular field theory for nematic and smectic A liquid crystals to study five problems arising from experimental work on biaxial molecules by other groups. A main theme, with the exception of chapter 6 is to stabilise thermotropic biaxial nematic or smectic A phases formed from low molar mass molecules. An overview of the classical molecular field theory for nematic phases is presented in chapter 2. We have left a review of this theory for smectic A phases to chapter 7 since this is the only chapter in this thesis which involves these phases. The essence of the molecular field theory is an assumption that a molecule only interacts with a long-range molecular field generated by other molecules through a potential of mean torque and short-range correlations are ignored. This molecular field approximation can often be tested and verified using lattice Monte Carlo simulations of intermolecular pair potentials analogous to the molecular field potential. Additionally, there are other drastic assumptions about the isotropic distribution of the intermolecular vector and the dominance of the second-rank interaction. These assumptions affect both the molecular field potential and the pair potential. Either assumption can be relaxed in order to explain relevant effects. The molecular field theory also assumes pairwise intermolecular interaction as dominant, hence ignoring N-body interaction, where N is greater than two. Moreover, we assume volume changes at phase transitions as constant, thus we can use the Helmholtz free energy to determine the equilibrium of a system. This is clearly in comparison with the lattice Monte Carlo simulation since in this simulation the molecular positions are confined and so the volume of the system does not change.

After all these assumptions are made, we identify a system to study by making assumptions about symmetry of the phase and the constituent molecules. Usually, in constructing a theory we assume that the lowest symmetry of the system is the same as the molecular symmetry. This result can be tested in the Monte Carlo simulation, where no symmetry of the phase is assumed. Often we also assume that the constituent molecules are rigid. The resulting system then depend on a set of order parameters, temperature and intermolecular interaction coefficients. Each liquid crystal phase is determined by some non-vanishing order parameters. By scaling the temperature with an interaction coefficient, which is often the second-rank uniaxial anisotropic term,

we can treat the system as general and not dependent on any specific molecular model. In addition, the other interaction coefficients can be scaled with the second-rank uniaxial anisotropic term to give interaction parameters. In the calculations, we fix the temperature and the interaction parameters and minimise the free energy in order to find the order parameters at a given temperature, hence determining the stable phase at that temperature. After that, we vary the temperature to determine the phase transition temperature. Finally, the interaction parameters are varied to determine the phase maps relating the transition temperature with them.

A recent analysis on experimental results for biaxial nematics suggested that the classically assumed symmetry of these phases should be C_{2h} instead of D_{2h}. In chapter 3, we fixed the assumptions about the symmetry of the constituent molecules and the phase by assuming that they are both C_{2h} instead of D_{2h}. We get a theory with nine order parameters and five interaction parameters. The theory can be simplified further by keeping only the dominant interaction terms in the potential of mean torque. Thus, our system is reduced to a more manageable set of only three second-rank order parameters and two interaction parameters. Even with this simplified model, we still found that the biaxial nematic phase with C_{2h} symmetry is stabilised at the ground state of the system. It is all the more stable the more the constituent molecules deviate from D_{2h} symmetry. We also found that the nematic phase with C_{2h} symmetry also has an axial first-rank order parameter, in addition to the three second-rank ones. In going from the nematic phase with C_{2h} symmetry to the isotropic phase, the system may go through the uniaxial nematic phase or the biaxial nematic phase with D_{2h} symmetry. In fact we found two biaxial nematic phases with D_{2h} symmetry but with different molecular organisation. In one phase, the assigned molecular minor axes tend to be parallel whereas in the other they tend to be perpendicular. Thus this model produces a rich phase behaviour of biaxial nematics.

In chapter 4, we aimed to explain a disagreement between the molecular field theory and the experiments of biaxial nematic phases formed from V-shaped molecules. While for this particular V-shaped molecule, the theory predicts that biaxial nematics cannot be formed in real system, they are stabilised at high temperature in the experiment. To explain this disagreement, we add a first-rank interaction term to the potential of mean torque to describe dipolar interaction. This first-rank interaction is expected theoretically since the molecules have polar shape and possess a large electrostatic dipole. The first-rank interaction strength is governed by a first-rank order parameter and a first-rank interaction parameter. Our calculations show that the dipolar interaction stabilises the biaxial nematic phase at high temperature for the V-shaped molecule analogous to that used in the experiments. Thus this model explains the disagreement between theory and experiment. In addition, we show that the dipolar interaction stabilises the polar biaxial nematic phase. This is another nematic phase of symmetry lower than D_{2h}, namely C_{2v}.

The assumption on molecular rigidity is relaxed when we study the effect of molecular flexibility on the stability of biaxial nematic phases in chapter 5. We study a simple system of liquid crystal dimers whose constituent molecules can adopt a large number of shapes, or conformation. Our model is simplified in that there are only two conformers: linear and bent with tetrahedral interarm angle. Hence one is uniaxial whereas the other has maximal biaxiality. We find that, when we assume the Boltzmann factor in the conformational distribution to be independent of temperature, the linear conformer is more favoured by both biaxial and uniaxial nematic systems. However, this effect is less important when we allow the Boltzmann factor in the conformational distribution to be temperature dependent. Importantly, we find that in order

for the biaxial nematic phase to stabilise, the conformational energy of the bent conformer needs to be lower than the linear one and the difference between the conformational energies should be sufficiently large.

The motivation for chapter 6 is a recent success in observing a significant increase in the magnetic-field induced uniaxial nematic to isotropic transition temperature in experiments. This success is partially attributed to a high magnetic field strength of 31 Tesla used in the experiment. We have proposed that this success is also due to high molecular biaxiality of the constituent molecules. Hence, we extended the classical model for uniaxial nematic formed from biaxial molecules to include an interaction with the magnetic field. We found that, for systems with high molecular biaxiality, the effect of the magnetic field on the transition temperature is more pronounced than for those with low molecular biaxiality. In addition, the magnetic critical point for systems with high molecular biaxiality is closer to the clearing point than for those with low molecular biaxiality, thus might require a smaller critical field strength to observe. Moreover, the critical exponent is cubic. We also related our theory with the Landau-KKLS theory to build up molecular structure into the Landau expansion. Hence, the results which we obtained by solving the molecular field theory are analytical in the Landau-KKLS theory and they agree qualitatively with the molecular field theory.

Finally, we developed a molecular field theory for biaxial smectic A phases in chapter 7. To keep the problem simple, we assume that the phase and the constituent molecules have D_{2h} symmetry. We use the KLZ approximation which assume that a mixed orientational-translational order parameter can be written as a product of an orientational order parameter and the translational order parameter. In addition, we considered two cases where we used either the SVD approximation or the geometric mean approximation for the orientational interaction parameters. Thus our theory for the biaxial smectic A phases is greatly simplified to only three order parameters and three interaction parameters. We set the interaction parameter which scales the pure translational interaction to zero, hence we are left with only two interaction parameters. The calculations show that, for high smectic interaction, the biaxial smectic A phases are easier to form than the biaxial nematic phase. In addition, using this simplified model, we can produce results that are in qualitative agreement with experiments.

8.2 Future Directions

There are several research directions which can be taken to extend the works in this thesis. One thing could be done is to build in more complexities within each chapter in order to study more realistic systems. Another direction is to combine the theories in some chapters into one model. This allows us to include many effects into a molecular field model and to see how they influence each other to stabilise or destabilise the biaxial phases.

For the model of biaxial nematics with C_{2h} symmetry in chapter 3, we may include more terms in the potential of mean torque, thus we can see the effect of the minor interaction parameters and order parameters. In addition, we can explore the molecular organisation with respect to the phase axes. We may be able to see if the molecular ordering tensors S_{xx}^{AA}, S_{yy}^{AA}, S_{xy}^{AA} and S_{zz}^{AA} have the same eigenframes or not which we have not been able to answer in the simplified

model. In order to relate all five interaction parameters to the molecular structure, we may use the excluded volume method. However, the resulting theory with nine order parameters is still challenging to solve. Hence ingenious computer algorithms and coding should be exploited to resolve this issues.

The calculation results on rigid V-shaped molecules which we have presented in chapters 4 and 6 are aimed to explain some experimental results. More work can also be done in these directions to explore the theory further. One may add more dipolar interactions in the directions perpendicular to the existing dipole, in order to see if the biaxial nematic phase is stabilised or not. The question about how local ordering influences the stability of the biaxial nematic phase also permits further exploration. This would involve adding more complication into the molecular field theory to a different level. Thus instead of one molecule interacting with the molecular field, we may have two or more molecules interacting with the field. Moreover, we could use the lattice Monte Carlo simulation in which the intermolecular vector distribution is anisotropic. Again, this would require ingenious methods to solve. For the magnetic interaction case, it is still unclear why the ratios in the experiment are much larger than the molecular field theory. One possible explanation is that the theory has a poor prediction of the supercooling temperature. This can also be tested by using the many-site molecular field theory or lattice Monte Carlo simulation.

In chapters 3 and 4 we study biaxial nematic phases of lower symmetry than usually assumed. However, assuming that second-rank interaction in liquid crystals is dominant, biaxial nematic phases with symmetries even lower than C_{2h} and C_{2v} are allowed to exist. They are C_i and C_s symmetries. Thus we may develop molecular field theories for these phases. They would be a combination of the extension of the models in chapters 3 and 4. Such systems would have a very rich phase behaviour with several nematic phases of different symmetries.

The model which we have used in chapter 5 is a very basic model of how molecular flexibility influences the stability of the biaxial nematic phases. It is then significant to extend this model to allow us to study real systems of nematic liquid crystals. This could be achieved through several steps. Ideally, we may start with flexible molecules, generate its many conformations which may have different symmetries. Then we solve the molecular field theory for these many conformations. This appears to be a formidable challenge in modelling and solving the theory.

In chapter 7, we have developed a model for biaxial smectic A phases with D_{2h} symmetry. Thus a valid question would be whether the biaxial smectic A phases can adopt lower symmetries as the biaxial nematic phases. This can simply be done by introducing the order parameters and interaction parameters which are responsible for smectic ordering into the theories of biaxial nematic with symmetries lower than D_{2h}. Assuming the second-rank interaction is also dominant in the smectic A phases, the symmetry of biaxial smectic A phases can be C_{2h}, C_i and C_s. In addition, if first-rank interactions are also allowed, we may have a polar biaxial smectic A phases with ferroelectric character. Moreover, biaxial smectic A phases have been found to stabilise by some liquid crystal dimers. These molecules are highly flexible. Therefore, in order to have a realistic model of these systems, we need to allow the molecules in the molecular field theory to change their shape. This would be a joined project with the extension of chapter 5.

Appendix A

Explicit Expressions for some Clebsch-Gordan Coefficients and Small Wigner Rotation Matrices

The explicit expressions for some of the Clebsch-Gordan coefficients $C(22L;mm')$ that are used in this thesis are:

$$\begin{gathered}
C(220;00) = C(220;2-2) = C(220;-22) = 1/\sqrt{5}, \\
C(222;00) = C(220;02) = C(220;0-2) = C(220;2-2) = C(220;-22) = \sqrt{2/7}, \\
C(224;00) = 3\sqrt{2/35}, \\
C(224;02) = C(224;0-2) = (1/2)\sqrt{6/7}, \\
C(224;22) = C(224;-2-2) = 1, \\
C(224;-22) = C(224;2-2) = 1/\sqrt{70}.
\end{gathered} \tag{A.0.1}$$

The explicit expressions for the small Wigner rotation matrices $d^L_{mn}(\beta)$ used in this thesis are

$$\begin{gathered}
d^0_{00}(\beta) = 1, \\
d^1_{00}(\beta) = \cos\beta, \\
d^1_{11}(\beta) = d^1_{-1-1}(\beta) = \cos^2\beta/2, \\
d^1_{1-1}(\beta) = d^1_{1-1}(\beta) = \sin^2\beta/2, \\
d^2_{00}(\beta) = (3\cos\beta^2 - 1)/2, \\
d^2_{02}(\beta) = d^2_{0-2}(\beta) = d^2_{20}(\beta) = d^2_{-20}(\beta) = \sqrt{3/8}\sin^2(\beta), \\
d^2_{22}(\beta) = d^2_{-2-2}(\beta) = \cos^4(\beta/2), \\
d^2_{2-2}(\beta) = d^2_{-22}(\beta) = \sin^4(\beta/2), \\
d^4_{00}(\beta) = (35/8)\cos^4(\beta) - (15/4)\cos^2(\beta) + (3/8), \\
d^4_{02}(\beta) = d^4_{0-2}(\beta) = d^4_{20}(\beta) = d^4_{-20}(\beta) = (\sqrt{10}/8)\sin^2(\beta)\left[7\cos^2(\beta) - 1\right] \\
d^4_{04}(\beta) = d^4_{0-4}(\beta) = d^4_{40}(\beta) = d^4_{-40}(\beta) = \left(\sqrt{(}70)/16\right)\sin^4(\beta).
\end{gathered} \tag{A.0.2}$$

Appendix B

Minimisation Methods

In order to minimise the free energy, we use the MATLAB function *fmincon*. An example of a free energy function is in equation (2.4.35) for a system formed from identical molecules with D_{2h} symmetry using the geometric mean approximation. This appendix describes the specific algorithms which we choose to minimise the free energy. Suppose we want to minimise a general function $f(\mathbf{x})$ of a vector variables $\mathbf{x}$ with a vector function $G_i(\mathbf{x})$ containing the values of the equality and inequality constraints evaluated at $\mathbf{x}$. We take a few steps in developing the complexity in our algorithm. First of all we show how Newton's method can be used to solve a nonlinear non-constrained minimisation problem in appendix B.1. Next, in appendix B.2, we apply Newton's method to show that the solutions to a general equality constraint nonlinear minimisation problem are the same as a Sequential Quadratic Programming problem. After that, in appendix B.3, we show how to use the Sequential Quadratic Programming to solve minimisation problem with inequality constraints which is analogous to minimisation problems with equality constraints. This last case has been used in the function *fmincon* in order to find the global minimum of the free energy of our system. In order to deal with inequality constraints, an algorithm called null-space active set method is employed which is discussed in B.4. Finally, in appendix B.5 we discuss an algorithm to find a step length at each iteration in our algorithm.

B.1 Application of Newton's Method for Non-constrained Nonlinear Minimisation Problems

Newton's method is a method for solving a system of nonlinear equations of general form $f(\mathbf{x}) = \mathbf{0}$ where f is a vector function of a vector variables $\mathbf{x}$. Suppose at iteration k in the algorithm the estimate of the solution $\mathbf{x}^*$ is $\mathbf{x}^{(k)}$. Newton's method computes the improved estimate $\mathbf{x}^{(k+1)}$ at step $k+1$ by setting the local linear approximation to the function f at $\mathbf{x}^{(k)}$ to zero and then solve to get $\mathbf{x}^{(k+1)}$. The estimate at step $k+1$ is given by

$$\mathbf{x}^{(k+1)} = \mathbf{x}^{(k)} - \mathbf{J}^{-1} f(\mathbf{x}^{(k)}), k = 0, 1, 2, ..., \tag{B.1.1}$$

provided that the Jacobian matrix $\mathbf{J}$ of f is non-singular. Newton's method has been proved to converge quadratically to a solution.

Newton's method can be applied to a non-constrained nonlinear minimisation problem to find the direction in the variables to go to the next iteration

$$\min f(\mathbf{x}), \tag{B.1.2}$$

by setting the first derivative to zero and solve the corresponding nonlinear system $\nabla f(\mathbf{x}) = 0$. The solution then gives us the direction to the minimum, provided sufficient conditions of the first and second derivatives of f are satisfied. The Newton's direction is then

$$\mathbf{x}^{(k+1)} = \mathbf{x}^{(k)} - \left(\mathbf{H}f(\mathbf{x}^{(k)})\right)^T \nabla f(\mathbf{x}^{(k)}), k = 0, 1, 2, ..., \tag{B.1.3}$$

where $\mathbf{H}f(\mathbf{x}^{(k)})$ denotes the estimate of the Hessian matrix of the function $f(\mathrm{x})$ at step k in the iteration.

B.2 Sequential Quadratic Programming for Solving Equality Constrained Nonlinear Minimisation Problems

Before deriving the Sequential Quadratic Programming method, we present the theorem which gives the first order necessary conditions for a general nonlinear minimisation problem. Given the following minimisation problem

$$\min f(\mathbf{x}) \tag{B.2.1}$$

subject to

$$\begin{aligned} &\mathbf{g}(\mathbf{x}) = \mathbf{0}, \\ &\mathbf{h}(\mathbf{x}) \geq \mathbf{0}. \end{aligned} \tag{B.2.2}$$

We define the Lagrangian to be $L(\mathbf{x}, \gamma, \theta) = f(\mathbf{x}) - \gamma\mathbf{g}(\mathbf{x}) + \theta\mathbf{h}(\mathbf{x})$ with arbitrary γ and θ. Then there are Lagrange multiplier vectors γ^* and θ^*, with components γ_i^* and θ_i^*, such that the following conditions are satisfied at the minimum $(\mathbf{x}^*, \gamma^*, \theta^*)$

$$\begin{aligned} &\nabla_{\mathbf{x}} L(\mathbf{x}^*, \gamma^*, \theta^*) = \mathbf{0}, \\ &\mathbf{g}(\mathbf{x}^*) = \mathbf{0}, \\ &\mathbf{h}(\mathbf{x}^*) \geq \mathbf{0}, \\ &\theta^* \geq \mathbf{0}, \\ &\gamma^*\mathbf{g}(\mathbf{x}^*) = \mathbf{0}, \\ &\theta^*\mathbf{h}(\mathbf{x}^*) = \mathbf{0}. \end{aligned} \tag{B.2.3}$$

The conditions in this theorem are often known as the Karush-Kuhn-Tucker conditions. The proof of this theorem is complex so we do not include here, for interested reader see in Nocedal

and Wright [129].

Now we come back to our minimisation problem which only include equality constraints

$$\min_{\mathbf{x}} f(\mathbf{x}), \tag{B.2.4}$$

subject to

$$\mathbf{g}(\mathbf{x}) = \mathbf{0}. \tag{B.2.5}$$

If $\mathbf{x}^*$ and γ^* are the solution and the corresponding Lagrange multiplier vectors, respectively, then the followings are satisfied according to the first order optimality conditions

$$\begin{aligned} \nabla f(\mathbf{x}^*) - \nabla \mathbf{g}(\mathbf{x}^*)^T \gamma^* = \mathbf{0}, \\ -\mathbf{g}(\mathbf{x}^*) = \mathbf{0}. \end{aligned} \tag{B.2.6}$$

Hence the minimum can be found by applying Newton's method to the following system to solve for $\mathbf{x}$ and γ

$$\begin{aligned} \nabla f(\mathbf{x}) - \nabla \mathbf{g}(\mathbf{x})^T \gamma = \mathbf{0}, \\ -\mathbf{g}(\mathbf{x}) = \mathbf{0}. \end{aligned} \tag{B.2.7}$$

An iterative step in Newton's method applying to this system of nonlinear equations is

$$\begin{pmatrix} \mathbf{H}L(\mathbf{x}^{(k)}, \gamma^{(k)}) & -\nabla \mathbf{g}(\mathbf{x}^{(k)}) \\ -\nabla \mathbf{g}(\mathbf{x}^{(k)})^T & \mathbf{0} \end{pmatrix} . \begin{pmatrix} \mathbf{p}^{(k)} \\ \gamma^{*(k)} \end{pmatrix} = - \begin{pmatrix} \nabla L(\mathbf{x}^{(k)}, \gamma^{(k)}) \\ -\mathbf{g}(\mathbf{x}^{(k)}). \end{pmatrix} \tag{B.2.8}$$

Here, $\mathbf{p}$ is the desired step from the estimate $\mathbf{x}$ to the minimum $\mathbf{x}^*$, $\mathbf{p} = \mathbf{x}^* - \mathbf{x}$ In fact these conditions above also satisfy the first-order necessary conditions for the following quadratic program

$$\min \qquad \frac{1}{2}\mathbf{p}^T.\mathbf{H}L(\mathbf{x}^{(k)}, \gamma^{(k)})\mathbf{p} + \nabla L(\mathbf{x}^{(k)}, \gamma^{(k)})^T \mathbf{p} + L(\mathbf{x}^{(k)}, \gamma^{(k)}) = 0, \tag{B.2.9}$$

subject to

$$\nabla \mathbf{g}(\mathbf{x}^{(k)})^T \mathbf{p} + \mathbf{g}(\mathbf{x}^{(k)}) = 0. \tag{B.2.10}$$

Hence the Sequential Quadratic Programming method is equivalent to Newton's method applied to the first order necessary conditions, solving the quadratic program generates the quasi-Newton steps. Because of the constraints, the quadratic program is equivalent to

$$\min \qquad \frac{1}{2}\mathbf{p}^T.\mathbf{H}L(\mathbf{x}^{(k)}, \gamma^{(k)})\mathbf{p} + \nabla f(\mathbf{x}^{(k)}, \gamma^{(k)})^T \mathbf{p} + f(\mathbf{x}^{(k)}, \gamma^{(k)}), \tag{B.2.11}$$

subject to

$$\nabla \mathbf{g}(\mathbf{x}^{(k)})^T \mathbf{p} + \mathbf{g}(\mathbf{x}^{(k)}) = 0. \tag{B.2.12}$$

Finally, we can drop the last term $f(\mathbf{x}^{(k)}, \gamma^{(k)})$ since it is irrelevant in determining $\mathbf{p}^{(k)}$. Therefore the quadratic program is

$$\min \qquad \frac{1}{2}\mathbf{p}^T.\mathbf{H}L(\mathbf{x}^{(k)}, \gamma^{(k)})\mathbf{p} + \nabla f(\mathbf{x}^{(k)}, \gamma^{(k)})^T \mathbf{p}, \tag{B.2.13}$$

subject to

$$\nabla \mathbf{g}(\mathbf{x}^{(k)})^T \mathbf{p} + \mathbf{g}(\mathbf{x}^{(k)}) = 0. \tag{B.2.14}$$

B.3 Sequential Quadratic Programming for Solving General nonlinear Minimisation Problems

A general nonlinear minimisation problem has both equality and inequality constraints

$$\min_{\mathbf{x}} \mathbf{f}(\mathbf{x}), \tag{B.3.1}$$

subject to

$$\begin{aligned} \mathbf{g}(\mathbf{x}) &= 0, \\ \mathbf{h}(\mathbf{x}) &\leq 0. \end{aligned} \tag{B.3.2}$$

Following the analysis for equality constrained minimisation, the Sequential Quadratic Programming can be extended to a general nonlinear programming problem. This is the method used in *fmincon* to locate minima of a general nonlinear smooth constrained problem. The quadratic program is now replaced by

$$\min \qquad \frac{1}{2}\mathbf{p}^T.\mathbf{H}L(\mathbf{x}^{(k)}, \gamma^{(k)})\mathbf{p} + \nabla f(\mathbf{x}^{(k)}, \gamma^{(k)})^T.\mathbf{p}, \tag{B.3.3}$$

subject to

$$\begin{aligned} \nabla \mathbf{g}(\mathbf{x}^{(k)})^T.\mathbf{p} + \mathbf{g}(\mathbf{x}^{(k)}) &= 0, \\ \nabla \mathbf{h}(\mathbf{x}^{(k)})^T.\mathbf{p} + \mathbf{h}(\mathbf{x}^{(k)}) &\leq 0. \end{aligned} \tag{B.3.4}$$

In fact this quadratic program also generates Newton steps.

In practice, quasi-Newton methods are often used instead of Newton's method. Quasi-Newton methods are like Newton's method except the Hessian of the Lagrangian is approximated instead of calculated directly as in Newton's method. The most popular quasi-Newton algorithm is the BFGS method, named after its discoverers Broyden, Fletcher, Goldfarb and Shanno. The method converges superlinearly, which is slower than Newton's method which is quadratic but faster than linear convergence. However Newton's method requires the calculations of second derivatives at each step which is more expensive and so the BFGS method is more favourable. The derivation of the approximation formulae for the Hessian matrix is rather complex and we only give the formular here for completeness

$$\mathbf{H}^{(k+1)} = \mathbf{H}^{(k)} + \frac{\nabla L^{(k)}.\nabla L^{(k)T}}{\nabla L^{(k)T}.\mathbf{p}^{(k)}} - \frac{\left(\mathbf{H}^{(k)}\mathbf{p}^{(k)}\right)\left(\mathbf{H}^{(k)}\mathbf{p}^{(k)}\right)^T}{\mathbf{p}^{(k)T}.\mathbf{H}^{(k)}\mathbf{p}^{(k)}}, \tag{B.3.5}$$

where $\mathbf{H}^{(k)}$ is the approximation of the Hessian matrix at step k, $\mathbf{H}^k$.

B.4 Null-space Active Set Method for Solving Quadratic Programs

At each step, a general quadratic program has the form

$$\min \qquad \frac{1}{2}\mathbf{p}^T.\mathbf{H}L(\mathbf{x}^{(k)},\gamma^{(k)})\mathbf{p} + \nabla f(\mathbf{x}^{(k)},\gamma^{(k)})^T\mathbf{p} = 0, \tag{B.4.1}$$

subject to

$$\nabla \mathbf{h}(\mathbf{x}^{(k)})^T\mathbf{p} + \mathbf{h}(\mathbf{x}^{(k)}) \leq 0, \tag{B.4.2}$$

here we do not include equality constraints since it is irrelevant to our problem anyway. For simplicity we rewrite the quadratic program as

$$\min \qquad \frac{1}{2}\mathbf{p}^T\mathbf{H}\mathbf{p} + \mathbf{c}^T\mathbf{p}. \tag{B.4.3}$$

subject to

$$\mathbf{A}\mathbf{p} \leq \mathbf{b}. \tag{B.4.4}$$

The active set method involves two phases. In the first phase a feasible starting point is calculated. In the second phase the method generates an iterative sequence of feasible points that converge to the solution. Now we define an active set $\bar{\mathbf{A}}$ which is the set that keeps information about the active constraints (those that are on the constraint boundaries). The number of columns of the active set is equal to the dimension of $\mathbf{p}$ and is always fixed, we call it m. The number of rows of the active set at each step is the number of the active constraints at that step and we call it l. At each iteration, the active constraint is updated, and is used to form a basis for a search direction. The search direction is then calculated and minimises the objective quadratic function while remaining on any active constraint boundary.

The first phase involves the computation of a feasible starting point $\mathbf{p}^{(0)}$ is not discussed in details in the documentation [130] so we obmit here. However some strategies can be found in Nocedal and Wright [129].

After the feasible starting point is found, the quadratic programming starts. At each step the quadratic programming is solved for the search direction $\mathbf{d}^{(j)}$ with the intention of setting $\mathbf{d}^{(j)} = \mathbf{p}^{(j)} - \mathbf{p}^{(j-1)}$. The problem now has the form

$$\min \qquad \frac{1}{2}\mathbf{d}^T\mathbf{H}\mathbf{d} + \mathbf{c}^{(j)T}\mathbf{d}. \tag{B.4.5}$$

subject to

$$\bar{\mathbf{A}}^{(j)}\mathbf{d} = \mathbf{0}, \tag{B.4.6}$$

where

$$\begin{aligned} \mathbf{d} &= \mathbf{p} - \mathbf{p}^{(j)}, \\ \mathbf{c}^{(j)} &= \mathbf{H}\mathbf{p}^{(j)} + \mathbf{c}. \end{aligned} \tag{B.4.7}$$

Now it is clear from the constraints that the search direction $\mathbf{d}^{(k)}$ must be in the null space of the active set $\bar{\mathbf{A}}$ (the space formed of vectors whose products with $\bar{\mathbf{A}}$ give the zero vector).

Therefore the search direction can be formed from a basis $\mathbf{Z}^{(j)}$ whose columns are orthogonal to the active set such that $\bar{\mathbf{A}}^{(j)T}\mathbf{Z}^{(j)} = 0$. This null space matrix can be formed from the last $m - l$ columns of the QR decomposition of the matrix $\bar{\mathbf{A}}$. Now since the search direction is in the null space of the active constraints, it is a linear combination of the columns of $\mathbf{Z}^{(j)}$, in other words $\mathbf{d}^{(j)} = \mathbf{Z}^{(j)}\mathbf{s}^{(j)}$, for some vector $\mathbf{s}^{(j)}$. Then the quadratic program is now in terms of $\mathbf{s}^{(j)}$ instead of $\mathbf{d}^{(j)}$

$$\min \qquad \frac{1}{2}\mathbf{s}^T\mathbf{Z}^{(j)T}\mathbf{H}\mathbf{Z}^{(j)}\mathbf{s} + \mathbf{c}^T\mathbf{Z}^{(j)}\mathbf{s}. \tag{B.4.8}$$

The search direction $\mathbf{s}^{(j)}$ can be found by setting the gradient of this function to zero and solve the corresponding linear equations. After that $\mathbf{d}^{(j)}$ can be found. If we can take $\mathbf{p}^{(j+1)} = \mathbf{p}^{(j)} + \mathbf{d}^{(j)}$ without violation of any inactive constraints then that step is accepted. Otherwise we move to the nearest boundary by taking $\mathbf{p}^{(j+1)} = \mathbf{p}^{(j)} + \delta\mathbf{d}^{(j)}$ where

$$\delta = \min_i \frac{-(\mathbf{A}_i\mathbf{p}^{(j)} - \mathbf{b}_i)}{\mathbf{A}_i\mathbf{p}^{(j)}} \tag{B.4.9}$$

Then the active set is updated. The quadratic subprogram is terminated when $\mathbf{d}^{(j)} = \mathbf{0}$ and the corresponding Lagrange multipliers are non-negative. The Lagrange multipliers are found by solving the first order optimality conditions

$$\bar{\mathbf{A}}^{(j)T}\gamma^{(j)} = \mathbf{c}. \tag{B.4.10}$$

If any Lagrange multiplier is negative then the columns of the active set corresponding to that Lagrange multiplier does not correspond to an equality constraint and is removed from the active set and a new iterate is sought.

B.5 Line Search Method for the Determination of Step Length

Now we have solved the quadratic subprogram to find the search direction $\mathbf{p}^{(k)}$ to move along. The new point in the next iterate has the form $\mathbf{x}^{(k+1)} = \mathbf{x}^{(k)} + \alpha^{(k)}\mathbf{p}^{(k)}$ where the step length $\alpha^{(k)}$ can be found by line search method. In line search method there are two phases. The first phase is the *bracketing phase* which finds an interval $[a, b]$ containing acceptable step lengths $[a, b]$. The second phase is called the *selection phase* that iteratively reduce the interval of acceptable step lengths by interpolating some of the function and derivative information gathered on earlier steps to guess the location of the minimiser. There are several methods that can be used in these phases and we are not sure which one is employed in *fmincon*. Some of the methods are listed in chapter 3 of Nocedal and Wright [129]. During the selection phase, the optimal solution is found when it satisfies the Wolfe conditions

$$\Psi(\mathbf{x}^{(k)} + \alpha^{(k)}\mathbf{p}^{(k)}) \leq \mathbf{x}^{(k)} + c_1\alpha^{(k)}\nabla\Psi^{(k)T}\mathbf{p}^{(k)}, \tag{B.5.1}$$

$$\nabla\Psi(\mathbf{x}^{(k)} + \alpha^{(k)}\mathbf{p}^{(k)})^T\mathbf{p}^{(k)} \geq c_2\nabla\Psi^{(k)T}\mathbf{p}^{(k)}, \tag{B.5.2}$$

where c_1 and c_2 are constants with $0 < c_1 < c_2 < 1$. Ψ is called merit function which is the same as the objective function f in non-constrained minimisation. In constrained minimisation, the merit function is an addtion of the objective function and terms which takes into account

the constraints to ensure that the next iterate does not go to far from the feasible region. The discussion of the merit function in this case, especially the one used in *fmincon* is rather complex and we refer reader to references in the documentation [130] and the book by Nocedal and Wright [129]. The first condition ensures that the step length $\alpha^{(k)}$ give sufficient decrease in the merit function Ψ. We see that the reduction in Ψ should be proportional to both the step length and the directional derivative $\nabla\Psi^{(k)T}\mathbf{p}^{(k)}$. The second condition is called the curvature condition which ensures the the algorithm makes reasonable progress by ruling out unacceptably short steps. This second condition means that, if the slope is two small then we cannot expect much more decrease in the merit function in this direction so we should stop the algorithm. In practice the values of c_1 and c_2 are about 10^{-4} and 0.9, respectively for Newton and quasi-Newton methods [129].

Appendix C

Analytical Results for the Biaxial Nematic-to-Uniaxial Nematic Phase Transition

We consider the relation at the second-rank biaxial nematic-to-uniaxial nematic phase transition

$$\frac{k_BT}{u_{200}} = 2Q^{-1}\int \left(F_B(\Omega)\right)^2 \exp\left(-\frac{U_U(\Omega)}{k_BT}\right) d(\Omega). \tag{C.0.1}$$

The function inside the exponential function is the potential of mean torque in the uniaxial phase and so it is independent of the angle α. Hence we can write this as

$$\frac{k_BT}{u_{200}} = 2Q_U^{-1}\int \left\{\left[\int \left(F_B(\Omega)\right)^2 d\alpha\right] \exp\left(\frac{-U_U(\omega)}{k_BT}\right)\right\} d(\omega), \tag{C.0.2}$$

where

$$F_B(\Omega) = \left(R^2_{20}(\Omega)\right)^2 + 2\gamma R^2_{20}(\Omega)R^2_{22}(\Omega) + \left(R^2_{22}(\Omega)\right)^2. \tag{C.0.3}$$

This can be expressed in terms of the quadratic products of the Wigner rotation matrices by writting the R functions in terms of them. The quadratic products of the Wigner rotation matrices are given by

$$D^2_{mn}(\Omega)D^2_{m'n'}(\Omega) = \sum_L C(22L;mm')C(22L;nn')D^L_{m+m',n+n'}(\Omega), \tag{C.0.4}$$

Bearing in mind that the Wigner rotation matrices $D^4_{\pm 4,n}(\Omega)$ vanish under the integration with respect to α, the results of the quadratic products which are non-zero under the integration over

α are

$$
\begin{aligned}
D^2_{20}(\Omega) \times D^2_{-20}(\Omega) &= (1/5) - (2/7)D^2_{00}(\Omega) + (3/35)D^4_{00}(\Omega), \\
D^2_{20}(\Omega) \times D^2_{-22}(\Omega) &= (2/7)D^2_{02}(\Omega) + (1/2)\sqrt{2/35}(1/2)\sqrt{6/7}D^4_{02}(\Omega), \\
D^2_{20}(\Omega) \times D^2_{-2-2}(\Omega) &= (2/7)D^2_{0-2}(\Omega) + (1/2)\sqrt{2/35}(1/2)\sqrt{6/7}D^4_{02}(\Omega), \\
D^2_{20}(\Omega) \times D^2_{-2-2}(\Omega) &= (2/7)D^2_{02}(\Omega) + (1/2)\sqrt{2/35}(1/2)\sqrt{6/7}D^4_{0-2}(\Omega), \\
D^2_{-20}(\Omega) \times D^2_{2-2}(\Omega) &= (2/7)D^2_{0-2}(\Omega) + (1/2)\sqrt{2/35}(1/2)\sqrt{6/7}D^4_{0-2}(\Omega), \\
D^2_{22}(\Omega) \times D^2_{-2-2}(\Omega) &= (2/7)D^2_{00}(\Omega) + (1/70)D^4_{00}(\Omega), \\
D^2_{22}(\Omega) \times D^2_{-22}(\Omega) &= 1/\sqrt{70}D^4_{04}(\Omega), \\
D^2_{2-2}(\Omega) \times D^2_{-22}(\Omega) &= 1/5 + (2/7)D^2_{00}(\Omega) + (1/70)D^4_{00}(\Omega), \\
D^2_{2-2}(\Omega) \times D^2_{-2-2}(\Omega) &= 1/\sqrt{70}D^4_{0-4}(\Omega).
\end{aligned}
\tag{C.0.5}
$$

Averaging these order parameters over the orientational distribution function for the uniaxial phase we get the relation of the biaxial nematic-to-uniaxial nematic phase transition temperature and the uniaxial order parameters

$$
\begin{aligned}
\tfrac{k_B T}{u_{200}} &= \tfrac{1+2\gamma^2}{5} + \left(\tfrac{-2+4\gamma^2}{7}\right)\langle R^2_{00}\rangle + \tfrac{8}{7}\gamma\langle R^2_{02}\rangle \\
&+ \left(\tfrac{3+\gamma^2}{35}\right)\langle R^4_{00}\rangle + \tfrac{2}{7}\sqrt{\tfrac{3}{5}}\gamma\langle R^4_{02}\rangle + \sqrt{\tfrac{2}{35}}\gamma^2\langle R^4_{04}\rangle.
\end{aligned}
\tag{C.0.6}
$$

Appendix D

A Proof of The Rotation Tensor

Let $\mathbf{R}$ be a rotation tensor which rotate a vector $\mathbf{v}$ around a unit vector $\mathbf{a} = (a_1, a_2, a_3)^T$ over an angle θ and send it to a new vector $\mathbf{v}'$. We want to prove that

$$\mathbf{R} = e^{\mathbf{A}\theta}, \tag{D.0.1}$$

where $\mathbf{A}$ is a skew symmetric tensor associated with the unit vector $\mathbf{a}$

$$\mathbf{A} = \begin{pmatrix} 0 & -a_3 & a_2 \\ a_3 & 0 & -a_1 \\ -a_2 & a_1 & 0 \end{pmatrix} \tag{D.0.2}$$

The proof is as follows. First we note that the new vector $\mathbf{v}'$ is related to the original vector $\mathbf{v}$ via the Rodriguez rotation formula

$$\mathbf{v}' = \mathbf{v}\cos\theta + \mathbf{a}(\mathbf{a}.\mathbf{v})(1 - \cos\theta) + (\mathbf{a} \times \mathbf{v})\sin\theta. \tag{D.0.3}$$

Suppose now $\theta = \Delta\theta$ is very small, such that

$$\cos\Delta\theta \backsimeq 1, \qquad \sin\Delta\theta \backsimeq \Delta\theta. \tag{D.0.4}$$

so that

$$\mathbf{v}' \backsimeq \mathbf{v} + \Delta\theta(\mathbf{a} \times \mathbf{v}). \tag{D.0.5}$$

Now we let $\mathbf{A}$ be a skew symmetric tensor associated with the unit vector $\mathbf{a}$, such that $\mathbf{A}\mathbf{v} = \mathbf{a} \times \mathbf{v}$, clearly $\mathbf{A}$ is given by equation (D.0.2). Hence to first order, the rotation tensor is

$$\mathbf{R} = \mathbf{I} + \Delta\theta\mathbf{A}. \tag{D.0.6}$$

Now the rotation around $\mathbf{a}$ over an arbitrary angle θ consists of N small rotations, where N is a large number, each takes $\mathbf{v}$ around $\mathbf{a}$ over an angle θ/N with the rotation matrix

$$\mathbf{R}_N = \mathbf{I} + \frac{\theta}{N}\mathbf{A}, \tag{D.0.7}$$

and so the rotation tensor over θ is

$$\mathbf{R} = \left(\mathbf{I} + \frac{\theta}{N}\mathbf{A}\right)^N. \tag{D.0.8}$$

Letting N goes to infinity we then have equation (D.0.1) $\mathbf{R} = e^{\mathbf{A}\theta}$.

Appendix E

Numerical Method for Solving the Self-consistency Equations

In this appendix, we discuss the trust-region dogleg algorithm which is implemented in the MATLAB function *fsolve*. We have used this function to solve the self-consistency equations in chapter 7. The contents of this appendix are taken from the documentation for the MATLAB Optimization Toolbox [130].

We recall from appendix B.1 Newton's method can be applied to solve a system of nonlinear equations $f(\mathbf{x}) = \mathbf{0}$ by improving the estimate $\mathbf{x}^{(k)}$ of the solution at each step to give the new, better estimate $\mathbf{x}^{(k+1)} = \mathbf{x}^{(k)} + \mathbf{d}^{(k)}$. Here, $\mathbf{d}^{(k)}$ is the solution of the equation

$$\mathbf{J}(\mathbf{x}^{(k)})\mathbf{d}^{(k)} = -f(\mathbf{x}^{(k)}), \tag{E.0.1}$$

where $\mathbf{J}(\mathbf{x}^{(k)})$ is the Jacobian matrix.

There are cases where this Newton's method can run into difficulties, as pointed out in the documentation for the MATLAB Optimization Toolbox [130]. For example, $\mathbf{J}(\mathbf{x}^{(k)})$ may be singular, and so the Newton step $\mathbf{d}^{(k)}$ is not even defined. In addition, the exact Newton step $\mathbf{d}^{(k)}$ may be expensive to compute. In addition, Newton's method may not converge if the starting point is far from the solution.

In order to improve robustness when the starting point $\mathbf{x}^{(0)}$ is far from the solution and also to handle the case when the Jacobian matrix is singular, the *Trust-Region Methods* is used in the MATLAB function fsolve. To use this method, a merit function is needed to decide if the new estimate is better or worse than the old estimate. Instead of solving the equation (E.0.1), the problem becomes a minimisation

$$\min_{\mathbf{d}} \left\{ (1/2) f(\mathbf{x}^{(k)})^T f(\mathbf{x}^{(k)}) + \mathbf{d}^T \mathbf{J}(\mathbf{x}^{(k)})^T f(\mathbf{x}^{(k)}) + (1/2)\mathbf{d}^T \mathbf{J}(\mathbf{x}^{(k)}) \mathbf{J}(\mathbf{x}^{(k)})^T d \right\}, \tag{E.0.2}$$

subject to

$$\|\mathbf{D}\mathbf{d}\| \leq \Delta. \tag{E.0.3}$$

Here, $\mathbf{D}$ is a diagonal scaling matrix and Δ is a positive scalar which can be set in the algorithm.

In addition, $\|.\|$ denotes the 2-norm. In the algorithm, the step $\mathbf{d}^{(k)}$ is a convex combination of a Cauchy step (a step along the steepest descent direction) and a Gauss-Newton step for $f(\mathbf{x}^{(k)})$. The Cauchy step is given by

$$\mathbf{d}_C^{(k)} = -a\mathbf{J}(\mathbf{x}^{(k)})^T f(\mathbf{x}^{(k)}), \tag{E.0.4}$$

where a is chosen such that the expression in equation (E.0.2) is minimised. In other words, the expression like $\mathbf{d}_C^{(k)}$ is substituted into equation (E.0.2) and the minimisation is solved for a. In addition, the Gauss-Newton step is calculated by solving the equation (E.0.1) using a method discussed in the documentation [130] which give $\mathbf{d}_{GN}^{(k)}$. The step $\mathbf{d}^{(k)}$ is chosen so that

$$\mathbf{d}^{(k)} = \mathbf{d}_C^{(k)} + \lambda \left(\mathbf{d}_{GN}^{(k)} - \mathbf{d}_C^{(k)} \right), \tag{E.0.5}$$

where λ is the largest value in the interval [0, 1] such that $\|\mathbf{d}^{(k)}\| < \Delta$. If $\mathbf{J}(\mathbf{x}^{(k)})$ is nearly singular, λ is set to zero.

Appendix F

Solutions of the Landau-de Gennes Theory of Field Induced Uniaxial Nematics

F.1 Pure Landau-de Gennes theory

The Landau-de Gennes free energy expansion for uniaxial nematics in the absence of magnetic field is

$$A = (3/4)a(T - T_{\rm bf})Q^2 + (1/4)BQ^3 + (9/16)CQ^4. \tag{F.1.1}$$

The temperature and order parameter at the uniaxial nematic-to-isotropic phase transition can be found by solving the system

$$\begin{aligned} &A(Q^0_{NI}) = A(0), \\ &\frac{\partial A}{\partial Q}(Q^0_{NI}) = \frac{\partial A}{\partial Q}(0) = 0, \end{aligned} \tag{F.1.2}$$

for non zero Q^0_{NI}. The transition temperature is given by

$$T^0_{NI} = T_{\rm bf} + \frac{1}{27}\frac{B^2}{aC}. \tag{F.1.3}$$

And the order parameter at the phase transition is

$$Q^0_{NI} = -\frac{2}{9}\frac{B}{C}. \tag{F.1.4}$$

The Landau-de Gennes free energy expansion for uniaxial nematics under the interactions with the magnetic field is

$$A = (3/4)a(T - T_{\rm bf})Q^2 + (1/4)BQ^3 + (9/16)CQ^4 - hQ. \tag{F.1.5}$$

At the critical point, the free energy satisfies

$$\frac{\partial A}{\partial Q} = \frac{\partial^2 A}{\partial Q^2} = \frac{\partial^3 A}{\partial Q^3} = 0. \tag{F.1.6}$$

All three derivatives need to be equal to zero. The first two conditions ensure that the critical point is a stationary point of the free energy [102]. The third condition ensures that it is a minimum or maximum. In order for it to be a minimum, we also need the fourth derivative to be positive.

Solving the third derivative of the free energy equal to zero, we get the order parameter at the critical point

$$Q_c = \frac{-B}{9C} = (1/2)Q^0_{NI}. \tag{F.1.7}$$

In addition, the fourth derivative only depends on C. Therefore, we require $C > 0$. In order to simplify the problem, we change the variable to

$$x = Q + \frac{B}{9C}. \tag{F.1.8}$$

The free energy can be rewritten as

$$\begin{aligned} A =& \frac{9}{16}Cx^4 + \left(\frac{3}{4}a(T - T_{\rm bf}) - \frac{1}{24}\frac{B^2}{C}\right)x^2 \\ &+ \left(-\frac{1}{6}a(T - T_{\rm bf})\frac{B}{C} - h + \frac{1}{162}\frac{B^3}{C^2}\right)x + \frac{1}{108}a(T - T_{\rm bf})\frac{B^2}{C^2}. \end{aligned} \tag{F.1.9}$$

In order for the first two derivatives to vanish, we need

$$\frac{3}{4}a(T - T_{\rm bf}) - \frac{1}{24}\frac{B^2}{C} = 0, \tag{F.1.10}$$

and,

$$-\frac{1}{6}a(T - T_{\rm bf})\frac{B}{C} - h + \frac{1}{162}\frac{B^3}{C^2} = 0. \tag{F.1.11}$$

These two equations give us the critical temperature

$$T_c = T_{\rm bf} + \frac{1}{18}\frac{B^2}{aC}, \tag{F.1.12}$$

which can be related to the applied field

$$T = T_{\rm bf} + \frac{1}{27}\frac{B^2}{aC}\left(1 + \frac{h}{2h_c}\right). \tag{F.1.13}$$

This can also be written as

$$T_c - T^0_{NI} = \frac{1}{2}(T^0_{NI} - T_{\rm bf}). \tag{F.1.14}$$

We can eliminate $a(T - T_{\rm bf})$ in both equations (F.1.10) and (F.1.11) in order to get the critical field

$$h_c = -\frac{1}{324}\frac{B^3}{C^2}. \tag{F.1.15}$$

The transition temperature and transitional order parameter for a given field strength can be found by solving the system

$$\begin{aligned} &A(Q_1) = A(Q_2), \\ &\frac{\partial A}{\partial Q}(Q_1) = \frac{\partial A}{\partial Q}(Q_2) = 0. \end{aligned} \tag{F.1.16}$$

This can be simplified into a set of four equations

$$\frac{9}{4}Cx_{1,2}^3 + \left(\frac{3}{2}a(T-T_{\rm bf}) - \frac{1}{12}\frac{B^2}{C}\right)x_{1,2} + \left(-\frac{1}{6}a(T-T_{\rm bf})\frac{B}{C} - h + \frac{1}{162}\frac{B^3}{C^2}\right) = 0, \tag{F.1.17}$$

$$\frac{9}{4}C(x_1^2 + x_2^2 + x_1x_2) + \left(\frac{3}{2}a(T-T_{\rm bf}) - \frac{1}{12}\frac{B^2}{C}\right) = 0, \tag{F.1.18}$$

$$\begin{aligned} &\frac{9}{16}C(x_1^3 + x_2^3 + x_1^2x_2 + x_1x_2^2) + \left(\frac{3}{4}a(T-T_{\rm bf}) - \frac{1}{24}\frac{B^2}{C}\right)(x_1+x_2) \\ &+ \left(-\frac{1}{6}a(T-T_{\rm bf})\frac{B}{C} - h + \frac{1}{162}\frac{B^3}{C^2}\right) = 0. \end{aligned} \tag{F.1.19}$$

Using equation (F.1.17) we can eliminate the last term in equation (F.1.19) which gives

$$\frac{9}{16}C(-3x_1^3 - 3x_2^3 + x_1^2x_2 + x_1x_2^2) - \left(\frac{3}{4}a(T-T_{\rm bf}) - \frac{1}{24}\frac{B^2}{C}\right)(x_1+x_2) = 0. \tag{F.1.20}$$

This satisfies when either $x_1 + x_2 = 0$, or

$$-\frac{9}{16}C\left(2(x_1^2+x_2^2) + (x_1-x_2)^2\right) - \frac{3}{4}\left(a(T-T_{\rm bf}) - \frac{1}{18}\frac{B^2}{C}\right) = 0. \tag{F.1.21}$$

However this expression is always less than zero for T less than T_c. Therefore our solution satisfies $x_1 = -x_2$. Now adding the two equations in (F.1.17) gives

$$-\frac{1}{6}a(T-T_{\rm bf})\frac{B}{C} - h + \frac{1}{162}\frac{B^3}{C^2} = 0. \tag{F.1.22}$$

This can be solved to give the field induced transition temperature

$$T_{N-pN} - T_{\rm bf} = -\frac{6C}{aB}h + \frac{1}{27}\frac{B^2}{aC}. \tag{F.1.23}$$

We can also write this as

$$T_{N-pN} - T_{NI} = -\frac{4}{3}\frac{h}{aQ_{NI}^0}. \tag{F.1.24}$$

Now equation (F.1.18) can be solved with $x_1 = -x_2$ to give

$$x_{1,2}^2 = \frac{B^2}{81C^2}\left(3 - 54\frac{aC}{B^2}(T_{N-pN} - T_{\rm bf})\right). \tag{F.1.25}$$

From equation (F.1.23) we can write this as

$$x_{1,2}^2 = \frac{B^2}{81C^2}\left(1 - \frac{h}{h_c}\right). \tag{F.1.26}$$

Therefore the order parameter at the phase transition is

$$Q_{1,2} = Q_c\left(1 \pm \sqrt{1 - \frac{h}{h_c}}\right). \tag{F.1.27}$$

In order to find a relation between the order parameter and the temperature at the critical field, we substitute $h = h_c$ and equation (F.1.12) into equation (F.1.9) and differentiate with respect to x.

$$\frac{\partial A}{\partial x}(h = h_c) = -26244Cx^3 + 17496aC^3x(T_c - T) - 1944BaC^2(T_c - T). \tag{F.1.28}$$

Hence at the critical field, we have

$$\frac{3}{2}C(Q - Q_c)^3 = aQ(T_c - T). \tag{F.1.29}$$

This equation can be used to find the critical exponent β. In the limit as T tends to T_c, $(T - T_c)$ is a power of $(Q - Q_c)$. We set $t = T_c - T$, the equation becomes

$$\frac{3}{2}Cx^3 = a(x + Q_c)t. \tag{F.1.30}$$

In order to find the asymptotic behaviour of t against x, we expand t as a polynomial of x

$$t = t_0 + t_1x + t_2x^2 + t_3x^3. \tag{F.1.31}$$

Therefore, we get

$$\begin{aligned}(3/2)Cx^3 = {} & aQ_ct_0 \\ & + a(t_0 + Q_ct_1)x \\ & + a(t_1 + Q_ct_2)x^2 \\ & + a(t_2 + Q_ct_3)x^3.\end{aligned} \tag{F.1.32}$$

Equate the two sides, we get

$$t_0 = t_1 = t_2 = 0. \tag{F.1.33}$$

And

$$t_3 = \frac{3C}{2aQ_c}. \tag{F.1.34}$$

Hence $(T - T_c)$ behaves asymptotically as $(Q - Q_c)^3$

$$T - T_c = \frac{3C}{2aQ_c}(Q - Q_c)^3. \tag{F.1.35}$$

F.2 Landau-KKLS theory

Here we set $B = bT$ so this coefficient is linear in temperature. The Landau-KKLS free energy expansion for uniaxial nematics without interaction with the magnetic field is

$$A = (3/4)a(T - T_{\rm bf})Q^2 + (1/4)bTQ^3 + (9/16)CQ^4, \tag{F.2.1}$$

where the coefficients are given in equation (6.2.17). The temperature and order parameter at the uniaxial nematic-to-isotropic phase transition can be found by solving the system

$$\begin{aligned} &A(Q^0_{NI}) = A(0), \\ &\frac{\partial A}{\partial Q}(Q^0_{NI}) = \frac{\partial A}{\partial Q}(0) = 0, \end{aligned} \tag{F.2.2}$$

for non zero Q^0_{NI}. Thus, the transition temperature is the positive solution of the quadratic equation

$$T^2 - 27\frac{aC}{b^2}T + 27\frac{aC}{b^2}T_{\rm bf} = 0. \tag{F.2.3}$$

Hence,

$$T^0_{NI} = \frac{1}{2}\left(\frac{27aC}{b^2} \pm \sqrt{\left(\frac{27aC}{b^2}\right)^2 - 4T_{\rm bf}\frac{27aC}{b^2}}\right). \tag{F.2.4}$$

And the order parameter at the phase transition is

$$Q^0_{NI} = -\frac{2}{9}\frac{bT^0_{NI}}{C}. \tag{F.2.5}$$

At this stage we cannot choose between the plus and minus signs for the transition temperature. It is clear when we use the Landau-KKLS theory that taking the minus sign gives us a result closer to the transition temperature predicted by the molecular field theory. In addition, taking the plus sign gives us the order parameter at the phase transition greater than one which is not valid. Hence, within the Landau-KKLS theory the transition temperature is

$$T^0_{NI} = \frac{1}{2}\left(\frac{27aC}{b^2} - \sqrt{\left(\frac{27aC}{b^2}\right)^2 - 4T_{\rm bf}\frac{27aC}{b^2}}\right). \tag{F.2.6}$$

The Landau-KKLS free energy expansion for magnetic field induced nematics is

$$A = (3/4)a(T - T_{\rm bf})Q^2 + (1/4)bTQ^3 + (9/16)CQ^4 - hQ. \tag{F.2.7}$$

At the critical point, both the first, second and third derivatives of the free energy must be zero whereas the fouth derivative is strictly positive. In order for the third derivative to vanish, the order parameter at the phase transition must be

$$Q_c = -\frac{bT_c}{9C}. \tag{F.2.8}$$

We change the variable to

$$x = Q + \frac{bT}{9C}. \tag{F.2.9}$$

Now we can rewrite the free energy as

$$\begin{aligned} A =& \frac{9}{16}Cx^4 + \left(\frac{3}{4}a(T - T_{\mathrm{bf}}) - \frac{1}{24}\frac{b^2T^2}{C}\right)x^2 \\ &+ \left(-\frac{1}{6}a(T - T_{\mathrm{bf}})\frac{bT}{C} - h + \frac{1}{162}\frac{b^3T^3}{C^2}\right)x + \frac{1}{108}a(T - T_{\mathrm{bf}})\frac{b^2T^2}{C^2}. \end{aligned} \tag{F.2.10}$$

The critical temperature and critical magnetic field are the solutions of the system

$$\begin{aligned} &\frac{3}{4}a(T - T_{\mathrm{bf}}) - \frac{1}{24}\frac{b^2T^2}{C} = 0, \\ &-\frac{1}{6}a(T - T_{\mathrm{bf}})\frac{bT}{C} - h + \frac{1}{162}\frac{b^3T^3}{C^2} = 0. \end{aligned} \tag{F.2.11}$$

Now the critical temperature is the solution of the first equation

$$T_c = \frac{1}{2}\left(\frac{18aC}{b^2} \pm \sqrt{\left(\frac{18aC}{b^2}\right)^2 - 4T_{\mathrm{bf}}\frac{18aC}{b^2}}\right). \tag{F.2.12}$$

The critical field can be found by eliminating the term $a(T - T_{\mathrm{bf}})$ in the two equations which gives

$$h_c = -\frac{1}{324}\frac{b^3T_c^3}{C^2}. \tag{F.2.13}$$

The equation relating the order parameter and temperatue at the critical field can be found by substituting for h_c to equation (F.2.10) and solve for the first derivative equal to zero, we get

$$\frac{9}{4}C\left(Q - \frac{bT}{9C}\right)^3 = -\left(\frac{3}{2}a(T - T_{\mathrm{bf}}) - \frac{1}{12}\frac{b^2T^2}{C}\right)Q. \tag{F.2.14}$$

Note in this case we cannot find the critical exponent analytically since we cannot write the critical equation in terms of $t = T_c - T$ due to the appearance of the quadratic term in T. Thus, the transitional order parameter cannot be put into a simple formular. Hence we have to rely on numerical results for this.

Appendix G

Stability of The Equilibrium Free Energy for KLZ Approximation

In this appendix, we analyse the stability conditions for the equilibrium free energy in three cases: uniaxial smectic A fomed from uniaxial molecules with KLZ approximation, biaxial smectic A formed from molecules with D_{2h} symmetry with KLZ-GM and KLZ-SVD approximations. The stability conditions can only be obtained analytically at perfect order. The methodology and results for the first case were introduced to me through a private communication with Mr Hock Seng Nguan.

G.1 KLZ Theory

For convenience, we define the following functions

$$J(z,\beta) = (1+\alpha\tau^2)P_2(\cos\beta) + 2\alpha\eta\tau\cos 2\pi z/d. \tag{G.1.1}$$

$$K(z,\beta) = 2\alpha\eta\tau P_2\cos\beta + \alpha(\delta+\eta^2)\cos 2\pi z/d. \tag{G.1.2}$$

The second derivatives of the scaled free energy A^* in equation (7.3.6) with respect to the two order parameters are

$$\frac{\partial^2 A^*}{\partial\tau^2} = \frac{1}{T^{*2}}\left(\overline{K}^2 - \overline{K^2}\right) + \frac{1}{T^*}\left(\delta\alpha + 3\alpha S^2 - 2\alpha S\overline{P_2}\right). \tag{G.1.3}$$

$$\frac{\partial^2 A^*}{\partial S^2} = \frac{1}{T^{*2}}\left(\overline{J}^2 - \overline{J^2}\right) + \frac{1}{T^*}\left(1 + 3\alpha\tau^2 - 2\alpha\tau\overline{\cos\left(2\pi z/d\right)}\right). \tag{G.1.4}$$

$$\frac{\partial^2 A^*}{\partial\tau\partial S} = \frac{1}{T^{*2}}\left(\overline{J}\times\overline{K} - \overline{JK}\right) + \frac{1}{T^*}\left(6\alpha\tau S - 2\alpha\tau\overline{P_2} - 2\alpha S\overline{\cos\left(2\pi z/d\right)}\right). \tag{G.1.5}$$

Here, we make a clear distinction between S and $\overline{P_2}$, and between τ and $\overline{\cos 2\pi z/d}$. The overline represents the integration

$$\overline{A} = \int\int A(z,\beta) f(z,\beta) dz d\beta. \tag{G.1.6}$$

They come from the derivative of the partition function. The values of $\overline{P_2}$ and $\overline{\cos 2\pi z/d}$ are only equal S and τ at the solutions of the self-consistency equations. The first terms in the three derivatives are thermodynamic fluctuations and vanish at perfect order. In addition, at perfect order we have $S = \overline{P_2} = 1$ and $\tau = \overline{\cos(2\pi z/d)} = 1$. Hence the values of the determinant of the Hessian matrix at the self consistency solutions at perfect order are

$$\det H = \frac{1}{T^{*2}} \left((1+\alpha)\delta\alpha + \alpha - 3\alpha^2 \right). \tag{G.1.7}$$

For simplicity, we let $\delta = 0$. It is then easy to see that the second derivatives of the form $\partial^2 A/\partial a^2$ are possitive. Hence, from multivariate analysis, the condition for stability is $\det H > 0$, or $0 < \alpha < 1/3$. In the next two sections, we also set δ to 0 for the GM-KLS approximation and for the SVD-KLS approximation.

G.2 Geometric Mean Approximation with KLZ Theory

For convenience, we define the following three functions as

$$J_1(z,\Omega) = \left(\delta\alpha + \alpha(\langle F_U\rangle^2 + 2\langle F_B\rangle^2)\right)\cos(2\pi z/d) + 2\alpha\tau\left(\langle F_U\rangle F_U(\Omega) + 2\langle F_B\rangle F_B(\Omega)\right). \tag{G.2.1}$$

$$J_2(z,\Omega) = 2\alpha\langle F_U\rangle\tau\cos(2\pi z/d) + \left(1+\alpha\tau^2\right)F_U(\Omega). \tag{G.2.2}$$

$$J_3(z,\Omega) = 4\alpha\langle F_B\rangle\tau\cos(2\pi z/d) + 2\left(1+\alpha\tau^2\right)F_B(\Omega). \tag{G.2.3}$$

The second derivatives of the KKLS free energy in equation (7.4.9) can be written in terms of these three functions

$$\frac{\partial^2 A^*}{\partial\tau^2} = \frac{1}{T^{*2}}\left(\overline{J_1}^2 - \overline{J_1^2}\right) + \frac{1}{T^*}\left\{\delta\alpha + 3\alpha\left(\langle F_U\rangle^2 + 2\langle F_B\rangle^2\right) - 2\alpha\left(\langle F_U\rangle\overline{F_U} + 2\langle F_B\rangle\overline{F_B}\right)\right\}. \tag{G.2.4}$$

$$\frac{\partial^2 A^*}{\partial\langle F_U\rangle^2} = \frac{1}{T^{*2}}\left(\overline{J_2}^2 - \overline{J_2^2}\right) + \frac{1}{T^*}\left(1 + 3\alpha\tau^2 - 2\alpha\tau\overline{\cos(2\pi z/d)}\right). \tag{G.2.5}$$

$$\frac{\partial^2 A^*}{\partial\langle F_B\rangle^2} = \frac{1}{T^{*2}}\left(\overline{J_3}^2 - \overline{J_3^2}\right) + \frac{1}{T^*}\left(2 + 6\alpha\tau^2 - 4\alpha\tau\overline{\cos 2\pi z/d}\right). \tag{G.2.6}$$

$$\frac{\partial^2 A^*}{\partial\tau\partial\langle F_U\rangle} = \frac{1}{T^{*2}}\left(\overline{J_1}\times\overline{J_2} - \overline{J_1 J_2}\right) + \frac{1}{T^*}\left(6\alpha\tau\langle F_U\rangle - 2\alpha\langle F_U\rangle\overline{\cos(2\pi z/d)} - 2\alpha\tau\overline{F_U}\right). \tag{G.2.7}$$

$$\frac{\partial^2 A^*}{\partial\tau\partial\langle F_B\rangle} = \frac{1}{T^{*2}}\left(\overline{J_1}\times\overline{J_3} - \overline{J_1 J_3}\right) + \frac{1}{T^*}\left(12\alpha\tau\langle F_B\rangle - 4\alpha\langle F_B\rangle\overline{\cos(2\pi z/d)} - 4\alpha\tau\overline{F_B}\right). \tag{G.2.8}$$

$$\frac{\partial^2 A^*}{\partial\langle F_U\rangle\partial\langle F_B\rangle} = \frac{1}{T^{*2}}\left(\overline{J_2}\times\overline{J_3} - \overline{J_2 J_3}\right). \tag{G.2.9}$$

Here, we make a clear distinction between $\langle F_U \rangle$ and $\overline{F_U}$, $\langle F_B \rangle$ and $\overline{F_B}$, and between τ and $\overline{\cos(2\pi z/d)}$. They only equal each other at the solution of the self-consistency equations. The overline represents the integration

$$\overline{A} = \int\int A(z,\beta) f(z,\Omega) dz d\Omega. \tag{G.2.10}$$

Again, at perfect order, the fluctuation terms vanish. Setting the limit for rod-like molecules, $\langle F_U \rangle = \overline{F_U} = 1$, $\langle F_B \rangle = \overline{F_B} = \gamma$ and $\tau = 1$, the determinant of the Hessian matrix is

$$\det H = 2\alpha(1+2\gamma^2)(1+\alpha)(1-3\alpha). \tag{G.2.11}$$

In addition, it is easy to see that the second derivatives of the form $\partial^2 A/\partial a^2$ are possitive. Here, the condition for the de Gennes' free energy to be well-behaved is the same as for the uniaxial smectic A phase formed from uniaxial molecules.

G.3 SVD Approximation

Again, for convenience, we define the following three functions

$$\begin{aligned} K_1(z,\Omega) = &\left(\delta\alpha + \alpha(\langle R_{00}\rangle^2 + 2\lambda\langle R_{22}\rangle^2)\right)\cos(2\pi z/d) \\ &+2\alpha\tau\left(\langle R_{00}\rangle R_{00}(\Omega) + 2\lambda\langle R_{22}\rangle R_{22}(\Omega)\right). \end{aligned} \tag{G.3.1}$$

$$K_2(z,\Omega) = 2\alpha\langle R_{00}\rangle\tau\cos(2\pi z/d) + \left(1+\alpha\tau^2\right)R_{00}(\Omega). \tag{G.3.2}$$

$$K_3(z,\Omega) = 4\alpha\lambda\langle R_{22}\rangle\tau\cos(2\pi z/d) + 2\left(1+\alpha\tau^2\right)\lambda R_{22}(\Omega). \tag{G.3.3}$$

The KKLS free energy in equation (7.4.2) can be written in terms of these three functions

$$\begin{aligned} \frac{\partial^2 A^*}{\partial\tau^2} = &\frac{1}{T^{*2}}\left(\overline{K_1}^2 - \overline{K_1^2}\right) + \frac{1}{T^*}\left\{\delta\alpha + 3\alpha\left(\langle R_{00}\rangle^2 + 2\lambda\langle R_{22}\rangle^2\right)\right. \\ &\left.-2\alpha\left(\langle R_{00}\rangle\overline{R_{00}} + 2\lambda\langle R_{22}\rangle\overline{R_{22}}\right)\right\}. \end{aligned} \tag{G.3.4}$$

$$\frac{\partial^2 A^*}{\partial\langle R_{00}\rangle^2} = \frac{1}{T^{*2}}\left(\overline{K_2}^2 - \overline{K_2^2}\right) + \frac{1}{T^*}\left(1+3\alpha\tau^2 - 2\alpha\tau\overline{\cos(2\pi z/d)}\right). \tag{G.3.5}$$

$$\frac{\partial^2 A^*}{\partial\langle R_{22}\rangle^2} = \frac{1}{T^{*2}}\left(\overline{K_3}^2 - \overline{K_3^2}\right) + \frac{1}{T^*}\left(2\lambda + 6\lambda\alpha\tau^2 - 4\lambda\alpha\tau\overline{\cos 2\pi z/d}\right). \tag{G.3.6}$$

$$\begin{aligned} \frac{\partial^2 A^*}{\partial\tau\partial\langle R_{00}\rangle} = &\frac{1}{T^{*2}}\left(\overline{K_1}\times\overline{K_2} - \overline{K_1 K_2}\right) \\ &+\frac{1}{T^*}\left(6\alpha\tau\langle R_{00}\rangle - 2\alpha\langle R_{00}\rangle\overline{\cos(2\pi z/d)} - 2\alpha\tau\overline{R_{00}}\right). \end{aligned} \tag{G.3.7}$$

$$\frac{\partial^2 A^*}{\partial\tau\partial\langle R_{22}\rangle} = \frac{1}{T^{*2}}\left(\overline{K_1}\times\overline{K_3} - \overline{K_1K_3}\right)$$
$$+\frac{1}{T^*}\left(12\lambda\alpha\tau\langle R_{22}\rangle - 4\lambda\alpha\langle R_{22}\rangle\overline{\cos\left(2\pi z/d\right)} - 4\lambda\alpha\tau\langle R_{22}\rangle\right). \tag{G.3.8}$$

$$\frac{\partial^2 A^*}{\partial\langle R_{00}\rangle\partial\langle R_{22}\rangle} = \frac{1}{T^{*2}}\left(\overline{K_2}\times\overline{K_3} - \overline{K_2K_3}\right). \tag{G.3.9}$$

Here, we make a clear distinction between $\langle R_{00}\rangle$ and $\overline{R_{00}}$, $\langle R_{22}\rangle$ and $\overline{R_{22}}$, and between τ and $\overline{\cos\left(2\pi z/d\right)}$. They only equal each other at the solution of the self-consistency equations. We note that, at perfect order, the fluctuation terms vanish. Setting the limit at perfect order $\langle R_{00}\rangle = \overline{R_{00}} = 1$, $\langle R_{22}\rangle = \overline{R_{22}} = 1$ and $\tau = \cos\left(2\pi z/d\right) = 1$, the determinant of the Hessian matrix is

$$\det H = 2\lambda\alpha(1+\lambda)(1+\alpha)(1-3\alpha). \tag{G.3.10}$$

In this case, we can also see that the second derivatives of the form $\partial^2 A/\partial a^2$ are positive. Hence, we conclude that in all three cases, the condition for the solution of the self-consistency equations to coincide with the minimum of the KKLS free energy is $0 < \alpha < 1/3$.

List of Publications

G. R. Luckhurst, S. Naemura, T. J. Sluckin, T. B. T. To and S. Turzi, *Molecular field theory for biaxial nematic liquid crystals composed of molecules with C_{2h} point group symmetry*, Phys. Rev. E. **84**, 011704 (2011).

G. R. Luckhurst, T. J. Sluckin and T. B. T. To, *Molecular field theory for polar biaxial nematics formed from V-shaped molecules*, in preparation.

G. R. Luckhurst, T. J. Sluckin and T. B. T. To, *Molecular field theory for magnetic field induced uniaxial nematics formed from biaxial molecules*, in preparation.

G. R. Luckhurst, T. J. Sluckin and T. B. T. To, *Molecular field theory for biaxial smectic A liquid crystals*, in preparation.

Bibliography

[1] T. J. Sluckin, Cont. Phys. **41**, 37 (2000).

[2] P. G. de Gennes, *The Physics of Liquid Crystals* (Oxford University Press, Oxford, 1990).

[3] G. R. Luckhurst, Thin Solid Films **393**, 40 (2001).

[4] I. Dierking, *Textures of Liquid Crystals* (Wiley-VCH, Darmstadt, 1999).

[5] J. P. Collings, *Liquid Crystals - Nature's Delicate Phase of Matter* (Princeton University Press, Princeton, 1990).

[6] W. L. McMillan, Phys. Rev. A **4**, 1238 (1971).

[7] G. Vertogen and W. H. de Jeu, *Thermotropic Liquid Crystals, Fundamentals* (Springer, 1988).

[8] S. Chandrasekhar, *Liquid Crystals* (CUP, 1992).

[9] T. J. Sluckin, D. A. Dunmur, and H. Stegemeyer, *Crystals That Flows - Classic Papers from the History of Liquid Crystals*, edited by T. J. Sluckin, D. A. Dunmur, and H. Stegemeyer (Taylor & Francis, 2004).

[10] M. A. Osipov, "Handbook of liquid crystals," (Wiley-VCH, Germany, 1998) Chap. 3.

[11] G. R. Luckhurst, "Molecular physics of liquid crystals," (Academy Press, London, 1979) Chap. 4.

[12] W. M. Gelbart, J. Chem. Phys. **86**, 4298 (1982).

[13] A. Sonnet, E. G. Virga, and G. E. Durand, Phys. Rev. E **67**, 061701 (2003).

[14] M. J. Freiser, Phys. Rev. Lett. **24**, 1041 (1970).

[15] M. J. Freiser, Mol. Cryst. Liq. Cryst. **14**, 165 (1971).

[16] P. W. Atkins and R. S. Friedman, *Molecular Quantum Mechanics*, 3rd ed. (OUP, Oxford, 1996).

[17] J. P. Straley, Phys. Rev. A **10**, 1881 (1974).

[18] N. Boccara, R. Mejdani, and L. de Seze, J. de Phys **7**, 149 (1977).

[19] D. K. Remler and A. D. J. Haymet, J. Phys. Chem. **90**, 5426 (1986).

[20] F. Biscarini, C. Chiccoli, P. Pasini, F. Semeria, and C. Zannoni, Phys. Rev. Lett. **75**, 1803 (1995).

[21] P. I. C. Teixeira, A. J. Masters, and B. M. Mulder, Mol. Cryst. Liq. Cryst. **323**, 167 (1998).

[22] G. De Matteis and Virga, Phys. Rev. E **71**, 061703 (2005).

[23] G. De Matteis, S. Romano, and E. G. Virga, Phys. Rev. E **72**, 041706 (2005).

[24] L. Longa, P. Grzybowski, S. Romano, and E. G. Virga, Phys. Rev. E **71**, 051714 (2005).

[25] F. Bisi, E. G. Virga, E. C. Gartland, Jr, G. De Matteis, A. M. Sonnet, and G. E. Durand, Phys. Rev. E **73**, 051709 (2006).

[26] F. Bisi, G. R. Luckhurst, and E. G. Virga, Phys. Rev. E **78**, 021701 (2008).

[27] D. Allender and L. Longa, Phys. Rev. E **78**, 011704 (2008).

[28] L. J. Yu and A. Saupe, Phys. Rev. Lett. **45**, 1000 (1980).

[29] K. Severing and K. Saalwachter, Phys. Rev. Lett. **92**, 125501 (2004).

[30] K. Merkel, A. Kocot, J. K. Vij, R. Korlacki, G. H. Mehl, and T. Meyer, Phys. Rev. Lett. **93**, 237801 (2004).

[31] J. L. Figueirinhas, C. Cruz, D. Filip, G. Feio, A. C. Ribeiro, Y. Frere, T. Meyer, and G. H. Mehl, Phys. Rev. Lett. **94**, 107802 (2005).

[32] K. Neupane, S. W. Kang, S. Sharma, D. Carney, T. Meyer, G. H. Mehl, D. W. Allender, S. Kumar, and S. Sprunt, Phys. Rev. Lett. **97**, 207802 (2006).

[33] G. R. Luckhurst, Nature **430**, 413 (2004).

[34] D. W. Bruce, The Chemical Record **4**, 10 (2004).

[35] B. R. Acharya, A. Primak, and S. Kumar, Phys. Rev. Lett. **92**, 145506 (2004).

[36] L. A. Madsen, T. J. Dingemans, M. Nakata, and E. T. Samulski, Phys. Rev. Lett. **92**, 145505 (2004).

[37] C. D. Southern, P. D. Brimicombe, S. D. Siemianowski, S. Jaradat, N. Roberts, V. Gortz, J. W. Goodby, and H. F. Gleeson, EPL **82**, 56001 (2008).

[38] J. H. Lee, T. K. Lim, W. T. Kim, and J. I. Lin, J. Appl. Phys. **101**, 034105 (2007).

[39] R. Berardi, L. Muccioli, and C. Zannoni, J. Chem. Phys. **128**, 024905 (2008).

[40] T. Ostapenko, D. B. Wiant, S. N. Sprunt, A. Jákli, and T. J. Gleeson, Phys. Rev. Lett. **101**, 247801 (2008).

[41] P. I. C. Teixeira, M. A. Osipov, and G. R. Luckhurst, Phys. Rev. E **73**, 061708 (2006).

[42] A. G. V. P. K. Karahaliou and D. J. Photinos, J. Chem. Phys. **131**, 124516 (2009).

[43] G. R. Luckhurst, Angew. Chem. Int. Ed. **44**, 2836 (2005).

[44] A. Ferrarini, G. R. Luckhurst, P. L. Nordio, and S. J. Roskilly, Chem. Phys. Letts **214**, 409 (1993).

[45] P. J. Wojtowicz and P. Sheng, Phys. Lett. **48A**, 235 (1974).

[46] A. J. Stone, "Molecular physics of liquid crystals," (Academy Press, London, 1979) Chap. 2.

[47] C. G. Gray and K. E. Gubbins, *Theory of Molecular Fluids* (OUP, New York, 1984).

[48] C. Zannoni, "Molecular physics of liquid crystals," (Academy Press, London, 1979) Chap. 3.

[49] L. Blum and A. J. Torruella, J. Chem. Phys. **56**, 303 (1972).

[50] M. E. Rose, *Elementary Theory of Angular Momentum* (Wiley, 1957).

[51] Luckhurst, Liq. Cryst **36**, 1295 (2009).

[52] F. Biscarini, C. Chiccoli, P. Pasini, and C. Zannoni, Mol. Phys. **73**, 439 (1991).

[53] S. J. Blundell and K. M. Blundell, *Concepts in Thermal Physics* (OUP, New York, 2006).

[54] B. Mulder, Phys. Rev. A **39**, 360 (1989).

[55] G. De Matteis, F. Bisi, and E. G. Virga, Con. Mech. Therm. **19**, 1 (2007).

[56] G. R. Luckhurst, C. Zannoni, P. L. Nordio, and U. Segre, Mol. Phys. **30**, 1345 (1975).

[57] F. Bisi, S. Romano, and E. G. Virga, Phys. Rev. E **75**, 041705 (2007).

[58] G. R. Luckhurst and S. Romano, Mol. Phys. **40**, 129 (1980).

[59] X. Zheng and P. Palffy-Muhoray, Disc. Cont. Dyn. Syst. Series B **15**, 475 (2011).

[60] R. Rosso and E. G. Virga, Phys. Rev. E **74**, 021712 (2006).

[61] G. De Matteis and S. Romano, Phys. Rev. E **78**, 021702 (2008).

[62] S. Romano, Phys. Rev. A **333**, 110 (2004).

[63] J. Katriel, G. F. Kventsel, G. R. Luckhurst, and T. J. Sluckin, Liq. Cryst **1**, 337 (1986).

[64] G. R. Luckhurst, S. Naemura, T. J. Sluckin, K. S. Thomas, and S. S. Turzi, (2009).

[65] M. V. Gorkunov, M. A. Osipov, A. Kocot, and J. K. Vij, Phys. Rev. E **81**, 061702 (2010).

[66] M. A. Osipov and M. V. Gorkunov, J. Phys.: Condens. Matter **22**, 362101 (2010).

[67] N. D. Mermin, Rev. Mod. Phys. **51**, 591 (1979).

[68] Y. Galerne, Mol. Cryst. Liq. Cryst. **323**, 211 (1998).

[69] M. Liu, Phys. Rev. A **24**, 2720 (1981).

[70] U. D. Kini, Mol. Cryst. Liq. Cryst. **112**, 265 (1984).

[71] N. Boccara, Ann. Phys. **76**, 72 (1973).

[72] S. Goshen, D. Mukamel, and S. Shtrikman, Mol. Cryst. Liq. Cryst. **31**, 171 (1975).

[73] T. C. Lubensky and L. Radzihovsky, Phys. Rev. E **66**, 031704 (2002).

[74] B. Mettout, Phys. Rev. E **72**, 031706 (2005).

[75] B. Mettout, Phys. Rev. E **74**, 041701 (2006).

[76] A. Ferrarini, G. J. Moro, P. L. Nordio, and G. R. Luckhurst, Mol. Phys. **77**, 1 (1992).

[77] A. Ferrarini, G. R. Luckhurst, P. L. Nordio, and S. J. Roskilly, J. Chem. Phys. **100**, 1460 (1994).

[78] A. Ferrarini, G. R. Luckhurst, P. L. Nordio, and S. J. Roskilly, Liq. Cryst. **21**, 373 (1996).

[79] F. Bisi, L. Longa, G. Pajak, and R. Rosso, Mol. Cryst. Liq. Cryst. **525**, 12 (2010).

[80] F. Bisi and R. Rosso, Eur. J. App. Math., 2011 in the press. DOI: 10.1017/S0956792510000379.

[81] E. W. Weisstein, "Binet-Cauchy Identity." From *MathWorld*–A Wolfram Web Resource. http://mathworld.wolfram.com/Binet-CauchyIdentity .html.

[82] M. Bates and G. R. Luckhurst, Phys. Rev. E **72**, 051702 (2005).

[83] M. Bates, Chem. Phys. Letts **437**, 189 (2007).

[84] P. Grzybowski and L. Longa, cond-mat.soft , arXiv:0911.4174v1 (2009).

[85] T. Watanabe, S. Miyata, T. Furukawa, H. Takezoe, T. Nishi, M. Sone, A. Migita, and J. Watanabe, Jpn. J. Appl. Phys. **35**, L 505 (1996).

[86] H. Takezoe and J. Watanabe, Mol. Cryst. Liq. Cryst. **328**, 325 (1999).

[87] J. Watanabe, L. Yuqing, H. Tuchiya, and H. Takezoe, Mol. Cryst. Liq. Cryst. **346**, 9 (2000).

[88] O. Francescangeli, V. Stanic, S. I. Torgova, A. Strigazzi, N. Scaramuzza, C. Ferrero, I. P. Dolbnya, T. M. Weiss, R. Berardi, L. Muccioli, S. Orlandi, and C. Zannoni, Adv. Funct. Mater. **19**, 2592 (2009).

[89] P. Palffy-Muhoray, M. A. Lee, and R. G. Petschek, Phys. Rev. Lett. **60**, 2303 (1988).

[90] B. Park, J. W. Wu, and H. Takezoe, Phys. Rev. E **63**, 021707 (2001).

[91] D. Wei and G. N. Patey, Phys. Rev. Lett. **68**, 1992 (1992).

[92] B. Mettout, P. Toledano, H. Takezoe, and J. Watanabe, Phys. Rev. E **66**, 031701 (2002).

[93] F. Bisi, R. Rosso, E. G. Virga, and G. E. Durand, Phys. Rev. E **78**, 011705 (2008).

[94] J. Peláez and M. R. Wilson, Phys. Rev. Lett. **97**, 267801 (2006).

[95] G. R. Luckhurst and S. Romano, J. Chem. Phys. **107**, 2557 (1997).

[96] G. R. Luckhurst and S. Romano, Phys. Chem. Chem. Phys. **5**, 1242 (2003).

[97] G. Luckhurst, Liq. Cryst **32**, 1335 (2005).

[98] L. Longa, G. Pajak, and T. Wydro, Phys. Rev. E **76**, 011703 (2007).

[99] M. Bates, Phys. Rev. E **74**, 061702 (2006).

[100] R. L. Humphries and G. R. Luckhurst, Chem. Phys. Letts **23**, 567 (1973).

[101] A. Kloczkowski and G. R. Luckhurst, J. Chem. Soc., Faraday Trans. 2 **84**, 155 (1988).

[102] I. Lelidis and G. Durand, Phys. Rev. E **48**, 3822 (1993).

[103] T. W. Stinson and J. D. Litster, Phys. Rev. Lett. **25**, 503 (1970).

[104] C. Rosenblatt, Phys. Rev. A **24**, 2236 (1981).

[105] D. Wiant, S. Stojadinovic, K. Neupane, S. Sharma, K. Fodor-Csorba, A. Jákli, J. T. Gleeson, and S. Sprunt, Phys. Rev. E **73**, 030703 (2006).

[106] J. Hanus, Phys. Rev. **178**, 420 (1969).

[107] G. R. Luckhurst and P. Simpson, Chem. Phys. Letts **95**, 149 (1983).

[108] Warsono, K. Abraha, Y. Yusuf, and P. Nurwantoro, Int. Jour. Bas. Appl. Sci. **10**, 19 (2010).

[109] P. Palffy-Muhoray and D. A. Dunmur, Mol. Cryst. Liq. Cryst. **97**, 337 (1983).

[110] E. I. Rjumtse, M. A. Osipov, , T. A. Rotinyan, and N. P. Yevlampieva, Liq. Cryst **18**, 87 (1995).

[111] E. F. Gramsbergen, L. Longa, and W. H. de Jeu, Phys. Rep. **135**, 195 (1986).

[112] Z. D. Zhang, D. X. Zhang, and Y. B. Sun, Chin. Phys. Lett. **17**, 749 (2000).

[113] H. R. Brand, P. E. Cladis, and H. Pleiner, Macromolecules **25**, 7223 (1992).

[114] H. R. Brand, P. E. Cladis, and H. Pleiner, Int. Jour. Eng. Sci. **38**, 1099 (2000).

[115] T. Hegmann, J. Kain, S. Diele, G. Pelzl, and C. Tschierske, Angew. Chem. Int. Ed. **40**, 887 (2001).

[116] K. Kaznacheev and T. Hegmann, Phys. Chem. Chem. Phys. **9**, 1705 (2007).

[117] A. Eremin, S. Diele, G. Pelzl, H. Nádasi, W. Weissflog, J. Salfetnikova, and H. Kresse, Phys. Rev. E **64**, 051707 (2001).

[118] C. V. Yelamaggad, S. K. Prasad, G. G. Nair, I. S. Shashikala, D. S. S. Rao, C. V. Lobo, and S. Chandrasekhar, Angew. Chem. Int. Ed. **43**, 3429 (2004).

[119] C. V. Yelamaggad, I. S. Shashikala, D. S. S. Rao, G. G. Nair, and S. K. Prasad, J. Mater. Chem. **16**, 4099 (2006).

[120] B. K. Sadashiva, R. A. Reddy, R. Pratibha, and N. V. Madhusudana, J. Mater. Chem. **12**, 943 (2002).

[121] H. N. S. Murthy and B. K. Sadashiva, Liq. Cryst **31**, 567 (2004).

[122] M. Matsushita, Mol. Cryst. Liq. Cryst. **68**, 949 (1981).

[123] R. Berardi and C. Zannoni, J. Chem. Phys. **113**, 5971 (2000).

[124] A. G. Vanakaras, M. A. Bates, and D. J. Photinos, Phys. Chem. Chem. Phys. **5**, 3700 (2003).

[125] E. M. Averyanov and A. N. Primak, Liq. Cryst **13**, 139 (1993).

[126] W. L. McMillan, Phys. Rev. A **6**, 936 (1972).

[127] G. F. Kventsel, G. R. Luckhurst, and H. B. Zewdie, Mol. Phys. **56**, 589 (1985).

[128] R. G. Marguta, E. Martín del Río, and E. de Miguel, J. Phys.: Condens. Matter **18**, 10335 (2006).

[129] J. Nocedal and S. J. Wright, *Numerical Optimisation*, edited by P. Glynn and S. M. Robinson (Springer, 1999).

[130] See http://www.mathworks.co.uk/help/toolbox/optim/.